# Hidden capacity of thin prestressed concrete deck slabs with T-beams

# Hidden capacity of thin prestressed concrete deck slabs with T-beams

A thesis submitted to the Department of Civil Engineering in conformity with the requirements for the degree of Master of Science.

Delft University of Technology
Delft, the Netherlands
2016

Author:

K.G.S. Pawirotaroeno

Thesis committee:

Dr.Ir. C. van der Veen

Prof.Dr.Ir. D.A.Hordijk

Ir. S.W.H. Ensink

Dr.Ir. M.A.N.Hendriks

Ir. L.J.M.Houben

# Preface

This research is fulfilled as a Master Thesis to obtain the degree of Master of Science. The thesis finalizes the study Civil Engineering with the master track Structural Engineering and specialty Concrete Structures at the University of Technology Delft.

My gratitude is given to the supervisors: Dr.Ir. C. van der Veen, Prof.Dr.Ir. D.A.Hordijk, Ir. S.W.H. Ensink, Dr. Ir. M.A.N.Hendriks, and Ir. L.J.M.Houben.

K.G.S. Pawirotaroeno

Delft, 2016

# Summary

The main objective considers a situation with a prestressed concrete bridge with T-girders and in between a thin deck cast in-situ. The main girder of the system is loaded directly until failure in shear is reached. At a certain load point, the main beam is assumed to fall out, leaving only the slab to carry the load. It is questioned whether the slab is able to carry the load, and to which extent compressive membrane action in the slab plays a role in that occuring mechanism.

The first step is understanding compressive membrane action. It is a mechanism occurring in laterally restraint (un)reinforced and prestressed concrete, and increases the slab bending and punching capacity. Methods exist that calculate membrane action in concrete slabs. Certain conditions have to be met in order to use them. Of importance is the slenderness ratio that has to be met, and the considered span and slab have to meet certain criteria of their own as well.

Returning to the main situation, in the first method, the bridge system is presented as a disconnected system of key elements: main beam, slab, and neighbor beams. For each, the capacity can be calculated. For the main beam it is the shear capacity (tensile splitting or flexural shear, depending on factors such as load location and the amount of shear reinforcement). For the slab the three considered methods (CAN, UK, RK) are used to determine the bending capacity with arching.

The load determined for the girder capacity only is considered a lower bound limit for the total load of the bridge system. For the upper bound limit a higher bridge load is possible. When the critical deflection condition--the relative girder deflection exceeding the slab midspan deflection--is met, the slab bending capacity can be added to the girder capacity. In this case, girder and slab are assumed to work together.

The second method determines the linear load distribution with a numerical plate model with the T-girders modelled as ribs. The numerical model determines the relative girder displacement and compares it with the slab midspan displacement also determined numerically. With this, a part of the span can be determined that is activated when the main girder reaches its maximum deflection. And once the activated span is known the deck capacity can be determined, summating the capacities (determined with one of the three methods) of the slab strips, with a pre-determined effective width, dividing the total activated area.

The load-displacement behavior of the slab itself is important. To understand the whole system, the slab ductility needs to be known, the deflection at its peak lead and the ultimate deflection. More research on laterally restraint slabs is done to gain more insight into this. It shows that when the lateral restraint is high enough, capacities can be reached, about four to six times higher than for simply supported slabs. Moreover, the slab seems to show higher deflections when failing in bending, compared to punching.

Which is favorable for when loading the girder directly, since bending is assumed to be the governing failure mechanism.

The bridge 'De Vecht' was tested with two different test load locations: 4 and 2.25 m from the end. The material and geometrical parameters were taken into account, and used for a numerical plate model and the calculation of the slab and girder capacity.

For the calculation of the total bridge load, the numerical model is combined with assumed deflections derived from the research done on the laterally restraint slabs. Furthermore, the linear load distribution limits the redistribution possibility.

Afterwards, the test results were compared with the calculations. The calculations overall show to be a safe underestimate of the reality. This holds for the calculated bearing capacity of the whole bridge system and the slab bending capacity.

The assumed failure mechanism bending for the slab seemed to be correct, since punching did not occur, meaning that more capacity of the slab due to arching was activated, and the slab deflected more than usual for slabs failing in punching.

However, the assumed deflections deviated from the actual ones, this probably was due to the used research, which only took into account a certain slenderness ratio deviating from the one from 'De Vecht'.

The test results and numerical model showed that multiple girders take part in carrying the load, which is also shown in the deflections of the girders. From the total of fifteen considered beams of a field, five or seven girders are activated. This is caused by the unique situation of 'De Vecht', with four crossbeams and a short c.t.c distance between girders. The crossbeam probably behaved so stiff that it, as it is loaded and as it deflects, activated more girders.

Finally, it was the question whether compressive membrane action was present in 'De Vecht' bridge. Analytically, the slab meets all the criteria to assume it was. However, numerically it is uncertain whether this is the case. The relative displacements were too low, even with a seven-girder model, meaning it is uncertain whether cracking occurs in the slab. And this cracking is essential in order to determine if compressive membrane action develops in the slab.

Ultimately, for the initial main problem of loading the bridge system, a set of methods, and solutions, and simple components are provided, for which various insights are given. The slab and girder seem to be the key to this complex situation, and they need to be investigated and modelled more in depth, since they showed nonlinear behavior in the test results, and this project only dealt with linear assumptions. Moreover, the slab seemed to be critical concerning the bearing capacity and ductility of the system as a whole. So more research needs to be done on laterally restraint slabs, with different concrete strengths and slenderness ratios, to determine the deflections, at peak load and failure.

# Contents

# Part 1 Objectives of the research on compressive membrane action

# Chapter 1 *Main Objective Thesis*

## Introduction

The first chapter discusses the main objective of this research on compressive membrane action. The subject, sub-objectives and an outline of the thesis are described too.

## Background

Rijkswaterstaat (RWS) is part of the Dutch Ministry of Infrastructure and Environment. The main functions of RWS are: design, construction, and maintenance of the infrastructural works of the Netherlands. A very important part of these infrastructural works are the widely considered concrete bridges. And especially the research on their residual strength is of concern for the main subject of this thesis.

In the Netherlands, there are about seventy prestressed concrete bridges designed between the sixties and seventies. These bridges are made of prefab prestressed concrete T-girders with in-situ concrete in between the girders to connect them (Figure 1). Because the deck slabs are transversely prestressed, they have a low reinforcement ratio, and the slenderness, the span/depth ratio, is very high.

Over time a lot has changed: traffic situations changed and extra lanes were implemented on top of the bridges. Back then the bridges were designed for lower traffic loads and the Dutch code has been altered as well. All leading to the question whether the bridges are still structurally safe. A large part of the research concerning the strength of these old bridges has been done at University of Technology Delft as requested by RWS.

A great deal of these bridges are being recalculated according to the current norms to ensure structural safety. Several recalculated bridges do not comply with the norms regarding the shear capacity. This is partly because the current code is stricter. The newer norms, changed traffic situations and higher traffic loads create the impression that there might be issues with the old concrete bridges regarding structural safety and durability.

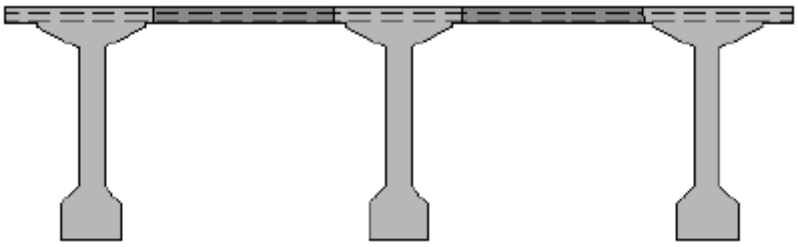

*Figure 1 In-site concrete cast in between girder*

A significant note: the current Dutch norms do *not* take into account the full theoretical capacity of concrete deck slabs. There is known to be an extra, hidden capacity left in the deck slab, due to the mechanism compressive membrane action (CMA). CMA increases the slab bending and punching shear capacity. The workings of CMA and its benefits, regarding the bearing capacity, is the focus of this thesis. CMA could provide residual capacity in concrete deck slabs of most bridges, which might be overlooked during recalculations.

CMA has been recognized by the engineering community and mentioned in past research. This is especially apparent in foreign codes of Canada, New Zealand and the UK. However CMA has yet to be included in the Dutch codes, even though a lot of research has been done at the University of Technology Delft. This is why it is the hope of the author that this project combined with the other past researches will provide a nudge in using CMA in the Dutch codes.

# Approach of the research on compressive membrane action

## Past research on compressive membrane action

Past research (Chapter 2 till 4) focuses on a situation where the traffic is modelled with a point load on the slab between girders. The slenderness was found to be an important factor (Figure 2 and Figure 3). The past research focuses mainly on directly loaded slabs.

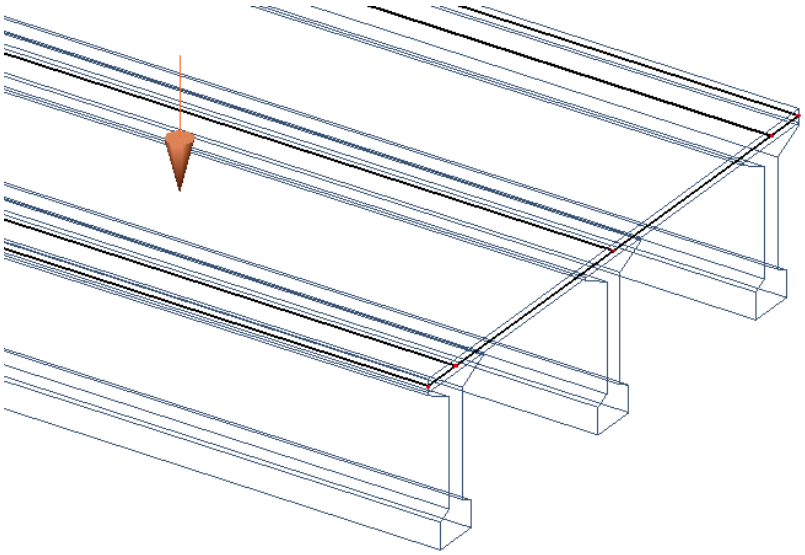

*Figure 2 isometric view of loading situation past research: slab loaded directly*

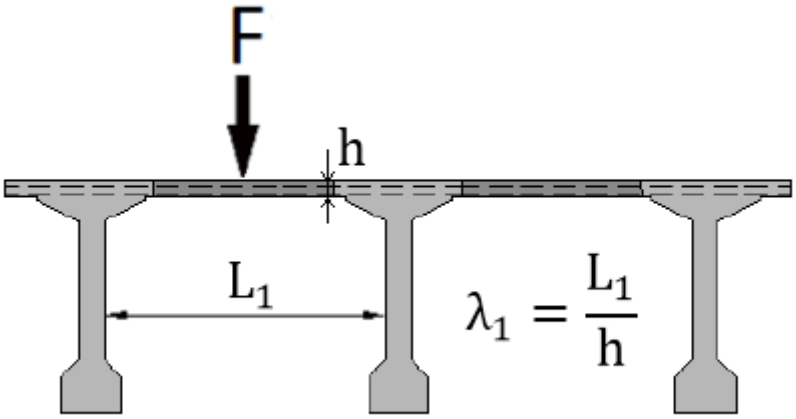


*Figure 3 front view of loading situation past research with certain slenderness*

Figure 4 enlarges the loaded slab and shows the development of membrane action for a laterally restraint situation (chapter 2). As the load increases, the slab wants to move outwards, but this movement is hindered by the restraints. And because of this restraint, in-plane compressive membrane forces (CMF) develop in the cracked slab. The compressive membrane forces result in a compressive arch that increases the slab moment bending and punching capacity, compared to past flexural theories (Figure 5).

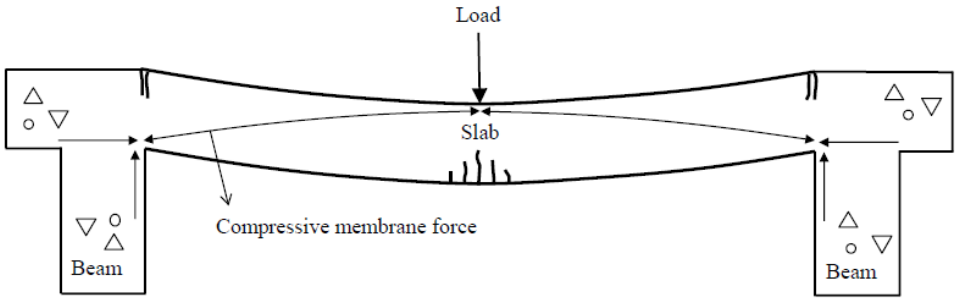


*Figure 4 activation of membrane action in a laterally restraint slab*

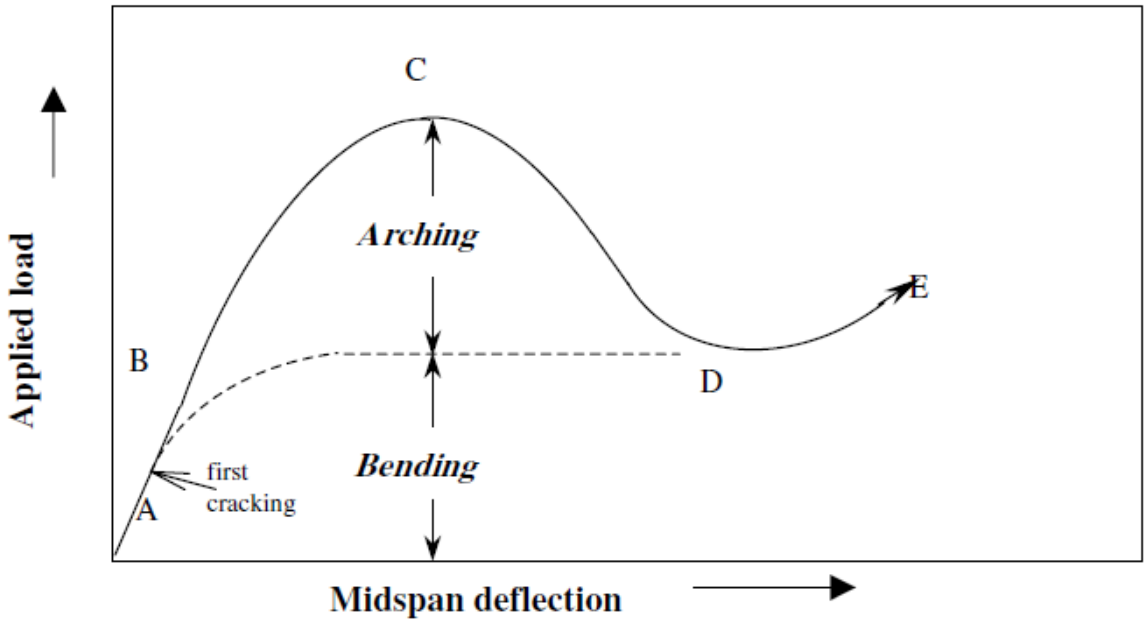


*Figure 5 increase of slab capacity with CMA compared to flexural theory*

**Focus of this research on compressive membrane action**

This research focuses on a similar situation, only with the load placed directly on a beam (Figure 6 and Figure 7). In this case, it is assumed that punching of the slab will not occur, since the beam is loaded directly. The higher bending with arching capacity is assumed to be governing.

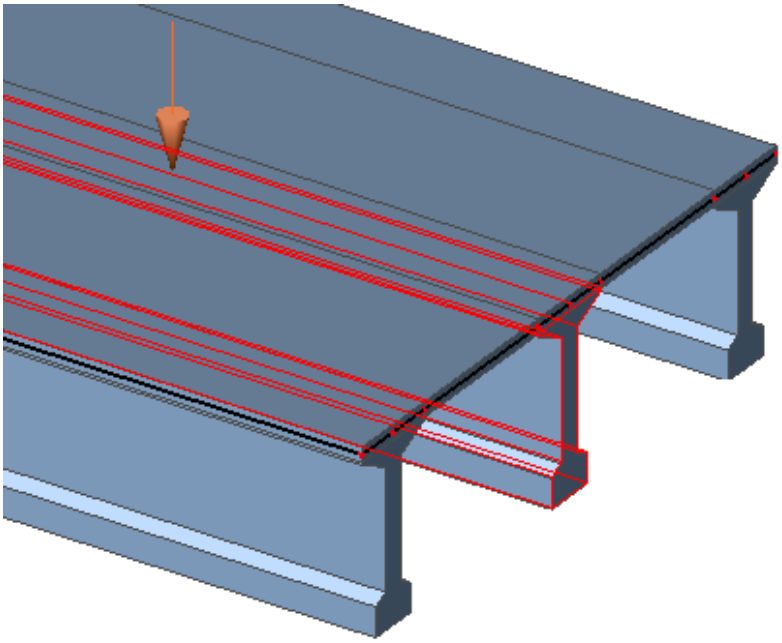

*Figure 6 isometric view loading situation of this research: beam load directly*

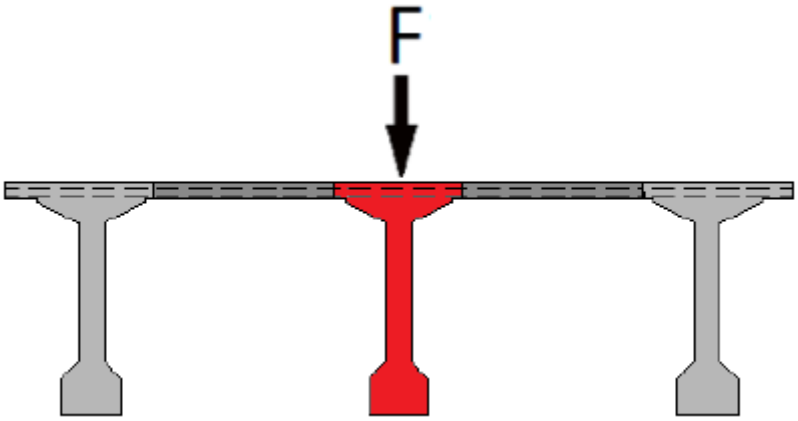


*Figure 7 front view loading situation*

It is assumed that at one point the loaded beam fails. When this occurs the loaded bridge system is assumed to change to a recognizable slab situation (Figure 8), similar to the past (chapter 5).

For this situation, the slab bending capacity with arching can be determined. It is questioned whether the load of the beam can be carried by the slab (Figure 9), if there is enough capacity to carry and redistribute to the neighbor beams (chapter 5). This redistribution is possible through membrane action.

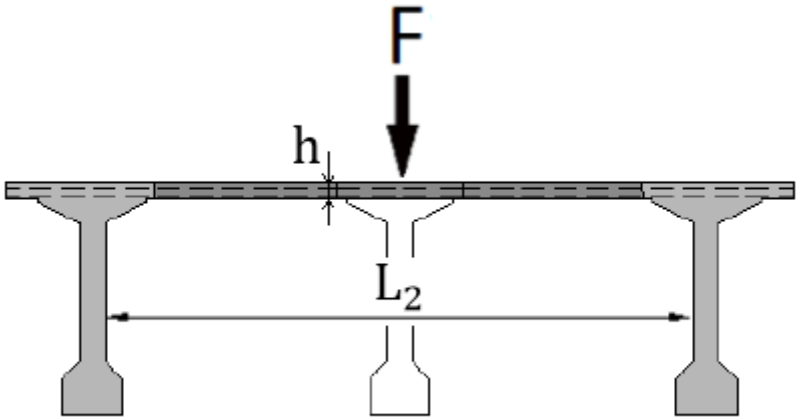


*Figure 8 slab situation with main beam not present*

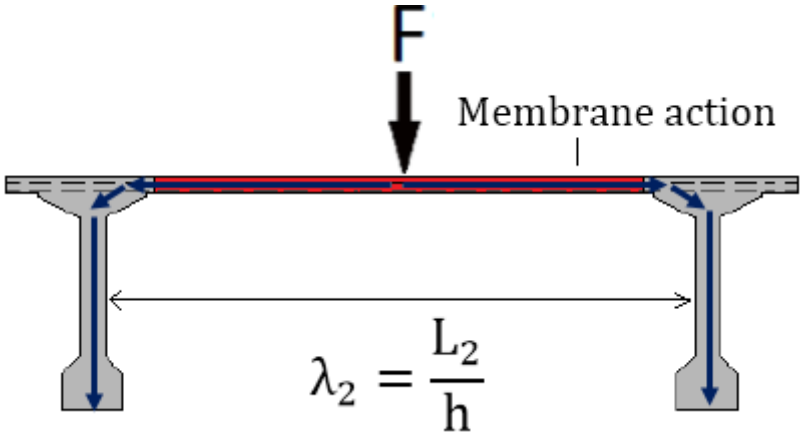


*Figure 9 redistribution of the loads*

### Considered load-displacement graphs for beam and slab

Two important components of this research is the behavior of the beam and slab. Figure 10 till Figure 13 give a rough sketch of their possible behaviors. The numbers are arbitrary and only to give an impression of the behavior, the size order of the displacement and load. In this research, the beam is assumed to have linear elastic behavior with brittle failure and bilinear plastic behavior (Chapter 5). For the slab only bilinear behavior is considered (Chapter 5). These behaviors are used throughout the research and will be discussed more in depth later.

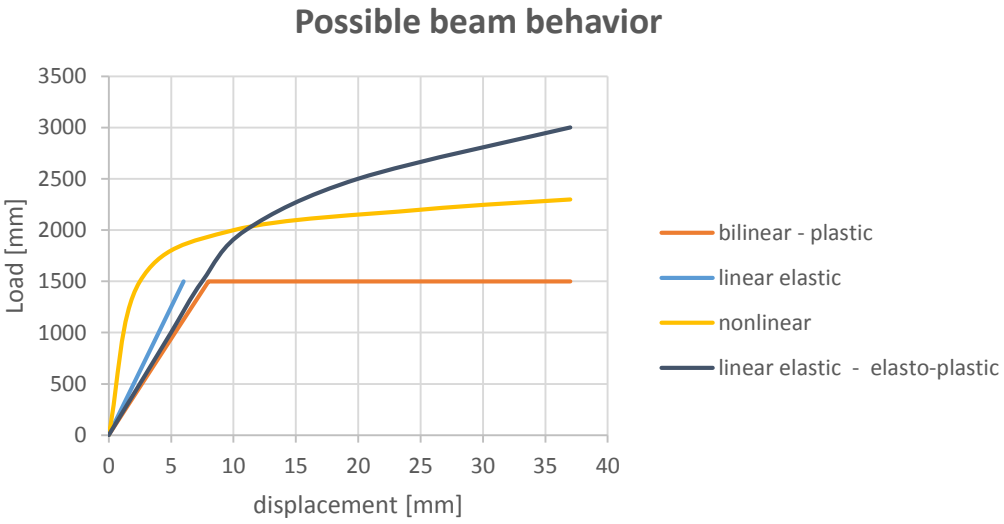


*Figure 10 possible beam behaviors*

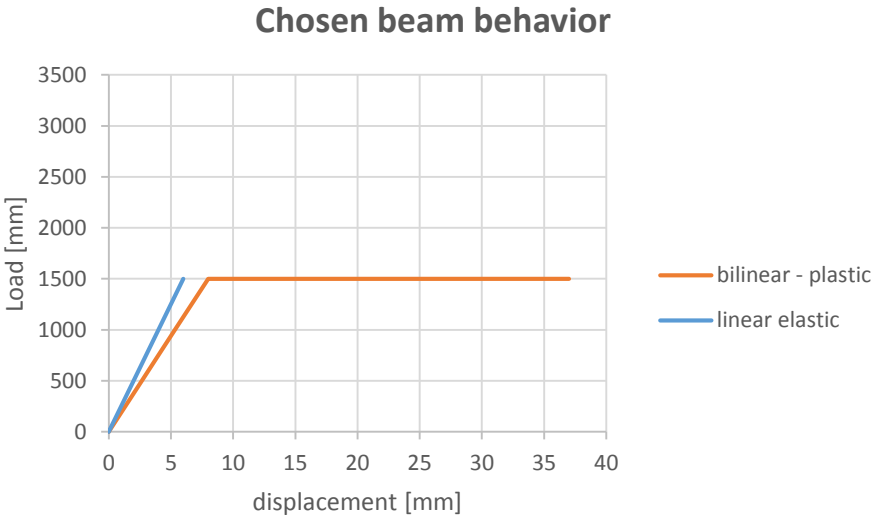


*Figure 11 chosen beam behavior*

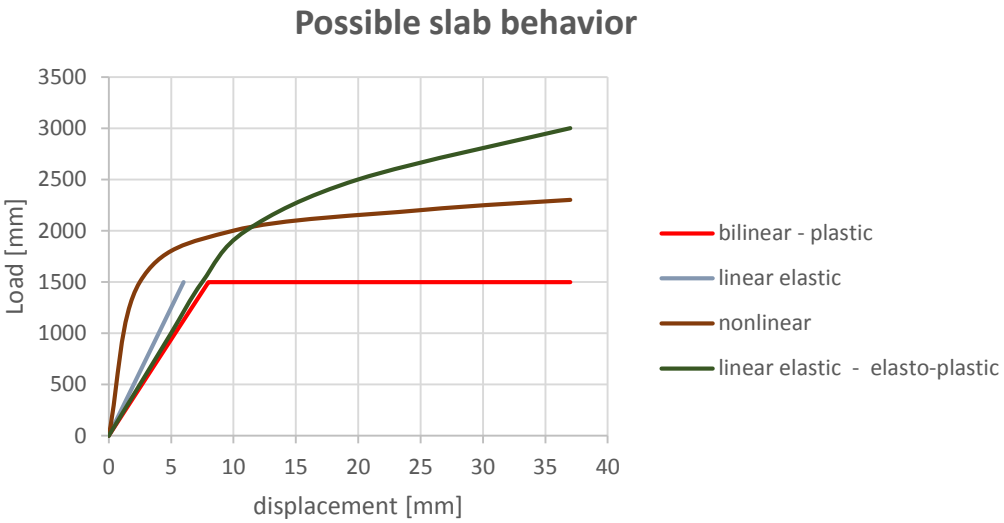


*Figure 12 possible slab behaviors*

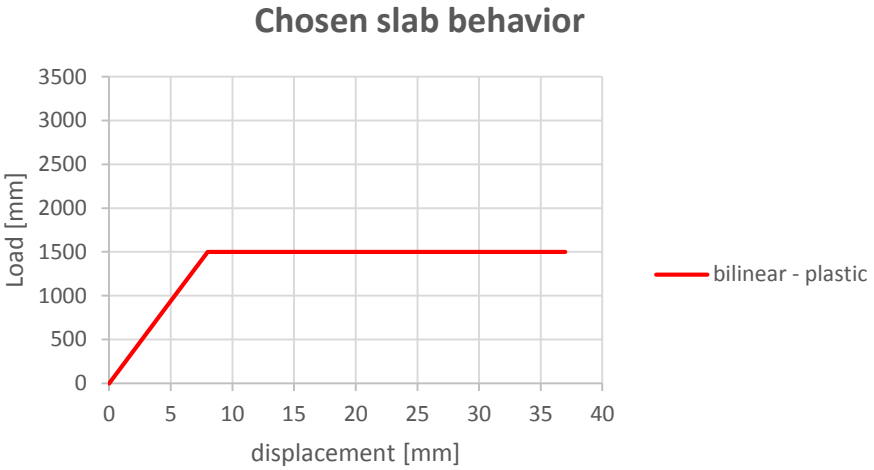


*Figure 13 chosen slab behavior*

## Main Objective Thesis

*Investigate to which extent compressive membrane action provides additional capacity during the loading of a T-beam integrated in a prestressed concrete deck slab.*

Former research has shown that a positive effect of compressive membrane action on the bearing capacity of a bridge system is present. This project uses this past research to understand the mechanism that occurs in the deck slab when one T-beam is loaded till failure. It is questioned whether a secondary load path occurs to the neighbor beam, through the slab when the T-beam is being loaded till failure.

If load redistribution takes place, the load will carried by the slab with the compressive membrane forces. Moreover, if the main beam and slab work together, their respective capacities can be added to create an upper bound value of the total bridge load. Ultimately, if membrane action is present, the slab helps the main beam in carrying the load to the neighbor beams, and their supports and foundation.

### Method One

Two methods are discussed to investigate the mechanism mentioned above. The first one disconnects the bridge system into two components: slab and main beam. This is done to understand the role of the components in the main problem.

In the first method three loading phases of the bridge system are studied. Phase one describes the main girder being loaded till its shear capacity. The girder capacity is used for scenario 1, the lower bound limit of the total bridge load.

Then Phase two begins, and this is the elasto-plastic phase. Compressive membrane action is assumed to be activated after first cracking, causing the load to be carried through the slab and to the neighbor beams. The main beam behaves plastically and carries the orginal load, while the slab carries the additional load through compressive membrane action. For scenario 2, the upper bound limit, a higher total bridge load is possible.

Finally, the load is distributed to the neighbor beams and then their supports and the foundation. The details of this methods is discussed more in depth in Chapter 5.

During the study of the role of membrane action and the hidden capacity that it provides, analytical methods are created for thin prestressed concrete deck slabs made of T-beams with in-situ cast concrete in between.

The calculative methods deal with the slab behavior when a T-beam fails and membrane action activates in the slab, describing the secondary load path that brings the load through the slab and neighbor beams to the supports. It is also investigated during which part of the loading the bridge system, membrane action activates. This can for example be in the linear phase of loading the girder or after. And after knowing when the membrane action activates, the activated part of the slab is determined, the part which provides the residual strength through membrane action. And the slab bending capacity is determined.

**Method Two**

The second method is based on numerical modelling. The second method follows from the first and they show a lot of similarities. However the second method uses different assumptions, and the numerical model is used heavily. And the second method actually takes into account the questions raised in the first method.

To determine the total slab capacity, the activated slab area has to be determined with use of the numerical model (Figure 14 and Figure 15).

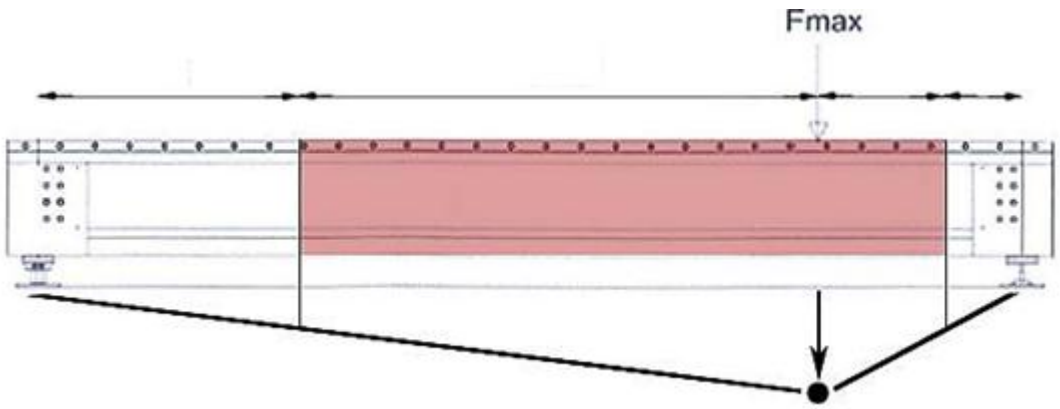


*Figure 14 activated part of the deck*

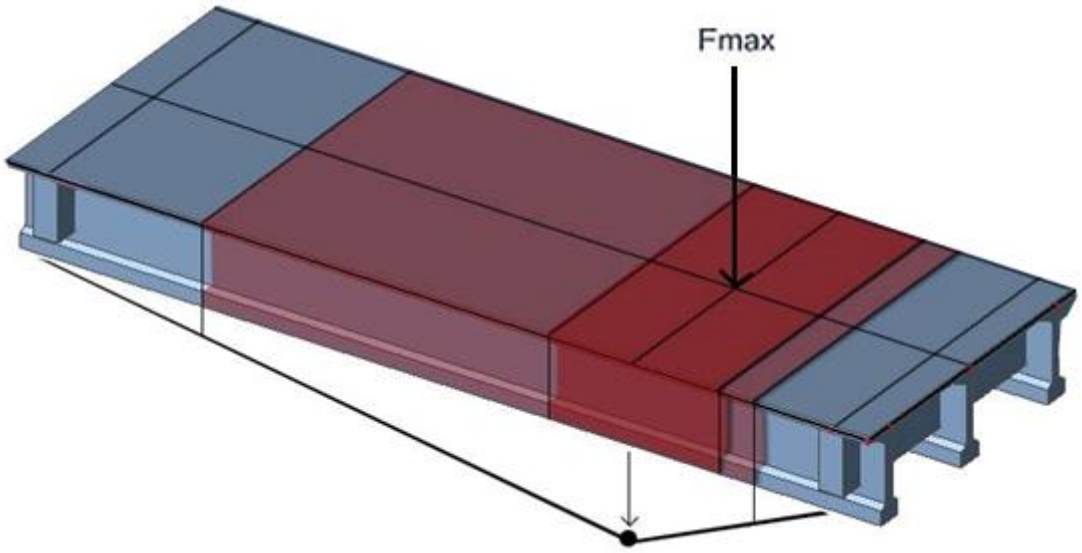


*Figure 15 activated slab area (details discussed more in depth in Chapter 5)*

After identifying the activated part, it is divided in laterally restraint concrete slab strips, with a certain effective width, and with a certain capacity, which is determined using calculative methods of past research. Finally, the total slab capacity is determined by summing up the capacities of individual slab strips.

The guidelines of the two methods provide practical tools, which can be used when facing a comparable situation and bridge. Ultimately, these tools are used on 'De Vecht' bridge to predict the total failure load with a range, bounded by an upper and lower value limit.

## Overall Research Objectives

The main objective loads a bridge system with a T-beam integrated in the slab. And to understand the main objective, it is broken down into smaller objectives that are considered during the research:

1. What is the total load of the bridge systems sketched in the main problem?

Discussed in part 2, chapter 5.

2. What roles do slab and beam have in the main problem?
    a. How do they behave?

Part 1 focuses on slab research and the failure mechanism in the main problem. In part 2 the beam behavior is discussed. Additional research on laterally restraint slabs is done in part 2, chapter 8.

    b. What are their respective capacities?

In part 1, chapter 3 discusses methods that calculate slab bending capacity with arching.
In part 2 the linear beam capacity is determined.

3. When do slab and beam work together and can their respective capacities summed?
    a. And does CMA activate?

Mentioned in chapter 2. It discusses when CMA is present in a slab. Chapter 3 discusses when enough restraint is present in a system and when one can calculate with CMA. Part 2, chapter 5 discusses the critical deflection condition.

4. How does linear load distribution influence the situation?

Discussed in part 2, chapter 5 till 7.

## Chapter Outline

The thesis is comprised of four parts. The first part deals with past research on compressive membrane action and how to calculate it.

Chapter 2 and 3 describe the mechanism and its presence in reinforced concrete deck slabs. Chapter 4 describes the assumptions and conditions for calculating with compressive membrane action in prestressed concrete. The 'Brienenoord' bridge and its prototype are used as examples.

Part 2 describes two methods to investigate the mechanism.

Chapter 5 gives the first method: disconnected bridge system. This simplifies the main problem and mechanism. It explains the secondary load path that occurs when a T-beam integrated in the bridge is loaded. Possible bridge failure scenarios are discussed, which occur during loading of the main beam, and the total slab capacity is calculated.

Chapter 6 discusses a numerical linear model to determine the slab deflections, using them as reference points for the second method discussed in Chapter 7. The load spreading is also determined. Chapter 8 deals with additional research on laterally restraint slabs and their deflections.

Part 3 discusses 'De Vecht' bridge in Muiden.

Chapter 9 describes the material and geometrical properties of the bridge, which is modelled using the information from part 1 and 2. And the capacity of the bridge, main beam and slab is estimated. Chapter 10 discusses the results of the tested bridge, and compares them with the determined calculations.

And ultimately in Part 4, it is discussed whether CMA activates in the slab of 'De Vecht' bridge, closing off with conclusions and recommendations.

# Chapter 2 *Introduction Compressive Membrane Action*

## Introduction

This chapter discusses the concept of compressive membrane action (CMA). This part discloses what kind of mechanism it is and gives a short chronology of relevant research done on the subject, which is used for the remainder of this thesis.

## Compressive membrane action

Every concrete deck slab has the potential for residual bearing capacity through compressive membrane action (CMA), if it is well restrained, laterally. Which gives the slab an extra, hidden capacity for moment- and punching shear capacity.

(Liebenberg, 1966) described compressive membrane action, and how and when it takes place. Compressive membrane action is a mechanism occurring in a laterally restrained, hardly able to displace laterally, concrete slab. As the vertical load increases, the deflection of the slab does also, causing the edges of the slab want to move to the outside. And this movement is hindered, and when the slab is hindered, compressive membrane action with in-plane compressive membrane forces (CMF) occur. The membrane action increases the slab's moment and punching shear capacity. Compressive membrane action is found in reinforced and unreinforced slabs. Later research such as (Amir, 2014) indicates its presence in prestressed concrete.

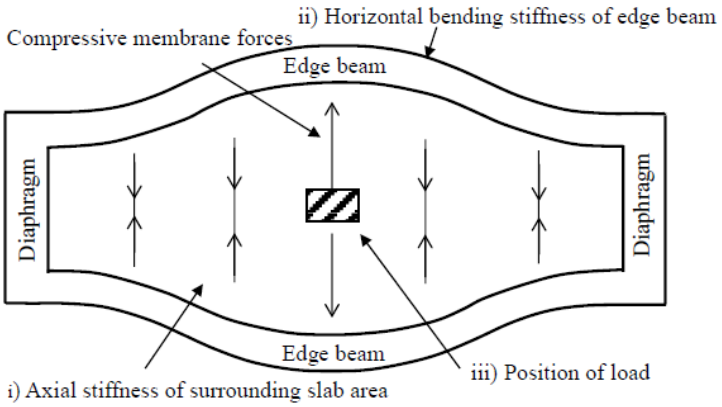


*Figure 16 Contributions to lateral restraint stiffness. (Hon, Taplin, & Al-Mahaidi, 2005)*

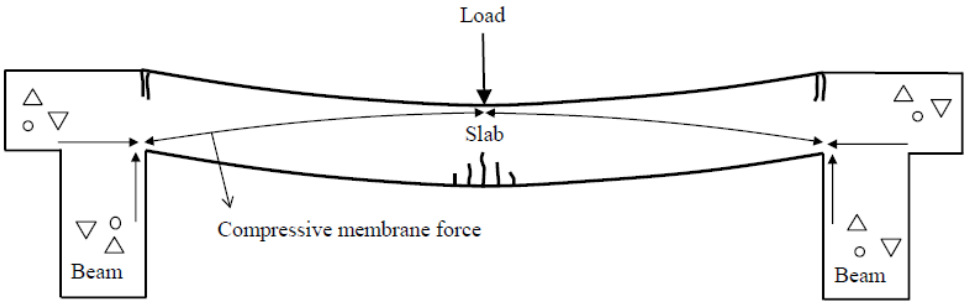


*Figure 17 CMA in a reinforced concrete bridge deck slab. (Hon, Taplin, & Al-Mahaidi, 2005)*

Taking a closer look at the restraints, (Hon, Taplin, & Al-Mahaidi, 2005) explained that the extent of compressive membrane action developed in a system depends on the level of horizontal translational restraint stiffness (Figure 16 and Figure 17), the effect of lateral restraint. This lateral restraint depends on:

- Axial stiffness of the surrounding slab area
- Horizontal bending stiffness of edge beams
- Position of the load regarding cross-beams. The restraint stiffness increases if the loaded area moves toward the ends of the specimen, closer to the end-beams.

Compressive membrane action can *only* develop after cracking occurs in a slab (shown at the bottom and top of the slab in Figure 17), and gives net in-plane forces at the slab boundaries. This phenomenon cannot occur in slabs with the same strength in tension and compression. Moreover the presence of reinforcement is not necessary ( (Amir, 2014) and (Taylor & Tharmarajah, 2014)).

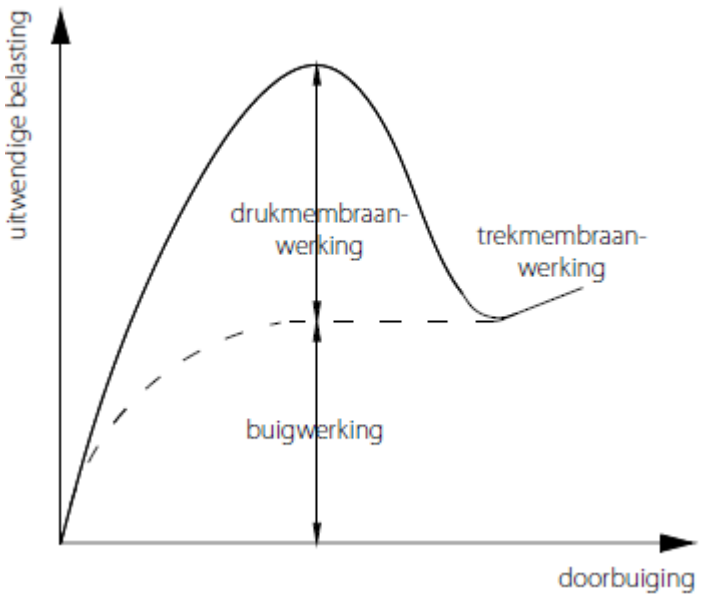


*Figure 18 typical load deflection curve showcasing CMA and flexural working (Van der Veen, Gijsbers, & de Boer, 2012)*

## Chronology of research on compressive membrane action

A lot of research has been done on the mechanism compressive membrane action in the past. It was first reported by (Ockleston, 1955) during tests on a three-storey building in South Africa. Subsequent research in bending strength area was done by (Wood, 1961) and (Park, 1964). Further research conducted at Queen's University, Canada, in the late sixties has led to compressive membrane action being incorporated in the current CHBDC, Canada Highway Bridge Design Code (CAN/CSA-S6-06, 2006) and the Transit Code (new zealand transport agency, 2014) Finally, research of CMA has been done in the UK Highway Agency standard (81/02, 2002). This method is simplified, as one assumes the concrete decks as rigidly restrained (Rankin & Long, 1997).

During test and experiments the moment and punching capacity was significantly higher due to membrane action. And the test slabs all failed in brittle punching failure. Meaning punching shear failure was decisive when the deck slab was loaded with a concentrated load in these experiments. This is due to fact that membrane action increases the moment capacity that much, causing it to be larger than the punching shear capacity. This will be noticed especially in Chapter 3.

# Chapter 3 *Calculative Methods On Determining Compressive Membrane Action*

## Introduction

Chapter 3 discusses methods that deal with compressive membrane action in reinforced concrete deck slabs only: the CHBDC ('Canadian Highway bridge design code'), the New Zealand's 'Transit Bridge manual', and the UK Highway agency BD 81/02. The first two foreign codes are comparable and apply the 'empirical method', while the second uses the 'simplified method'. Finally, the Rankin method is discussed, which is used in many researches regarding laterally restraint slab strips to calculate the bearing capacity.

## Canadian Highway Bridge Design Code and the 'Empirical method'

Canada has registered compressive membrane action in their code (CAN/CSA-S6-06, 2006). Moreover, the Transit Manual (new zealand transport agency, 2014) is similar to the CHBDC in certain relevant aspects. Similar graphs such as the one in Figure 141 are used in both codes to determine the allowable axle load.

Research done by (Dorton & Csagoly, 1977) functioned as the base for the CHBDC and studied the most important parameters with the largest influence on the effect of CMA:

- Slenderness $\lambda$ (span/depth ratio of the slab between the girders)
- Cylindrical Compressive concrete strength $f_c$
- Reinforcement ratio $\rho$ (plays a smaller part)

The experiments concern a reinforced concrete deck slab, which was modeled with scale 1:8. From the experiments one found that when the slab was loaded, the failure mechanism was always explosive and with no warning, in the form of brittle punching shear. Parameters such as load location and stresses due to sustained loading were not as significantly important regarding the total fail load compared to the stated ones above.

From the tests one concludes concrete slabs have a considerable amount of hidden strength left. This applies even for unreinforced deck slabs. Also slabs with reinforcements at mid-depth of the slab (isotropic) behaved similarly to slabs designed with top and bottom mesh reinforcement. Meaning that in traditional calculation methods, the concrete deck slabs are being underestimated regarding strength. In the Canadian research, fatigue was also considered, but was finally deemed not decisive.

In the British design code, to use the positive effect of membrane action in the design of a concrete bridge, a certain degree of restraint must be applicable to the bridge. The continuous concrete deck needs to be restrained laterally by the stiffness of the deck and transverse end beam. And an edge zone needs to be present, for example provided by reinforced edge beams. The effect of lateral restraint was stressed earlier in Chapter 2.

The total restraint effect is incorporated in an empirical restraint factor $\eta$ (Hewitt & Batchelor, 1975). In theory $\eta = 1$ means the slab is completely enclosed and fully restraint. And $\eta = 0$ means the slab is statically determined with free supports loaded under bending. In practice the restraint factor is usually somewhere in between (Table 1).

In accordance with the theory the restraint factor was determined for a number of bridge types:

- Steel girders with reinforced concrete deck, non-compositely
- Steel girders with reinforced concrete deck, compositely
- Reinforced concrete girders with reinforced concrete deck slab, compositely
- Prestressed prefab concrete girders with reinforced deck, compositely

From the test results a safe lower bound value $\eta = 0.5$ for type 2, 3 and 4 was determined. The restraint factor was determined with model lab experiments, where the compressive membrane forces was a function of the restraint factor.

Significant is the fourth type, prestressed girders with reinforced deck, showing two values higher than $\eta = 0.5$: $\eta = 0.66$ and $\eta = 1.0$ with an average of $\eta = 0.83$ (Table 1). Most of the factors are around 0.8 and many were 1.0 (Figure 19). And for the last three types almost all tests had a factor higher than 0.5, meaning most slabs are between fully enclosed and simply supported.

*Table 1 Restraint factors in tested bridge slabs. (Van der Veen, Gijsbers, & de Boer, 2012)*

| niet-composiete staalbetonligger | | composiete staalbetonligger | | betonnen balken en plaat | | voorgespannen ligger en betonnen plaat | |
|---|---|---|---|---|---|---|---|
| brug | $\eta$-waarde | brug | $\eta$-waarde | brug | $\eta$-waarde | brug | $\eta$-waarde |
| 1<br>2<br>3<br>4<br>5<br>6<br>7<br>8<br>9 | 0,23; 0,25<br>0,21; 0,33<br>0,31; 0,33<br>0,71<br>0,61; 0,63<br>0,24<br>0,34; 0,55<br>1,0<br>0,.21; 0,25 | 10<br>11<br>12<br>13<br>14<br>15<br>16<br>17<br>18 | 1,0<br>1,0; 1,0; 1,0<br>0,8; 1,0<br>0,75; 0,83; 1,0<br>0,96<br>0,75<br>1,0<br>0,98<br>0,94 | 19<br>20<br>21<br>22<br>23<br>24<br>25<br>26 | 1,0<br>0,48; 0,5; 0,71; 0,75<br>0,75; 0,75; 0,75<br>0,63; 0,75; 1,0<br>1,0<br>0,4<br>0,82; 1,0<br>1,0; 1,0 | 27<br>28 | 0,66<br>1,0 |
| gemiddelde $\eta$-waarde | 0,41 | | 0,93 | | 0,78 | | 0,83 |

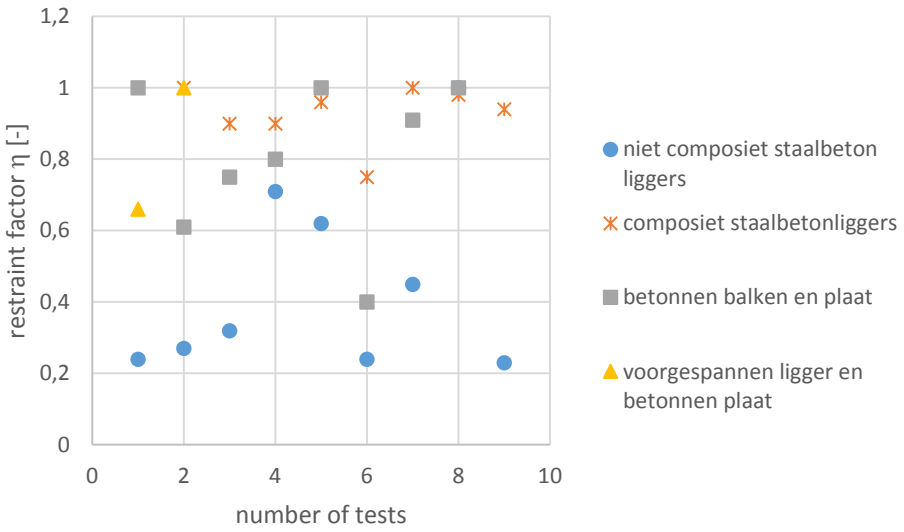


*Figure 19 restraint factors of test slabs from Table 1*

In order to calculate the bridge's capacity, according to (Dorton & Csagoly, 1977), using the safe lower bound restraint factor $\eta = 0.5$, certain conditions must be met:

- Minimum reinforcement ratio $\rho = 0.3\%$ in two directions, top and bottom, is advised.

- Concrete deck is part of a beam-deck system working together. (This is nearly always the case in the Netherlands.)

- Concrete deck, massive with a constant thickness of $h = 200\,mm$ Changed later in Transit Bridge manual to a minimum thickness of $h = 150\,mm$ (new zealand transport agency, 2014)

- The span of the slab between the girders $L_s \leq 3.7\,m$
  It is noted that in the tests CMA was activated until a girder c.t.c distance of 4.0 m. Later this condition changed to $L_s \leq 4.5\,m$ (new zealand transport agency, 2014)

For a concrete deck with haunches monolithically connected to the webs of girders, the span $L_s$ is defined as the distance between the midpoints of the haunches (new zealand transport agency, 2014).

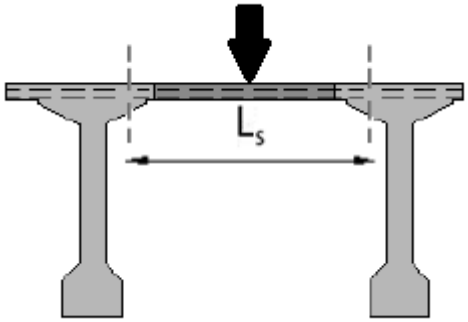


*Figure 20 definition span $L_s$ between haunches with loading location*

- The slenderness $\lambda = \frac{L_s}{h} \leq 15$
  CMA has been found with a slenderness of 20. And this is now the current demand (new zealand transport agency, 2014), and will be used later again in Chapter 4.

- The distance between cross girders not larger than 24.0 m

- Distance between the reinforcement bars not larger than 300 mm

- The edge stiffness for the concrete deck slab should be provided with a system consisting of:

  - Extra reinforcement in the deck or
  - A reinforcement edge beam (usually the case in the Netherlands) or
  - A reinforcement thickening (edge zone) of the concrete deck

If all the conditions above are met, then enough lateral restraint is available to guarantee a restraint factor $\eta = 0.5$. Generally the Dutch bridges comply with these conditions, but there are exceptions. When this is the case, compressive membrane action may be taken in to account, if the necessary restraint factor can be validated. It is also possible that the criteria of slenderness or span length is not met. This fact will be of importance later in the modelling phase in Part 2.

The method described in the Transit Manual and the Canadian HBD code is often called the 'Empirical method' because of its base in test results and experiments on bridges where membrane action occurred. The allowable axle load is:

$$P_{axle} = \frac{\frac{\phi * 0.6 * R_i}{\gamma_L * 40 * I} * 8200}{100} \quad [\text{kN}] \tag{1}$$

$\phi$ = variable strength reduction factor = $\phi_d * 1 = 0.5$ (assumed low cracking)
$\gamma_L$ = partial load factor for normal loading = 1.9
$I$ = 1.0 (impactfactor)

Factors taking into account dynamic effects have already been taken into account in the characteristic values of the vertical load. Shown in table 4.2 (NEN-EN 1991-2, 2005).

The value for $R_i$ can be determined by using Figure 141 in Appendix A, $R_d$, $F_q$, $F_c$ and using the formula:

$$R_i = R_d * F_q * F_c \quad [\text{kN}] \tag{2}$$

$F_c$ and $F_q$ are correction factors for concrete strength and reinforcement ratio respectively. $R_d$ is determined with Figure 141 for a certain deck thickness. The factor $F_c$ is determined for concrete strengths between 20 and 40 MPa, outside that range, one needs to extrapolate, leading to less accurate results. This is significant when dealing with Dutch bridges, as 'De Vecht,' that usually apply a concrete strength higher than 40 MPa.

$$q = 50 * \left(\frac{A_{sl}}{b * d_l} + \frac{A_{st}}{b * d_t}\right) \tag{3}$$

$$0.2\% \leq q \leq 1\%$$

$A_{sl}$ = longitudinal bottom steel areas
$A_{st}$ = transverse bottom steel areas
$b$ = width
$d_l$ = longitudinal effective depth of the deck slab
$d_t$ = transverse effective depth of the deck slab

The total axle load in Equation (1) is given in kg and converted to kN with factor 100. Furthermore in Equation (1) the reduction factor $\phi$ depends on the properties of the deck slab. It tells if the slab is in good condition, cracked or severely cracked (Table 23, Appendix A). The code is for a load surface area of 250*250 mm.

## UK code and the 'Simplified method'

### Background

The background of this code is also experimental. (Kirkpatrick, Long, & Thompson, 1982) performed tests with a scale of 1:3. The results contain information about deck slabs with a centrically placed reinforcement (at 0.5*d) only. Some comparisons can be made with prestressed concrete deck slabs where a continuous centrically placed prestress runs through the slab and connects the in-situ concrete with the T-girders.

Also (Taylor, Rankin, & D.J., 2001) found that when lateral restraint was provided, the slabs could be efficiently reinforced with the bars located centrally due to the benefits of arching action, and it avoided the need for two reinforcement layers, when looking at the bearing capacity. However top and bottom reinforcement seem to have merit, since it influences the slab's ductility in a positive manner.

The UK code deals with reinforced concrete only and assumes a fully restrained slab with a factor $\eta = 1$. This simplifies the expressions that calculate the influence of compressive membrane action very much.

When a slab is fully restrained, the effect of the reinforcement on the failure load will be small (Van der Veen & Gijsbers, 2014). The effect of laterally restraining slabs and inducing compressive membrane forces, is so significant that fully restrained unreinforced concrete slabs show a higher capacity than statically determined *reinforced* concrete slabs with free supports.

It seems an underestimation of the slab strength is apparent. This gives the conclusion that compressive membrane action and its effect is usually governing for the slab bearing capacity. And the influence of the traditional bending capacity on the total capacity is less significant.

**Perfect plastic behaviour**

When a perfect plastic material is present, the maximum arch capacity according to (Christiansen, 1963) gives:

$$M_{ar} = 0.85 * f_c' * \left(\frac{h}{2}\right)^2 = \ 0.21 * f_c' * h^2 \quad (4)$$

$f_c'$ = cylindrical compressive concrete strength
$h$ = thickness slab

It is assumed that the internal lever arm is equal to half of the height of the slab (Equation (4)). This applies *only* for perfect plastic material, since it reduces in concrete which deforms.

**Elastic plastic behaviour**

(Rankin G. , 1982) established a relation between maximum arch capacity and slenderness of a slab for an ideally elastic-plastic concrete behavior. (McDowell, McKee, & Sevin, 1956), and then derived the deformation in relation to the bearing capacity used in the UK method. With this a new arching capacity $M_{ar}$ is calculated.

$$R = \varepsilon_c * \frac{{L_r}^2}{h^2} \ [-] \quad (5)$$

$L_s$ = span of slab
$L_r = 0.5 * L_s$
$h$ = slab thickness
$0 < R < 0.26$

The considered span $L_s$ is defined as the clear span for slabs monolithically connected with beams, according to BD (81/02, 2002). Noted that the UK method defines the span differently than the 'empirical method'.

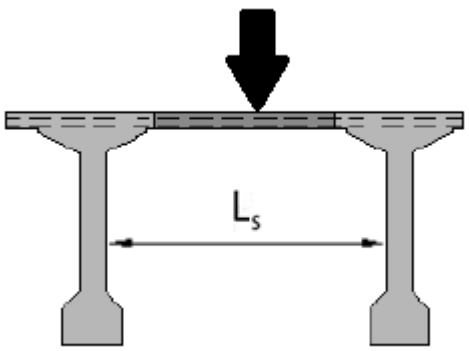


*Figure 21 span $L_s$ defined as the clear span between girders*

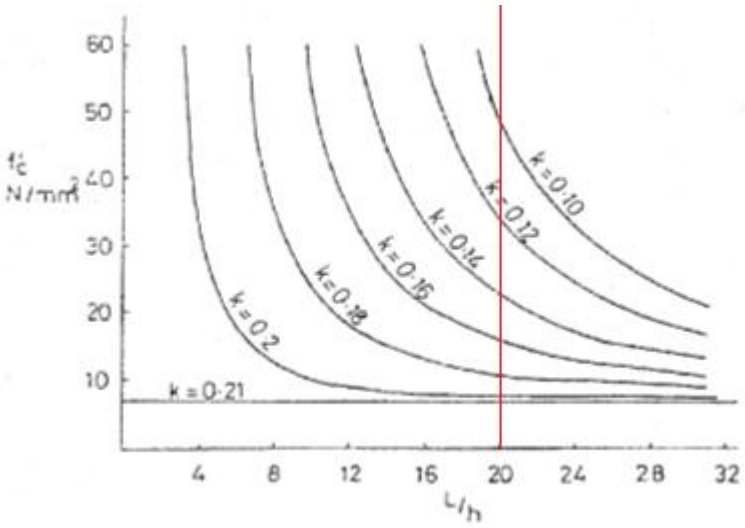


*Figure 22 k-values for maximum arching moments (Kirkpatrick, Long, & Thompson, 1982). The red line indicates the earlier defined maximum slenderness of* $\lambda = 20$

$$\varepsilon_c = (-400 + 60 * f_c' - 0.33 * f_c') * 10^{-6} \quad [-] \tag{6}$$

Figure 22 shows that concrete strengths up till 60 MPa can be used for the 'simplified method.'

Finally, the theoretical maximum arching capacity through compressive membrane action is given again:

$$M_{ar} = k * f_c' * h^2 \ \text{[kNm/m]} \tag{7}$$

$$\begin{aligned} k &= \frac{0.21}{4} * M_r \\ M_r &= 4.3 - 16.1 * \sqrt{3.3 * 10^{-4} + 0.1243 * R}\ ) \ [-] \\ M_r &= 4 \text{ for rigid plastic behavior} \end{aligned} \tag{8}$$

The relations above apply for concrete with elasto-plastic behavior. In Equation (8) the k-factor acts as a reduction factor and reduces the maximum arching capacity of a perfect plastic situation for an elasto-plastic situation. When $M_r = 4$ the relation returns to the original one. Once the moment capacity is known, the moment [kNm/m] can be converted to a comparable force [kN] using Figure 23, in this specific situation:

$$P_b = \frac{M_{ar}}{0.23}\ [kN] \text{ (restrained at both sides)} \tag{9}$$

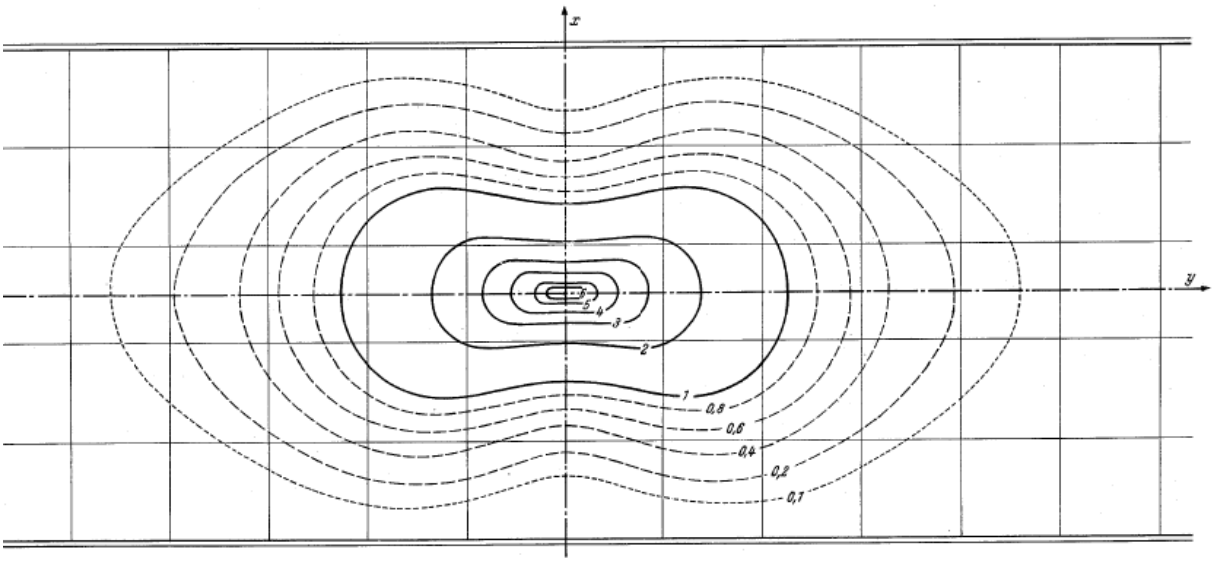


*Figure 23 influence surfaces for a plate with two restrained edges (Pucher, 1964)*

As mentioned before concrete deck slabs usually fail in brittle punching shear. This is shown in experiments. The reason why is that the bending capacity increases considerably more than the punching shear capacity due to occurring arching action ( (Hewitt & Batchelor, 1975), (McDowell, McKee, & Sevin, 1956)).

Which means usually punching shear failure is governing. To calculate the punching capacity a formula is derived by (Long, 1975). Where a circular shape load is used instead of a square load of a wheel print, which is converted with use of an equivalent punching diameter $\phi$. A circular shaped load surface is assumed to have a 15% higher shear capacity because it is assumed free of stress concentrations.

$$P_p = 1.52 * (\phi + d) * d * \sqrt{f_c'} * (100 * \rho_e)^{0.25} \quad [\text{kN}] \tag{10}$$

$\phi$ = equivalent punching diameter
$d$ = average effective height tensile reinforcement
$f_c'$ = cyllindrical compressive concrete strength

The reinforcement ratio in Equation (10) is an equivalent reinforcement ratio $\rho_e$:

$$\rho_e = \frac{k * f_c' * h^2}{f_{ye} * d * z} \tag{11}$$

$z$ = internal leverarm = $0.75 * d$
$f_{ye}$ = 320 MPa

The internal lever arm $z$ is assumed as 75% of the effective depth, common for heavily reinforced concrete cross sections with a fully restrained concrete slab (Van der Veen & Gijsbers, 2014).

In the test results of BD (81/02, 2002) the reinforcement yield stress was 320 MPa and remained constant. When dealing with a concrete deck where only a centrical prestress is placed as the main reinforcement, the effective depth $d$ is taken up till the center of the centrical prestress. An example is given in Chapter 4.

**Punching shear**

Punching shear is also called *two-way shear*, and is generally a *brittle punching* failure (Figure 24) with no warning in advance; where some warning is shown, the case is classified as *flexural* punching. Flexural punching was observed in some cases when the transverse prestressing level was too low or when the single loads were applied above a duct at midspan (Amir, 2014). Flexural punching gives a ductile load-deflection behavior, which is more desired than the behavior for brittle punching. Also for (Hwang, 2010), the level of prestressing influences the mode of failure, with low prestressing levels giving *flexural punching* as the failure mode.

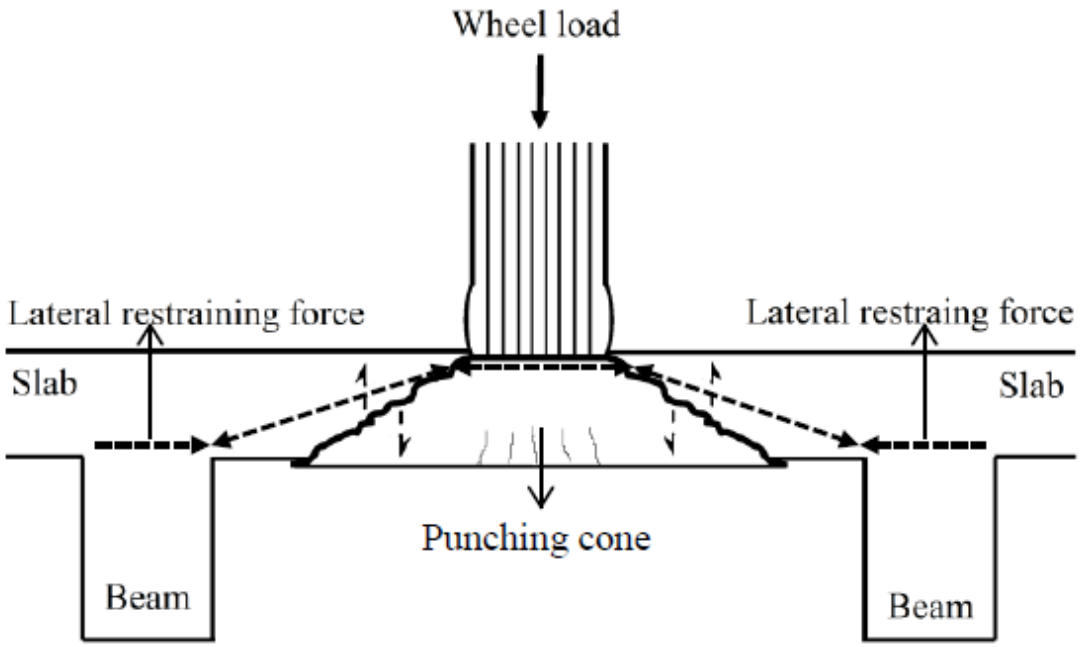


*Figure 24 brittle punching shear in lateral restrain slabs (Kirkpatrick, Long, & Thompson, 1982)*

**Side notes and summary**

First, according to the test results the amount of available bending reinforcement has no influence on the punching capacity of the concrete slab. Since the CMA is more decisive in delivering the strength. Second, the increase in bending capacity is given by the equivalent reinforcement ratio. Moreover, the critical cross section is placed at d/2 from the perimeter (Figure 25) of the loaded surface (contrary to (NEN-EN 1992-1-1, 2005) where the distance is 2d) (81/02, 2002).

The UK method described here and the calculated arching capacity lean heavily on the parameters concrete strength $f_c'$ and the slenderness, span/depth ratio. Which were mentioned in Chapter 2 as important factors for the bearing capacity.

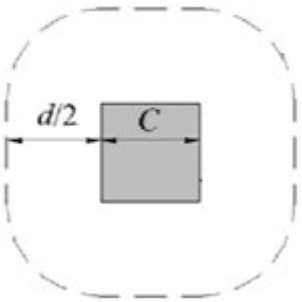


*Figure 25 loaded critical perimeter*

## Rankin method

### Background

The UK method in BD (81/02, 2002) calculates an arching capacity $M_{ar}$. Which is based on theory described by (Rankin & Long, 1997). Here Rankin determines the capacity of laterally restrained *concrete slab strips,* which in turn is essential to determine the total deck capacity. This method splits the arching and bending action components.

### Effective width

Taylor devised a method to estimate the effective width of an activated slab strip (Figure 27). This method takes into account the loading area and range which is loaded. The previously discussed methods make no mention of an effective width.

$$b_{eff} = c_y + 2 * L_e + 2 * h \tag{12}$$

$c_y$ = length of load area in y − direction
$L_e$ = effective span of the slab subjected to arching force
$L_e = \frac{L_s}{2} - \frac{c_x}{2}$
$c_x$ = length of load area in x − direction
$L_s$ = clear span of considered slab

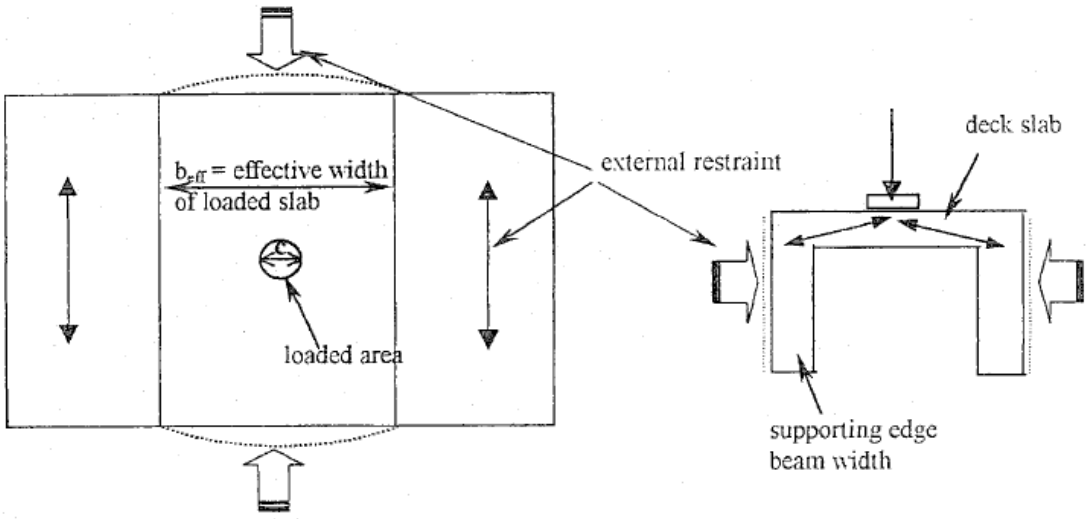


*Figure 26 Restraint model (Taylor, Rankin, & Cleland, 2002)*

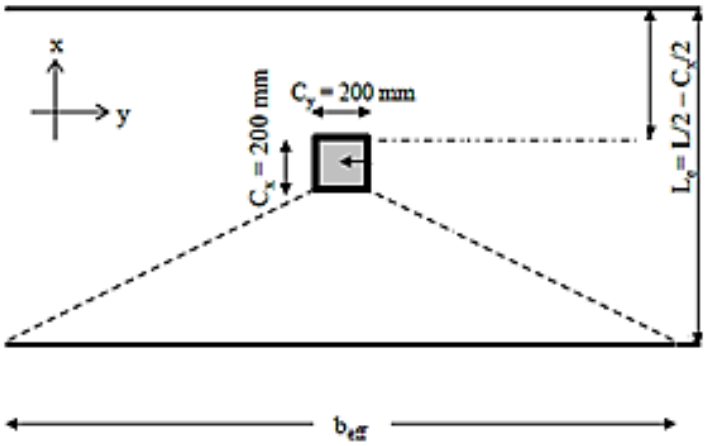


*Figure 27 Calculation for effective width (Taylor, Rankin, & Cleland, 2002)*

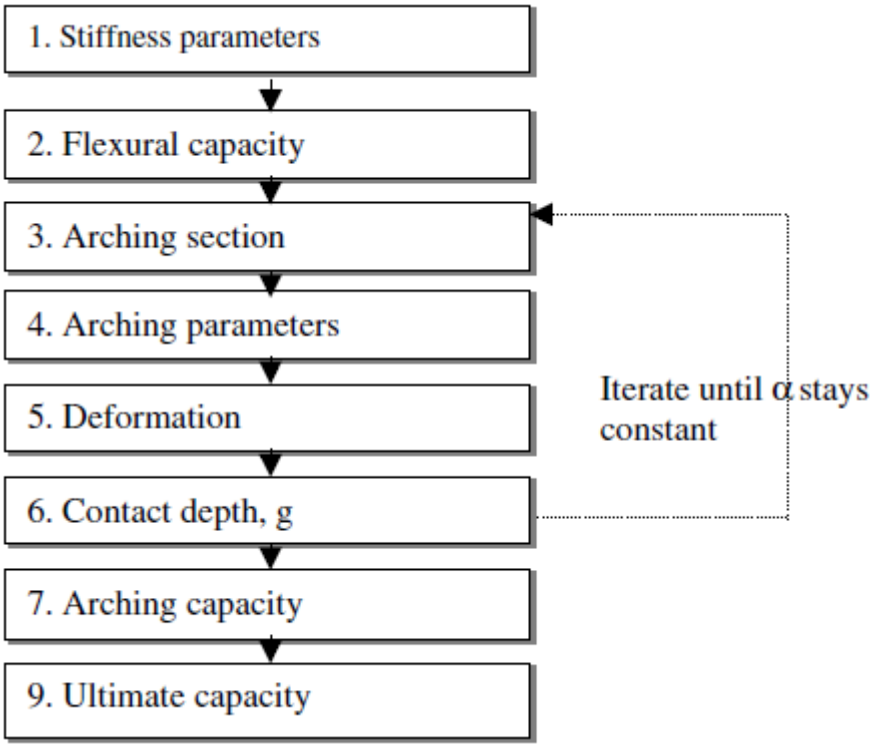


*Figure 28 flow diagram for calculating ultimate capacity of laterally restraint slabs (Taylor & Mullin, 2006)*

A procedure for assessing the strength of laterally restrained slabs is followed. It is outlined by the flow diagram (Taylor & Mullin, 2006) in Figure 28. Some of the expressions or parameters might seem familiar, since the UK method is influenced by Rankin.

The method uses a model restraint system (Figure 26) where the supporting edge beams, end diaphragms and surrounding area of unloaded slab are equated to a spring of an equivalent stiffness (Taylor, Rankin, & Cleland, 2002).

**Stiffness parameters**

The value for the elastic modulus is based on (Hognestad, Hanson, & McHenry, 1955), and has given good estimations for the measured elastic modulus in experiments (Taylor, Rankin, & D.J., 2001).

$$E_c = 4.23 * f_{cu}^{0.5} \tag{13}$$

$$K_s = \frac{E_c * b_{eff} * h}{L_e} \tag{14}$$

The area outside the effective width acts parallel to the end diaphragms in resisting the outward arching thrust. The areas are cumulative and can be summed to give a total area $A_d$. Which consists of the total area diaphragms and the slab area outside of the effective width.

$$K_d = \sum \frac{A_d * E_c}{L_e} \tag{15}$$

$$K_b = \frac{A_b * E_c}{L_e} \tag{16}$$

$$A_b = \frac{\zeta * I_b * L_e}{b_{eff}} \tag{17}$$

$\zeta = 114.5$ (SS)
$\zeta = 985$ (FE)
$\zeta = 550$ (SS/FE)

SS stands for simply supported, FE for fixed ended, and for most bridges $\zeta$ is somewhere in between those two. A comparison can be made with BD (81/02, 2002), where a restraint factor $\eta = 0$ means the bridge can be considered simply supported (SS). For restraint factor $\eta = 1$ the bridge can be considered fixed ended (FE). So SS/FE with $\zeta = 550$ corresponds with the factor of about $\eta = 0.5$.

Stiffness of the edge beams act in parallel to the end diaphragms as opposed to additionally. Which accumulate to an overall lesser restraint than each component given by:

$$K_r = \frac{1}{(\frac{1}{K_b} + \frac{1}{K_d})} \tag{18}$$

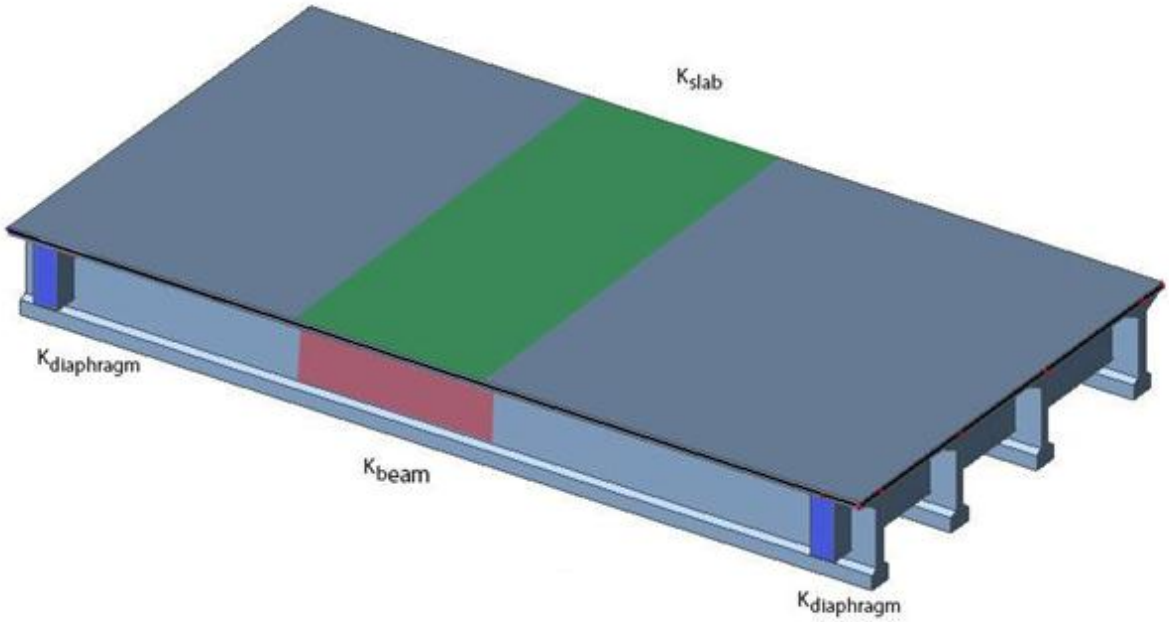


*Figure 29 Stiffness parameters of bridge*

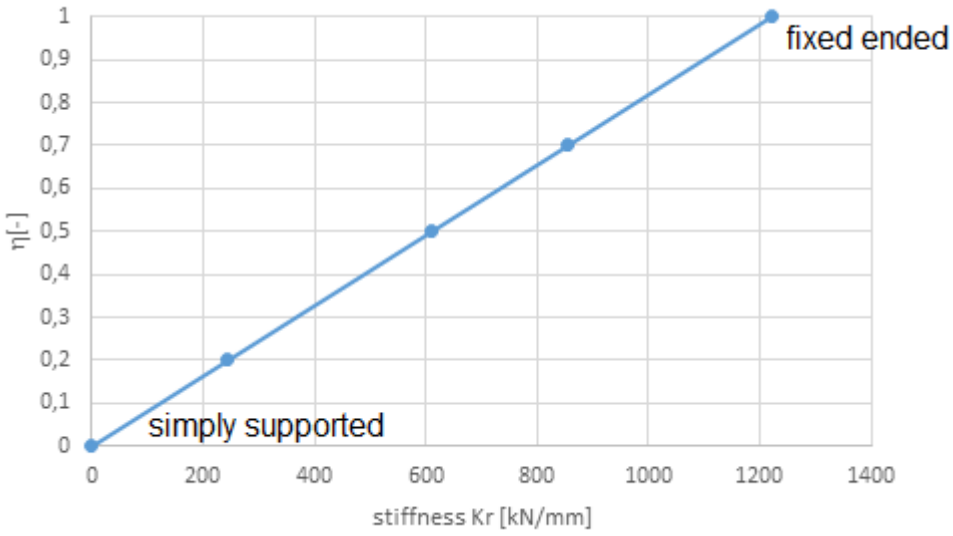


*Figure 30 stiffness vs restraint factor*

An in-plane stiffness $K_r$ of 855 kN/mm is equivalent to 70% of the rigid restraint stiffness described by ( (Rankin & Long, 1997) and (Taylor, Rankin, & D.J., 2001)). This becomes important when calculating the stiffness parameters of slabs. A slab's lateral restraint can be determined:

$$For\ K_r = 855\frac{kN}{mm}, 70\%\ of\ rigid\ restraint, meaning\ \eta = 0.7$$

This gives:

$$K_r = \frac{855}{70} * 100 = 1221\frac{kN}{mm}, 100\%\ rigid\ restraint, with\ \boldsymbol{\eta = 1.0}\ (\text{(Figure 30)})$$

This means that for a stiffness of at least $K_r$ 1221 kN/mm means the slab can be considered rigidly restraint, equivalent to restraint factor $\eta = 1.0$ (Figure 30).

**Flexural Capacity**

This capacity is determined using the standard flexural theory but with a modified stress block which accounts for high stress concrete, between 35 and 115 MPa ( (Taylor, Rankin, & D.J., 2001)).

**Flexural parameters**

Depth of stress block

$$\beta = 1 - 0.003 * f_{cd} < 0.9 \tag{19}$$

Depth of neutral axis

$$x = \frac{f_y * A_s}{0.67 * f_{cd} * \beta * b_{eff}} \tag{20}$$

Lever arm

$$z = d - 0.5 * \beta * x \tag{21}$$

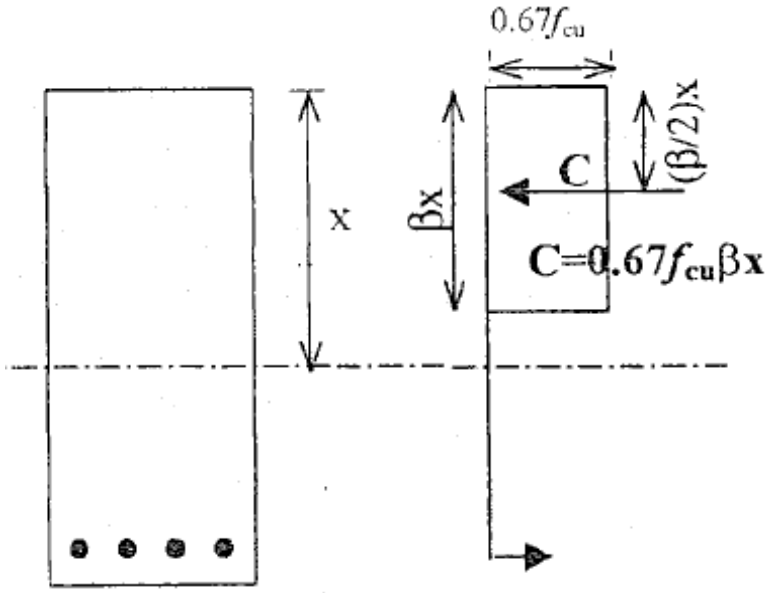


*Figure 31 proposed stress block Rankin method for normal reinforced concrete (Taylor, Rankin, & Cleland, 2002)*

Flexural moment capacity

$$M_b = f_y * A_s * z \tag{22}$$

Load capacity attributed to flexure

$$P_b = k_b * M_b \tag{23}$$

**Arching section**

The arching section can be described as the depth available for arching and depends upon the depth of the compression zone due to flexure. Depth available for arching:

$$2 * d_1 = h - 2 * x * \beta \tag{24}$$

$d_1$ from the previous iteration is used. The contact area due to arching is then given by:

$$A = \alpha * b_{eff} * d_1$$
$$\alpha = 1 \text{ for the first iteration} \tag{25}$$

Rankin uses a three-hinged analogy (Figure 32) and takes into account the less than rigid restraint an "equivalent" rigidly restrained arch length $L_R$ is used:

$$L_R = L_e \sqrt[3]{\left(\frac{E * A}{K * L_e}\right) + 1} \tag{26}$$

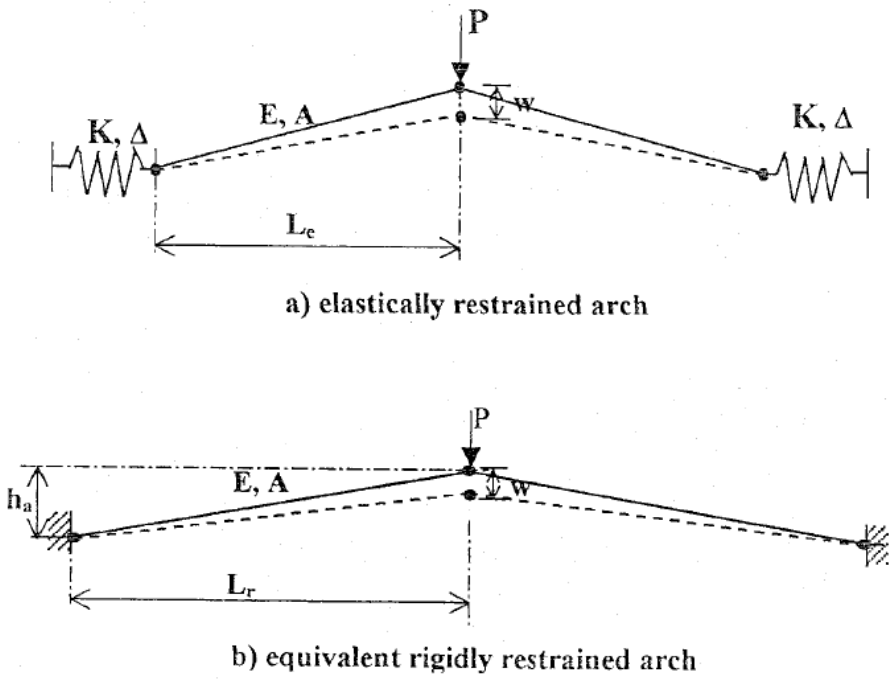


*Figure 32 analogy of three-hinged arch (Rankin G. , 1982)*

### Arching parameters

The theory uses an idealized elasto-plastic concrete with concrete ultimate and plastic strains, given as:

$$\varepsilon_u = 0.0043 - [(f_{cd} - 60) * 2.5 * 10^{-5}] < 0.0043$$
$$\varepsilon_c = 2 * \varepsilon_u * (1 - \beta) \tag{27}$$

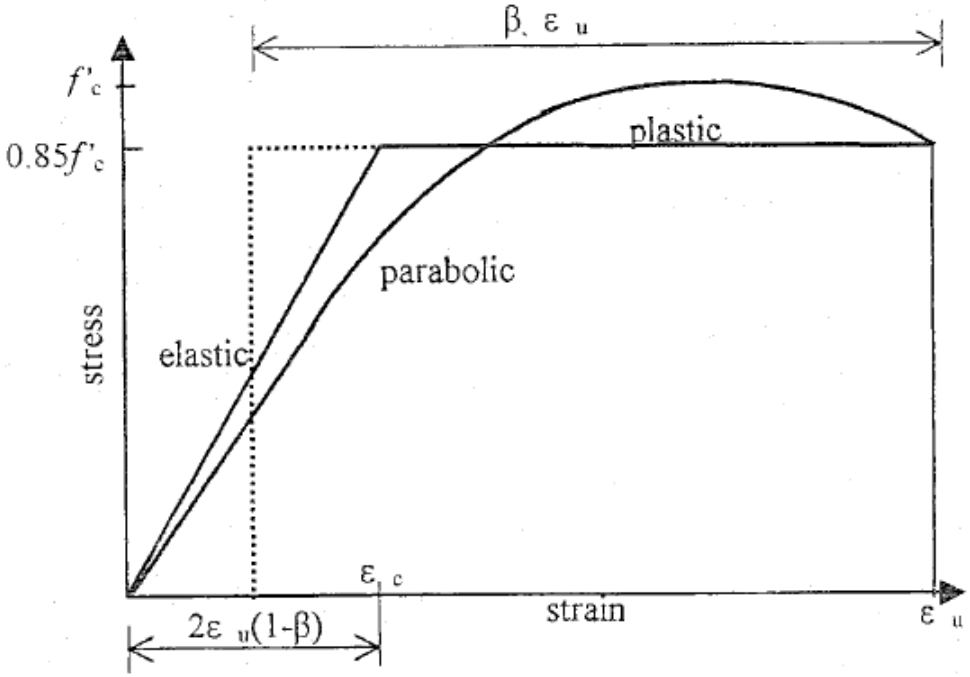


*Figure 33 elastic plastic strain relationship (Taylor, Rankin, & Cleland, 2002)*

**Deformation**

The similarity between material properties of masonry and concrete provided a justifiable base for Rankin's extension of McDowell's theory to restrained reinforced concrete slab strips. He described the lateral thrust and arching moments in terms of two non-dimensional parameters, $R$, a measure of the elastic deformation and, $u$, a non-dimensional measure of the deflection of the slab strip ( (Taylor & Mulin, 2005)).

$$R = \frac{\varepsilon_c * {L_r}^2}{4 * d_1^2} \ [-] \tag{28}$$

$$0 < R < 0.26;\ u = -0.15 + 0.36 * \sqrt{0.18 + 5.6 * R} \tag{29}$$

$$R > 0.26;\ u = 0.31 \text{ (constant)} \tag{30}$$

**Contact Depth**

$$\alpha = 1 - \frac{u}{2} \tag{31}$$

$\alpha * d_1$ is used for refined arching section above until value remains constant (iterative process).

**Arching Capacity**

$$0 < R < 0.26;\ M_r = \ 4.3 - 16.1 * \sqrt{3.3 * 10^{-4} + 0.1243 * R}\ )\ [-] \tag{32}$$

$$R > 0.26;\ M_r = \frac{0.3615}{R}\ [-] \tag{33}$$

$$M_{ar} = 0.168 * b_{eff} * f_c' * d_1^2 * M_r * \frac{L_e}{L_r}\ [kNm/m] \tag{34}$$

Maximum arching for $L_e = L_r$

Then converting the moment to a load:

$$P_a = M_{ar} * k_a \tag{35}$$

$k_a$ and $k_b$ in Equation (35) and Equation (23) differ for different slab restraints, for example when both sides are restrained (Pucher, 1964) gives:

$$P_a = \frac{M_{ar}}{0.23}$$

**Flexural punching capacity**

The ultimate capacity is the sum of the flexural and arching capacity:

$$P_{pf} = P_b + P_a \tag{36}$$

However it is possible that punching shear is governing, with the critical perimeter located at 0.5d from the face of the loaded area (Figure 25):

$$P_{pv} = \frac{0.43}{r_f} * \sqrt{f_{cd}} * (\phi + d)\pi * d * (\rho_e)^{0.25}$$
$$r_f = 1.0 \text{ (circular wheel load)} \tag{37}$$
$$r_f = 1.15 \text{ (rectangular wheel load)}$$

**Ultimate capacity**

It needs to be checked whether: $P_{pf} > P_{pv}$ or $P_{pf} < P_{pv}$

Meaning whether the flexural shear capacity exceeds the punching shear capacity or not. Usually punching shear is governing, then: $P_u = P_{pv}$

## Summary

First, the methods differ in the conditions that must be met, in order to use their respective methods. Table 2 shows an overview of the differences in conditions. These experimental conditions are very important to consider in order to take compressive membrane action into account. The further one goes away from the theory and results from the experiments, the harder it is to know if membrane action is present in the deck. Which is shown in the second part when the extra total deck capacity is determined with the numerical model.

Second, each method determines the bearing capacity according to their own assumptions and conditions. But generally the span/depth ratio, concrete strength, deck thickness, and lateral restraint are four significant factors to consider when determining the bearing capacity of a slab. Of the three methods, the CAN method is applicable with a certain accuracy between concrete strengths 20 and 40 MPa, and the other two methods can be used for higher strength concretes.

The simplified method is one of the quickest to use. It mainly depends on the slenderness, span/depth ratio, and the concrete strength. The empirical method does not calculate a flexural shear capacity, compared to the other two. And the Rankin method takes into account a lot of different factors, modeling the surrounding bridge as a spring system to determine the stiffness, and it also mentions an effective width for single slab strips to calculate with, which the other methods do not.

Finally, all the methods calculate a punching capacity. But the UK and Rankin method calculate a bending capacity, and the CAN method does not. It is important to keep these two failure modes in mind when dealing with other cases of slab failure discussed later.

*Table 2 certain differences in stated conditions of the foreign codes*

| | CHBDC (CAN) | BD 81/02 (UK) | Rankin method |
|---|---|---|---|
| **Span** | Distance between midpoints of haunches: $L_s < 4.5\ m$ | Defined as clear span: $L_s < 3.7\ m$ | N/A |
| **Slenderness** | $\lambda < 20$ | $\lambda < 15$ | N/A |
| **Concrete strength** | 20-40 MPa | 10-60 MPa | 35-115 MPa |

# Chapter 4 *Compressive Membrane Action In Prestressed Concrete*

## Introduction

Previous studies on compressive membrane action was for reinforced concrete only, so chapter 4 deals with research concerning compressive membrane action, its role and application in prestressed concrete.

It is assumed that the methods described in Chapter 3 can be applied to prestressed concrete as well. Prestressed concrete generally meets the aforementioned criteria in order for compressive membrane action to be present in the slab: low reinforcement ratio (which is favorable for cracking, and consequently CMA), sufficient lateral restraint (Chapter 3 discussed research where restraint factor was around $\eta = 0.8$), and cross and edge beams are present.

## Background

The previously discussed methods are for reinforced concrete deck slabs only. And it is expected that transverse prestressing will not only improve the bearing capacity, but also compensate for the high slenderness ratio, making thinner deck slabs possible with no problems of serviceability and structural safety (Amir, 2014). The use of prestressing is economical and improves durability as slab deformations and cracking are reduced.

A linear correlation exists between the punching load and the transverse prestressing level (Figure 34), a conclusion which is also drawn in (Amir, 2014). The higher the transverse prestressing level is, the higher the punching load. The cracking load varied between 23% to 38% of the failure load and increases with the transverse prestressing level (TPL). This further showed that transverse prestressing acts as an effective crack controller.

However subtracting the initial prestress from the overall in-plane force corresponding to that particular TPL gives a constant value of the compressive membrane force ($CMF \approx 370\ N/mm$ for the example of (Amir, 2014)). This shows that compressive membrane action is *independent* of the transverse prestress level.

This implies that for a particular deck slab having a certain lateral stiffness, the compressive membrane action developed remains constant if all other parameters (e.g. concrete strength, type of loading) remain the same. A certain level of *default* compressive membrane force is developed in the plane of the deck slab due to the built-in restraint available in the form of edge supports (girders), diaphragms and surrounding slab area (Amir, 2014).

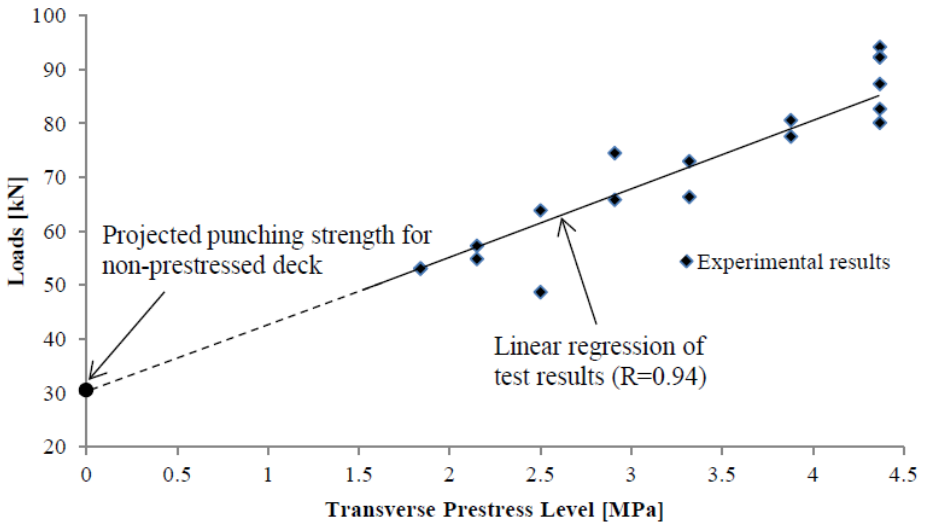


*Figure 34 Relationship between TPL and ultimate punching load He et al. (1992)*

This agrees well with the concept of compressive membrane action given in literature that the level of the compressive membrane action depends on the level of the external restraint available. And this is further proven numerically, showing the relationship between the transverse prestressing and the in-plane force (sum of the transverse prestressing force and the compressive membrane force) developed in the bridge deck.

It can be concluded that a linear relationship exists between the punching shear capacity and the in-plane forces arising from the transverse prestressing and compressive membrane action, where the prestressing is an external action, and compressive membrane force is an inherent, internal structural property (Amir, 2014).

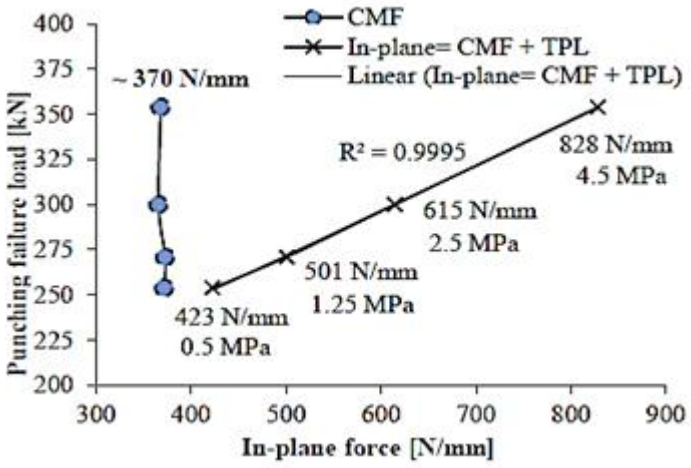


*Figure 35 independence of CMA to transverse prestress level.*

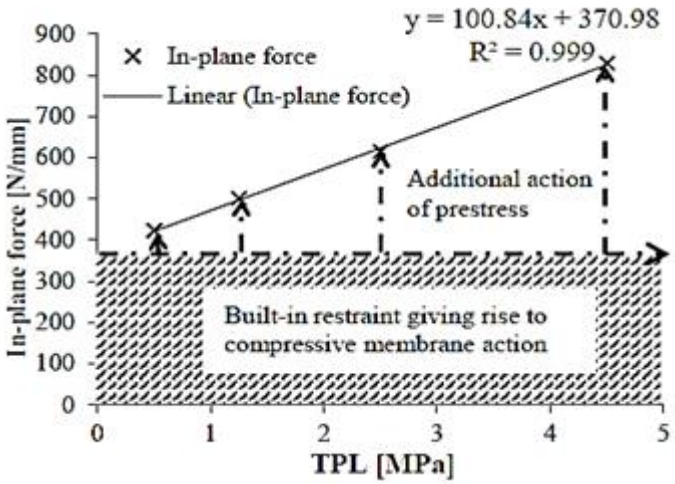


*Figure 36 Built-in restraint, and compressive membrane forces (CMF) in the deck slab (Amir, 2014)*

## Calculation Brienenoord bridge

The discussed calculation methods are used on the approach bridge of the 'Brienenoord' bridge and its prototype. First, the 'empirical method' is considered, then the 'simplified method' and finally the Rankin method. Usually the methods are used for reinforced concrete only.

It is noted that the conditions that must be met to use the respective codes. The methods differ slightly, for example the conditions of the slenderness and length span differ, or the considered span differs.

### Empirical method (NZ/CAN)

Checking the prescribed conditions, according to (new zealand transport agency, 2014), to see if the 'empirical method' is applicable (Van der Veen & Gijsbers, 2014):

- Continuous end cross beams present cast between outer girders. Agreed.
- Slenderness (span to depth ratio): $\lambda = \frac{L_s}{h} = \frac{3210}{200} = 16.1 < 20$. Agreed.
  The old condition stated $\lambda < 15$ (Dorton & Csagoly, 1977). This condition would not be met.
- Concrete strength not lower than 20 MPa. C40/50 applied. Agreed.
- Slab span 3.21 m (Figure 37) < 4.5 m. Agreed.
  The condition used to be $L_s \leq 3.7$ (Dorton & Csagoly, 1977). This condition is met as well.
- Minimal deck thickness $h \geq 150\,mm$. 200 mm is present. Agreed.
- There needs to be a minimum distance of 0.8 m at the edge. A guiding rail at 1.41 m from the edge is present, so the condition is met.

A local check is sufficient and all the conditions are met, so the method can be used. The rest of the calculation, as described in Chapter 3, is found in Appendix A.

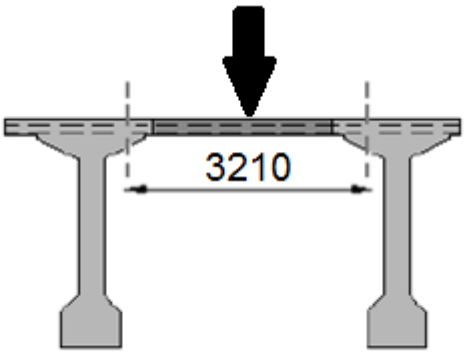


*Figure 37 considered span $L_s$ real live bridge Brienenoord for the CAN method (Van der Veen & Gijsbers, 2014)*

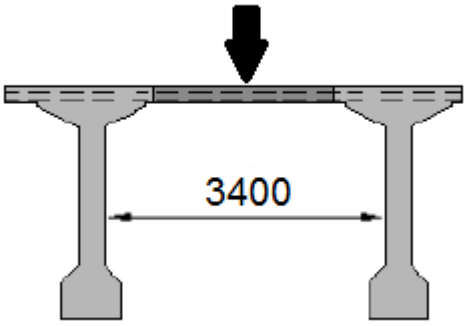


.

*Figure 38 span defined as the clear span UK and Rankin method*

**Simplified method (UK)**

Conditions to be met (Van der Veen & Gijsbers, 2014):

- Slab clear span 3.4 m (Figure 38) < 3.7m. Agreed.
- A small overhang of concrete of 1.0 m is present. Agreed.
- Slenderness: $\frac{3400}{200} = 17 > 15$. *Not agreed.*

  Compressive membrane action has been experimentally proven to be present for up to slenderness 20 though, shown in (Dorton & Csagoly, 1977).

- Continuous end cross beams present. Agreed.
- Edge beams integrally cast with deck. Agreed.

With exception of one, all the conditions are met again, which means the method can be used. And the rest of the calculation, as described in Chapter 3, is found in Appendix A.

### Rankin Method

For this method no specific conditions need to be met in order to use it or to justify a certain restraint (simply supported, or fixed ended). The stiffness of the slab and surrounding concrete, for example end beams, is calculated and represent the aforementioned restraint, as discussed in Chapter 3. Punching shear capacity was governing in this case, probably due to the high slenderness. The rest of the calculation is found in Appendix A.

The results of all the calculations are gathered and presented in Table 3. And the bending capacities (with full arching action through membrane action) are added in the last column for future reference. It is noted that for the Rankin method the bending capacity is almost four times larger than the punching capacity. And the UK method shows bending is governing, giving a lower capacity than punching.

### Summary

*Table 3 calculated results fail load with methods of foreign codes*

| Method | Punching Capacity [kN] | Bending Capacity [kN] |
|---|---|---|
| Empirical (NZ/CAN) | 369 | N/A |
| Simplified (UK) | 762 | 675 |
| Rankin | 501 | **1775** |

## Calculation Brienenoord Prototype

### Empirical method (NZ/CAN)

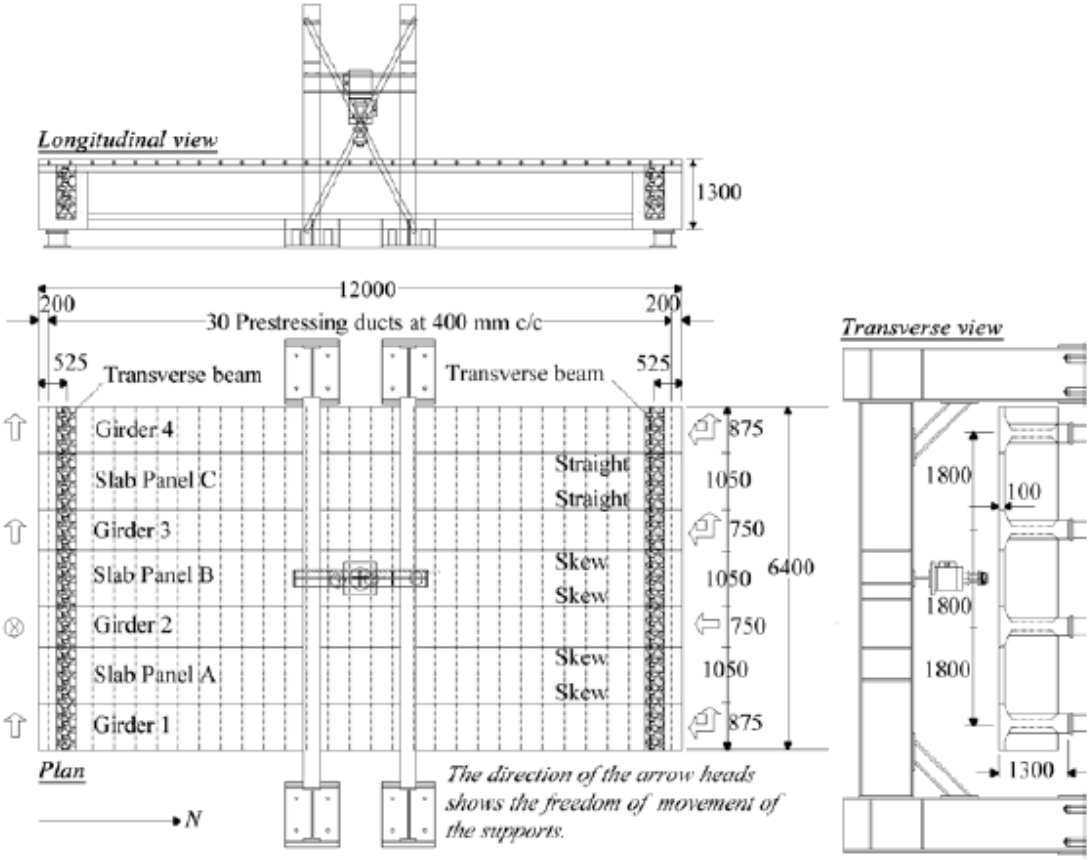


*Figure 39 overview of test setup and geometrical data of girders and slab (Stevin Report No. 25.5.13-06, 2013)*

In order to use the method certain conditions must be met (new zealand transport agency, 2014):

- End cross beam present. Agreed.
- End cross beams are continuously cast across the girders. Agreed
- The slenderness (span/depth ratio) must be smaller than 20:

$$\frac{L_s}{h} = \frac{L_{c.t.c} - 2 * d_{web} - 2 * 0.5 * d_{vout}}{h} = \frac{1800 - (2 * 75 - 2 * 240)}{100} = 11.7 < 20$$

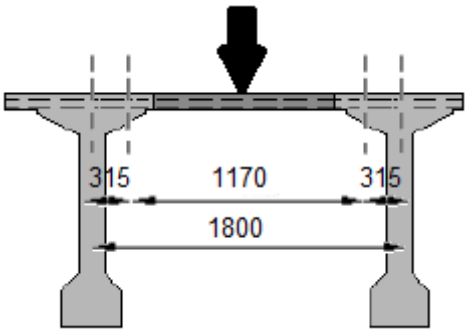


*Figure 40 defining span $L_s$ between the haunches*

- Compressive concrete strength not lower than 20 MPa. $f_c' = 38\,N/mm^2$. Check.
- Deck thickness not smaller than 150 mm. *Not agreed.*
  It is noted that the prototype deck thickness of 100 mm is smaller than the norm. It is assumed that the thin concrete slab has sufficient strength due to the transverse prestressing and the calculation will be done using the same method as before.
- Again a local check is done where dead load and other sustaining loads are neglected. It is difficult to assess combined effects of both local and global loads. Thereforee the two effects are mostly treated independently. In design and assessment of a beam-and-slab type bridge the local effects dominate (Taylor, Rankin, & Cleland, 2002).

The rest of the calculation is found in Appendix A.

### Simplified Method (UK)

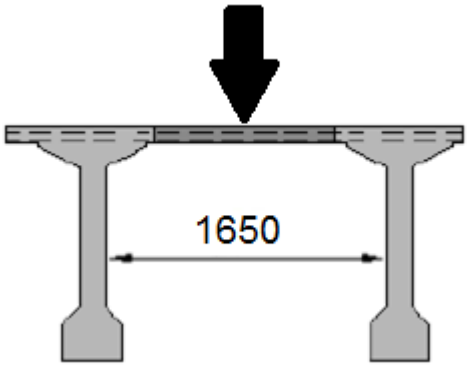


*Figure 41 clear span defined as* $L_s$

Concerning conditions:

- Slab span (Figure 41) 1.65 m < 3.7m. Agreed.
- A small overhang of concrete of 1.0 m is present. Agreed.
- Slenderness: $\frac{1650}{100} = 16.5 > 15$. *Not Agreed.*
  CMA has been proven to be present for up to slenderness 20 though.
- Continuous end cross beams present. Agreed.
- Edge beams integrally cast with deck. Agreed.

The rest of the calculation is found in Appendix A.

### Rankin Method

The same procedure is followed again as described in Chapter 3, and the full calculation is found in Appendix A, assuming a fixed ended (FE) slab.

## Conclusions of CMA in prestressed concrete

Table 6 shows tests done at midspan of a concrete slab, containing details about the total punching load capacity (Amir, 2014). Comparing the calculated punching load with the punching test results, with an average capacity of 333 kN--derived by averaging the four brittle punching with a transverse prestress level (TPL) of 2.5 MPa, indicated with red in Table 6--shows that the calculated values underestimate the actual punching load (Table 4).

The lowest value of Table 6 gives 257 kN, with a maximum capacity of 359 kN and an average capacity of 306 kN. Ultimately concluding that the discussed methods provide a safe but underestimated value for the failure load regarding punching shear capacity. Table 6 makes a distinction between the two possible failure modes brittle punching (indicated with red), and flexural punching/bending (indicated with blue).

The difference between the test and calculated capacity for the empirical method could be due to the fact that the method is not intended to be used for thin deck slabs below 150 mm, and 100 mm was applied. The simplified method, probably the quickest method to use, shows the best comparison with the test result. Rankin shows a severe underestimation for the punching capacity, as was shown for the real size bridge too.

*Table 4 comparing calculated punching capacity with tests results*

| Method | Calculated Punching Capacity $P_p$ [kN] | Average test Punching Capacity $P_t$ [kN] for TPL=2.5 MPa | Ratio $P_t/P_p$ [-] |
|---|---|---|---|
| Empirical(NZ)/(CAN) | 200 | 333 | 1.6 |
| Simplified (UK) | 268 | 333 | 1.2 |
| Rankin (F/E) | 140 | 333 | 2.3 |

*Table 5 comparing calculated bending capacity with test results*

| Method | Calculated Bending Capacity $P_p$ [kN] | Average Test Bending Capacity $P_t$ [kN] for TPL=1.25 MPa | Ratio $P_t/P_p$ [-] |
|---|---|---|---|
| Empirical(NZ)/(CAN) | N/A | N/A | N/A |
| Simplified (UK) | 328 | 341 | 1.04 |
| Rankin (F/E) | 320 | 341 | 1.07 |

The average failure load, 341 kN, for flexural punching (FP)--averaging the two flexural punching capacities for a TPL of 1.25 MPa, indicated with blue in Table 6--is used to compare the calculated bending capacity with (Table 5). The empirical method does not calculate the bending capacity. Both the UK and the Rankin method underestimate the actual capacity, where the bending capacity of the test is 1.04 times the calculated UK capacity. Here, too, the UK method shows a good comparison for the bending capacity with the test, and with a quick calculation, compared to the slower, more detailed Rankin method. One might expect the more nuanced method of Rankin to be more similar to the test results, seeing how it takes into account more parameters, but ultimately the most important factors, used in the UK method, are the concrete strength, the considered span, and the deck thickness.

Moreover, it is noted that the considered methods only take into account reinforced concrete slabs. The results derived from these methods were then compared with the tested prestressed concrete slabs. The results from this comparison could imply that the slabs are always an underestimation of the slab's strength, which is not always the case, since the prestressing was not taken into account. But if prestressing is taken into account, it can lead to higher calculated slab strengths, possibly higher than the ones from the test results.

Overall for punching, and bending, capacity, all three methods prove to be safe, and underestimate the slab's true capacity. With one important note, that the test capacities decrease as the TPL decreases too, so for example with a lower TPL of 1.25 MPa, lower slab capacities are found.

*Table 6 Fail load and deflections at midspan of deck slab, indicated in red and blue are the capacities used for Table 4 and Table 5 respectively*

| # | Test | Designation | TPL | $P_{CR,T}$ | $P_{CR0.1,T}$ (0.1 mm) | $S_T$ | $P_T$ | FMODE |
|---|---|---|---|---|---|---|---|---|
| | | | [MPa] | [kN] | [kN] | [mm] | [kN] | |
| 1. | BB1 | C-P1M-ST | 2.5 | 75 | 150 | 5.8 | 348.7 | BP |
| 2. | BB2 | A-P1M-SK | 2.5 | 75 | 150 | 4.92 | 321.4 | BP |
| 3. | BB7 | C-P1M-ST | 2.5 | 75 | 125 | 5.77 | 345.9 | BP |
| 4. | BB19 | B-P1M-SK | 2.5 | 75 | 125 | 4.15 | 317.8 | BP |
| 5. | BB8 | C-P1M-ST | 1.25 | 50 | 100 | 5.25 | 284.5 | BP |
| 6. | BB9 | A-P1M-SK | 1.25 | 50 | 100 | 5.00 | 258.2 | BP |
| 7. | BB13 | C-P1M-ST | 1.25 | 25 | 75 | 13.88 | 322.9 | FP |
| 8. | BB15 | A-P1M-SK | 1.25 | 50 | 125 | 13.96 | 359.7 | FP |
| 9. | BB21 | B-P1M-SK | 0.5 | 50 | 100 | 9.46 | 243.8 | FP |
| 10. | BB22 | B-P1M-SK | 0.5 | 25 | 75 | 9.09 | 257.5 | FP |

# Part 2 Methods on determining CMA and the total load of the bridge system

# Chapter 5 *Method 1: Disconnected Bridge System*

## Introduction

This chapter discusses the first method, which disconnects the bridge in more understandable components to simplify the main problem. The first method is an analytical method.

Moreover, this chapter deals with the failure mechanism and to what extent compressive membrane action plays a role in that. Furthermore, this chapter explains the important components of the bridge and the loading phases. Finally, an upper and lower bound limit of the bridge's capacity is determined.

## Main problem

The main problem investigates the failure mechanism of a directly loaded *T-beam* of a prestressed concrete bridge (Figure 42). This is contrary to past experiments where the *slab* between beams was loaded, usually failing in punching (Chapter 1, Approach of research on CMA). Eventually, the loaded main beam reaches its governing shear load and fails. Then the slab redistributes the beam load and possibly the additional load to the neighbor beams and supports. The redistribution of this load is the mechanism that is discussed. The governing failure mode of the slab in between the flanges of the neighbor beams (Figure 43) is assumed to be bending, instead of punching. This means one can calculate the slab bending capacity with arching, as done with the methods from part 1 (Chapter 3 and 4).

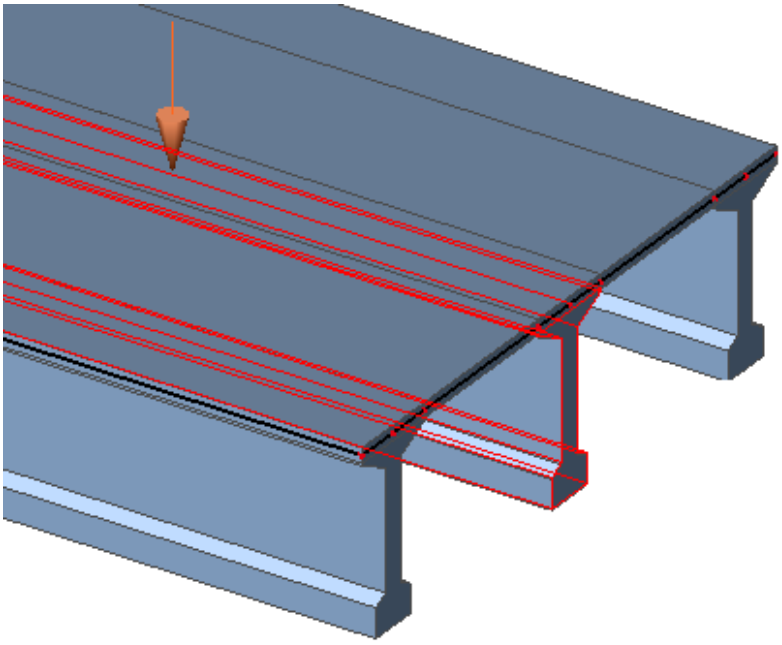

*Figure 42 load directly on main girder*

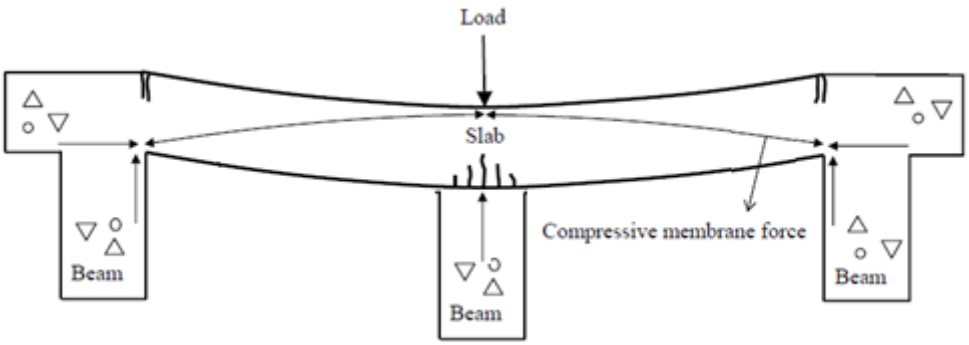


*Figure 43 loading the main beam, showing membrane action and lateral restraint*

## Disconnecting into key components

In order to simplify the failure mechanism, the first method *disconnects* the bridge in two components, with each their respective capacities, to understand their role in the failure of the whole bridge system. Considered are:

1. Main beam (Figure 44, red) => Shear capacity (Appendix A)
2. Slab (Figure 44, blue) => Bending capacity (Chapter 3)

It is noted that the span length of the slab increases, because the loaded beam failed. Only the top flange is assumed to behave as a part of the slab (Figure 44 and Figure 45).

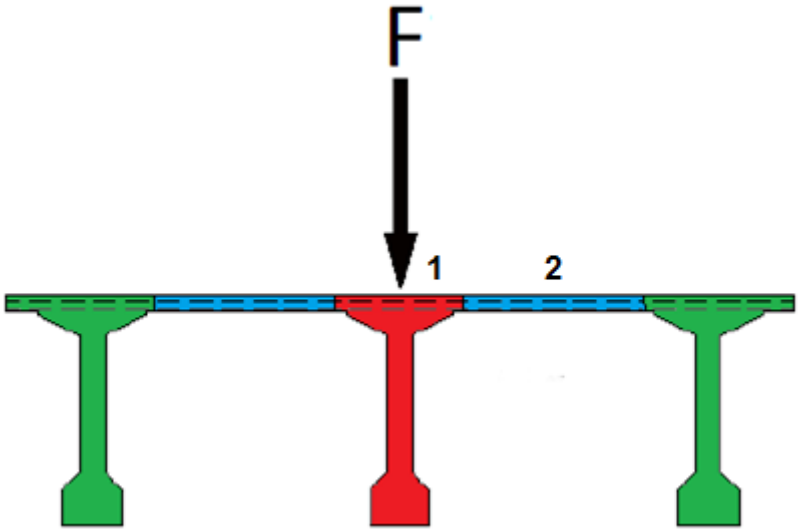


*Figure 44 three disconnected components*

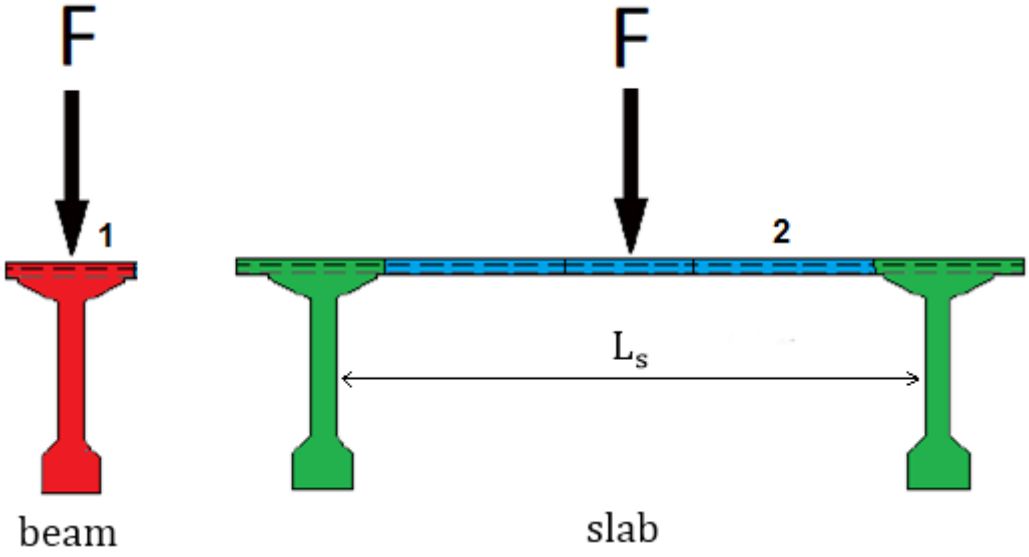


*Figure 45 two distinct situations considered: slab and main beam*

Basically, the method disconnects the first loading situation of the main problem into two other distinct situations, where slab and beam are taken into account and for which their respective capacities can be calculated (Figure 45).

The slab situation--without the main beam present--indicated on the right in Figure 45, has a bending capacity with arching which can be determined as shown in part 1, with one of the calculative methods (Chapter 3 and 4).

But first the main beam is considered more in depth, to understand its assumed load-deflection behavior and to determine its shear capacity.

And after that the two new distinct situations will be discussed more in depth, since they occur during the loading phases of the bridge system.

## Beam behavior

### Test result single beam load-displacement graph

In order to understand the beam behavior a *single* prototype beam was tested. And Figure 46 shows its load displacement graph. It shows a ductile behavior, which is desired when loading a similar beam, one that is integrated into a bridge system, as is the case for the main problem.

The single beam shows a peak load of around 3000 kN, with a displacement of 37 mm, and an ultimate displacement of 45 mm.

Point A till B shows linear elastic behavior and the corresponding girder load is reached around 1500 kN. At point B the linear cracking moment is reached, and from then on the beam shows non-linearity.

From point B till C, the beam and slab crack, part of the load is taken up by the steel, and elastic-plastic behavior sets in. Finally at point C, the peak load is reached. The same peak load is desired to be reached when loading a beam integrated in a bridge.

However, it is assumed that, due to load distribution through the slab to the neighbor beams, the main beam will not reach its maximum girder load, which is discussed later.

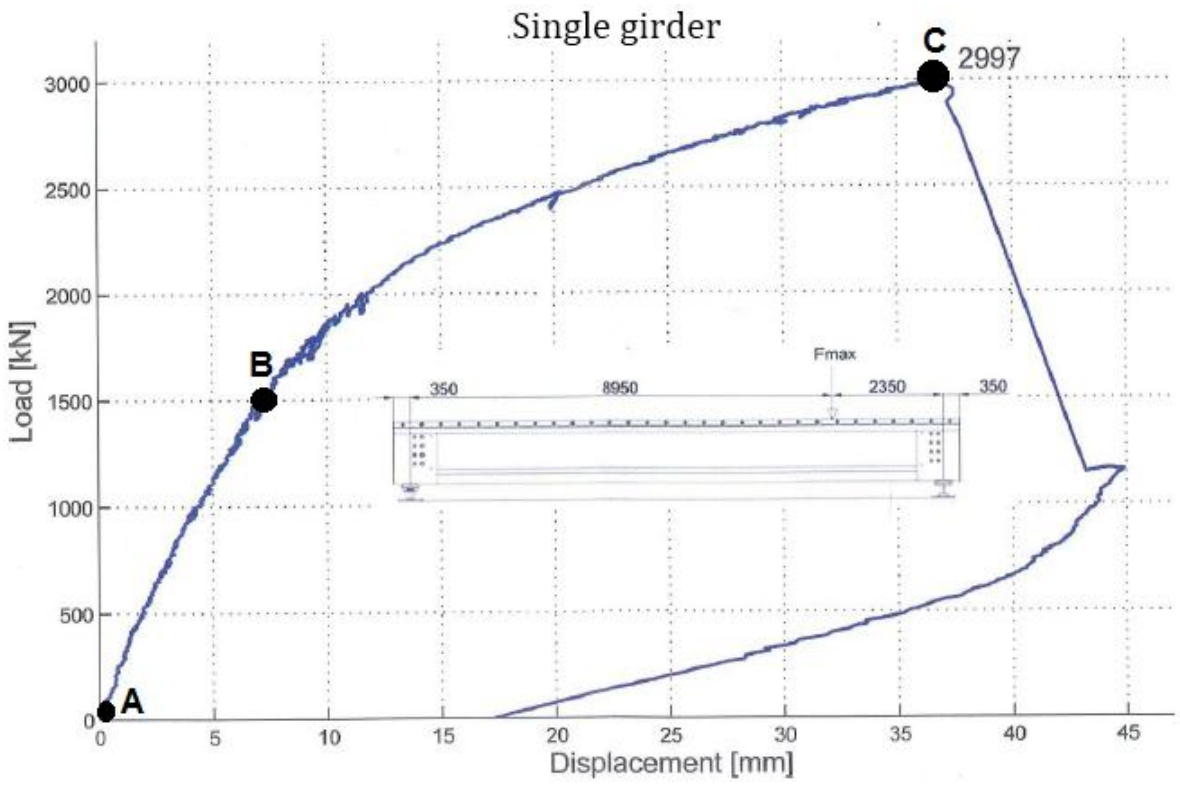


*Figure 46 load displacement graph of a single T-beam*

Overall, the beam shows non-brittle behavior and large deflections take place. The steel stirrups and reinforcement have the opportunity to yield and warn for failure, showing plastic behavior. Ultimately, the large girder deflections are favorable and necessary for membrane action to activate when loading a similar beam integrated in a bridge system. This has to do with the critical deflection condition mentioned earlier, which will be discussed later. It is noted that the tested single girder is heavily reinforced with shear stirrups, more than old bridges, causing it to behave more ductile.

And it is noted that usually one does not have test results of the single beam behavior, before actually testing a bridge system. So, one does not know how the nonlinear branch of the load-displacement curve looks like.

**Girder shear capacity**

But one can calculate the linear beam capacity. The calculation is given in Appendix A. The beam is calculated to have either its tensile splitting shear capacity or flexural shear, depending on the load location and amount of shear reinforcement.

For the 'Brienenoord' prototype beam, the linear capacity gives a girder load $F_{girder} = 1550\ kN$. This is a safe underestimate of the actual total beam load (Figure 47). It is in the same order as the linear load shown in the load-displacement graph with a certain margin of error. It is reached around a deflection of 7 mm.

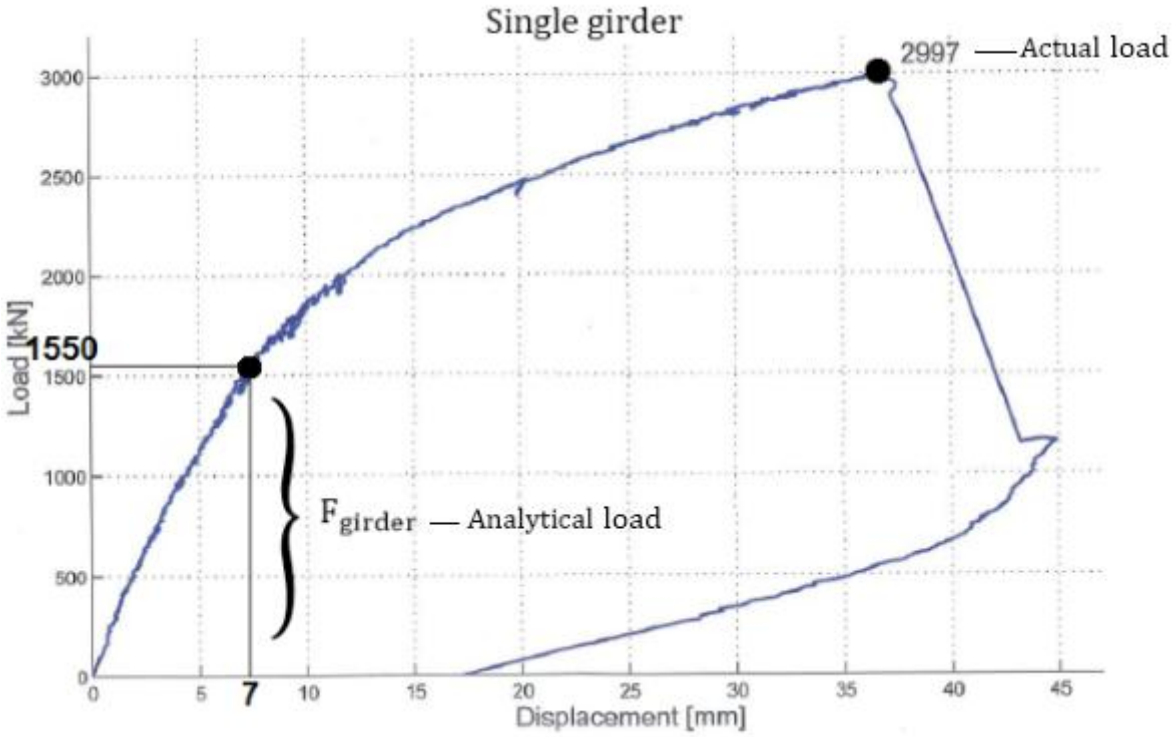


*Figure 47 linear girder capacity, an safe underestimate*

## Failure scenarios 1 and 2: lower and upper bound limit

### Scenario 1: the lower bound limit

In the linear loading phase, as the load on the bridge system increases, it is assumed that the linear capacity of the main beam is reached at the girder load $F_{girder}$. At the girder load first cracking occurs (shown for beam 1 in Figure 49). The instant of cracking is important and is discussed in depth later. The main beam reaches its shear capacity (Appendix A).

Moreover, it is noted that the linear elastic distribution is not taken into account for now in order to simplify the problem. To determine the distribution of the load a numerical model is needed, which is discussed later with method 2 (Chapter 6 and 7). For now it is assumed that the main beam takes 100% of the effect of the external load (Figure 48).

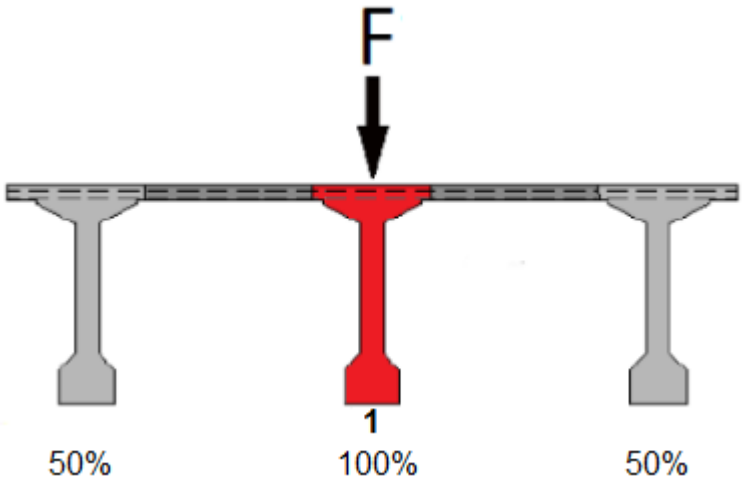


*Figure 48 linear elastic distribution is not taken into account yet (one is referred to Chapter 6)*


*Figure 49 Top: main beam loaded till shear capacity. Bottom: sideview of beam reaching tensile splitting shear*

For the bridge system, two failure scenarios are assumed. Now the first failure scenario is introduced, it occurs in the linear loading phase.

After the linear capacity at the girder load $F_{girder}$ is reached, it is assumed that the slab and beam do *not* work together. Therefore, the beam capacity and the slab bending capacity are *not* allowed to be summed up together. Consequently, the girder load is the lower bound limit of the total bridge load (Figure 50).

Furthermore, the it is assumed that the main beam does not have more capacity left after reaching its linear capacity. The beam fails brittle (Figure 50 and Figure 51). If the main beam fails brittle, the bridge system fails as well. And it is assumed that the slab is able to carry and redistribute the load to the neighbor beams. It is the question whether the slab bending capacity is sufficient to hold the beam load (this is discussed later in the chapter).

It is noted that the total bridge capacity only has the capacity of the two neighbor beams. This is because the main beam falls out. Each neighbor beam is assumed to have the same capacity as the main beam (Figure 51).

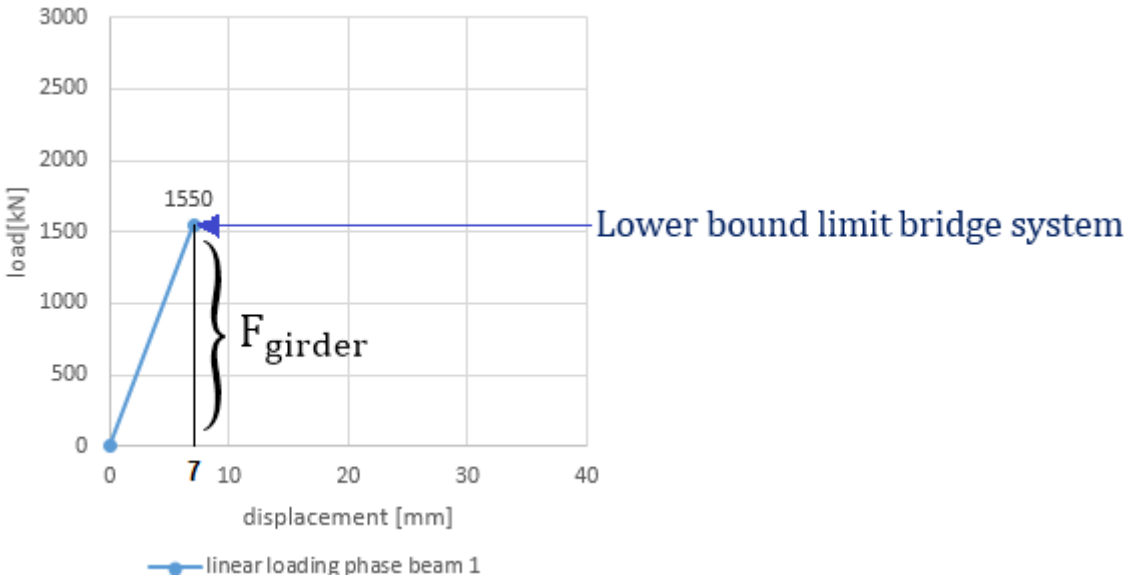


*Figure 50 first failure scenario: lower bound limit of the bearing capacity of the bridge system*

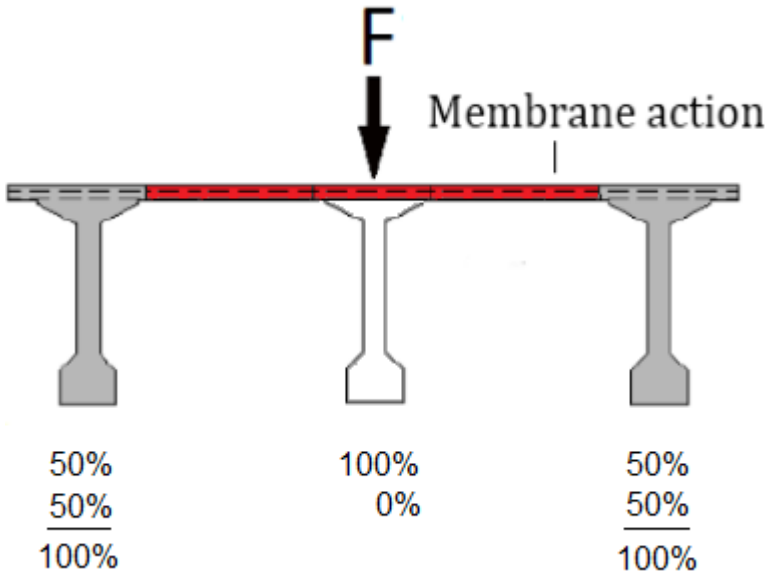


*Figure 51 the beam load is distributed through the slab to the neighbor beams*

Usually test results are not available before actually testing a bridge. Therefore, by assuming a lower bound, safety regarding the beam capacity is created. Because actually the beam has a certain plasticity, which can be a bilinear-like behavior or another nonlinear behavior. And the load distribution is not taken into account yet which would reduce the effect of the external load on the main beam. All of this means the beam has potential capacity left.

However, now considering the second failure scenario, the bridge is assumed to have a hidden capacity of the slab through membrane action. Where the bridge has a hidden capacity and load redistribution is possible. And this capacity is the slab bending capacity with arching, which can be calculated. Which will now be considered more in depth.

For this research, linear elastic behavior with brittle failure is assumed for the beam (Scenario 1: lower bound limit). And bilinear behavior is assumed too. By assuming these two behaviors, it was shown that a lower bound of the beam capacity is assumed, compared to the other possible beam behaviors (Chapter 1, Approach of research on CMA). This is why the lower bound limit of the bridge system can be considered a lower bound. Since $F_{girder}$ might be higher in practice.

**Comparison slab bending capacity and girder load**

If the main beam fails, the slab instantly needs to carry the load that was originally on the loaded beam. It is questioned whether the slab has enough capacity. For the parameters of the Brienenoord prototype, the slab bending capacity with CMA is determined (with Rankin in Appendix A): 178 kN. This is the bending capacity for the determined effective width (Appendix A).

Assuming that the membrane action activates after the linear girder load of 1550 kN is reached, it is concluded that the slab bending capacity is not sufficient and cannot redistribute the load.

This is a logical conclusion. Since it was determined earlier that is unlikely that membrane action is activated or has a significant strength contribution, because of the high slenderness. Even when the slenderness is reduced to 15 (Appendix C), the slab capacity is not sufficient.

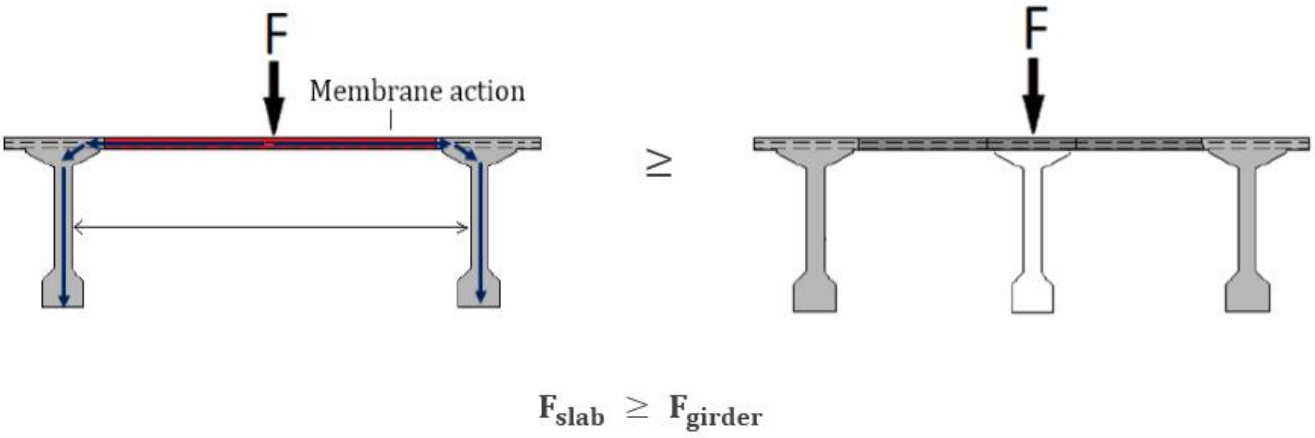


*Figure 52 Slab bending capacity needs to be higher than the girder load*

**Scenario 2: the upper bound limit**

The second failure scenario of the bridge system is introduced.

In this scenario it is assumed that after the linear capacity of the main beam is reached and first cracking occurs, membrane action in the slab is activated. The slab is able to carry and redistributes the additional load to the neighbor beams.

This is the elasto-plastic loading phase of the bridge system (Figure 53), where both the beam and slab are assumed to behave plastically, bilinear-like, till failure. The beam behaves plastically meaning it is assumed to carry the original load that was on it.

Basically, the situation goes from a beam situation to a slab situation, where the beam capacity stays constant (this is an underestimation of its actual capacity as discussed earlier). The main beam can be shown as a weak spring that keeps deflecting till failure. This is possible because of the assumed plastic behavior.

The new slab situation has a span length that has approximately doubled (Figure 53) where the top flange of the loaded beam behaves as a part of the slab. The slab has a bending capacity with arching that can be calculated (e.g. Rankin from Chapter 3).

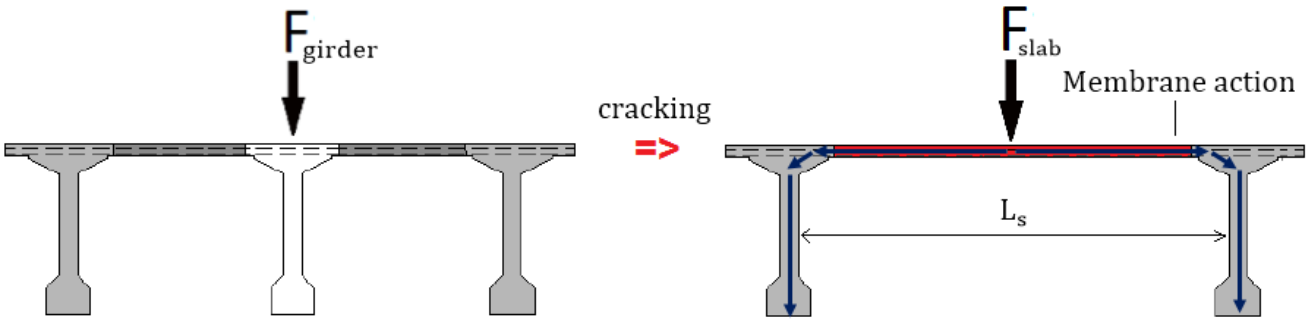


*Figure 53 elasto-plastic loading phase: redistribution of additional load due to membrane action*

The slab is assumed to reach its maximum arching capacity at the instant at which first cracking occurs (Figure 54). After that the slab is assumed to deform plastically till the total bridge load and failure is reached.

It is noted that membrane action can only be activated if the relative beam displacement--which is the displacement difference between the main beam and neighbor beams--is large enough (this is discussed in depth later). For now it is assumed in the first method that this is the case after the linear capacity is reached and first cracking occurs. At this instant, membrane action is activated and slab and beam are assumed to work together. This means that their respective capacities can be added together: $F_{total} = F_{girder} + F_{slab}$ (Figure 55).

The upper bound scenario assumes that the total bridge capacity is the capacity of all three beams together. It is noted that membrane action might activate earlier than the point of the linear girder load, this is discussed later. And a final note, it is assumed that only three beams will take the total external load.

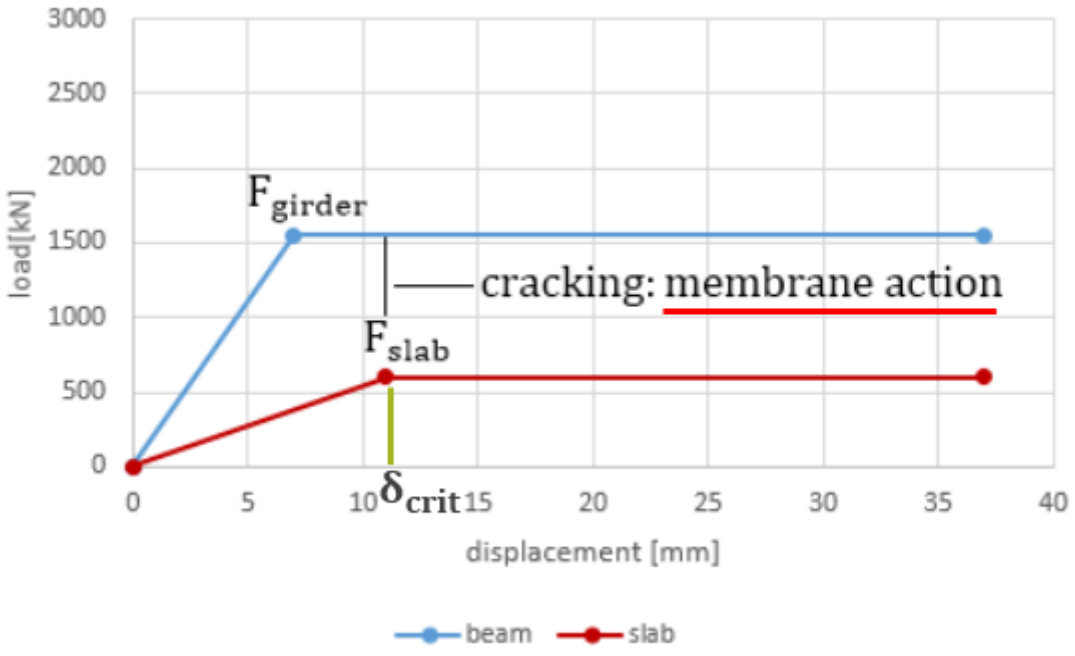


*Figure 54 After linear capacity is reached, and cracking occurs, is the instant at which membrane action activates*

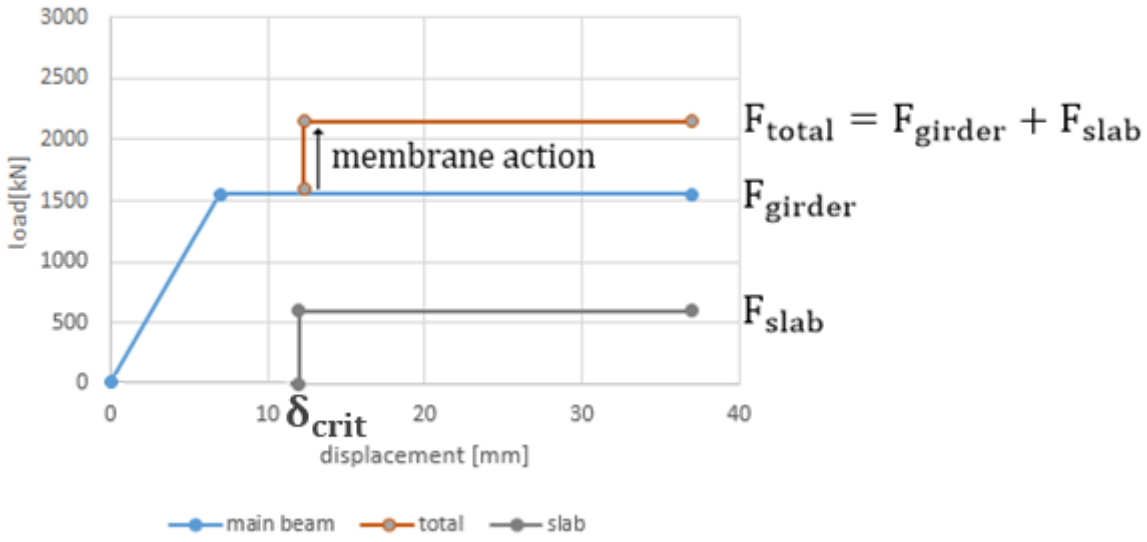


*Figure 55 Slab and beam capacities are added together*

## Span/depth ratio criteria

The considered clear span results in a high span/depth ratio. The effect of a high span/depth ratio is shown at the end during the calculation of the total deck capacity. The slenderness condition (mentioned in Chapter 3) must be met for membrane action to activate. To clarify the importance of the slenderness, the Brienenoord prototype is used as an example (Figure 56). This gives the following:

$$\lambda = \frac{L_s}{h} = \frac{3450}{100} = 34{,}5 > 20$$

The slenderness condition is *not* met for both the British and Canadian method. It was stated earlier that some conditions may not be met, such as the slenderness. And in this case membrane action may then be taken in to account if the necessary restraint factor can be validated. The stiffness parameters can also be validated when using Rankin's method of Rankin instead. And it is noted that the method of Rankin does not state a certain slenderness condition. However, the calculation of the effective width does take into account the clear span.

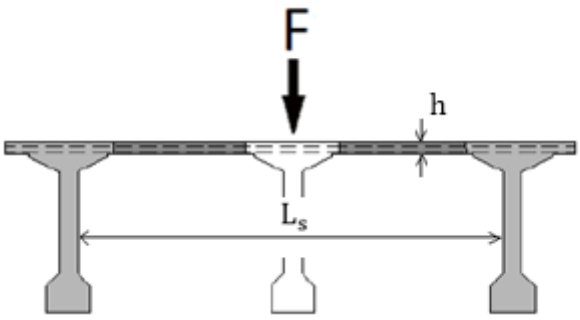


*Figure 56 determining the span/depth ratio*

A safe choice for the slenderness conform the criteria (of Chapter 3) is the maximum of 20. This gives the following:

$L = h * 20 = 2000\ mm$
$h = 100$

This means that up to a maximum clear span ('dagmaat') of 2000 mm for a thickness of 100 mm membrane action can be activated. When adding the web thickness of the Brienenoord prototype for example, this gives the following c.t.c. distance:

$L_{c.t.c.} = L_{clear} + d_{web} = 2150\ mm$
$d_{web} = 150\ mm$

Furthermore, two examples are given with more calculations (in Appendix C). One where the point load is placed at halfway the length of the beam (also a case where CMA contribution is negligible), and one with a safer span/depth ratio of 15. A slenderness of 15 gives the following:

$L = h * 15 = 1500\ mm$
$h = 100$
$L_{c.t.c.} = L_{clear} + d_{web} = 1650\ mm$
$d_{web} = 150\ mm$

**Conclusion activation membrane action**

Ultimately, it seems that the slenderness is a very important criteria for membrane action activation. It is advised that it needs to be lower than 20. A slenderness of 15 is safer.

However, it is hard to guarantee the restraint of the bridge system. Meeting the stated criteria is an indication of the restraint. Therefore, it is safer not to calculate with membrane action when one of the criteria is not met. This will be discussed later.

With the discussed slenderness larger than 20, it is assumed that it is unlikely that membrane action activates or that its contribution is not very high for the prototype. The following calculation is done to verify this.

## Slab bending capacity

The following combines past and new research to determine the slab bending capacity with arching. Most of it is explained without actual calculations with numbers. This is done in order for others to use it for similar bridge situations. Some calculations are made to enforce some points. For more details and calculations one is referred to Appendix A.

It was clear that an important part is the elasto-plastic loading phase. Here, membrane action activates and helps the main beam carry the load. It is important to understand to which extent membrane action plays a role. And it is important to give a quantity to the slab bending capacity with membrane action.

A simplified approach is made to understand which parts of the slab provide which part of the total deck capacity due to membrane action. Simply said, some parts of the slab provide strength and some parts do not play a role. To study the slab the following is determined:

1. Activated slab area => determined with critical deflections
2. Concrete slab strip bending capacity => determined with Rankin method
3. Total capacity of activated area => determined with (1) and (2)

First, the activated slab area is determined by using the linear girder deflection field and the critical deflection condition.

Then, the slab area is assumed to be made up of laterally restraint concrete strips. The strips are used to determine the total deck capacity. The capacity of a single strip is determined with the Rankin method. So, the total activated slab area has a capacity of 100% and each concrete strip is part of the total capacity.

### Activated slab area

First, it is determined which part of the total slab area is activated. Two situations are considered: a lower and upper bound situation.

### Lower bound situation

This situation activates an effective width of the slab. (Taylor, Rankin, & Cleland, 2002) devised a method to estimate the effective width of a laterally restraint slab strip (Figure 57). For the actual calculation of the effective width see Appendix A. This method takes into account the loading area over which the load is spread, activating a certain width for membrane action. So, the lower bound is the slab bending capacity that can be calculated for this width. It takes into account the considered clear span.

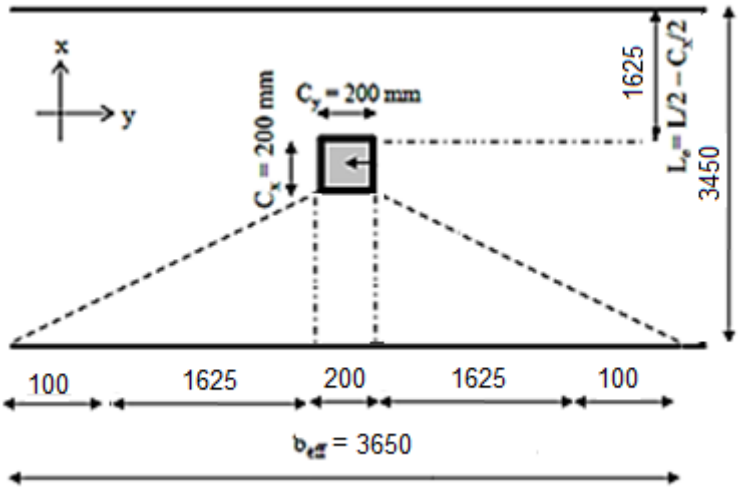


*Figure 57 effective width (Taylor, Rankin, & Cleland, 2002)*

**Lower bound slab bending capacity**

When loading the beam, a linear elastic deflection field is assumed to be present over the length of the beam. A plastic hinge forms at the loading point. The rest of the beam is modeled as rigid bodies (Figure 58). Basically, both slab and beam are assumed to behave plastically. This means that they will display plastic deformations. This is favorable for activation of membrane action.

After the main beam shows first cracking, the slab is assumed to be activated and takes over the additional load. Membrane action might activate earlier or later than the point of the linear girder load, this is discussed more with the numerical method.

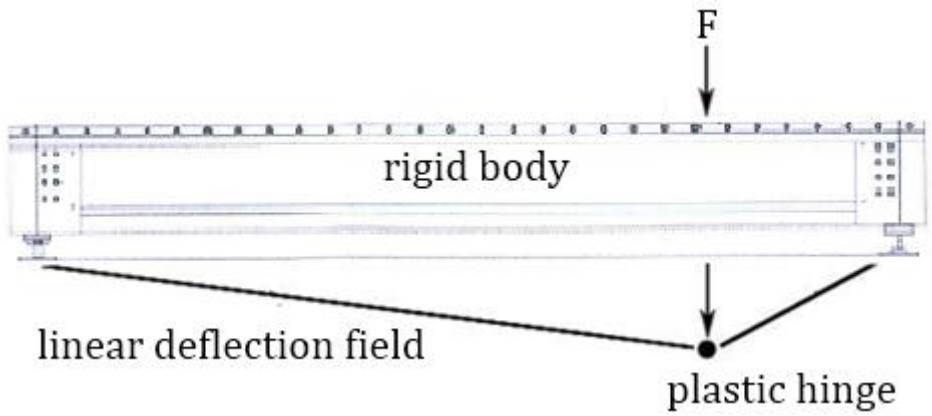


*Figure 58 displacement model*

The instant at which membrane action is activated is for the deflection $\delta_{crit}$ (Figure 59). Here the relative deflection, the deflection difference between the loaded beam and the neighboring beams, is large enough. The deflection $\delta_{crit}$ is important for the activation of membrane action.

At the deflection $\delta_{crit}$, an effective width is activated with the lower bound slab bending capacity (Figure 59). At this instant, the critical condition for membrane action to activate is reached.

In the second method, a numerical model is used instead to determine the critical deflection and the instant at which membrane action activates. An example calculation of the lower bound slab bending capacity of a laterally restraint concrete strip is given in Appendix A. Figure 60 shows the linear beam capacity with the lower bound slab bending capacity, adding membrane action.

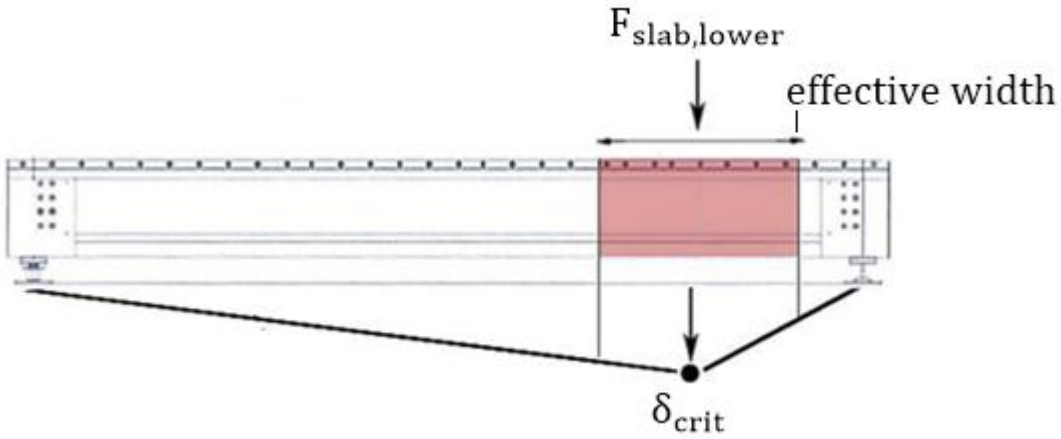


*Figure 59 instant at which membrane action activates according to first method*

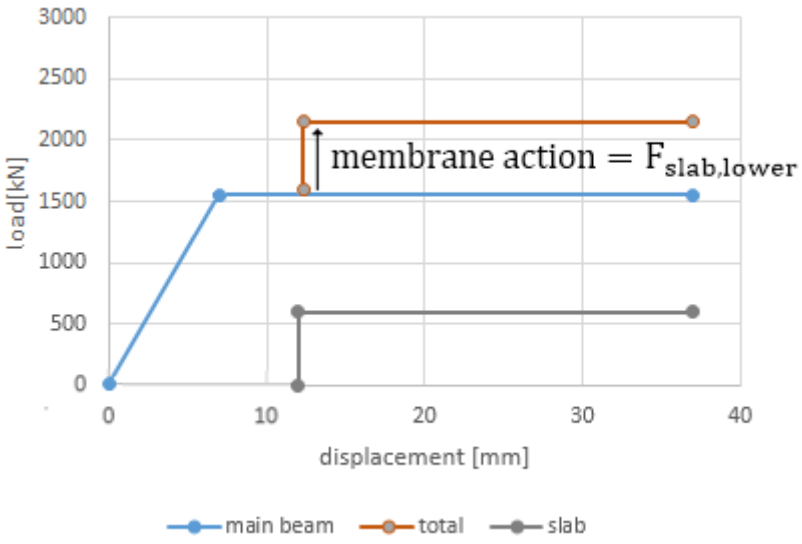


*Figure 60 lower bound slab bending capacity added to beam capacity (not on scale)*

### Upper bound slab bending capacity

Returning to the slab capacity, if it is assumed that there is still more capacity possible: the upper bound of the slab bending capacity. In this case it is assumed that after the first lower bound slab bending capacity is reached, the slab capacity increases as the slab keeps on deflecting up till failure for an ultimate deflection $\delta_{ultm}$ (Figure 61).

This is more realistic instead of keeping the slab capacity constant as shown in the lower bound slab situation. The maximum deflection can be derived empirically or numerically.

For the calculation in Appendix A, $\delta_{ultm}$ is derived from the single beam test results and is the deflection of the beam at peak load. With the maximum deflection, the activated beam span is determined (Figure 62).

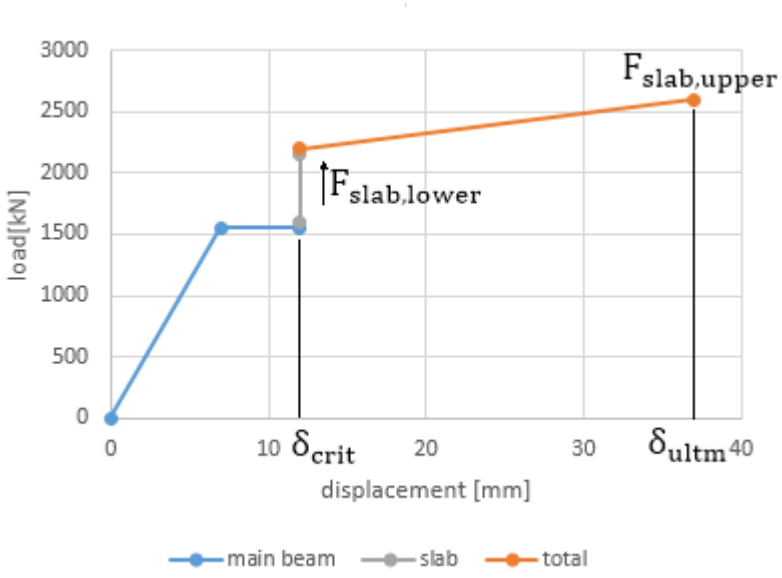


*Figure 61 upper bound slab bending capacity (not on scale)*

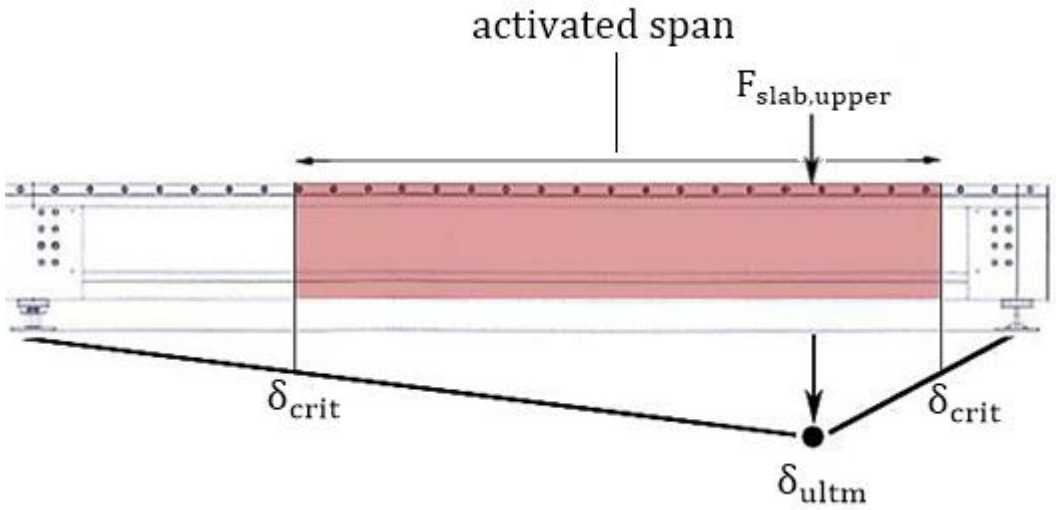


*Figure 62 upper bound: activated beam span (not on scale)*

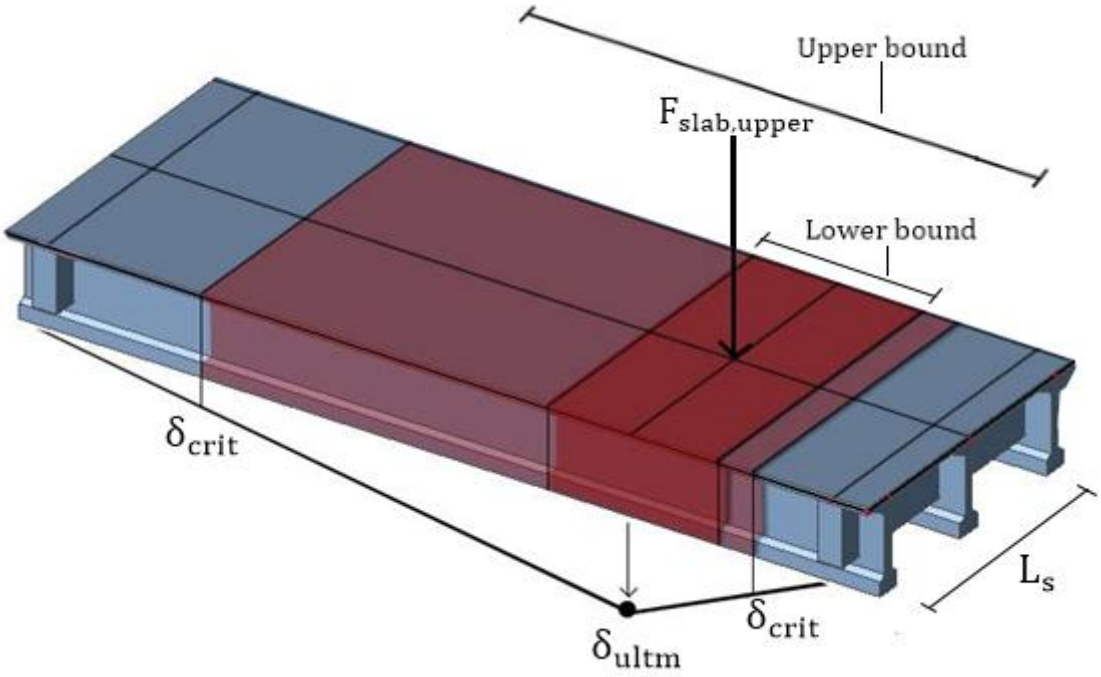


*Figure 63 lower and upper bound of activated beam span*

The slab bending capacity is determined for a certain span. This means that when a part of the beam is activated, in fact a part of the total slab area is activated. Figure 62 and Figure 63 display this activated slab area.

Summarizing, the capacity of the slab strip with the effective width (Figure 59) is considered a lower bound value and the whole activated span is considered to result in an upper bound value (Figure 63). Reality falls somewhere in between.

**Total slab capacity of activated slab area**

Now the total slab capacity is determined. Earlier parts discussed what area of the slab is activated for compressive membrane action, and how to determine the capacity of a single laterally restrained concrete slab strip. Now the full capacity of the total activated slab area is determined by combining these two informations.

The capacity of a single laterally restrained concrete strip with an effective width $b_{eff}$ was determined. And if one were to visualize shifting the load over the activated slab area along the span of the girder and constantly loading a 'new' $b_{eff}$ zone, the total activated slab area can be divided in smaller strips with known widths and capacities (Figure 64). So, the slab is assumed to be made of parts, some of which not as wide as $b_{eff}$, providing a lower capacity, and some of which provide the full capacity of a single slab strip. The total capacity given by the total activated slab area is given by:

$$F_{tot,a} = \sum F_{x,a} \tag{38}$$

The ratios of $B_{eff}$ in Figure 64 are an example of the slab calculation (Appendix A).

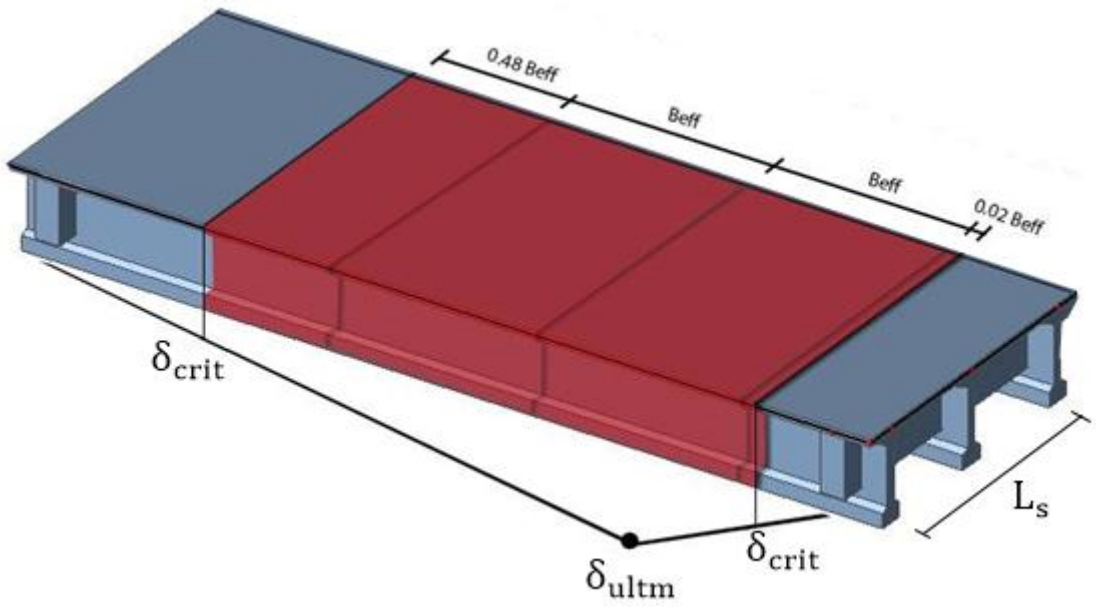


*Figure 64 total activated slab area divided by strips of effective widths (not on scale)*

**Total slab capacity**

Now the total slab capacity of the total slab area is determined. The calculation is shown in Appendix A.

$$n\,[-] = \frac{\text{activated slab span [m]}}{\text{effective width slab strip [m]}}$$

$$\text{total slab capacity } [\text{kN}] = n * \textbf{bending} \text{ capacity slab strip}$$

$$\mathrm{F_{slab,upper}} = n * \mathrm{F_{slab,lower}}$$

The linear girder load is added to give the total load, since it is assumed that slab and beam work together:

$$\mathrm{F_{total}} = \mathrm{F_{girder}} + \mathrm{F_{slab,upper}}$$

The same calculations are done again, for Rankin (SS/FE), (FE) and the UK method. For the last method the same effective width is assumed to be present. The CAN method does not calculate a bending capacity. Results are summarized (Table 24, Appendix A).

**Conclusions slab bending capacity**

A fixed ended slab gives a higher slab bending capacity than a simply supported one (Appendix A). The lateral restraint influences the slab bending capacity.

Moreover, the slab capacity depends on the total activated slab area, the activated beam span and the slab strip bending capacity.

Furthermore, the slab bending capacity is determined with the Rankin method for a certain effective width. The effective width plays an important part in determining the capacity. When the considered clear span becomes longer, the effective width becomes longer (Appendix A).

Finally, the calculation in Appendix A demonstrated that the contribution of the slab bending capacity is not very high for the Brienenoord prototype. For the experiment described in Appendix C, this was also the case. In that experiment, the slenderness was also higher than 20, which led to a slab bending capacity that was not very high.

Furthermore, a parameter study was done for a shorter span. The following was assumed: a slenderness of 15, a c.t.c distance of 1650 mm and a deck thickness of 100 mm (Appendix C). And there it is demonstrated as well that the slab contribution due to bending is not that high.

## Activation membrane action in the slab

Compressive membrane action can only develop if enough lateral restraint is present in the system. Also, it can only occur in a slab after cracking occurs and gives net in-plane forces at the slab boundaries. The mechanism cannot occur in slabs with the same linear elastic behavior strength in tension and compression. Cracking in the slab is essential in order for compressive membrane action to develop in the slab. Membrane action develops at the critical deflection. Therefore, in order to identify whether the mechanism develops in the slab, it needs to be verified if the critical deflection is reached.

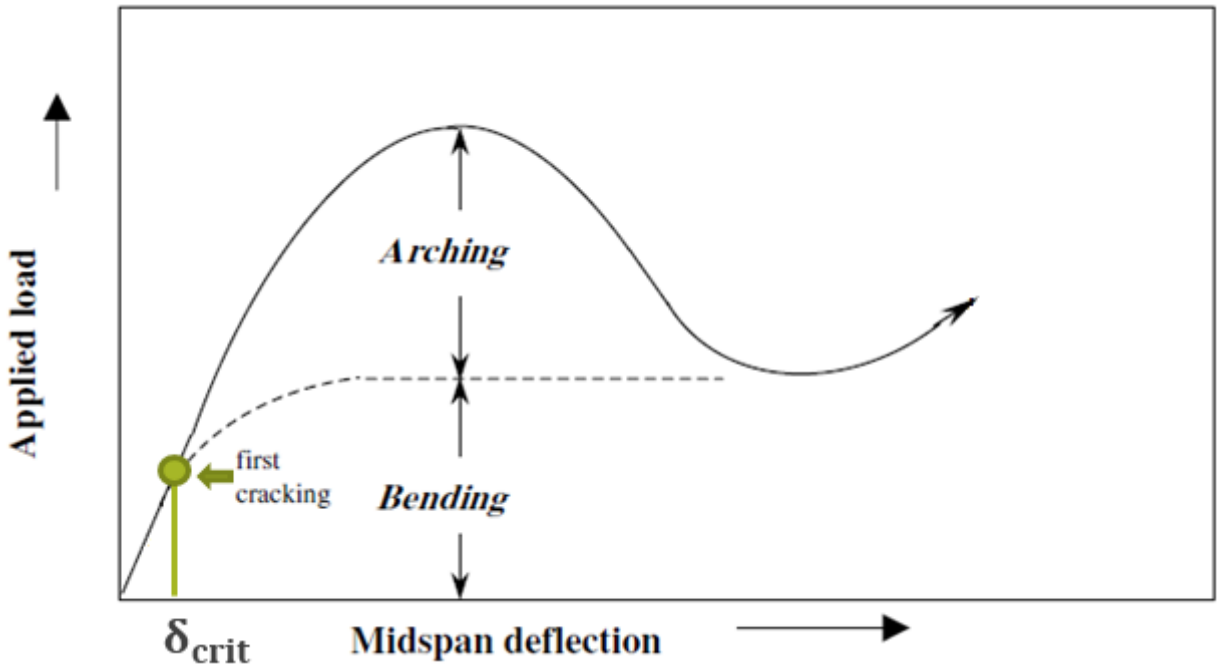


*Figure 65 Critical deflection reached at first cracking of the slab*

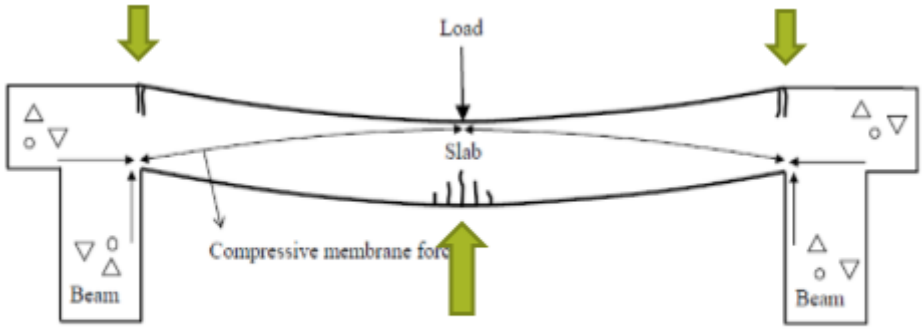


*Figure 66 cracking in the slab and CMA develops*

This means that the condition for which compressive membrane action develops, is that the main beam needs to displace more than the neighbor beams and slab at midspan. In other words, the relative deflection of the main beam needs to be larger than the slab deflection in order to develop membrane action (Figure 67). Basically, the relative girder deflection is the deflection difference between the main beam and the neighbor beams.

$$\delta_{rel,girder} \geq \delta_{slab} \tag{39}$$

So only if the relative deflection of the main beam is large enough, exceeding past the critical slab deflection (where cracking occurs), then and only then plastic behavior is initiated, causing activation of membrane action and providing the additional slab capacity. This condition must be met in order for slab and beam to work together and add their respective capacities.

In the method discussed in this chapter, it was assumed that membrane action was activated after cracking when the linear beam capacity was reached. But it is possible that membrane action could be activated earlier in the linear loading phase, this feature is discussed in later chapters.

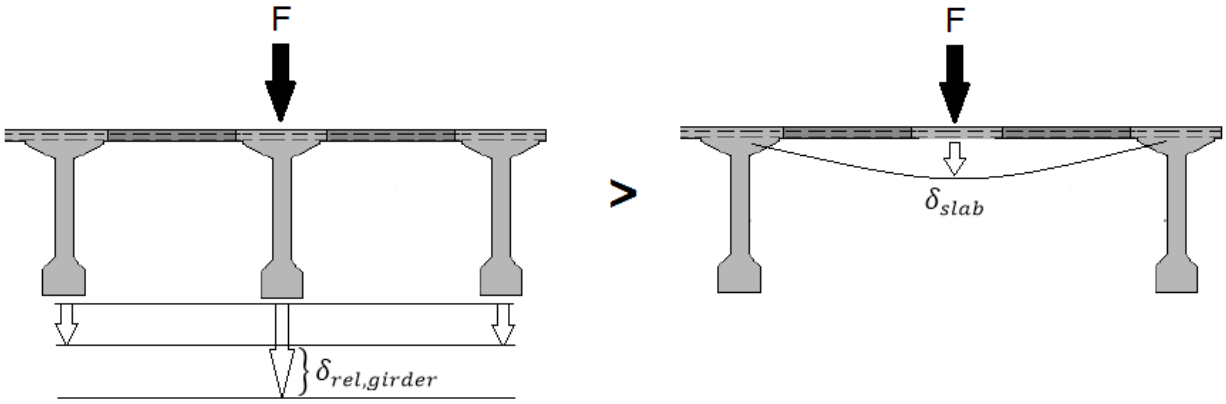


*Figure 67 critical deflection condition: relative girder deflection needs to be larger than slab deflection at midspan*

# Summary Chapter 5

### Summary of loading phases

Summarizing, from the linear till the final loading phase, the load is distributed from the initial load point and eventually to the neighbor beam supports and foundation, and during this load period membrane action is activated in the slab, helping the main beam to redistribute the load to the neighbor beams. It is noted that for a linear system the neighbor beams are assumed to have the same capacity as the main beam. This is discussed later more in depth.

All three load phases are shown in Figure 68.

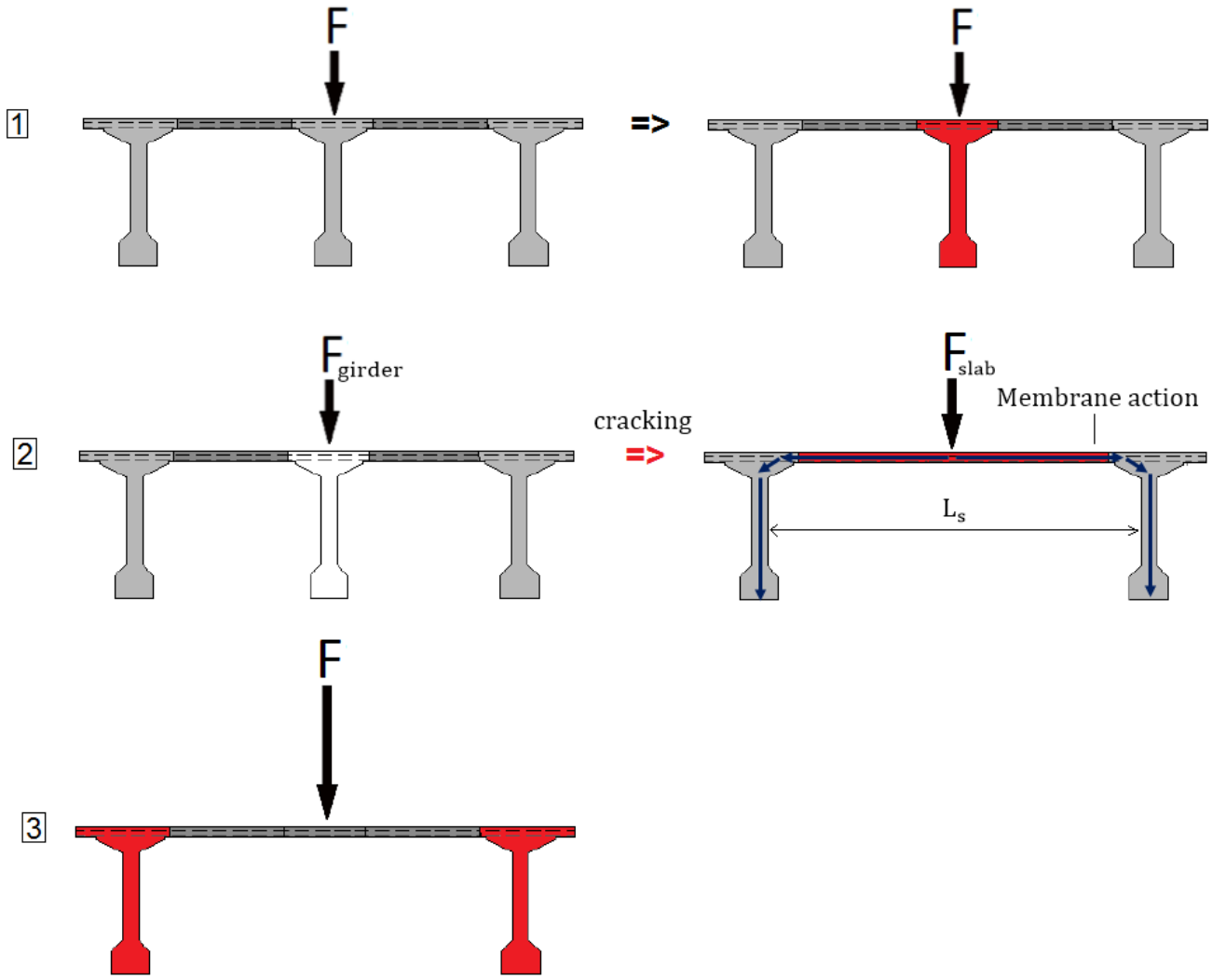


*Figure 68 summary of all three loading phases*

**Summary of failure scenarios**

Two possible failure scenarios are introduced that can occur when loading the bridge system of the main problem.

**Scenario 1 Lower bound limit**

Scenario 1 assumes a lower bound limit of the total bridge load. This is the girder load $F_{girder}$ that is reached for the linear capacity of the main beam. The lower bound limit is considered a safe underestimate of the bridge system bearing capacity (Figure 50).

Moreover, slab and beam are assumed *not* to work together, and their respective capacities are *not* summed up. The main beam is assumed to reach its brittle capacity, and the slab carries the load to the neighbor beams.

Sidenote: the linear elastic load distribution of the slab is not taken into account yet, which reduces the load on the main beam. To determine this distribution, a numerical model is needed, which is considered later.

**Scenario 2 Upper bound limit**

On the other hand, when the critical deflection is reached, main beam and slab work together. When slab and beam work together, a favorable upper bound limit of the bridge capacity is reached, their respective capacities can be added together: $F_{total} = F_{girder} + F_{slab}$ (**Error! Reference source not found.**). In reality the failure load of bridge system will be somewhere in between the two failure scenarios, between the lower and upper bound limit.

**Overall conclusions and further objectives**

The following questions are raised in using the first method, and combined with their answers they provide the conclusions. Some questions do not have direct answers and are considered more in depth in following sections.

1. How much slab capacity is available?

This is calculated with one of the slab bending methods of part 1 (e.g. Rankin)

2. When is membrane action activated?

At the instant linear beam capacity is reached and cracking occurs (Figure 53 and Figure 54). This leads to question 3.

3. Can membrane action be activated earlier in the linear loading phase before the linear capacity $F_{girder}$ is reached (Figure 69)?

To determine this, more details are needed about *when* membrane action is activated. And also a numerical model is needed to determine at what load and deflection this occurs, indicated with the question marks in Figure 69.

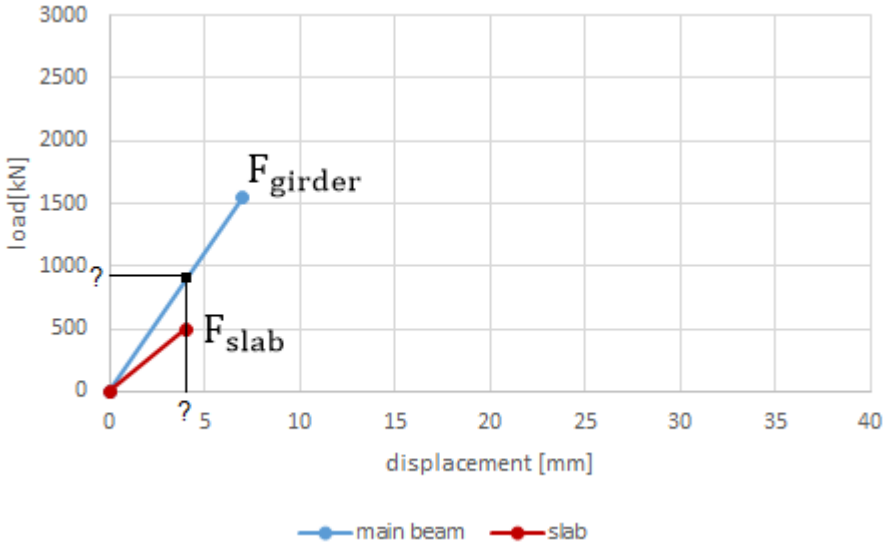


*Figure 69 instant at which membrane activates, needs more investigation*

4. How does linear load distribution influence the situation?

For this a numerical model is needed. But it is expected with an assumed load distribution (unknown for now, Figure 70) that the main beam is loaded less and spreads the load through the slab to the neighbor beams. And to carry this load a certain slab capacity is required. Basically, it is questioned whether the slab bending capacity is sufficient to carry the load.

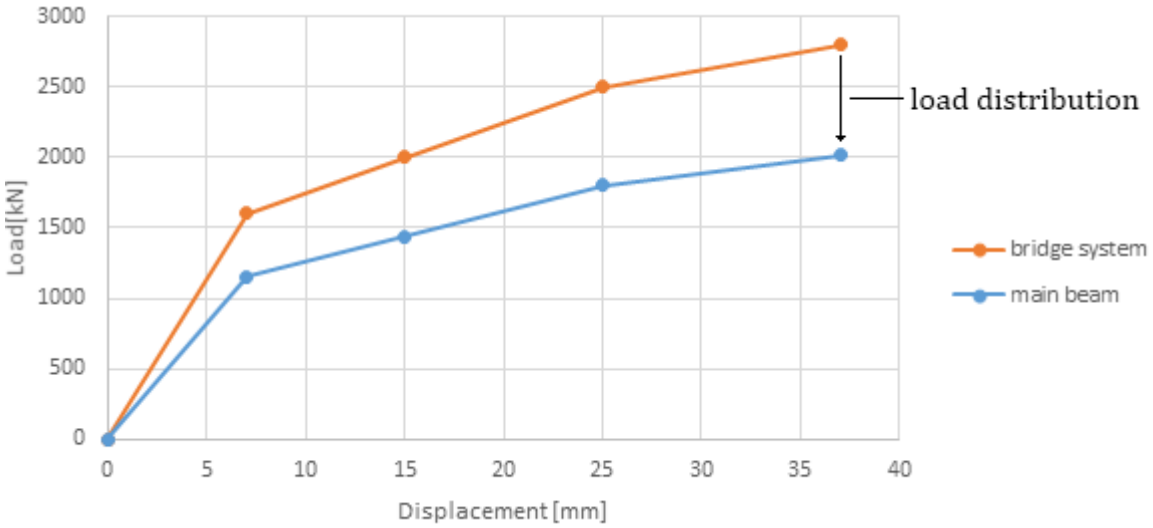


*Figure 70 expected behavior of system with load distribution*

5. How does the slab behave (Figure 71)?

a. Does it behave plastically?

For now the slab is assumed to behave bilinearly. More research on laterally restraint slabs is done later to verify (chapter 8).

b. How long is its plastic branch during which redistribution can take place?

Assumed to begin when maximum slab bending capacity is reached, at first cracking, up till failure of the bridge system. More research on laterally restraint slabs is done later to give a number to this plastic plateau (chapter 8).

c. At which deflection does the slab reach its full membrane/arching action?

More research on laterally restraint slabs is done later to give a number to this (chapter 8).
And a numerical model determines the midspan slab deflection for its bending capacity.

d. At which ultimate deflection does the slab fail?

More research on laterally restraint slabs is done later to give a number to this (chapter 8).

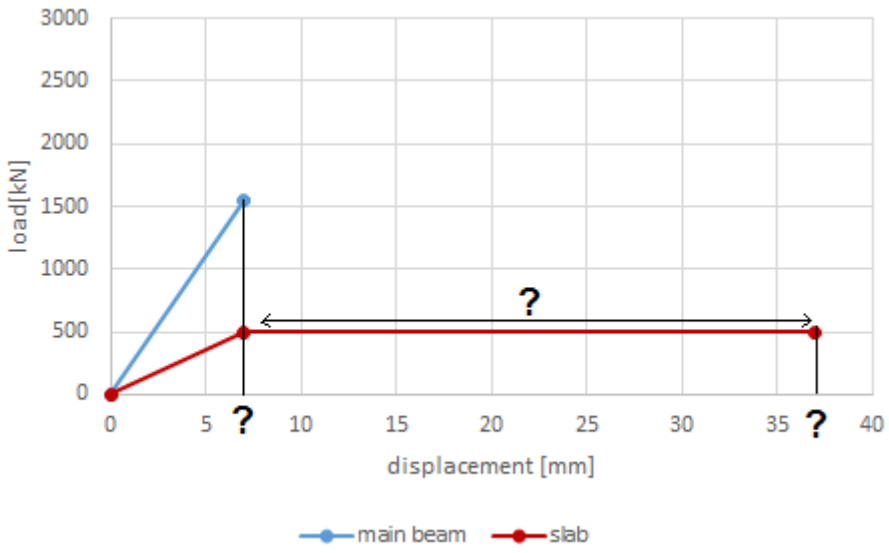


*Figure 71 questions regarding the slabs actual behavior*

**Important elements from the first method**

- Lower bound limit: girder shear capacity (tensile splitting or flexural shear)
- Total slab capacity
    - Critical deflections
    - Activated beam span and slab area
    - Slab strip bending capacity (effected by slenderness) $F_{slab,lower}$
- Upper bound limit: beam plus slab capacity
- Slenderness, span/depth ratio
    - Considered span
    - Slab thickness
- Effective width of a single slab strip (dependent on considered span)
- Location of the point load
- Concrete strength of beam and slab

**Summary of the first method**

- Determine Scenario 1: $F_{girder}$
- Determine activated slab area
    - Determine maximum deflection (empirically)
    - Determine critical deflection (empirically)
    - Determine activated beam span
- Determine effective width
    - Influenced by span/depth ratio
- Determine bending capacity of single slab strip $F_{slab,lower}$
- Determine if slab can hold the beam load: $F_{slab} \geq F_{girder}$
- Determine total slab capacity
- Determine Scenario 2: $F_{total} = F_{girder} + F_{slab,upper}$

**Important points for the second method**

- Linear elastic distribution with numerical model (Chapter 6 and 7)
- Slab deflections at midspan with numerical model (Chapter 6 and 7)

# Chapter 6 *Numerical Plate Model*

## Introduction

To study the linear elastic load distribution of the deck slab, a numerical plate model of the Brienenoord prototype is made with SCIA Engineering. It is modeled as an orthotropic plate with inverted T-beams as ribs, using plate-elements of the type Mindlin/Reissner. Numerical models with crossbeams are also considered.

Moreover, the questions raised in the first method are discussed. It is investigated whether compressive membrane action is not activated earlier when the main beam is still in the linear loading phase. And the critical deflections are determined numerically. At these deflections, membrane action is assumed to activate.

## Material and geometrical parameters

### Slab and crossbeams

For the slab and crossbeams of the numerical model, the mean concrete compressive cylinder strength $f_{cm}$ was taken as 65 MPa, the mean tensile strength $f_{ctm}$ was taken as 5.41 MPa and the mean modulus of elasticity $E_{cm}$ was calculated as 39 GPa.

### T-beams

For the beams as ribs integrated in the slab in the numerical model, the concrete compressive cylinder strength $f_{cm}$ was taken as 75 MPa, $f_{ctm}$as 6.30 MPa and $E_{cm}$ as 41 GPa, (Amir, 2014).

### Degrees of freedom

The freedom of movements of the supports of the prototype were used in the numerical model. On the south side, all beams are restricted in the x-direction. Except for support two, which is restricted both ways. On the north side all supports are free to move in x- and y-direction, except for support two, which has movement only in the x-direction. All supports have rotational movement about the x- and y-axes but not the z-axis, and are implemented as spring supports (Figure 72). The numerical model models the spring action of the actual rubber bearings, and a displacement of 1 mm is assumed to take place under permanent loading of the self-weight. After the geometrical and material data was put in the numerical model, the resultant force of the self-weight of the construction was determined and divided over the number of supports. And using the divided force and an assumed displacement of 1 mm the spring stiffness of a bearing was determined. The spring stiffness of the supports is given in Appendix B.

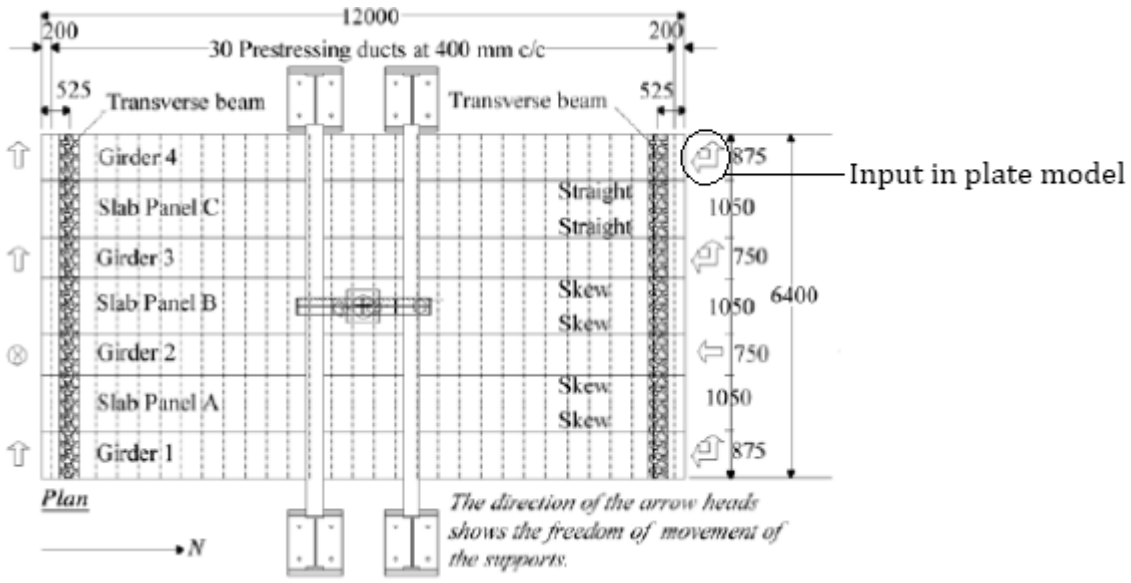


*Figure 72 overview of test setup and geometrical data of girders and slab (Stevin Report No. 25.5.13-06, 2013)*

## Load distribution

### Different models

First, five numerical models where made to study the load distribution. Ranging from a linear elastic plate, to a model with four T-beams as ribs and two crossbeams, similar to the lab prototype. It is noted that the loading point stayed at the same location, where the main beam was expected to fail in shear. Since, if the loading point changes location, the linear load distribution changes too. More information of the numerical models is found in Appendix B.

To study the displacements Model 2, a plate with three girders, is used. This simplified model determines the relative girder displacements relatively easy because of its symmetrical nature. The neighbor girders are loaded the same and displace the same. Furthermore, Model 2 is favored above Model 1 due to the implementation of the ribs beneath the plate, which is more realistic. And Model 3, with crossbeams, causes a high load spreading, resulting in very low girder displacements, complicating the calculation of the deck capacity. However, for bridge systems with multiple girders, such as 'De Vecht', the high load distribution indicates that it is possible that more girders outside of the main three participate in carrying the load, which means that a three-girder numerical model no longer would be sufficient and then the step must be made to a five- or seven-girder model. This will be discussed later.

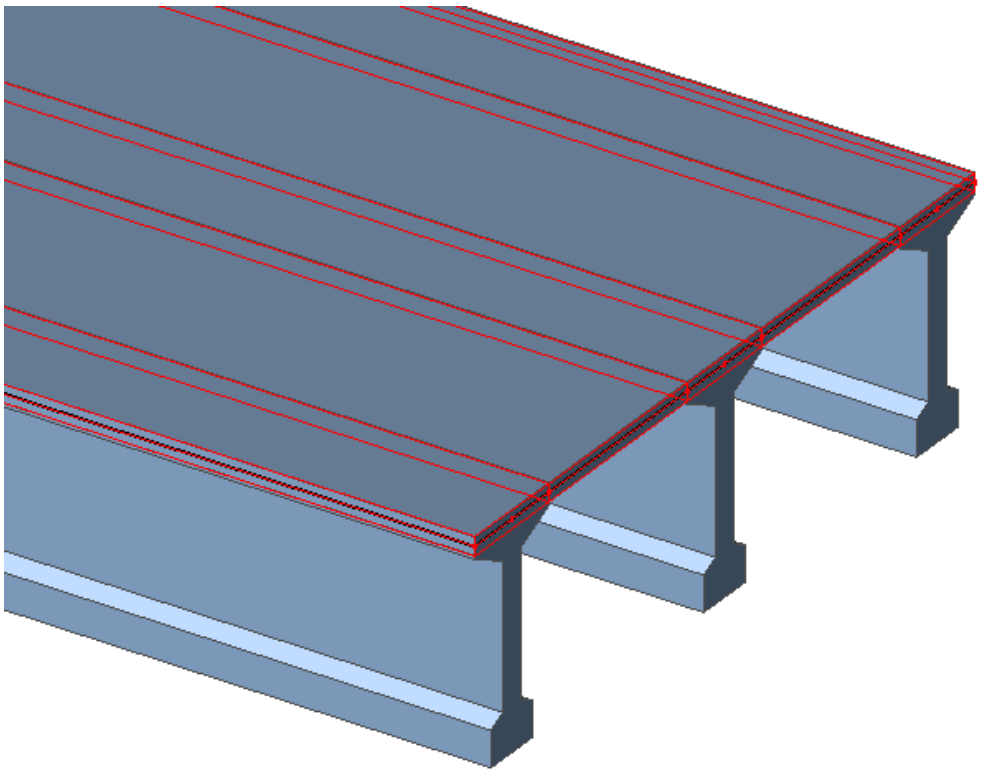

*Figure 73 the chosen plate model type with five sub regions of the deck*

### Load distribution

To further refine the model the deck was divided in five subregions assigned with their respective material properties. Basically, the plate parts above the girders were modeled as the flanges of the girders. Resulting in a more realistic representation of the lab prototype (Figure 73). The linear distribution was calculated: 14% 72% 14%. The main beam is loaded with 72 percent. With this, redistribution is possible up to a hundred percent (Figure 74). The reason why is the long span with high loading of the main beam. Later it is found that for shorter spans the load distribution is higher and the main beam is loaded with less than fifty percent, resulting in redistributions less than hundred.

### Midspan displacements

Membrane action is only activated if the relative girder displacement is larger than the slab midspan displacement. To determine the midspan displacements, another numerical model is made withhout the main beam present (Figure 75). They are determined numerically in the next section. A clear span of 3450 mm is considered (Figure 74).

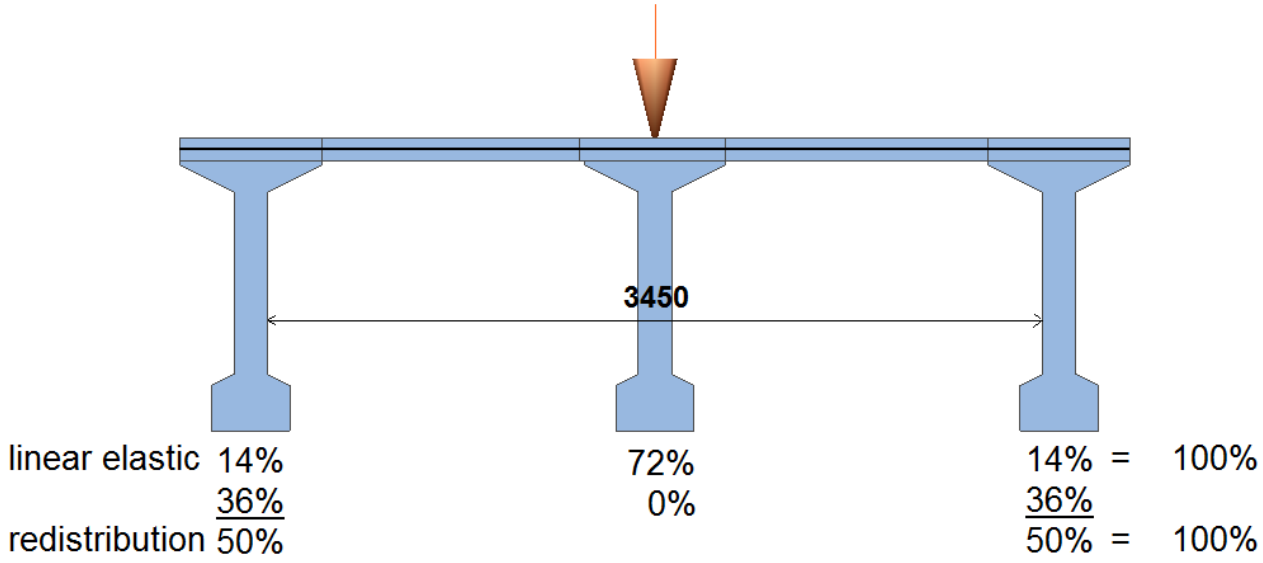


*Figure 74 linear elastic redistribution*

## Comparing displacements

### Determining slab midspan displacement

First, the slab bending capacity is determined with Rankin. The bending capacities with arching are between 133 and 178 kN (Table 7).

And then the numerical slab model is used to determine the midspan slab displacement Figure 75 shows that for a slab bending capacity of 133 kN, a displacement of 7.8 mm is found numerically. The rest of the displacements are determined in the same way (Table 7). In fact the slab midspan displacements are the critical displacements and the relative girder displacement needs to exceed these values.

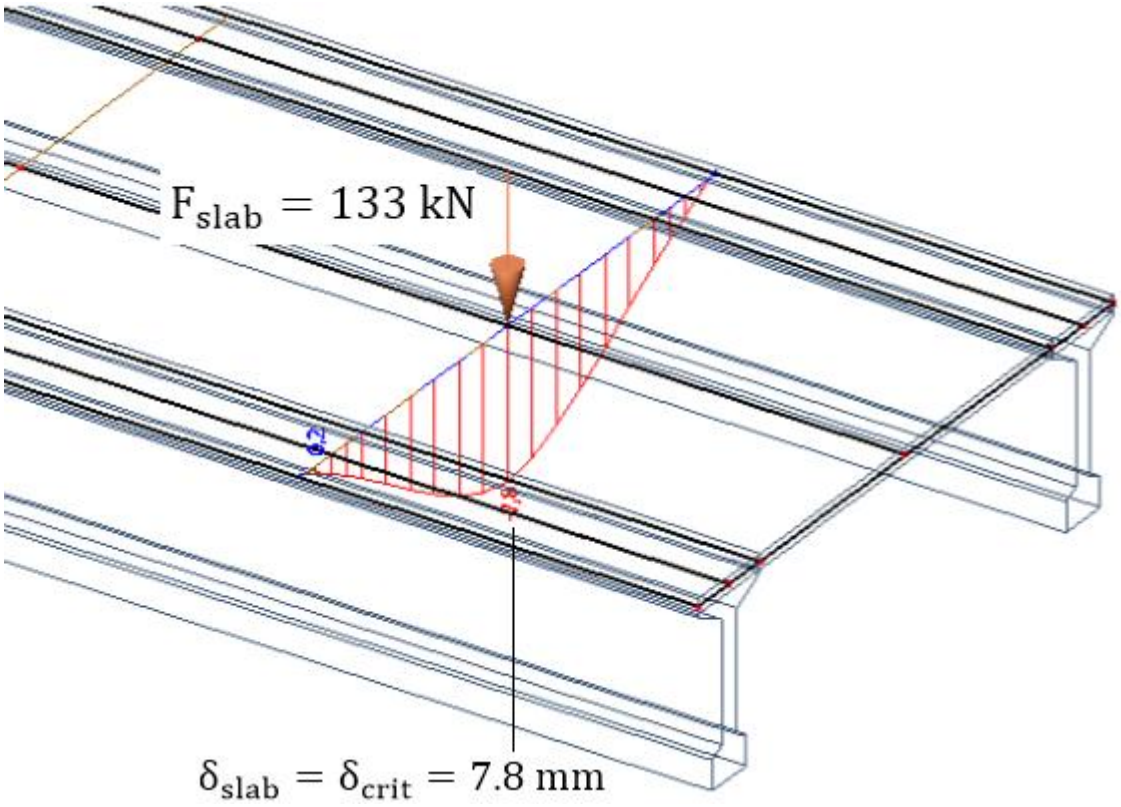


*Figure 75 midspan slab displacement determined for the slab bending capacity according to Rankin (SS)*

*Table 7 overview of results of bending capacities and slab midspan displacements*

| Method | Slab Bending Capacity $F_{slab,lower}$ [kN] | Slab midspan/critical displacement $\delta_{slab} = \delta_{crit}$ [mm] |
|---|---|---|
| **Rankin (SS)** | **133** | **7.8** |
| **Rankin(SS/FE)** | 172 | 10.1 |
| **Rankin (FE)** | 178 | 10.5 |
| **Simplified (UK)** | 75 | 4.5 |

### Determining the critical girder load

The critical girder load is defined as the load for which the relative girder displacement exceeds the slab midspan displacement (Figure 76). At the critical girder load membrane action is assumed to activate.

The slab midspan displacements were already determined. And the numerical model is used to determine the critical girder load (Figure 76 on the left, and Figure 77).

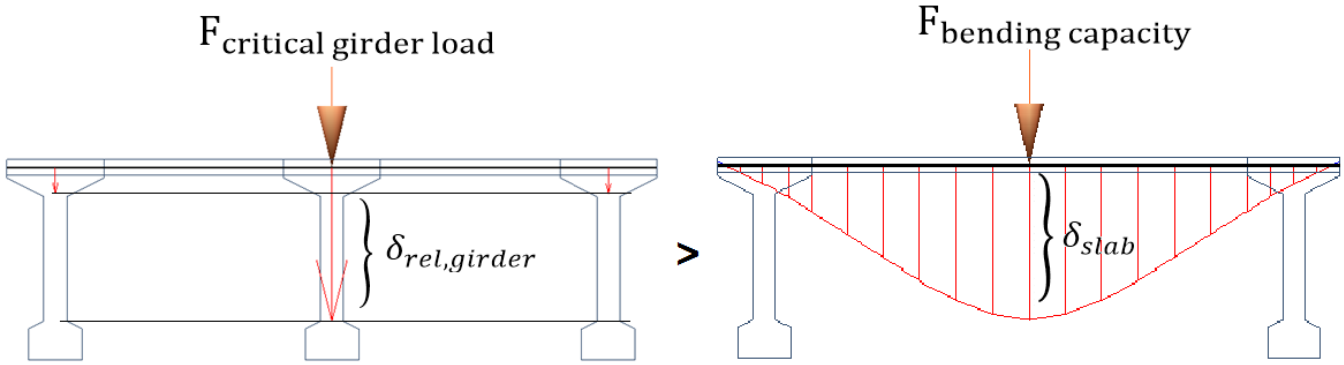


*Figure 76 numerically determining relative girder displacement*

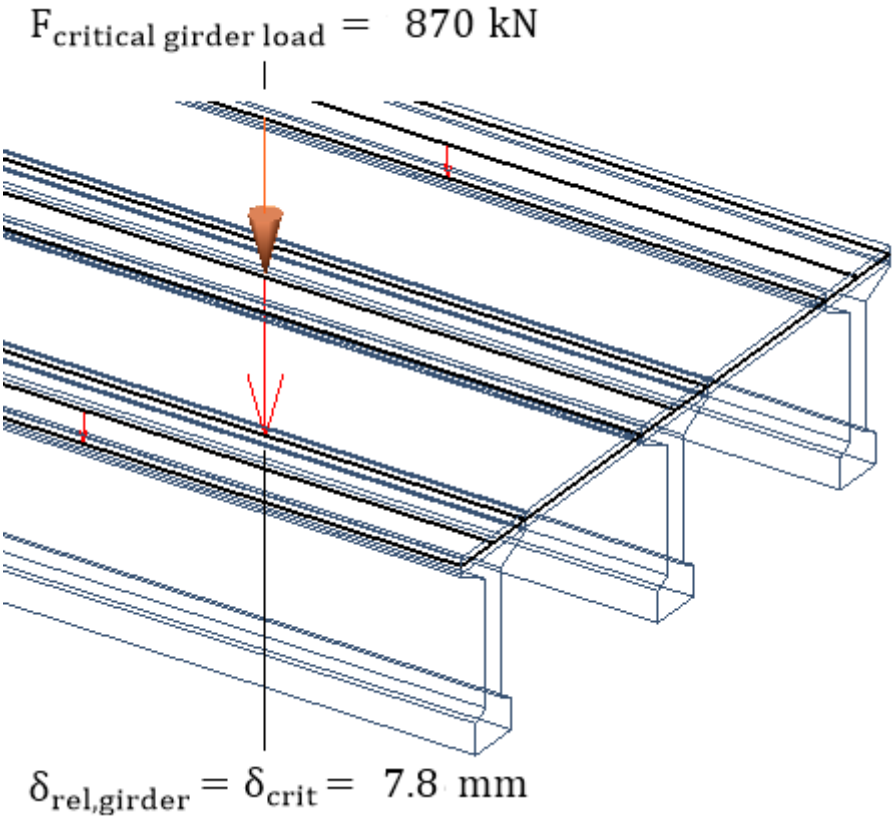


*Figure 77 determining the critical girder load, for which membrane action activates*

Figure 77 and Table 8 show that for a slab midspan/critical displacement of 7.8 mm, the critical girder load is 870 kN. After the critical girder load is reached and membrane action is activated, the slab is assumed to behave plastically up till failure. It is the question whether the slab can deflect that much. This is discussed later.

It was also questioned whether membrane action could be activated before the linear capacity was reached. The critical girder loads are smaller than the earlier determined linear beam load, 1550 kN (Table 8). Therefore, it is suggested numerically that membrane action could activate earlier. This is possible as soon as 870 kN is reached (Table 8). The load distribution causes the main beam to be loaded with 72 percent of the effect of the external load. This gives the following calculation:

$$870 * 0.72 = 626\ kN$$

When taking into account the load distribution, membrane action could be activated at a load of 626 kN, according to the numerical calculations (Figure 78).

*Table 8 overview of results of slab midspan displacements and critical girder loads*

| Method | Slab midspan displacement [mm] | Critical girder load [kN] |
|---|---|---|
| **Rankin (SS)** | 7.8 | 870 |
| **Rankin(SS/FE)** | 10.1 | 1117 |
| **Rankin (FE)** | 10.5 | 1160 |
| **Simplified (UK)** | 4.5 | 444 |

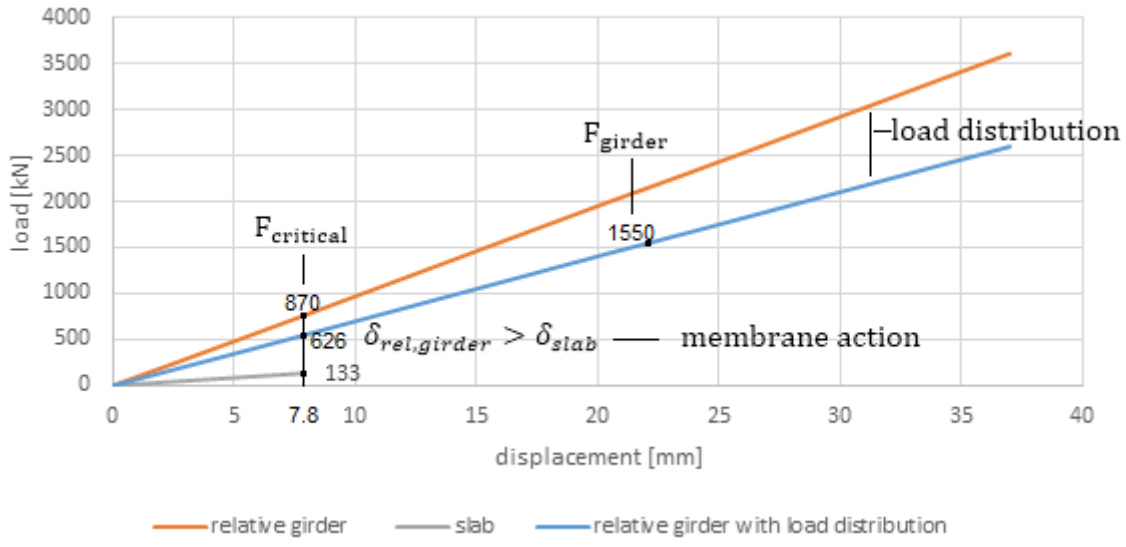


*Figure 78 membrane action activated at the instant the relative girder deflects more than the slab*

# Summary

### Summary of the numerical model

The questions from chapter 5 were partly answered. The load distribution of the bridge system was determined. And the behavior of the main beam and slab were modelled: the slabs displacements and relative girder displacements were determined.

The numerical model is used to see what the effect of the load distribution was on the main beam.

For a span of 3450 mm, 72 percent of the load was determined to be present on the main beam. This means the spreading is not high. However, it means that for a linear system, and for a long span, 3450 mm, redistribution till 100% is theoretically possible.

Finally, the main beam displaces more than the neighbor beams. This is favorable for the activation of membrane action. This is for a long span, later the situation for a short span is considered. And the numerical model is used to investigate if membrane action could be activated earlier in the linear loading phase.

# Chapter 7 *Method 2: Numerical Model*

## Introduction

The second method is similar to the first, but uses different assumptions and the numerical model. In order to determine the total slab capacity provided, the activated slab area is calculated again, but with the numerical plate model. And after identifying the activated part, the same method from Chapter 5 is used to determine the total slab capacity. And finally slab and beam capacity are added together to give the total bridge capacity.

## Activated slab area

### Lower bound limit

First, the earlier determined $\delta_{girder,max} = 37\,mm$ is used. It is assumed the slab behaves plastically and has sufficient capacity and ductility to deflect this much. This is discussed later.

The numerical model is used to check if the maximum girder displacement, 37 mm, is reached and this occurs at a load of $F_{bridge,max} = 2780\,kN$ (Figure 79).

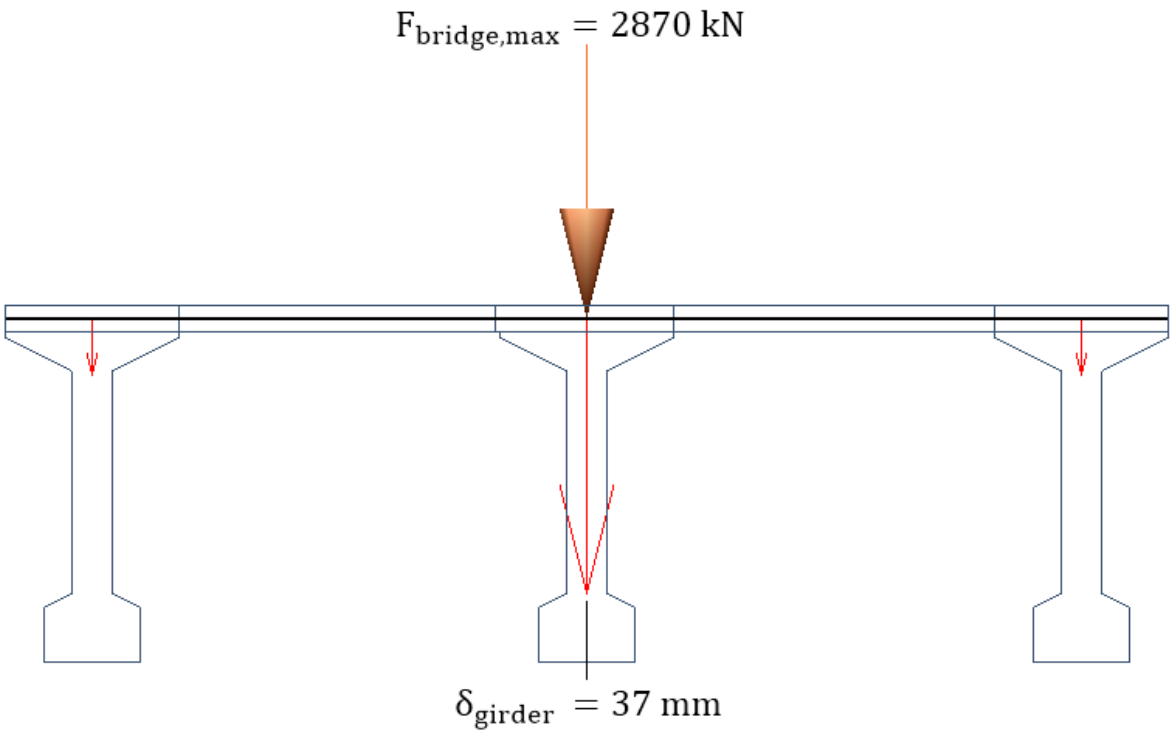


*Figure 79 maximum girder displacement of 37 mm*

With 72 percent of the effect of the external load on the main girder, this gives:
$F_{girder,max} = F_{bridge,max} * 0.72 = 2067\ kN$
The lower bound limit is the girder load $F_{girder}$, 1550 kN.
However, the load distribution is used to determine the equivalent load for the bridge:
$F_{bridge} = \frac{F_{girder}}{0.72} = \frac{1550}{0.72} = 2153\ kN$ (Figure 80).
The lower bound limit is given in Figure 81. Redistribution is assumed to be possible up to a 100%. And the girder is assumed to have a capacity between 1550 and 2067 kN, this is a safe underestimate (Figure 81).

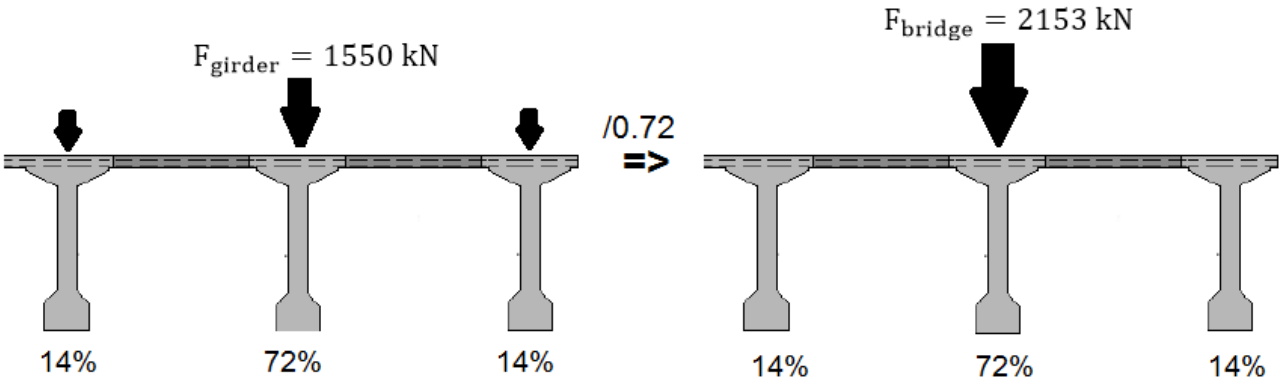


*Figure 80 converting load on single girder, top, to equivalent bridge load, bottom*

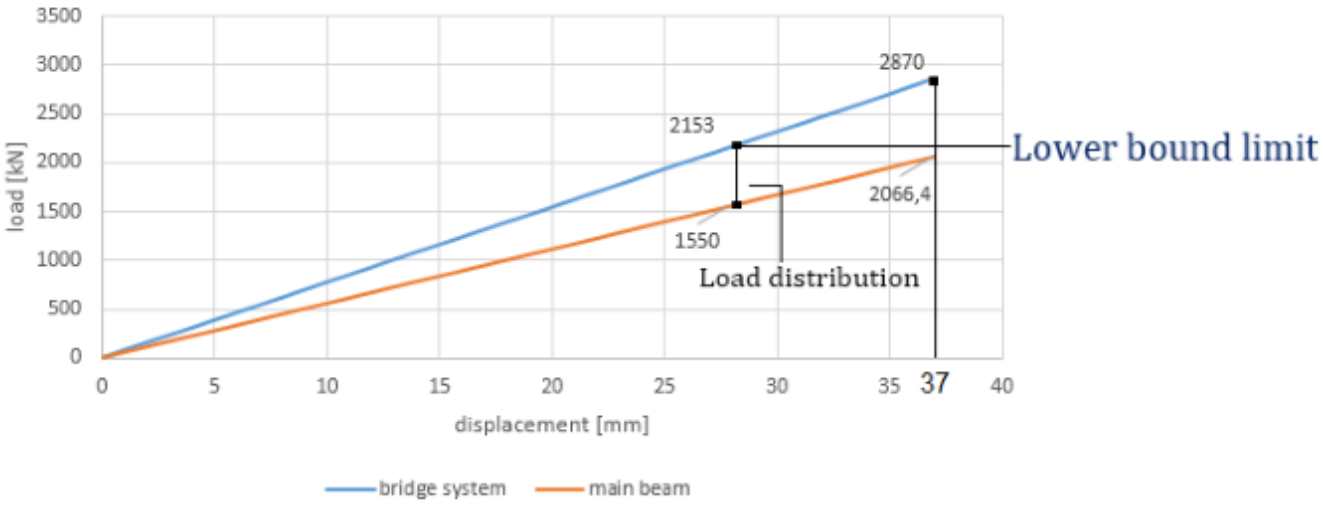


*Figure 81 lower bound limit of the bridge capacity of the numerical model*

### Critical deflection

The next step is to numerically determine the critical deflections. The slab midspan displacements are in fact the critical deflections: $\delta_{slab} = \delta_{crit}$ (Table 9).

First, the slab bending capacity $F_{slab}$ is determined. And then numerically the slab midspan displacement is determined. For a slab bending capacity of 133 kN, the critical deflection is 7.8 mm. This is the instant at which the relative girder deflections exceed the critical deflections and membrane action is activated. For a critical deflection of 7.8 mm, the critical girder load is 870 kN (Figure 82).

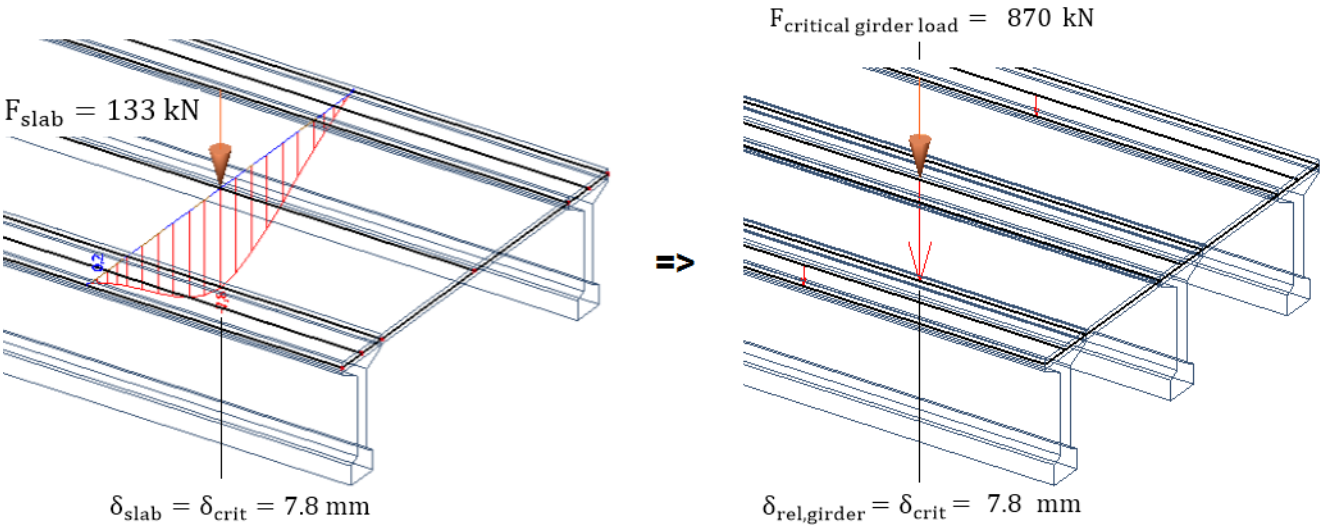


*Figure 82 determining critical deflection and critical girder load*

*Table 9 critical displacement for which CMA is activated*

| Method | Slab Bending Capacity [kN] | Critical deflection [mm] | Activated beam span [m] |
|---|---|---|---|
| **Rankin (SS)** | **133** | **7.8** | 8.9 |
| **Rankin(SS/FE)** | 172 | 10.1 | 8.2 |
| **Rankin (FE)** | 178 | 10.5 | 8 |
| **Simplified (UK)** | 75 | 4.5 | 10 |

### Activated beam span

After that, the activated beam span and slab area is determined with the maximum displacement of 37 mm and the critical deflection of 7.8 mm. Figure 83 shows the activated beam span, and Figure 84 the activated slab area, as part of the whole deck of the prototype, to display how much of the total slab area is activated.

And for the rest of the bending capacities, the same process is followed, the results are given in Table 10.

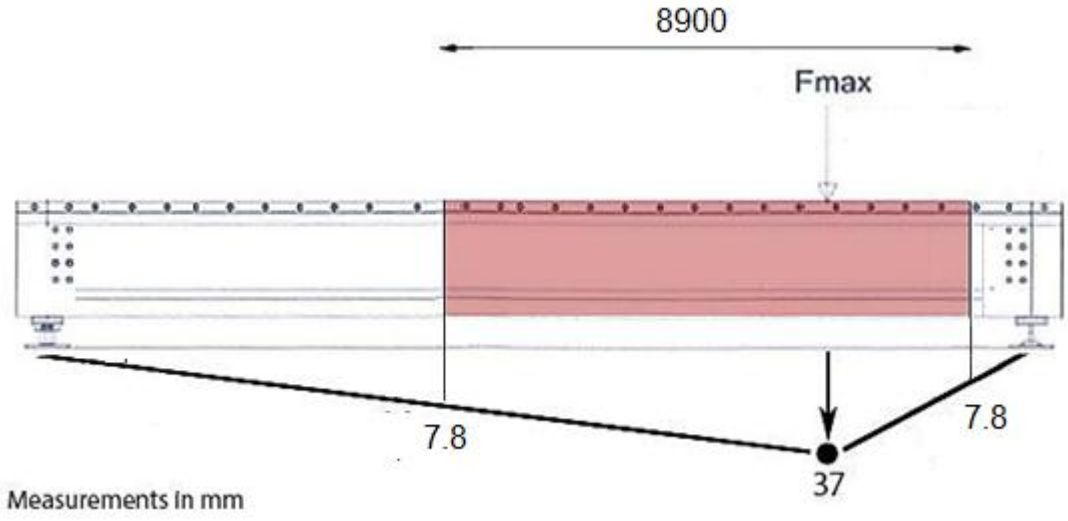


*Figure 83 activated beam span (not on scale)*

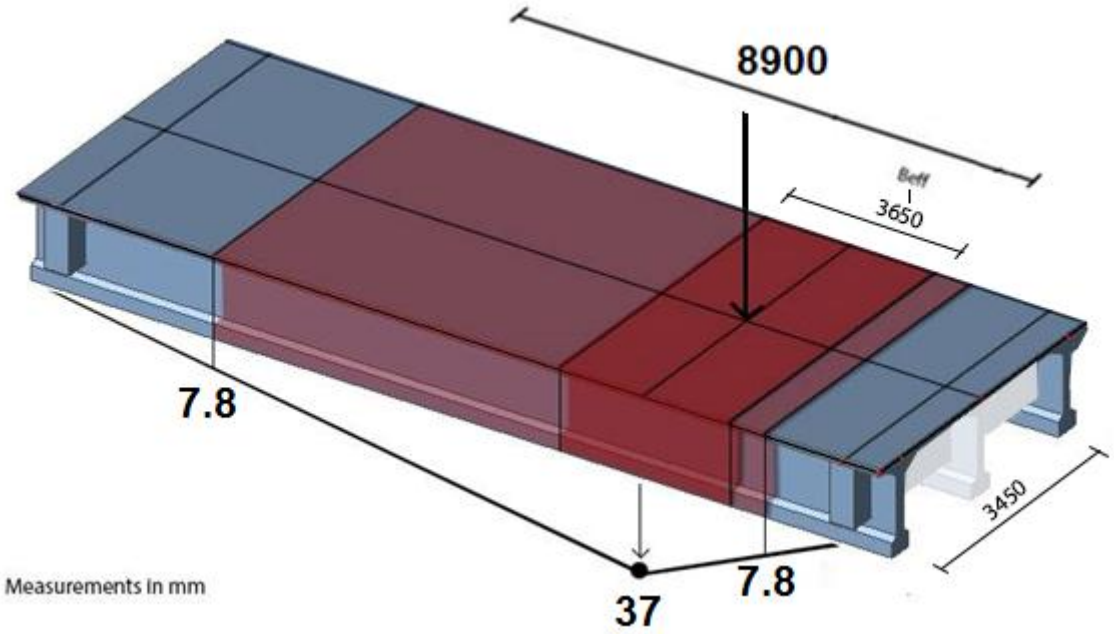


*Figure 84 effective width and activated length (not on scale)*

## Total slab capacity

The span of 8.9 m is activated (Figure 83 and Figure 84). Therefore an effective width of 3.65 m (shown in Figure 57 of Chapter 5) and a bending capacity of 133 kN per activated slab strip gives the following total slab capacity:

$$n[-] = \frac{\text{activated slab span[m]}}{\text{effective width slab strip[m]}}$$

$$\text{total slab capacity [kN]} = n * \text{slab } \mathbf{bending} \text{ capacity strip[kN]} \qquad (40)$$
$$\mathrm{F}_{\mathrm{slab,upper}} = n * \mathrm{F}_{\mathrm{slab,lower}}$$

$$n = \frac{8.9}{3.65} = 2.45$$

$$\mathrm{F}_{\mathrm{slab,upper}} = 2.45 * 133 = 325\ kN$$

The numerically determined maximum load for a maximum displacement of 37 mm is 2870 kN. The linear beam capacity, 2153 kN, after calculating the equivalent bridge load, can be contributed to the total capacity, since it is assumed that slab and beam work together.

This leads to the total bridge capacity of 2543 kN when the beam capacity, 2153 kN, and total slab capacity are summed up:

$$\mathrm{F}_{\mathrm{total}} = \mathrm{F}_{\mathrm{girder}} + \mathrm{F}_{\mathrm{slab,upper}} = 2153 + 325 = 2478\ kN$$

The same calculations were done again for Rankin (SS/FE), (FE), and the UK method, for which the same effective width is assumed to be present. The results are summarized in Table 10. And it is shown that none of the results reach the numerically determined maximum load, 2870 kN.

The lower and upper bound limit of the bridge load is given in Figure 85. With the load distribution it is checked how much the main beam is loaded for the lower and upper bound limit:

$0.72 * 2153 = 1550$ kN and $0.72 * 2543 = 1830$ kN

Which means the beam load is estimated to be between 1550 and 1830 kN. This seems a safe underestimate (Figure 86).

The discussed methods that calculated the slab bending capacity do not take into account the transverse prestressing of the slab (as mentioned at the end of Chapter 4).

*Table 10 results total deck capacity*

| Method | Slab Bending capacity $\mathbf{F_{slab,lower}}$ [kN] | Activated beam span [m] | Total slab capacity $\mathbf{F_{slab,upper}}$ [kN] | Total bridge load [kN] |
|---|---|---|---|---|
| **Rankin (SS)** | 133 | 8.9 | **325** | **2478** |
| **Rankin(SS/FE)** | 172 | 8.2 | 386 | 2539 |
| **Rankin (FE)** | 178 | 8 | 390 | 2543 |
| **Simplified (UK)** | 75 | 10 | 205 | 2358 |

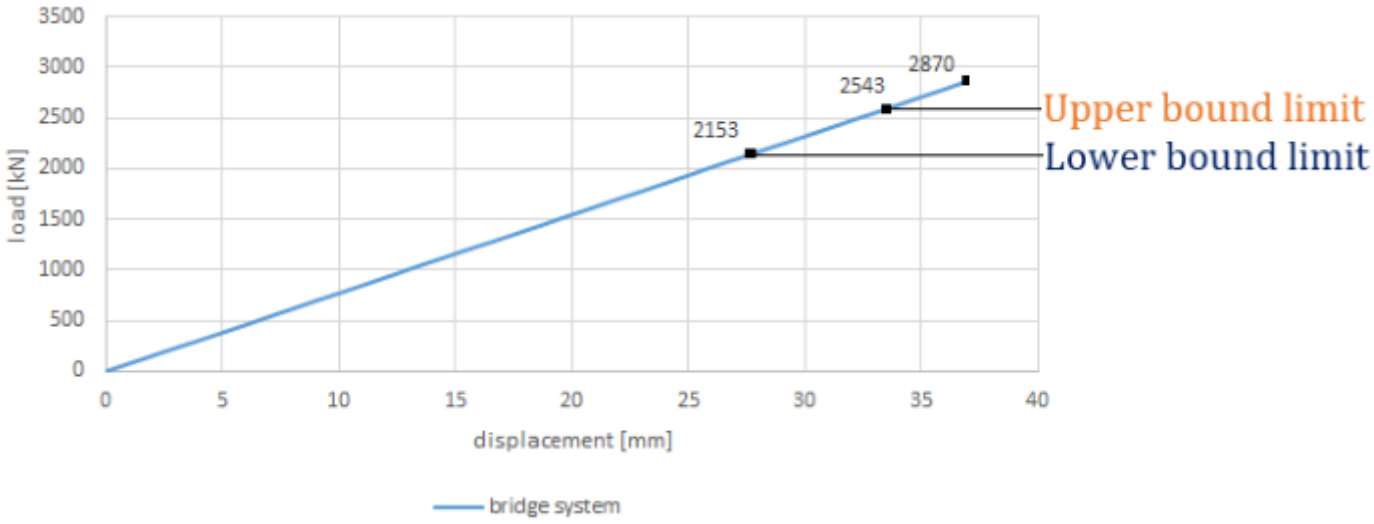


*Figure 85 range of the bridge's bearing capacity: lower, and upper bound limit using the numerical model*

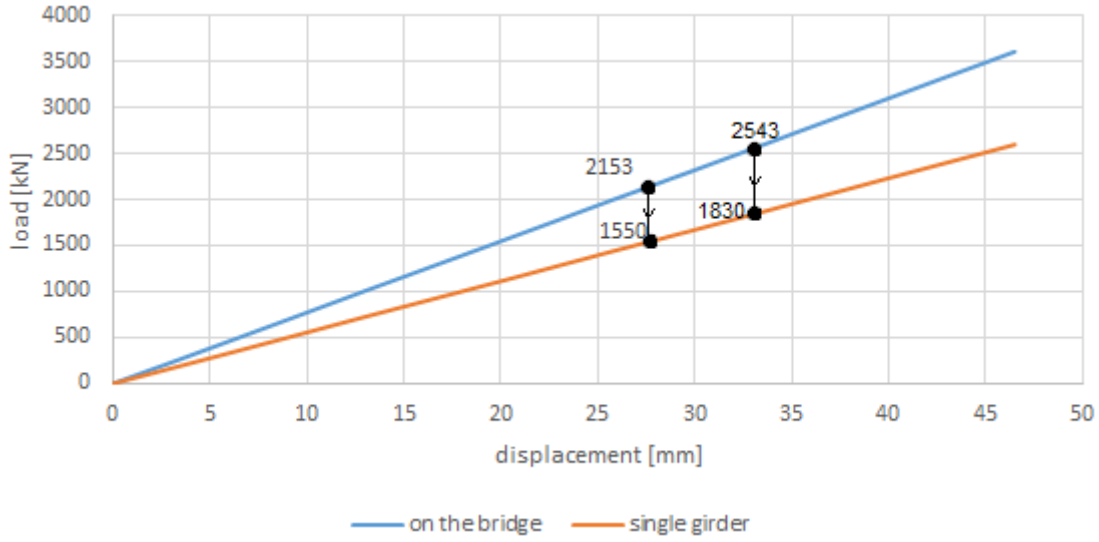


*Figure 86 load on the single girder after load distribution for the lower and upper bound limit values*

**Conclusions**

First, the load distribution plays a significant role in the calculation of the total slab capacity. Moreover, for different models with different load distributions the calculations and corresponding results would differ significantly.

Second, Table 10 shows that the resulting hidden slab capacity is 390 kN at most, which seems to be insufficient to achieve the maximum possible failure load determined numerically. And it is also insufficient to carry the girder load, as was shown in Chapter 5.

The slab has a too high span/depth ratio with a considered clear span, 3450 mm, and thin deck, 100 mm. This long clear span also influences the effective width, causing it to be long too, which means that the activated beam span is divided by long wide strips, ultimately causing a low calculated total slab capacity (Equation (40)).

In the second method, the maximum deflection for the maximum load $F_{total}$, 2543 kN, is 33 mm. This implies that the slab needs to deflect this much as well.

So assuming a slab defection of 10 mm at maximum bending capacity (Table 9) up to 33 mm, the slab needs to deflect for 23 mm more after reaching its maximum arching capacity, 178 kN, assuming a bilinear type of deflection behavior, where the slab's capacity is assumed constant (Figure 87). If this is possible, is researched more in Chapter 8.

And 100% redistribution was possible, but the slab has a limited bending capacity and limits the total bridge load. And finally, it is implied numerically that membrane action is activated before the girder load $F_{girder}$ is reached (Figure 87).

Overall method 2 seems to give a safe approach.

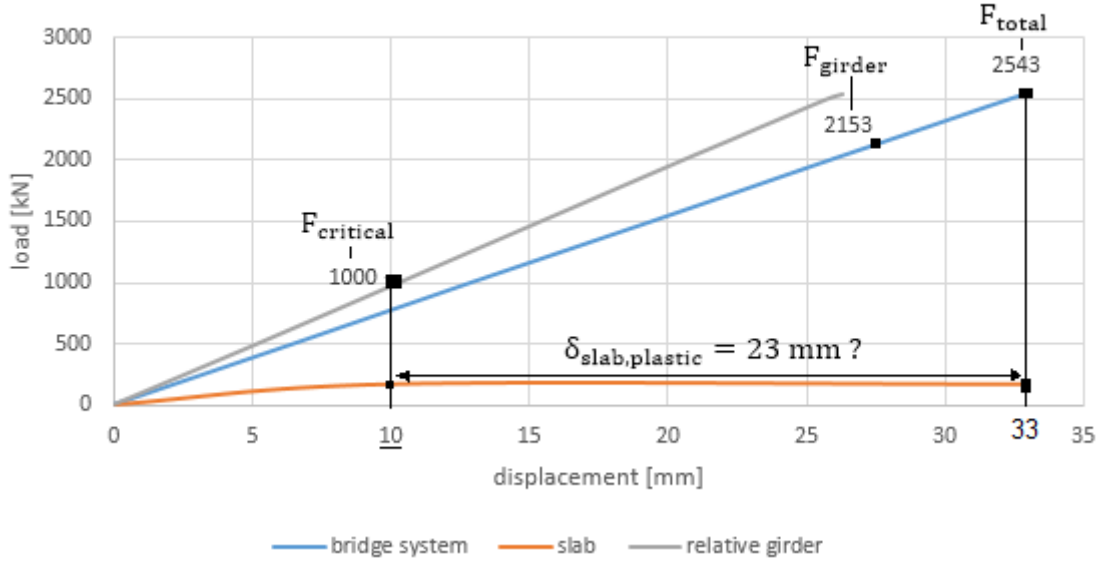


*Figure 87 possible deflection range of the slab*

## Comparison method 1 and 2

Method 1 and 2 are compared. Method 1 is the disconnected system approach, without load distribution. Method 2 is with the numerical model that determines the load distribution. Their maximum loads of the bridge system, the upper bound limits, are compared. And the upper bound slab bending capacities are compared (determined with Rankin F/E).

It shows that method 1 assumed that membrane action activated earlier at 7mm (Table 11). However, this was without load distribution, and the main beam took more load, reaching the critical deflection earlier than for method 2.

When the critical deflection is smaller, a longer span is activated with membrane action. This is also shown in (Table 11).

A longer activated span gives a higher total slab capacity $F_{slab,upper}$.

However, the main beam contribution to the total load on the bridge system is higher for method 2. This is because of the load distribution. In method 1, $F_{girder} = 1550\ kN$ was used. But in method 2 the load distribution was taken into account, with this the load on the bridge gives: $F_{bridge} = \frac{1550}{0.72} = 2153\ kN$.

This is an increase of $2153 - 1550 = 603\ kN$. This gives the higher total bridge load for method 2. Both methods however are safe underestimates of the reality, because of the assumptions taken into account.

One final note, the slab capacity does not exceed 500 kN. The reason for this might be the location of the load or the high slenderness ratio of the slab. This is considered more in depth in chapter 8.

*Table 11 comparison method 1 and 2*

| Method | Critical deflection [mm] | Activated beam span [m] | Total slab capacity $\mathbf{F_{slab,upper}}$ [kN] | Total bridge load [kN] |
|---|---|---|---|---|
| **1 Disconnected** | 7 | 9.2 | 445 | 1995 |
| **2 Numerical** | 10 | 8 | 390 | 2543 |

# Summary

### Summary of the second method

- Determine the linear load distribution (numerically)
- Establish $\delta_{girder,max}$ (empirically)
- Determine $F_{girder,max}$ of the model for $\delta_{girder,max}$
    - Determine equivalent $F_{bridge}$ with load distribution
- Determine bending capacity of single slab strip $F_{slab,lower}$
- Determine the critical girder load
- Determine the total activated slab area
    - Determine the critical deflection (numerically)
    - Determine the activated beam span
    - Determine the effective width of a single slab strip
- Determine the total slab capacity $F_{slab,upper}$
- Determine lower bound limit of the bridge capacity: beam capacity
- Determine upper bound limit of the bridge capacity: beam capacity plus total slab capacity

### Important points for further study

- Influence of load location (Appendix C)
- Influence of slenderness on the methods (Appendix C)
- Deflection behavior of laterally restraint slabs (Chapter 8)
    - Redistribution possibility
    - Slab deflection at peak load
    - Slab ultimate deflection
    - Material parameters: e.g. concrete strength, reinforcement, etc.
    - Geometrical parameters: e.g. span/depth ratio

# Chapter 8 *Research on compressive membrane action in concrete deck slabs*

## Introduction

This chapter investigates more research on the behavior of deck slabs. Extra attention is given to failure mode, failure load, thickness of the slab and the slenderness ratio. The research is meant to give insight about possible trend behaviors of the concrete deck slabs, especially laterally restraint ones.

## Background

In the next part the bridge ‘De Vecht’ is discussed. There the total theoretical failure load will be determined using the methods discussed in previous parts. An important part of that calculation will be the deck slab. Therefore, to make a good judgment of the failure load, more insight of the slabs is needed. That is why this chapter deals with more research on decks slabs.

Attention is given especially to research where the tested slabs are comparable with or give insight into the possible behavior of the slab of ‘De Vecht’. This concerns laterally restraint slabs with thicknesses larger than 100 mm and where *bending*, and not punching shear, is the main failure mechanism, the expected failure mechanism of the slab of ‘De Vecht’. All of the research mentioned in this chapter can be found in Appendix D.

## Laterally restraint reinforced concrete slabs

The tested slabs of (Taylor, Rankin, & D.J., 2001) are laterally restraint, thicker than 100 mm, have a slenderness of 9.5 and show bending as the prominent failure mechanism. The shown test results deal with full scale one-way spanning *reinforced concrete* slabs. The following observations are made.

### Compressive strength

First, a higher compressive strength does not necessarily mean a higher ultimate deflection or a higher deflection at peak load (shown in Figure 88 and Figure 89, where S1 till S5 are the laterally restraint slab strips tested in the study). The ultimate deflection follows a trend that a higher concrete strength could result in a higher ultimate deflection (Figure 88). The trend is less pronounced for the deflection at peak load (Figure 89).

It is important to know how far the test slabs deflect. The deflection of the slab of 'De Vecht" can be predicted later with the test slab information. The ultimate deflections range between 30 and 45 mm. And the found deflections at peak load range between 21 and 36 mm.

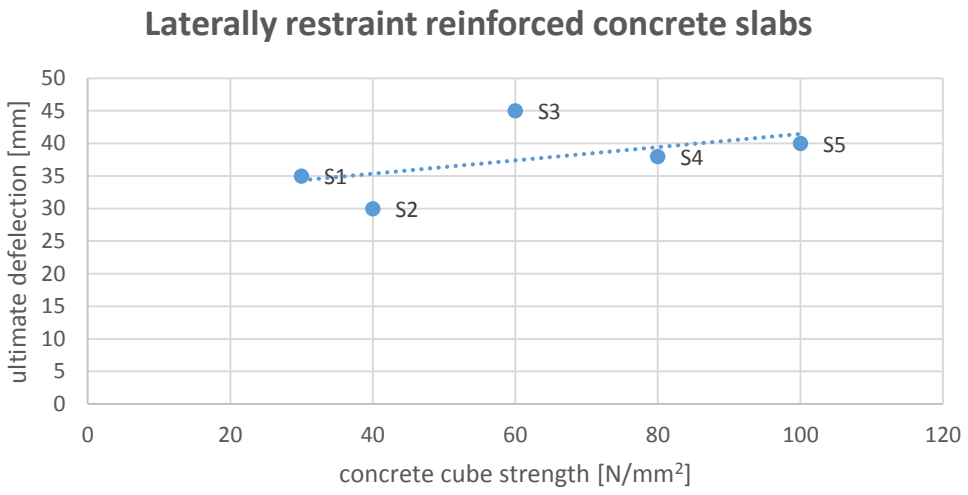


*Figure 88 concrete cube strength vs ultimate deflection, $\lambda = 9.5$ (Taylor, Rankin, & D.J., 2001)*

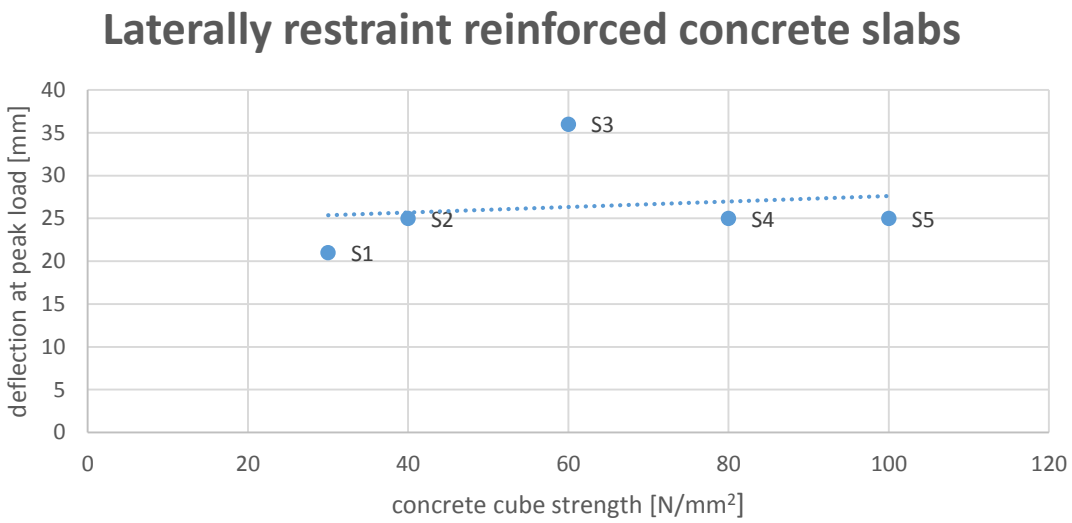


*Figure 89 concrete cube strength vs deflection at peak load, $\lambda = 9.5$ (Taylor, Rankin, & D.J., 2001)*

*Table 12 range $\delta_u/h$ ratio*

| Deflection | $\delta_u/h$ ratio [-] | | |
|---|---|---|---|
| | Lower bound | Upper bound | Average |
| **Ultimate** | 0.2 | 0.3 | 0.25 |
| **Peak load** | 0.14 | 0.24 | 0.19 |

The thickness of the five tested slabs is 150 mm, meaning that the $\delta_u/h$ ratio (Table 12) ranges between: 0.2-0.3, with an average of about 0.25, with $\delta_u$ as the ultimate deflection. For the deflection at the peak load this gives a ratio between: 0.14-0.24, with an average of 0.19.

Moreover, slabs with a higher compressive strength behave stiffer in the linear phase (Figure 196 of Appendix D). Higher compressive strength also means a higher failure load (Figure 90, and Figure 197 in Appendix D). (Muthu, 2006) and (Taylor & Mulin, 2005) agree with this trend. Generally, a higher concrete strength means a higher failure load (Table 45 and Table 48 of Appendix D).

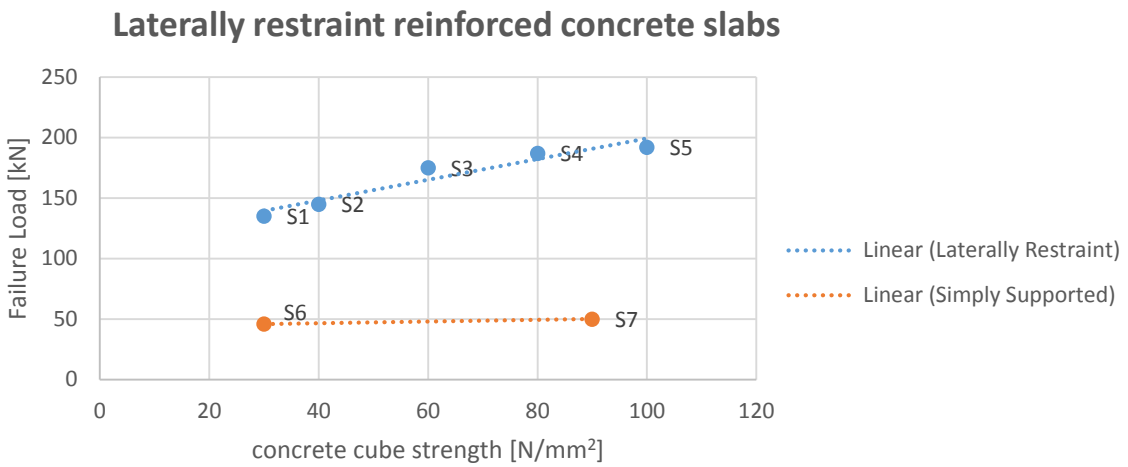


*Figure 90 concrete strength vs failure load displaying lateral restraint effect, $\lambda = 9.5$ (Taylor, Rankin, & D.J., 2001)*

### Effect of lateral restraint

In the tests some simply supported slabs were tested for comparison, too. These slabs have a much lower failure load than the laterally restraint ones. The difference in fail load between the two types of slabs is almost a factor 4 to 6 (Taylor, Rankin, & D.J., 2001) and (Taylor & Mulin, 2005). Here it is found again that the effect of laterally restraining the slabs has a positive influence on increasing the failure load (Figure 90).

This lateral external restraint effect, expressed as the stiffness factor $K_r$ calculated by the Rankin method, influences the failure load. The failure load increases when the restraint effect does too. (Taylor, Rankin, & D.J., 2001) ran two phases of tests, and the second had a higher restraint than the first (Table 46 and Figure 197 of Appendix C). Which indicated an increase in the arching action with increased external lateral restraint and suggested that any theory for the prediction of the ultimate capacity of laterally restrained slabs must take into account both the concrete strength and the degree of external restraint (Taylor, Rankin, & D.J., 2001).

It is noted that slabs with high deflections were fixed ended (Table 47 of Appendix D). The end restraint was provided by a self-straining stiff steel frame. And to ensure a fully encased support, provision was made for bolting through the depth of the slab at each end with a stiffness factor $K_r = 197\ kN/mm$ (Taylor, Rankin, & D.J., 2001).

## Failure load and failure mode

### Failure load

In (Taylor, Rankin, & D.J., 2001) the predicted failure loads were compared to the actual failure loads. The Rankin method was used to calculate the slab capacity, again showing a lower bound underestimate of the actual slab capacity (as was seen in Chapter 4). The ratio between the actual and the predicted load was on average 1.16 (Table 46 of Appendix D). This means that the Rankin method is a conservative method with a safety margin of about 16 percent (this conservative feature was also noticed in Chapter 4).

### Failure mode

In (Taylor, Rankin, & D.J., 2001) the main failure mode was *bending*, and ultimately crushing (Figure 91). The crushing in the compression zone became more pronounced in the slabs with higher concrete strengths, exhibiting behavior similar to an over-reinforced slab. The increase in capacity with increasing concrete strength and the evidence of high compressive forces characterized by concrete crushing between the end plates and the ends of the slab, in addition to the compression zones below the load point, indicated the development of membrane action (Taylor, Rankin, & D.J., 2001). And none of the slabs failed in punching shear. It is stressed again that reinforced concrete slabs were tested.

*Figure 91 bending, and ultimately crushing, as failure mode for a laterally restrained reinforced concrete slabs (Taylor, Rankin, & D.J., 2001)*

The results of all the different researches (Appendix D) are compared in Figure 92 and Figure 93. It is found that the ultimate slab deflections of (Taylor, Rankin, & D.J., 2001) are higher than the rest of the slab deflections of the other researches. The Taylor slabs are laterally reinforced concrete slabs, where bending seemed to be the failure mode. The other tests showed other failure mechanisms, where punching shear was common (Table 43 of Appendix D).

For the prestressed concrete models punching shear seemed to be the governing failure mechanism ( (Poston, 1988), (Marshe, 1997), and (Amir, 2014), shown in Figure 92 and Figure 93).

It is possible that slabs failing in bending provide higher ultimate deflections (Figure 93). The ultimate deflections for punching shear are lower, giving a good lower bound threshold, whereas the slab deflections for bending can be considered as an upper bound.

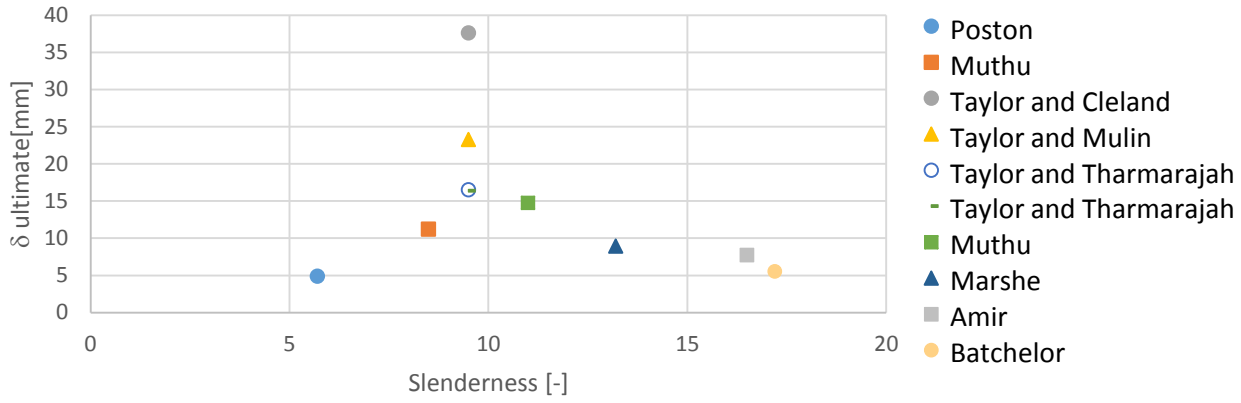


*Figure 92 slenderness vs ultimate deflection derived from the research on slabs*

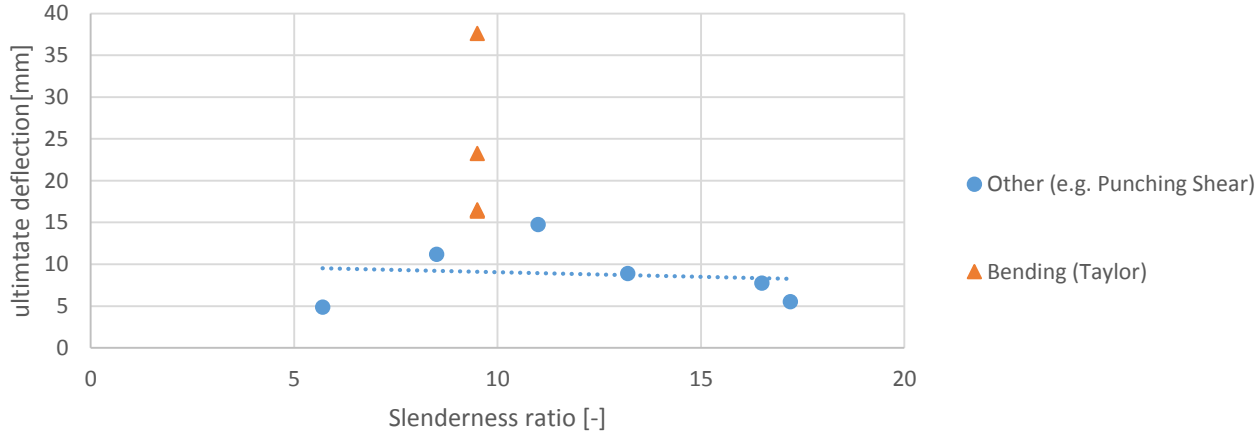


*Figure 93 comparison of possible failure modes for different slenderness ratios*

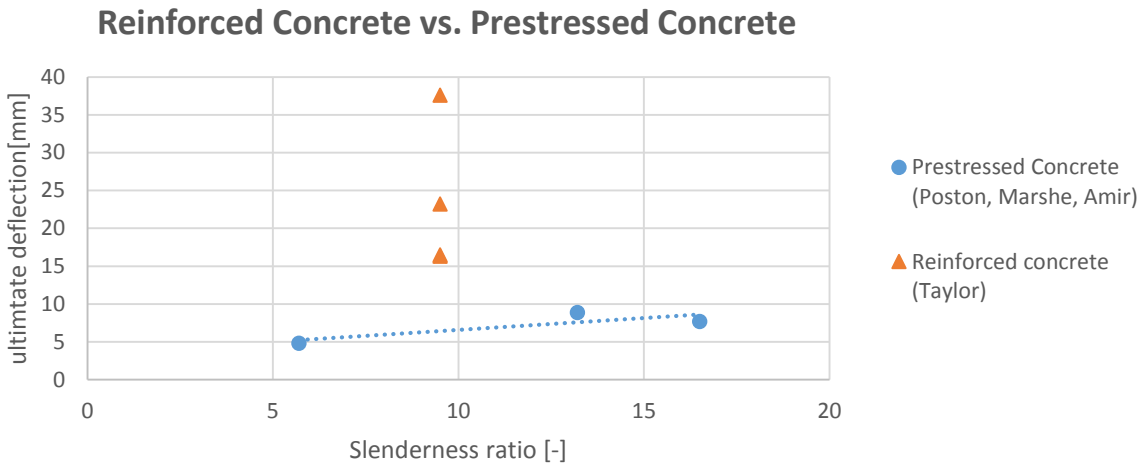


*Figure 94 comparison of reinforced and prestressed concrete*

In Figure 94 reinforced concrete is compared with prestressed concrete. The reinforced concrete slabs have higher ultimate deflections than was found for the prestressed concrete models. The reinforced concrete slabs failed in bending, and the prestressed concrete models failed in punching shear (Figure 93 and Figure 94).

Of all the researches discussed in this chapter, only (Taylor, Rankin, & Cleland, 2002) mentions bending as the main failure mechanism for the tested slabs. And in the past research discussed in Chapter 1 till 4, only (Amir, 2014) mentions bending as an occurring mechanism in the bridge deck slab. Therefore, a closer look is given to the respective results of these two researches. They are displayed again in Figure 95.

It is noted that the results of Taylor are valid for reinforced concrete and the results of Amir are valid for prestressed concrete. The Taylor slabs have a slenderness of 9.5, and the ones from Amir 16.5 (shown in Chapter 4). Overall, it is found that the lower the slenderness of the slab is, the higher the ultimate deflections are.

(Amir, 2014) also shows that when the transverse prestress level (TPL) of the slab is higher, the ultimate slab deflections are lower (Figure 96).

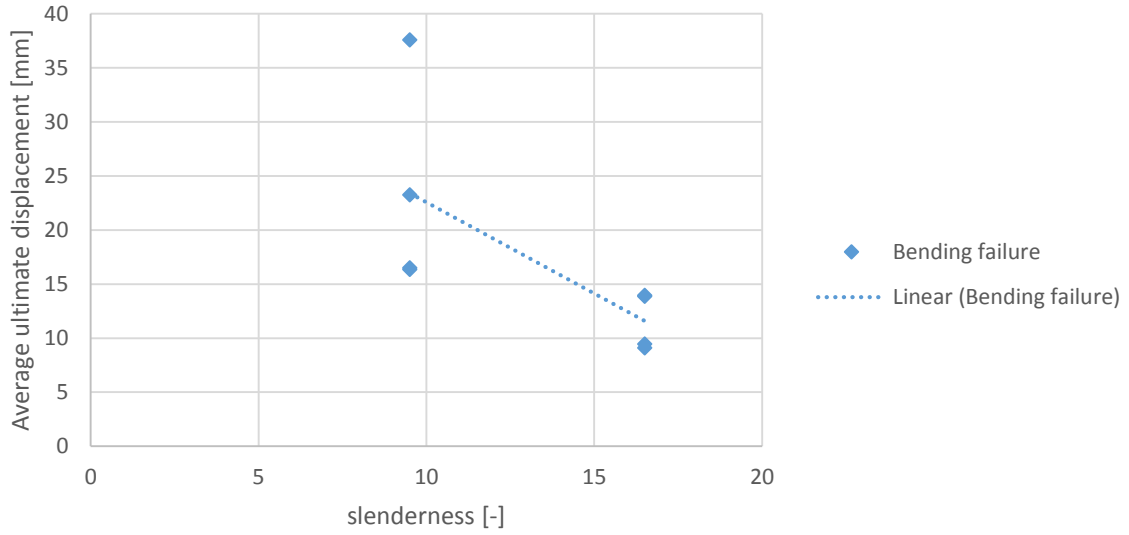


*Figure 95 relation between slab test results for failure in bending*

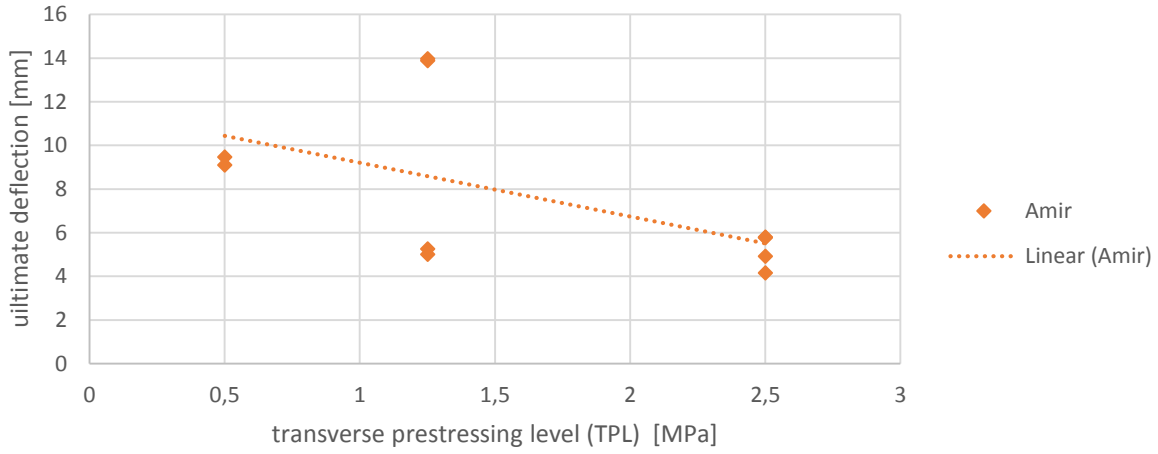


*Figure 96 relation between TPL and ultimate slab deflection, $\lambda$ = 16.5 (shown in Chapter 4) (Amir, 2014)*

### Deflection plateau

In the load deflection graphs of (Taylor, Rankin, & D.J., 2001), only, a deflection plateau was present. Meaning that the defection at peak load increased during loading and stopped at the ultimate deflection, showing a behavior which can be modeled as bilinear (Figure 97 and Figure 98). These tests were done on reinforced concrete.

The net panel load-deflection curves of (Marshe, 1997) were also bilinear. However, these tests were done on prestressed concrete.

The described plastic behavior leads to higher ultimate deflections. And if this plateau is present when loading other comparable slabs, such as from 'De Vecht', it provides an opportunity for redistribution of loads. When dealing with a directly loaded girder integrated in the deck this redistribution is beneficial for the total bearing capacity of the whole bridge deck.

Earlier the slab's ductility was questioned (Chapter 7). Therefore, this part gives more details regarding the slab's deflection behavior. For example, slab S5 showed a deflection of 25 mm at peak load and an ultimate deflection of 40 mm at failure, providing a range of 15 mm (Figure 98), during which redistribution can take place. Earlier (Chapter 7) it was stated that the slab needed to be able to displace 16 mm, which seems to be possible under the right conditions.

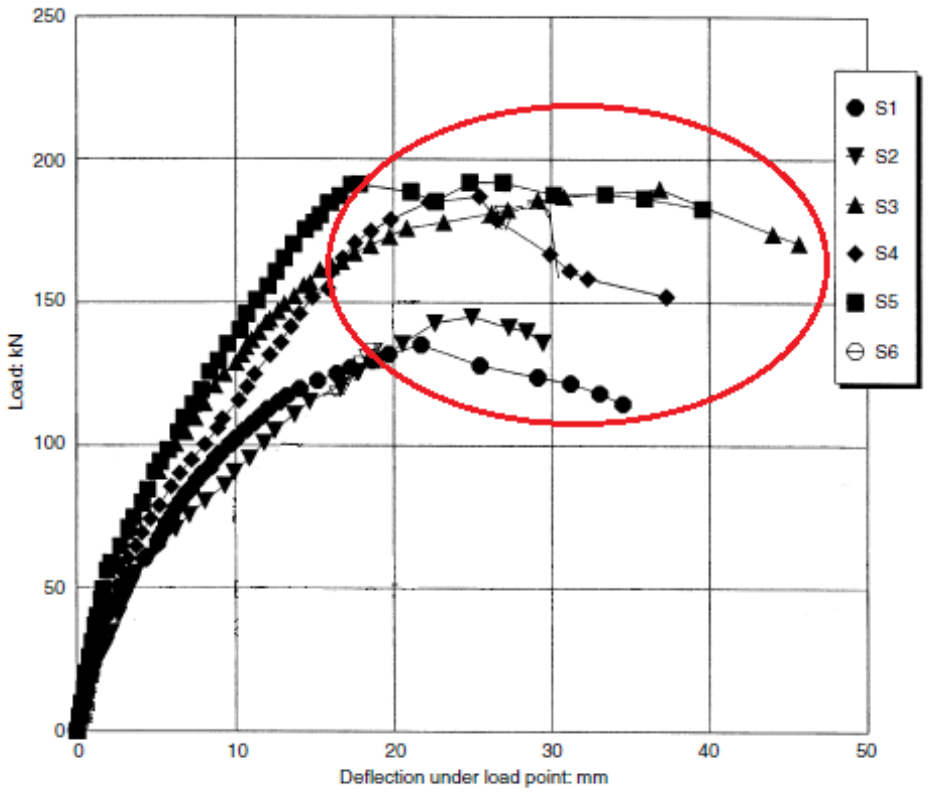


*Figure 97 plastic plateau possibly due to top and bottom reinforcment, $\lambda = 9.5$ (Taylor, Rankin, & D.J., 2001)*

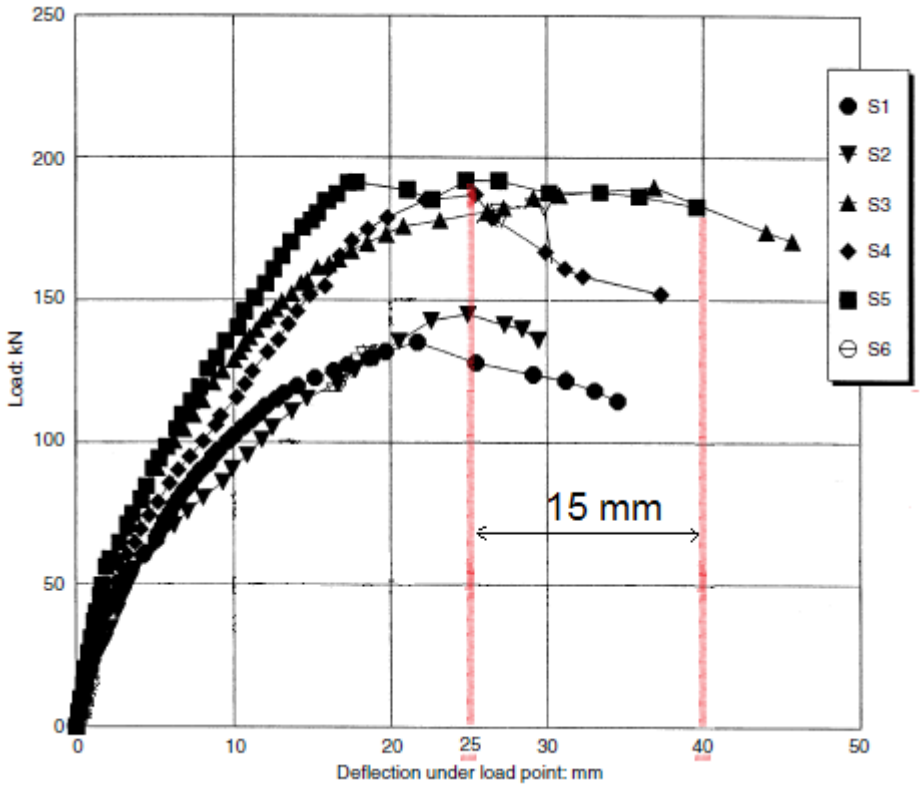


*Figure 98 plateau of 15 mm with deflection starting at 25, ending at 40 mm, for S5, $\lambda = 9.5$ (Taylor, Rankin, & D.J., 2001)*

### Reinforcement

High yield 12 mm diameter bars with a strength of 500 MPa were used. And top and bottom steel reinforcement was applied with a ratio of 0.68%. In other slabs different FRP reinforcement types were used, or reinforcement was only placed in the center ( (Taylor & Mulin, 2005) and (Taylor & Tharmarajah, 2014), shown in Appendix D). The effect of the reinforcement placing is also noticeable in Appendix D. Slabs S8 and S11 (Table 47, Figure 195, and Figure 196 of Appendix D) show a less ductile behavior than the rest of the slabs; S8 has only bottom reinforcement, and S11 only in the center. All the before mentioned aspects influenced the slab's ductility and need to be considered carefully when dealing with similar slabs.

## Summary

For the laterally restraint reinforced concrete slabs (Taylor, Rankin, & D.J., 2001), there is a strong correlation between failure load and concrete compressive strength: the higher the concrete strength, the higher the failure load (Figure 90). But a higher concrete strength does not necessarily mean a higher ultimate deflection (Figure 88 and Figure 89). And the failure load of the slabs never exceeded 500 kN, not even one designed with 100 MPa concrete compressive strength, but the considered span/depth ratio stayed constant.

Moreover, the effect of laterally restraining the slabs increased the bearing capacity with a factor 4 to 6 compared to simply supported slabs (Figure 196 and Figure 198 of Appendix D). And the more restraint the slabs were, the higher the failure load (Figure 197 of Appendix D).

Furthermore, the research showed that the Ranking method provides a conservative underestimate of the actual slab strip capacity with a safety margin of about 16 percent.

An observation was made that reinforced concrete slabs failing in bending showed higher deflections, ranging from 20 mm at peak load to 40 mm as ultimate deflection. The prestressed concrete slabs failing in punching shear had lower deflections around 10 mm (Figure 92 and Figure 93). Generally, according to the considered research, slabs failing in bending give higher deflections than slabs failing in punching. The tested slabs failing in bending were reinforced concrete slabs.

Finally, the fixed ended laterally restrained reinforced concrete slabs showed plastic behavior (Figure 97 and Figure 98) during which redistribution of loads can occur.

# Part 3 Calculating CMA In 'De Vecht' Bridge

# Chapter 9 *Calculations 'De Vecht' Bridge*

## Introduction

A series of tests are performed on 'De Vecht' bridge in Muiden. This is done in order to determine what the total bridge load is and how compressive membrane action in the slab plays a role in reaching that total load. It is the question whether the slab develops CMA and whether it is able to carry the load after the main beam fails, redistributing the load to the neighbor beams. This is the focus point of this chapter.

First, the geometrical and material parameters of 'De Vecht' bridge are discussed. The considered clear span and cross section of the deck is given. Other important factors such as slenderness, the span/depth ratio, lateral restraint and compressive strength are mentioned too.

All the before mentioned parameters are modeled with use of a numerical plate model, similar to the models shown before. The numerical model is used to determine the linear bearing capacity of the bridge (Appendix G), which is compared in Chapter 10 with the measured results.

But more importantly, the relative displacement is determined to determine whether the critical deflection is reached and compressive membrane action is developed.

Moreover, the slab capacity is determined using the considered methods. Punching as well as bending capacity is calculated where applicable. After that, the girder shear capacity is determined (Appendix F).

Finally, it is noted that the calculations in this chapter were made before the test results were available (given in Chapter 10).

## Geometrical and Material parameters

### Span/depth ratio

The center-to-center distance between two beams is 1225 mm (Figure 99). For the considered clear span 2270 mm is taken, after subtracting the thickness of the web, which is 180 mm (Figure 100).

$$L_s = 2 * L_{c.t.c} - b_{web} = 2 * 1225 - 180 = \mathbf{2270\ mm}$$

A low slenderness ratio of about 12.6 is present, which is favorable for activating compressive membrane action, since the fact that the girders are close to each other increases the lateral restraint effect and positively influences the bearing capacity and arching action.

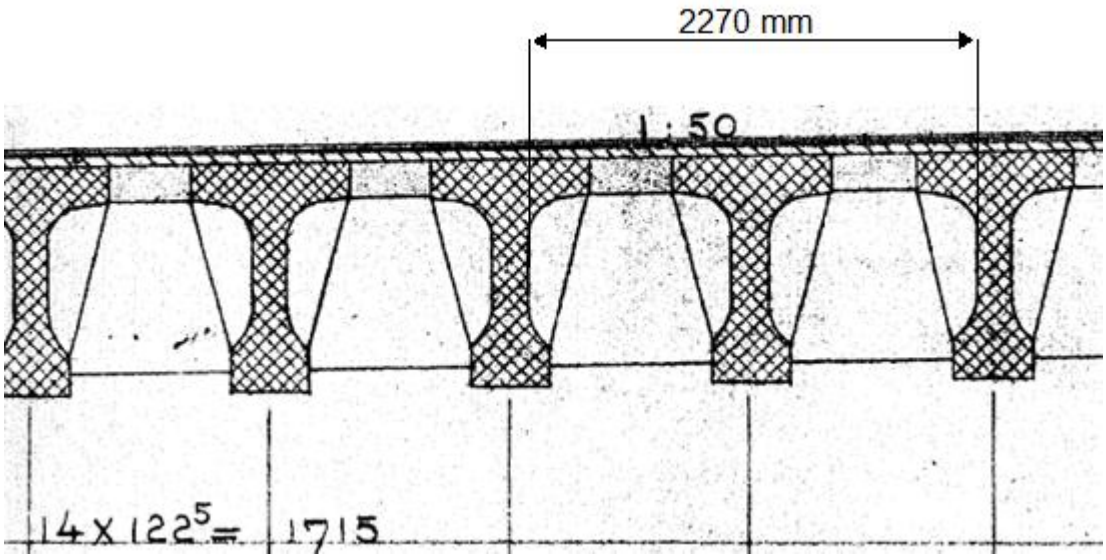


*Figure 99 c.t.c distance "De Vecht"*

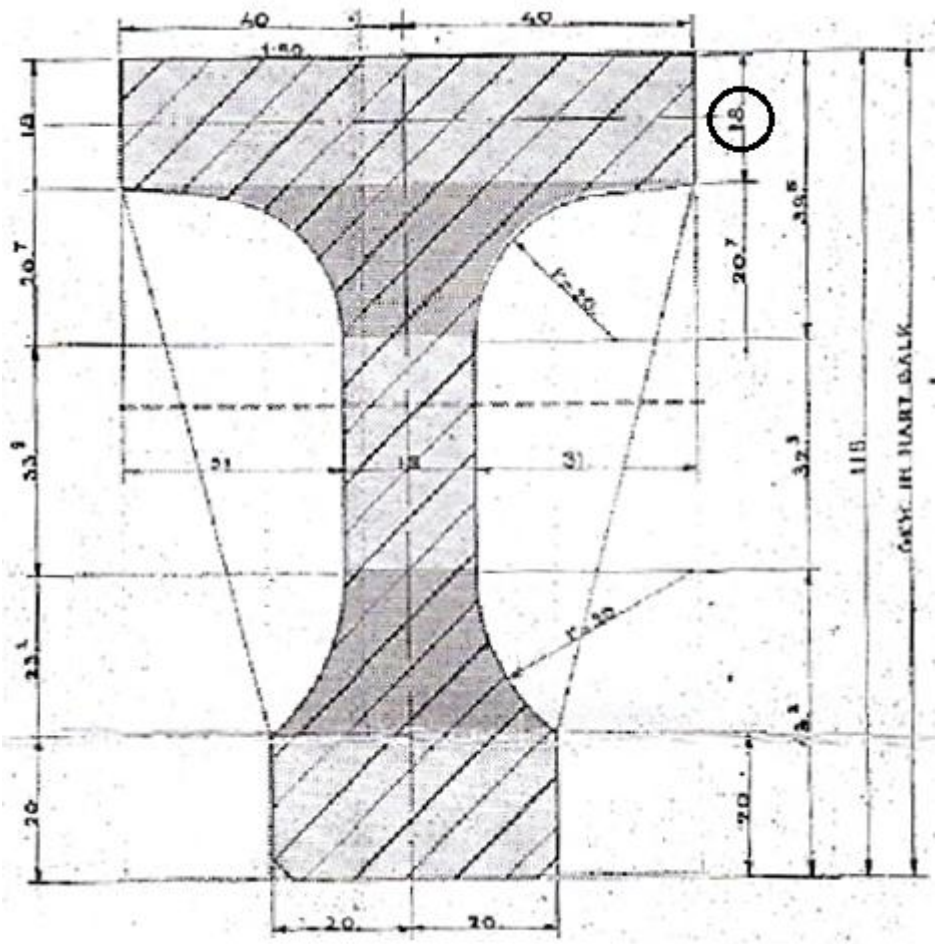


*Figure 100 cross section girder "de Vecht"*

The deck thickness is taken as 180 mm, which already includes the thickness of the girder top flange (Figure 100). The rest of the girder properties, such as the second moment of inertia, which is used for the calculation of the shear capacity, is found in Appendix E.

### Crossbeams and considered field

There are four crossbeams, two located at 150 mm from the ends of the bridge (Figure 101), and two at one-third and two-third--at 8 and 16 m--of the considered length of the bridge. The end crossbeams are 400 mm wide, and the other two are 500 mm. The total considered field length of the bridge is 24 m (Figure 103). These elements are modeled later.

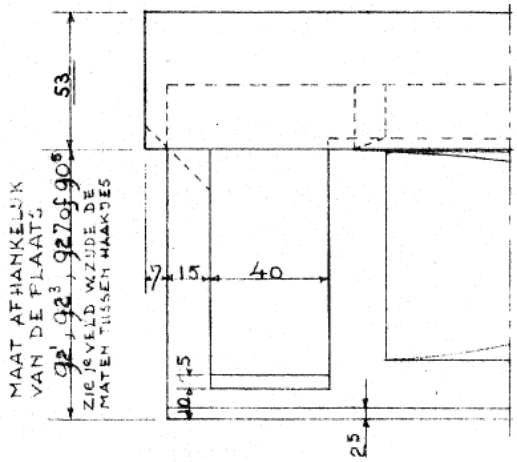


*Figure 101 cross section end cross beam*

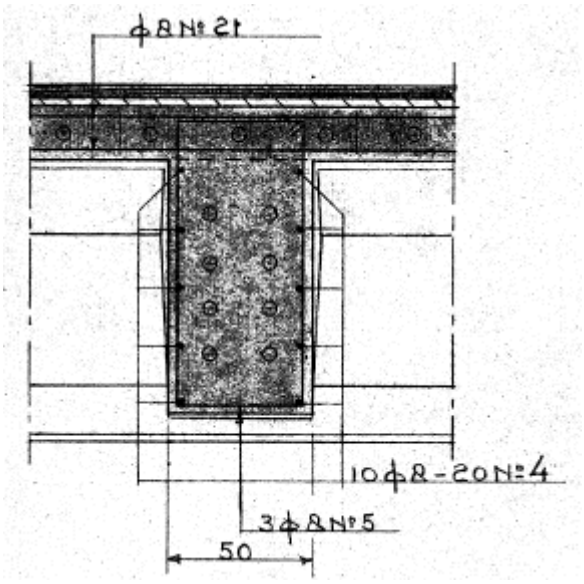


*Figure 102 cross section cross beam*

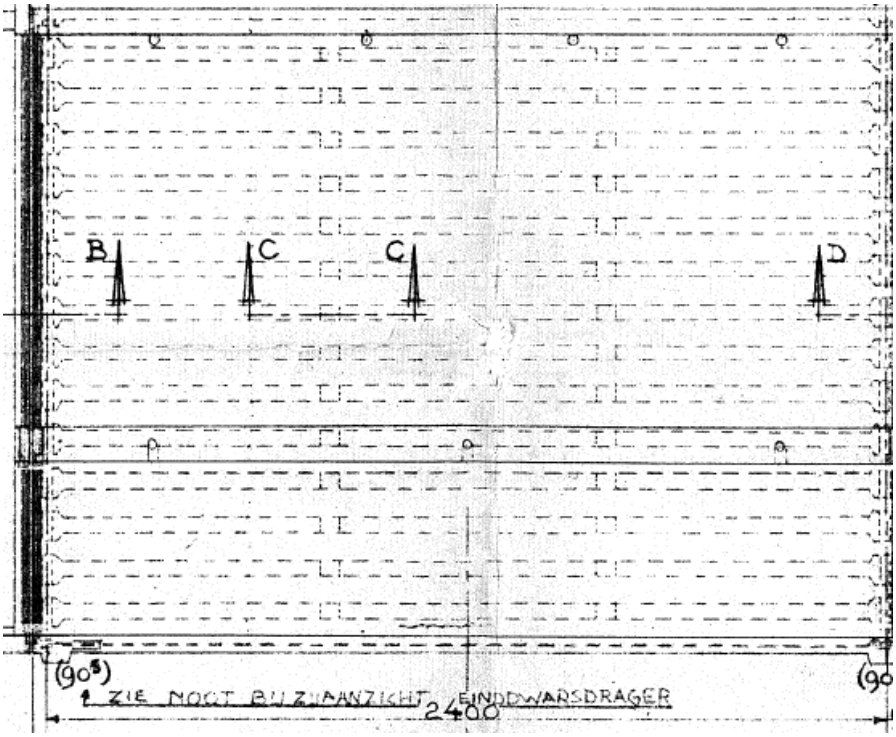


*Figure 103 considered field of bridge , 24 m, with cross beams at 8 and 16 m, and end beams 0.15 m from the ends.*

**Concrete parameters**

The deck and crossbeams are assumed to be C35/45, and the girders beneath the deck C55/67 (Table 13 and Table 14). The concrete strength could be higher than these values, because of the ongoing hydration over time

**Reinforcement steel**

6 mm steel bars are applied in the deck (Figure 104), estimated with a low yield strength of an average 280 MPa. Also, very low reinforcement is applied, 0.23% (0.44% for transverse prestressing, and 0.03% for the longitudinal reinforcement). The low reinforcement ratio is favorable for the development of cracking.

In Chapter 8, it seemed favorable for ductile behavior if 12 mm bars, top and bottom mesh, with 500 MPa yield strength were present. This is not the case for 'De Vecht'.

*Table 13 deck material properties*

| Deck | C35/45 | |
|---|---|---|
| $f_{cm}$ | 43 | [MPa] |
| $f_{ck}$ | 35 | [MPa] |
| $f_{ck,cube}$ | 45 | [MPa] |
| $f_{ck}$ | 36 | [MPa] |
| $y_c$ | 1,5 | [-] |
| $f_{cd}$ | 23,3 | [MPa] |
| $E_{cm}$ | 34077 | [MPa] |
| $f_{ctm}$ | 3,5 | [MPa] |

*Table 14 girder properties*

| Girder | C55/67 | |
|---|---|---|
| $f_{cm}$ | 63 | [MPa] |
| $f_{ck}$ | 55 | [MPa] |
| $f_{ck,cube}$ | 67 | [MPa] |
| $f_{ck}$ | 53,6 | [MPa] |
| $y_c$ | 1,5 | [-] |
| $f_{cd}$ | 36,7 | [MPa] |
| $E_{cm}$ | 38214 | [MPa] |
| $f_{ctm}$ | 4,21 | [MPa] |

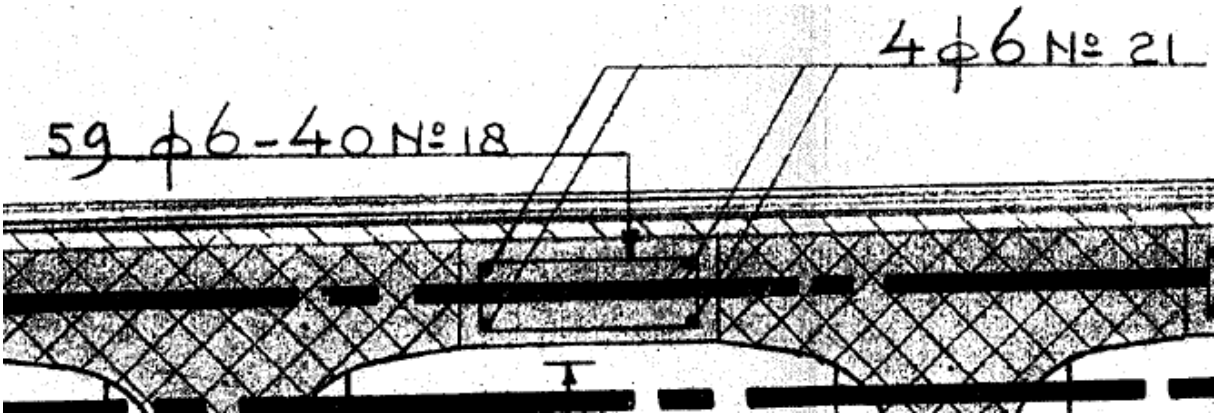


*Figure 104 reinforcement in deck*

### Prestressing steel

'De Vecht' was built in 1965. For the prestressing in both the girder, and deck, Freyssinet 12$\phi$7 is assumed. Prestressting steel with a surface area: $A_p = 462\ mm^2$ is assumed with a steel quality QP170. This steel quality is has a tensile strength of 1700 MPa.

### Test location

Two tests are performed on 'De Vecht' bridge, at 4 and 2.25 m from the end (Figure 105 and Figure 106). The test load surface is 400*400 mm. And the girder is loaded directly (Figure 109), where the slab is more likely to fail in bending than punching because the slab is integrated with the girder in the bridge (as discussed in Chapter 5).

*Table 15 prestressing information (Rijkswaterstaat, 2013)*

| Systeem | Toegepast vanaf | Groepering | Staalopp. [mm2] | Staal-kwaliteit | Max. blijvende voor-spankracht (= 55%) | Max. aanvangsvoor-spankracht (= 65%) | Opmerking |
|---|---|---|---|---|---|---|---|
| Freyssinet | 1960 | Kabel: 12Ø5 (d) | 236 | QP150 | 190 kN (19,4 tf) | | Na 1965 is QP 150 hiervoor niet meer veel toegepast. |
| | | | | QP170 | 216 kN (22,0 tf) | | |
| | 1960 | Kabel: 12Ø7 (d) | 462 | QP150 | 374 kN (38,1 tf) | | |
| | | | | QP170 | 424 kN (43,2 tf) | | |

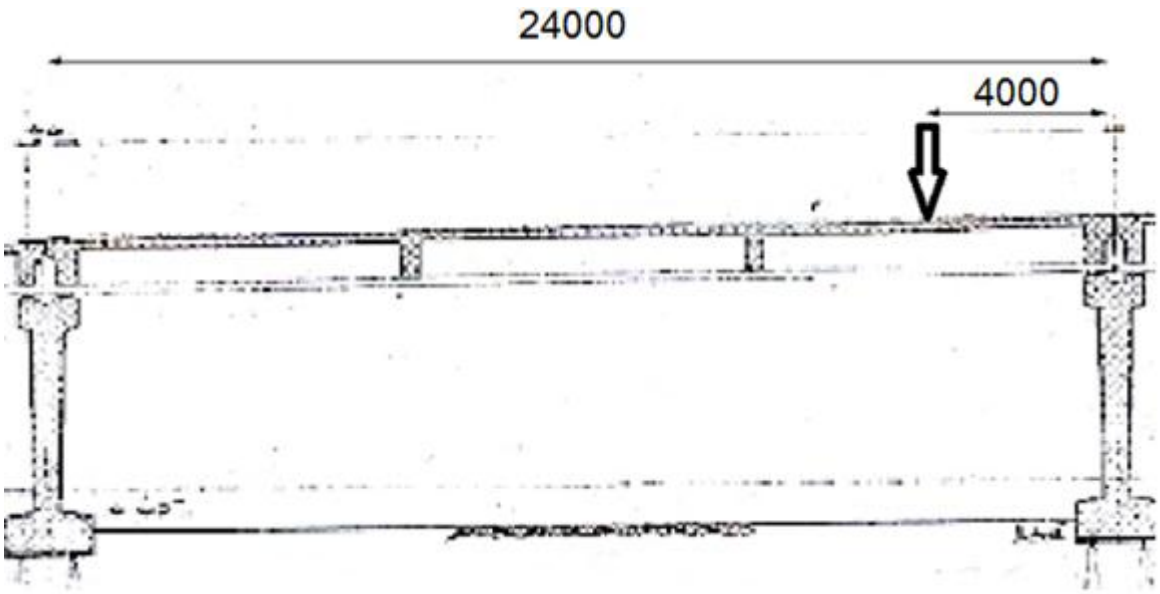


*Figure 105 location test load (1), distances in mm*

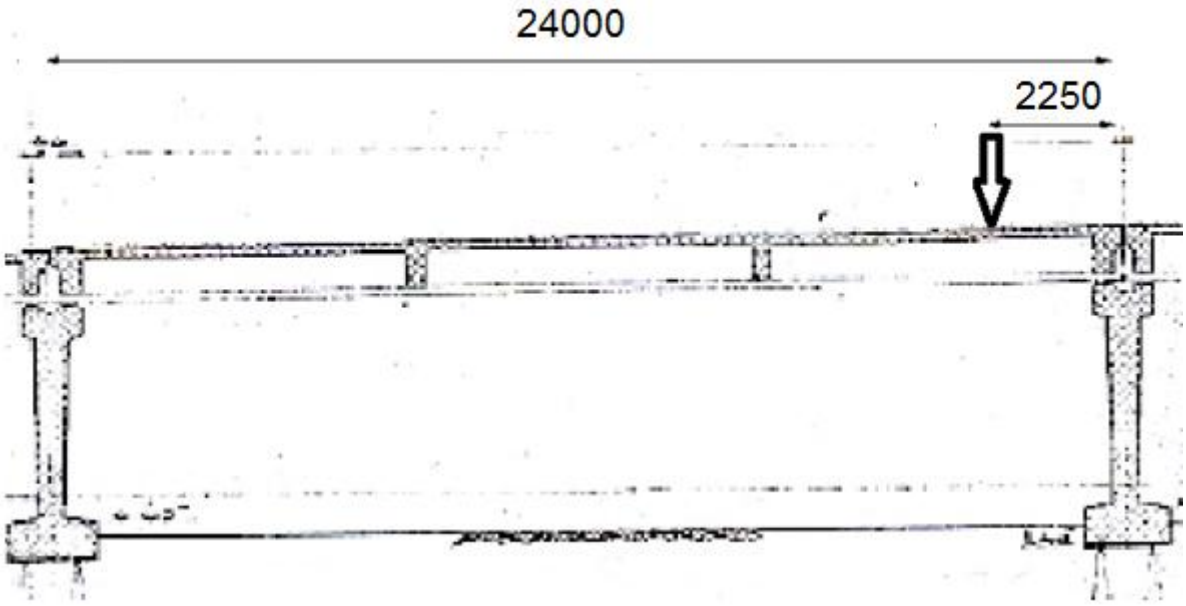


*Figure 106 location of the load (2), distances in mm*

## Analytically determining CMA in 'De Vecht' bridge

### Lateral restraint

According to (Dorton & Csagoly, 1977), one can calculate the bridge's capacity using a safe lower bound restraint factor $\eta = 0.5$, if the beforementioned conditions are met. Then, also the empircal and simplfied method are allowed to be used to determine the slab's bending and punching capacity.

'De Vecht' slab agrees with all mentioned conditions. A restraint factor of at least $\eta = 0.5$ is present, and the methods are allowed to be used. This is expected since earlier a stiffness factor $K_r$ larger dan 1221 kN/mm was determined, meaning the slab is considered fixed ended with an equivalent restraint factor of $\eta = 1.0$. Finally, the slab bending and punching capacities are determined (Table 16). The slab calculations are found in Appendix F.

### Empirical method (CAN)

- End cross beams present. Agreed.
- Continuous end cross beams present cast between outer girders. Agreed.
- Edge beams integrally cast with deck. Agreed.
- Concrete strength not lower than 20 MPa. C35/45 present. Agreed.
- Minimal deck thickness $h \geq 150\,mm$. 180 mm present. Agreed.
- Considered slab span 2.239 m $<$ 4.5 m. Agreed.
- A small overhang of concrete of 0.75 m is present. Agreed.
- Slenderness: $\lambda = \frac{L_s}{h} = \frac{2239}{180} = 12.4 < 20$. Agreed.

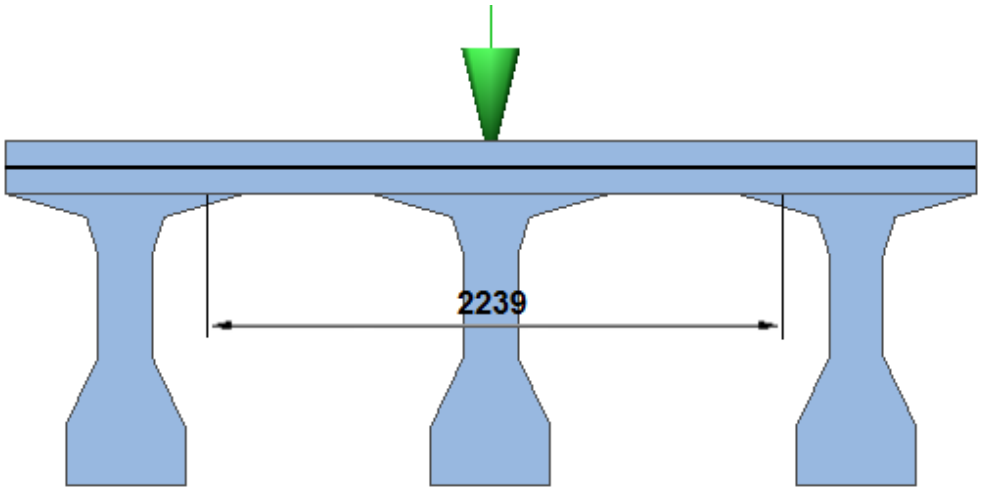


*Figure 107 considered clear span "De Vecht" empirical method*

**Simplified method (UK)**

- Slab clear span 2.27 m (Figure 109) < 3.7 m. Agreed.
- A small overhang of concrete of 0.75 m is present. Agreed.
- Slenderness: $\lambda = \frac{L_s}{h} = \frac{2270}{180} = 12.6 < 15$. Agreed.
- Continuous end cross beams present. Agreed.
- Edge beams integrally cast with deck. Agreed.

**Rankin method**

The effective width and considered clear span are given, and the rest of the calculation is found in Appendix F. The effective width stays the same when the point load changes location, from test load at 4 to 2.25 m. The test load surface is 400*400 mm.

$b_{eff} = 2630\ mm$ (Figure 108 and Figure 110)
$L_s = 2270\ mm$ (Figure 109)

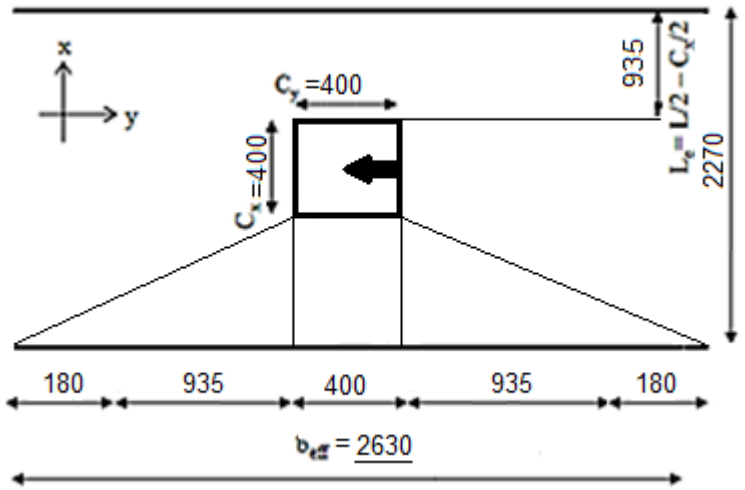


*Figure 108 effective width slab 'De Vecht' (measurements in mm, and not on scale)*

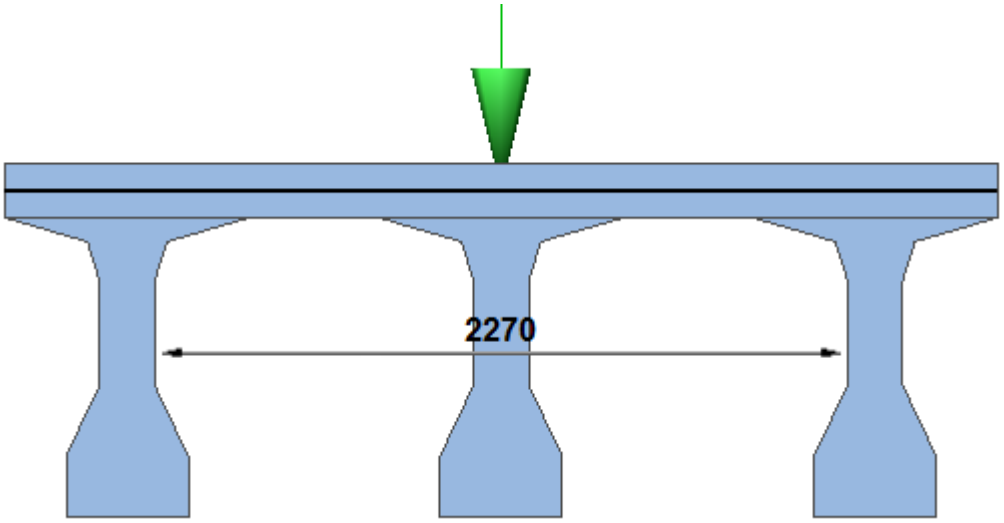


*Figure 109 considered clear span 'De Vecht' for UK and RK method*

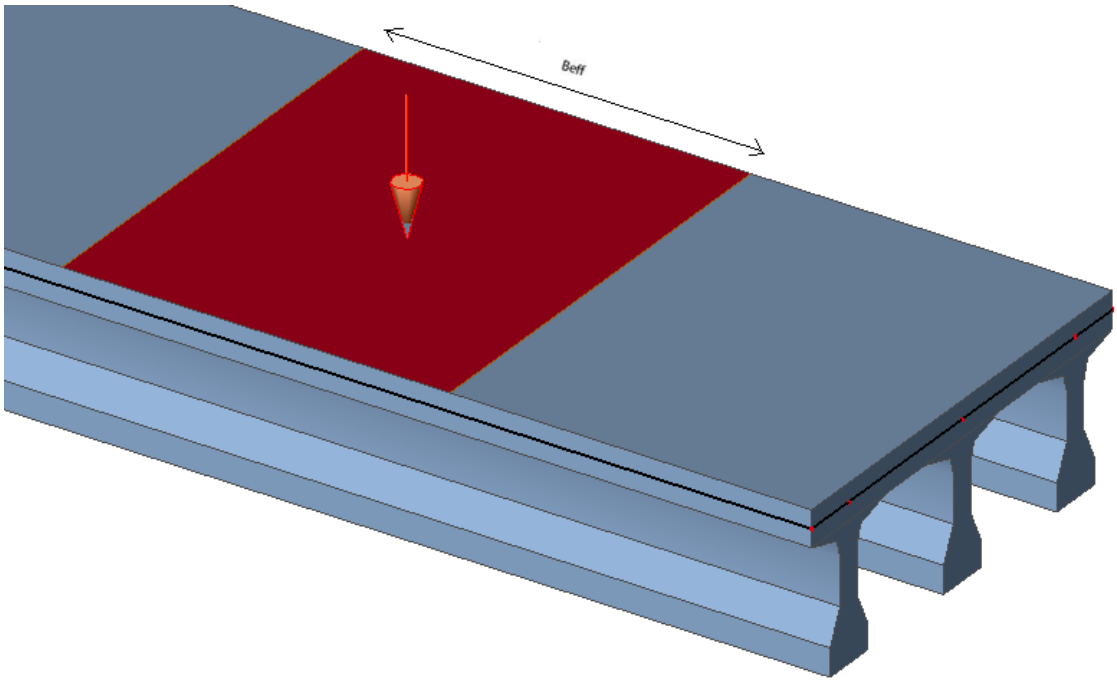


*Figure 110 calculated effective width represented on the bridge system*

### SCIA

The lower bound estimate deflection--10 mm for punching was used in combination with a numerical slab model to determine at which load the slab's punching capacity is reached (Appendix G). The load for the 10 mm deflection was 455 kN.

The same was done for the estimated deflection 25 mm at peak load (Appendix G), to determine the slab's bending capacity, according to SCIA a bending capacity of 1136 kN was found, it is assumed that during the deflection plateau of 10 mm up till 35 mm (Appendix G) this capacity remains unchanged, assuming a bilinear slab behavior where the slab's peak load remains unchanged during deflection.

**Conclusions analytically determining CMA in the slab**

The slab of 'De Vecht' meets all the criteria of the calculative methods. So analytically, it seems that the signs indicate that compressive membrane action might develop in the slab. Table 16 shows an overview of the calculated slab capacities for punching as well as bending.

The slab punching capacities of Rankin and UK method are comparable. The CAN method only calculates the punching capacity. The punching capacity was estimated with linear extrapolation for a load surface of 400*400 mm (Appendix F).

The highest value, 1200 kN, is determined with Rankin (Appendix F). The UK method has a higher punching capacity than bending. However it is expected that the system does not fail in punching and that bending is the governing failure method.

The methods calculating the slab capacity do not take prestressing into account (as mentioned before in Chapter 4 of Part 1) and are considered an underestimation. And also according to (Taylor, Rankin, & D.J., 2001), the slab bending capacity calculated with Rankin is considered to be an underestimation of the actual strength (with an average difference in strength of 16% (Appendix D)).

*Table 16 results slab capacity for load at 4m from the end*

| Method | Slab Punching Capacity [kN] | Slab Bending Capacity [kN] |
|---|---|---|
| **SCIA** | 455 | 1136 |
| **Empirical (NZ/CAN)** | 467 | N/A |
| **Simplified (UK)** | 635 | 558 |
| **Rankin (FE)** | 509 | 1200 |

## Numerically determining CMA in 'De Vecht' bridge

### Three-girder plate model

First a portion of the bridge deck is modeled (Figure 111 and Figure 112), and is made of an orthotropic plate with three beams as ribs. Generally, the material parameters as discussed earlier in this chapter is used for the numerical model (more information is found in Appendix E and H).

The main girder is loaded with a point load where it is expected the main girder fails in shear. There are two test locations; the point loads are located 4 and 2.25 m from the end of the girder (Figure 113 till Figure 115). A slab model with the main girder left out is used as well to determine the deflections at midspan (in a similar way as described in Chapter 6 and 7).

The supports are modeled as springs. The spring action of the real life rubber bearings is determined by assuming a deflection of 1 mm under loading of the self-weight. The cross section (Figure 100) is used to model the ribs underneath the plate model (Figure 115).

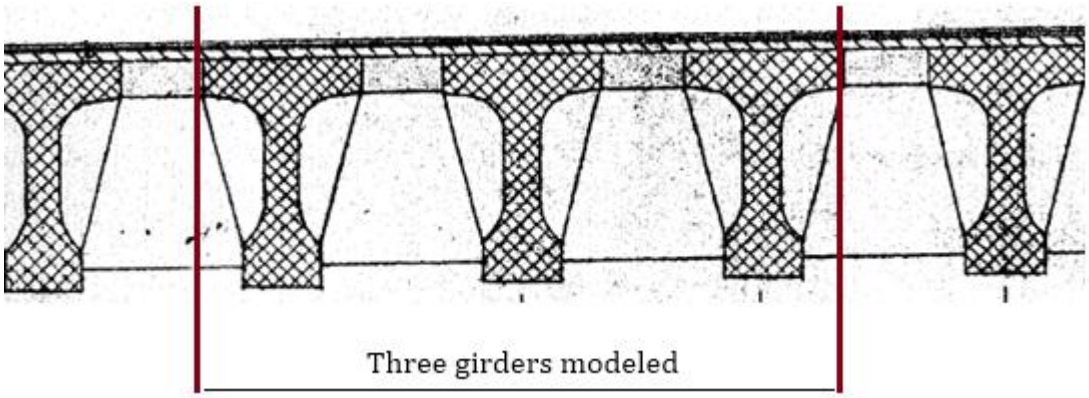


*Figure 111 portion of the deck modeled: three girders*

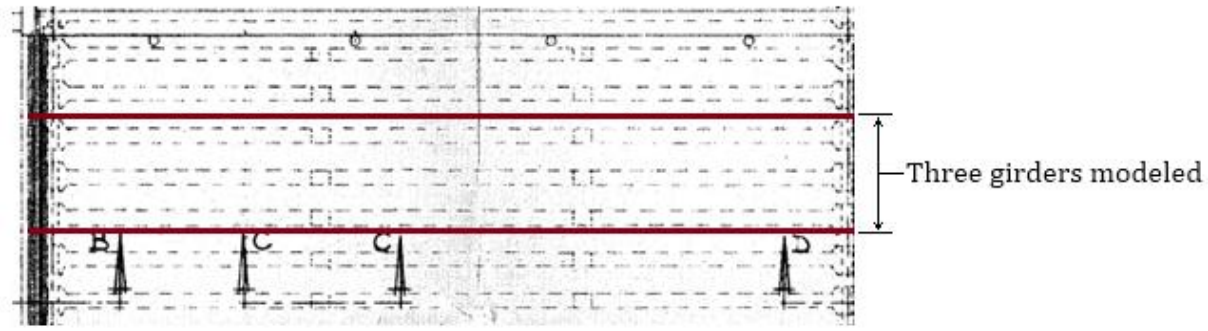


*Figure 112 portion of the deck modeled, top view, three-girders modeled*

*Figure 113 side view numerical model 'De Vecht" with test load at 4 m from the end*

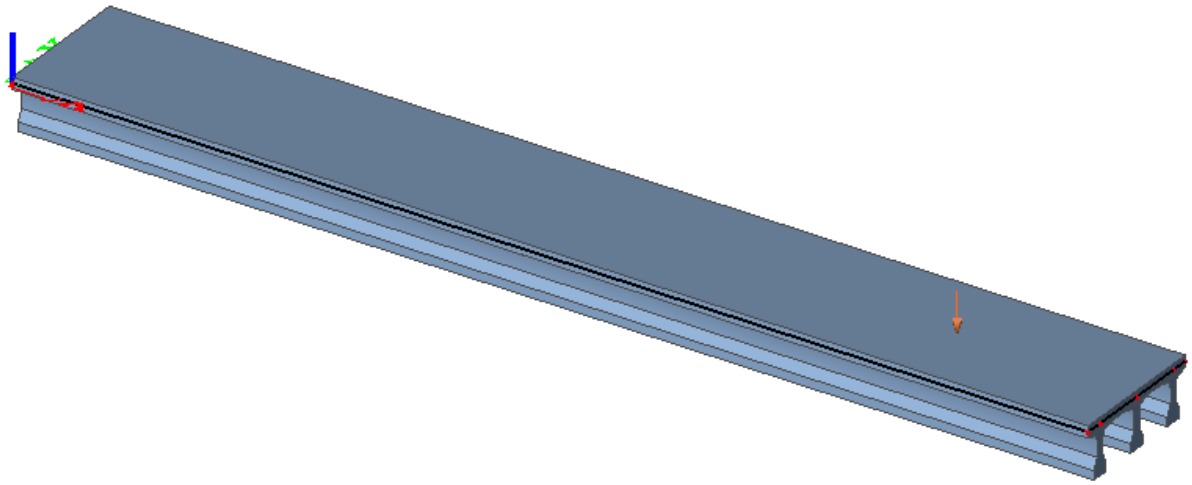

*Figure 114 3D view of 'De Vecht' plate model with ribs, and the load placed at 4 m*

### Load distribution over three girders

The linear load distribution is determined, giving over the three girders: 30% 40% 30%. This means only 20% of the load can be redistributed, 10% to each neighbor beam. This means that the neighbor beams can take only 80% of the total load (Figure 115). If the main beam is assumed to fail brittle, the bridge capacity is only the capacity of the two neighbor beams (the lower bound). But if the main beam behaves plastically, then the capacity of the bridge is three times the beam capacity, the upper bound.

This high load spread, which is without the presence of the crossbeams, suggests that a three-girder model might not be sufficient enough to cover the actual spreading. A five- or seven-girder numerical model might be more suited in this case, which is discussed later. One reason for the high load spread is the low slenderness ratio.

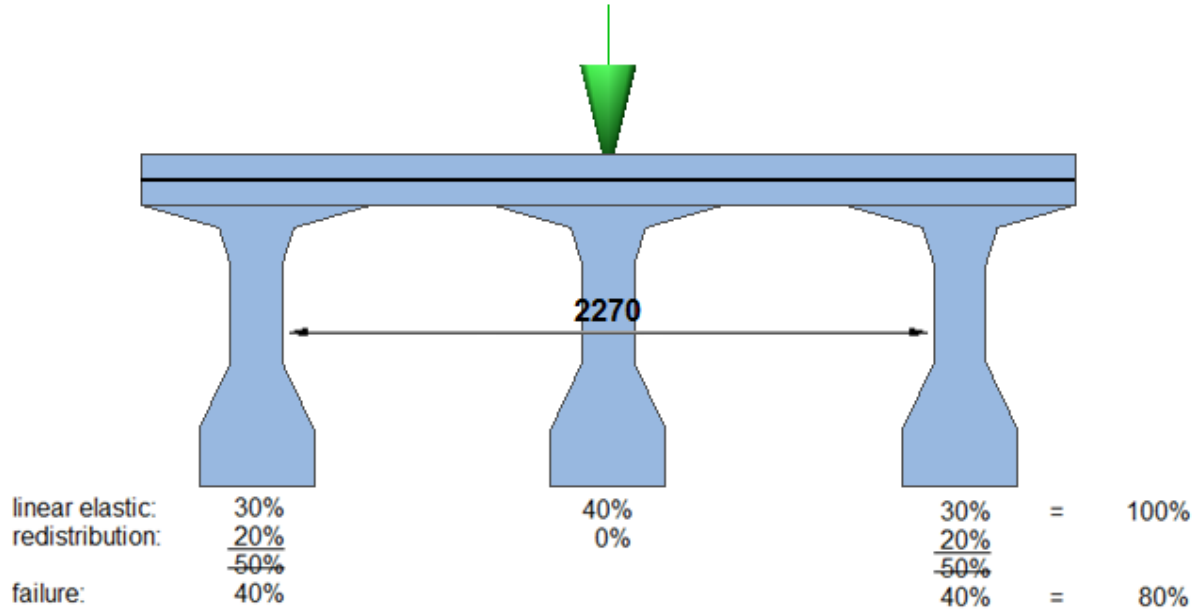


*Figure 115 cross section of plate model with girders with load distribution for load at 4m*

### Three-girder model with crossbeams

The load distribution is determined again but this time with crossbeams implemented in the plate model: 33.3% 33.3% 33.3% (Figure 115). No redistribution is assumed possible.

Moreover, the high spreading suggests that a three-girder model might not be sufficient enough to represent the actual spreading of the real bridge. A five- or seven-girder might be more suited in this case, which is discussed later (Figure 117).

The implementation of the crossbeams is another reason for the high load spread (as was noted already in Appendix B).

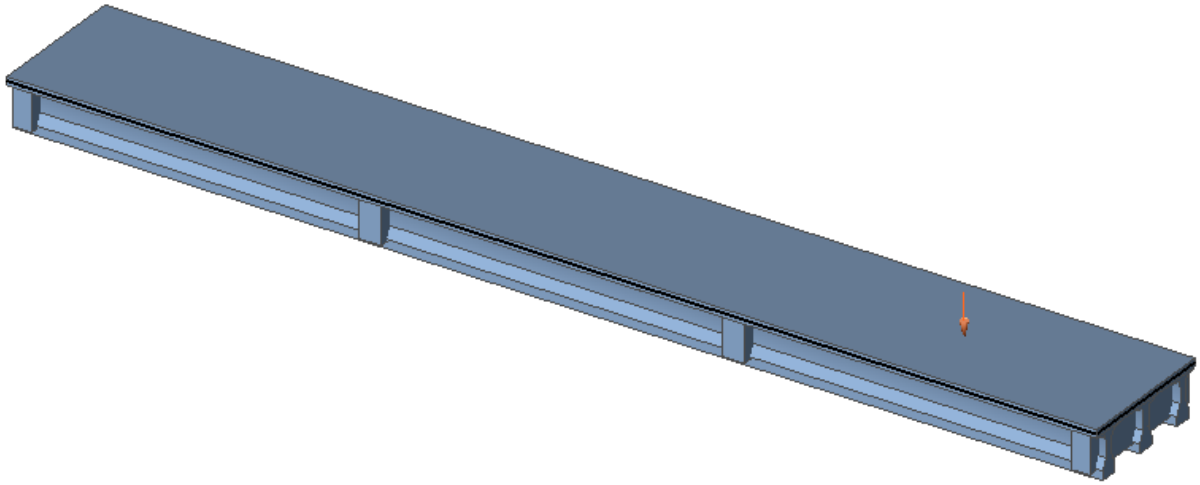

*Figure 116 bridge with crossbeams, and the load at 4 m*

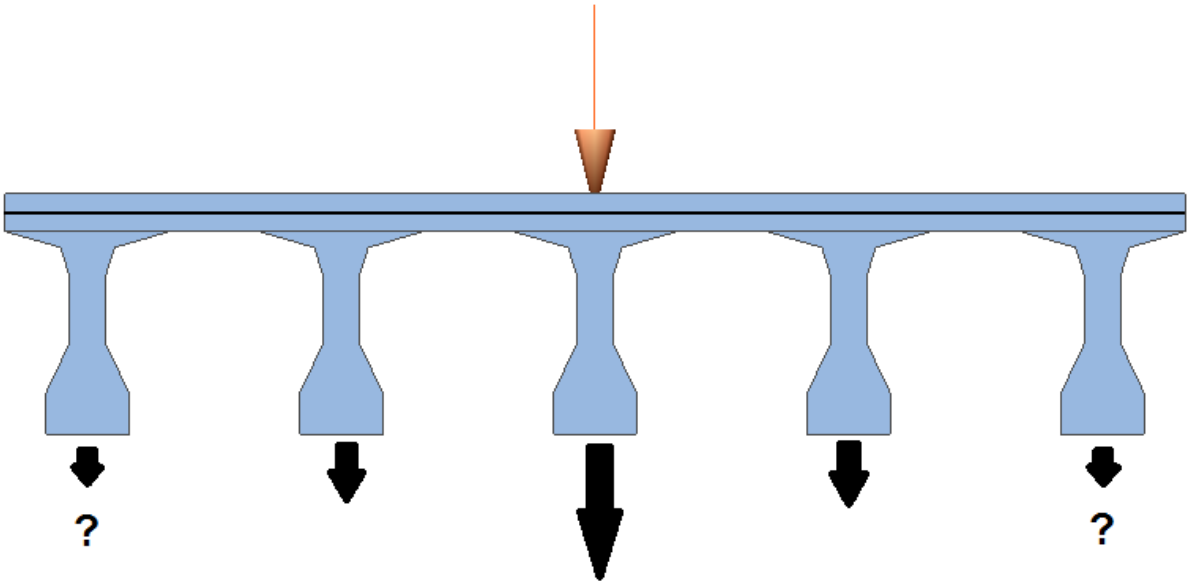


*Figure 117 numerical model with five-girders showing the possible deflections of the outer girders*

**Test load at 2.25 m**

The same was done for the test load at 2.25 m, only the location of the load changed. The same calculation was done as shown in Figure 115, giving a linear load distribution of: 26.5% 47% 26.5%. This means 41% of the total load can be redistributed, 20.5% to each neighbor beam.

Linear load distribution of the numerical model with the test load at 2.25 m, *with* four crossbeams gives: 33% 34% 33%. No redistribution is assumed possible. It is clear that the presence of the crossbeams has a significant effect on the load distribution.

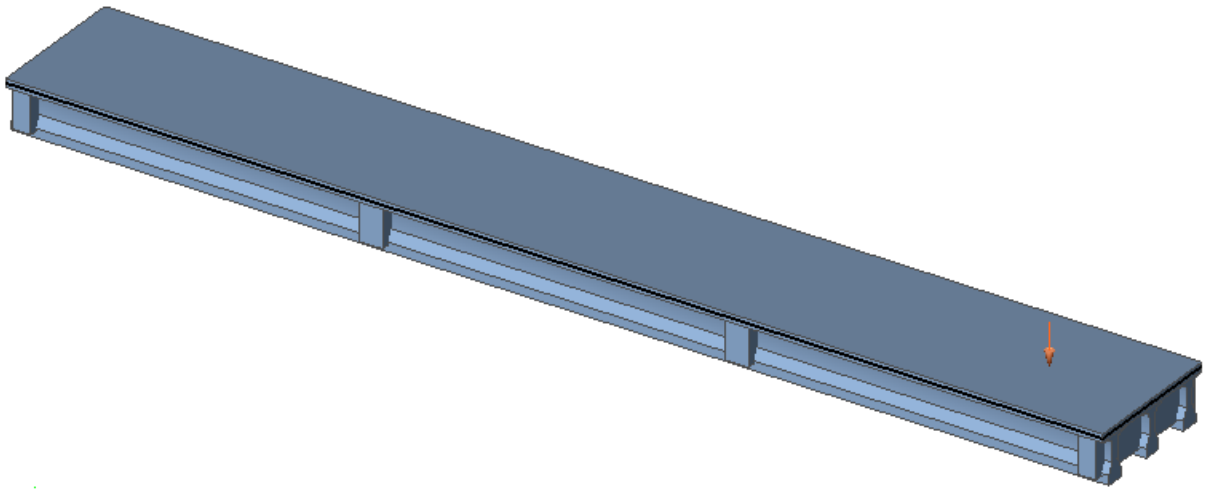

*Figure 118 bridge with crossbeams, and with the load at 2.25 m*

### Conclusions development CMA in slab

Numerically, for both the test load at 4 and 2.25 m, a high load spread is apparent and the three girders are loaded almost the same (Figure 119). The high load spread leads to a low relative displacement. And when the relative displacement is too low, it is uncertain whether the critical deflection is reached, cracking develops in the slab, and compressive membrane action is developed in the slab.

This is another indication that multiple girders need to be modelled for further research of the load distribution. So by using the numerical method described in Chapter 7, it is uncertain whether CMA activates during load and whether the slab can contribute to the upper bound value of the bridge load.

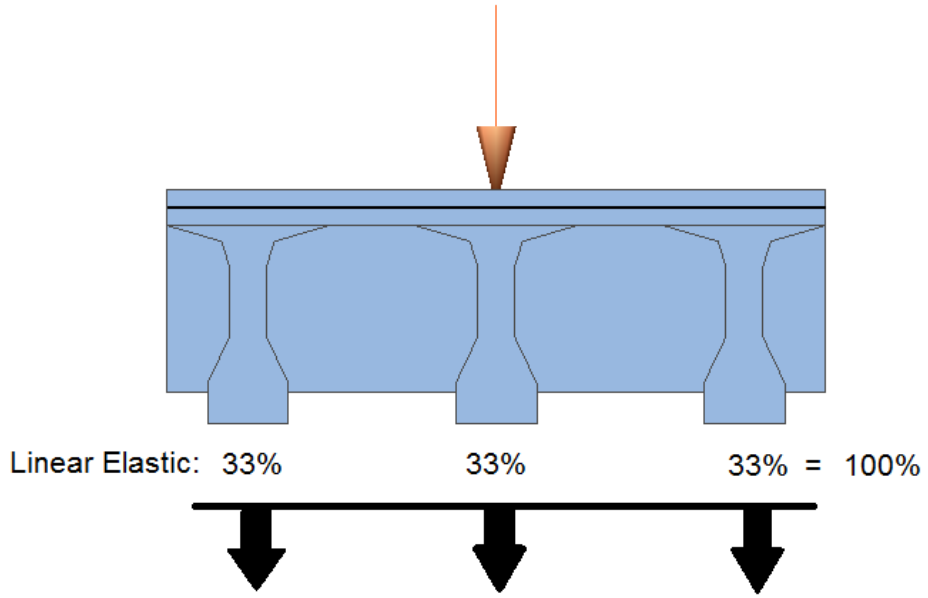


*Figure 119 high load spread leads to low relative girder displacement*

# Chapter 10 *Test Results 'De Vecht' Bridge*

## Introduction

This chapter discusses the test results from 'De Vecht'. Two point load locations are considered, at 4 and 2.25 m from the end. First, the load displacement graphs of the whole bridge system are discussed. Then single girder tests are discussed with their own load displacement graphs.

Moreover, a numerical modelling is done with five-girders and seven-girders in order to determine whether CMA developed in the concrete slab.

## Comparison between predicted and actual total bridge load

The load displacement graphs of the tests on the full bridge systems, with loads at 4 and 2.25 m, are given in Figure 237 and Figure 238 respectively (Appendix H). For both tests the total load, estimated linear loads, the ultimate deflection, and deflection at peak load are given in Table 17.

The bridge with the load at 2.25 m shows the higher external total capacity, compared to when loaded at 4 m from the end (Table 17). This is possibly due to the load location itself, when the load is closer to the end beam, which causes an increase in strength and stiffness of the whole bridge system. This was also noticed in numerical modelling. The fact that the load location influences the total bridge load was noticed earlier in Part 1.

However, the ultimate deflection of for the load at 4 m is higher than the load at 2.25 m (Table 17). This might be due to the ductility of the two key elements: the single girder or the slab. This is discussed later. And the linear capacity for the load at 2.25 m is the higher one, probably due to the higher single girder capacity, which is noticed later.

*Table 17 results of both tests, with the load at 4 and 2.25 m: bearing capacity and deflections*

| load location [m] | total load [kN] | displacement at peak load [mm] | ultimate displacement [mm] | linear load [kN] | displacement at linear load [mm] |
|---|---|---|---|---|---|
| **4** | 3000 | 19 | 22 | 1500 | 5.5 |
| **2.25** | 3400 | 10.5 | 13 | 1900 | 3.5 |

*Table 18 comparison actual and predicted total capacity with margin of errors for the loads at 4 and 2.25 m*

| load location [m] | actual total load [kN] | predicted total load [kN] | | margin of error [%] |
|---|---|---|---|---|
| 4 | 3000 | RK(nonlinear) | 3960 | 32 |
| | | SCIA(linear) | 2564 | 15 |
| | | UK(linear) | 1635 | 45 |
| 2.25 | 3400 | RK (nonlinear) | 5640 | 65 |
| | | SCIA(nonlinear) | 5422 | 60 |
| | | UK (nonlinear) | 2692 | 21 |

*Table 19 comparison actual and predicted ultimate deflections for the loads at 4 and 2.25 m*

| load location [m] | actual ultimate deflection [mm] | predicted ultimate deflection [mm] | Margin of error [%] |
|---|---|---|---|
| 4 | 22 | 35 | 60 |
| 2.25 | 13 | 35 | 170 |

The comparison between the actual and predicted bridge load (determined in Appendix G) is shown in Table 18. All methods considered failing in bending, since punching was not governing. And linear/nonlinear in the parantheses concern the assumed load distribution (Appendix G). And it is noted that the predicted capacities are determined for a set of assumed ultimate deflections, which is also discussed and compared with the actual ones (Table 19).

Two methods in Table 18 are considered a safe understimate. All of the other results overestimate the total bridge load. That being said, all the predicted bearing capacities were determined for assumed deflections, derived with the Taylor tests (Appendix G), deviating from the ones in reality (Table 19). The assumed deflections seemes to be a significant overestimation. Therefore, if the assumed deflections were closer to reality, the numerical model would have provided a safe understimate (Figure 241), regardless of the chosen calculative method for the slab bending capacity.

**Deflections**

The actual deflections of ‘De Vecht’ differ from the ones estimated with Taylor (Table 19). Which could be because the tested slabs had a slenderness of 9.5, while the slab of ‘De Vecht’ has a slenderness of 12.6. Also, as mentioned in Chapter 8, the tested laterally restraint strips show more ductility than the one applied in ‘De Vecht’ bridge.

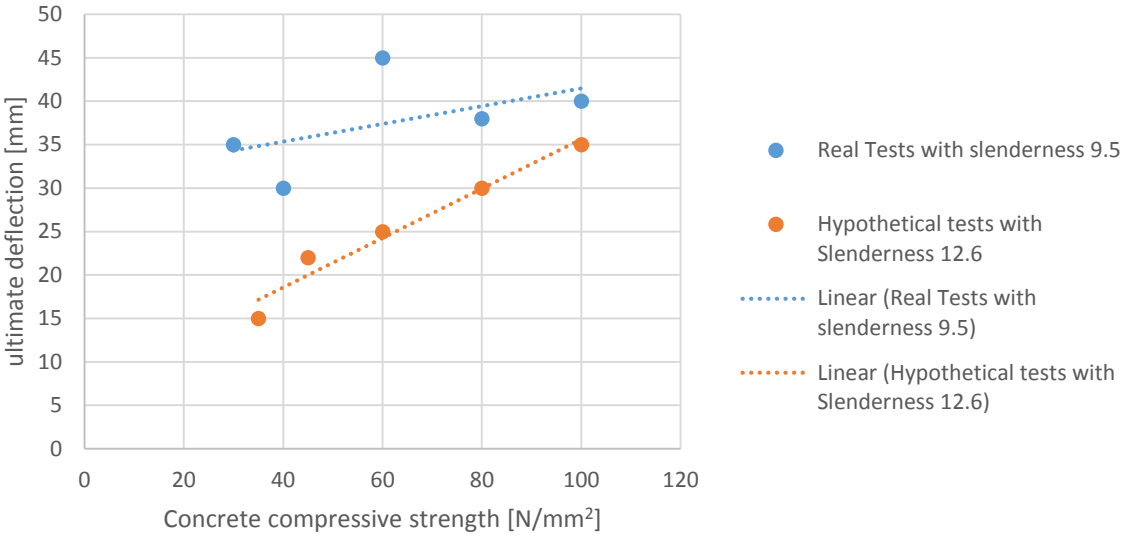


*Figure 120 hypothetical trendline for slenderness 12.6 compared with the trendline for slenderness 9.5 from the tests.*

With that known, Figure 120 shows a hypothetical trendline of a slab with slenderness 12.6, which would have been used to determine the actual ultimate deflection of 'De Vecht'. But in fact no real test data is available for such a trendline. So more research needs to be done on laterally restraint slabs with different slenderness ratios, with which one can create more trendlines which would be applicable for different situations with different concrete strengths and slenderness ratios.

### Failure mode

The slab did not fail in punching, and the ultimate deflections, which are larger than the estimated 10 mm for punching, seemed to agree with this conclusion. On the other hand, it also means that the assumption of using the slab bending capacity is plausible. If one calculates with the bending capacity, it will result in a higher capacity of the slab, as long as the right conditions are met (e.g. slenderness ratio).

## Comparison between predicted and actual girder loads

Besides the tests on the bridge system, individual girders were tested, again with the test load location being at 2.25 or 4 m from the end. For the load at 2.25 m, three tests were done, and for 4 m only one. And the results are given in Table 20. The actual load-displacement graphs are found in Appendix H.

Moreover, the single girder test shows that, for the load at 4 m, the ultimate deflection is the higher one (Table 20). This might be the reason why the whole bridge system fails at a higher ultimate deflection when loading at 4 m compared to the test load at 2.25 m. The ductility of the single girder influences the ductility of the bridge system as whole. In Table 21 the actual girder loads from the test results are compared with the predicted girder loads (determined in Appendix G).

*Table 20 results of single girder tests, with the load at 4 and 2.25 m: capacity and deflections*

| load location [m] | total load [kN] | displacement at peak load [mm] | ultimate displacement [mm] | linear load [kN] | displacement at linear load [mm] |
|---|---|---|---|---|---|
| 2.25 (1) | 1600 | 70 | 75 | 900 | 7 |
| 2.25 (2) | 1700 | 60 | 65 | 1000 | 7 |
| 2.25 (3) | 1750 | 65 | 70 | 1000 | 7 |
| 4 | 1000 | 120 | 130 | 600 | 18 |

*Table 21 comparison actual and predicted capacities of a single girder*

| load location [m] | actual girder load [kN] | predicted girder load [kN] | margin of error [%] |
|---|---|---|---|
| 4 | 1000 | 1197 | 20% |
| 2.25 | 1700 | 1097 | 35% |

**Load distribution determined with measured test results**

A more nuanced calculation for the load distribution is made using both the load-displacement graph of the bridge system and single girders. For example, for the test load at 4 m, the peak bridge load is 3000 kN, at this load, the deflection is 19 mm (Figure 237). And then the load-displacement graph of the single girder is used to determine at what load the girder displaces 19 mm, this gives: 625 kN (Figure 121).

And knowing how much the main beam is loaded, gives the load percentage of the main beam: $\frac{625}{3000} * 100\% = 20.8\,\%$.

Using the same process, the load percentage of the neighbor beams can be determined too. First, the ultimate deflections of the neighbor beams are determined (Figure 122), and then the same girder load-displacement graph as before is used to determine at what load the neighbor deflections are reached, this gives: 350 and 475 kN (Figure 123). This gives a load percentage of 15.8 and 11.7 %. An average deflection, of 7.5 and 10.5 mm, for the neighbor beams is assumed to maintain symmetry of deflections of the neighbor beams (Figure 122).

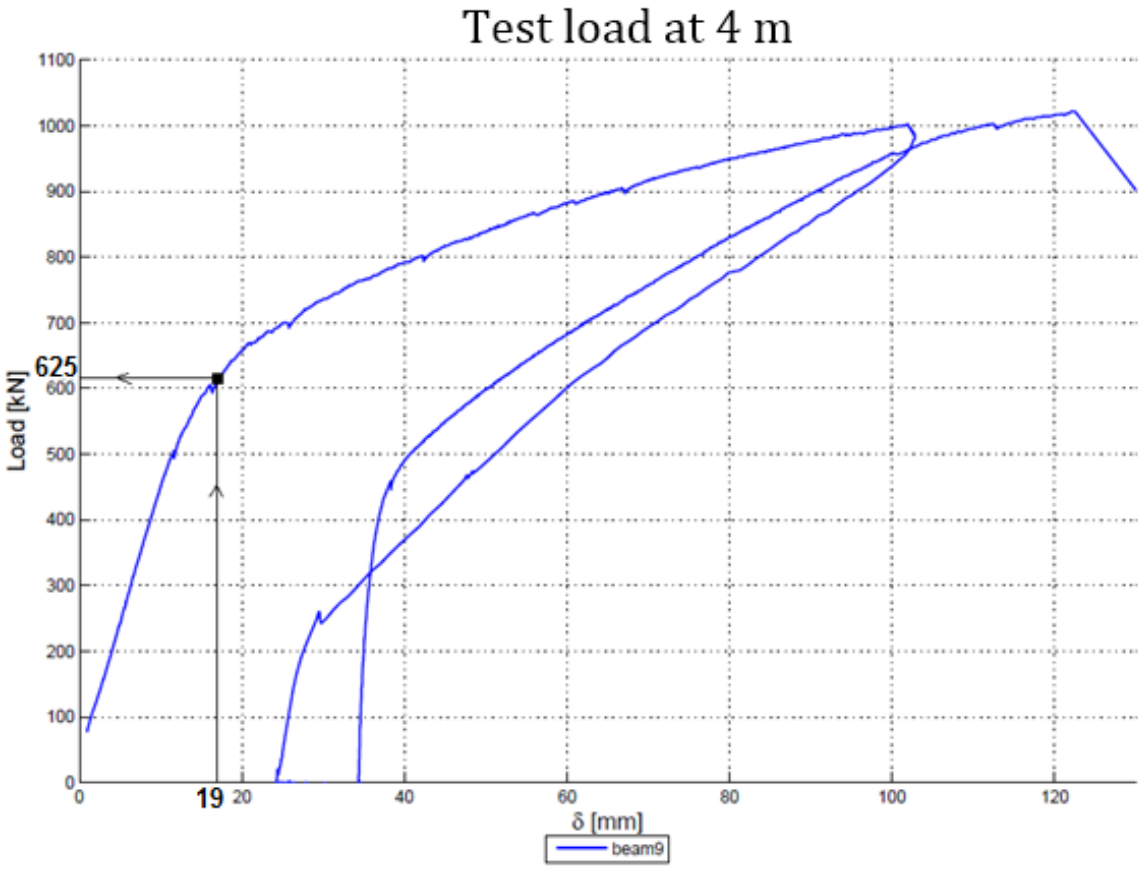


*Figure 121 determining at what load the ultimate deflection of the bridge system is reached, for the load at 4m*

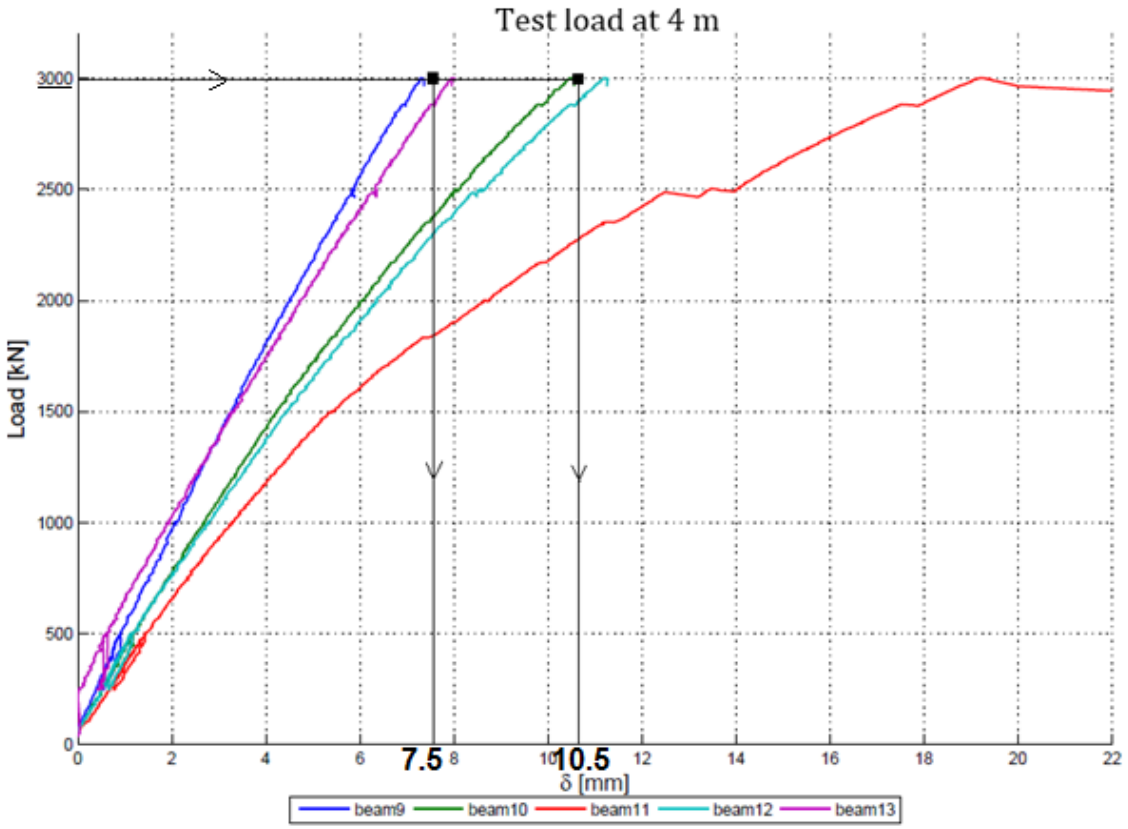


*Figure 122 ultimate deflections of the neighbor beams, for the load at 4 m*

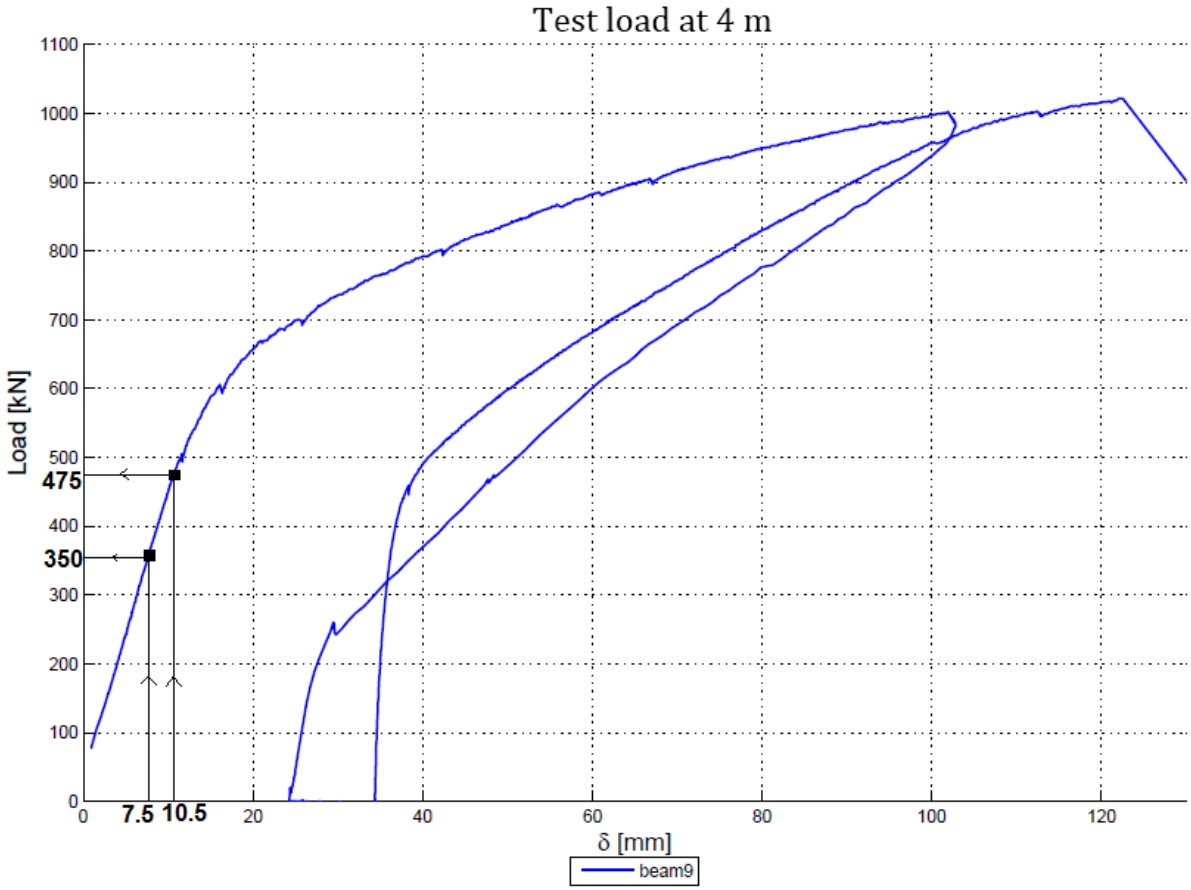


*Figure 123 determining at what load the ultimate deflection of the neighbor beams is reached*

As clarification, the determined deflections are given in Figure 124. And the load distribution is presented in Figure 125, with the determined girder load for each beam. The same process is done for the load at 2.25 m (shown in Appendix H, with Figure 244 and Figure 248), and all the results are given in Table 22.

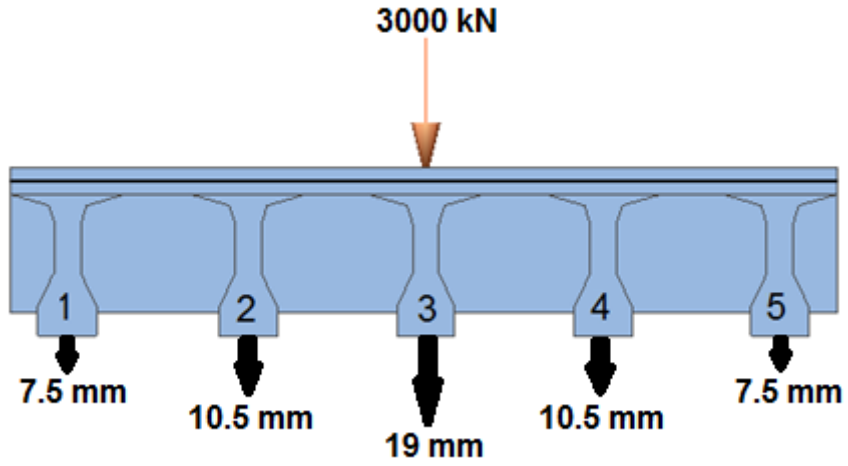


*Figure 124 displacements of the main beam and neighbor beams at the peak load 3000 kN, for the load placed at 4 m.*

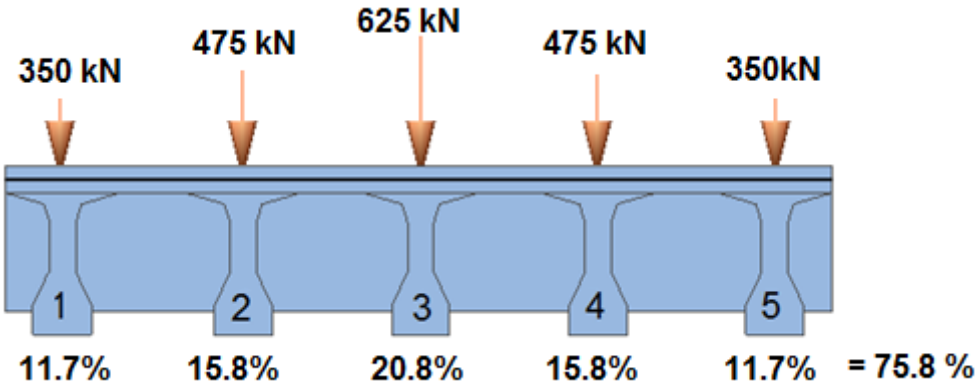


*Figure 125 load distribution determined with the tests results, over five girders with the girder load on each beam*

*Table 22 results of the comparison between the load distribution determined numerically and through the test results*

| Load location [m] | Total load percentage [%] | Load percentage of main beam (derived from test results) [%] | Load percentage of main beam (numerically determined) [%] | Margin of error [%] |
|---|---|---|---|---|
| 4 | 75.8 | 20.8 | 18.5 | 2.3 |
| 2.25 | 100 | 34 | 22 | 8 |

## Numerical modelling with multiple girders to determine CMA

Moreover, as suspected in Chapter 9, the short span of 'De Vecht' causes a high spreading of the load (Figure 237 and Figure 238). According to the measurements from the test (Figure 126), it appears that at least five girders take up a part of the load. This was what predicted before the test was done on the bridge. So in order to research the load distribution over the five girders, a five-girder numerical model was created (Figure 127). This is done in order to determine the relative girder displacement, to determine what the differnces are compared to the three-girder model.

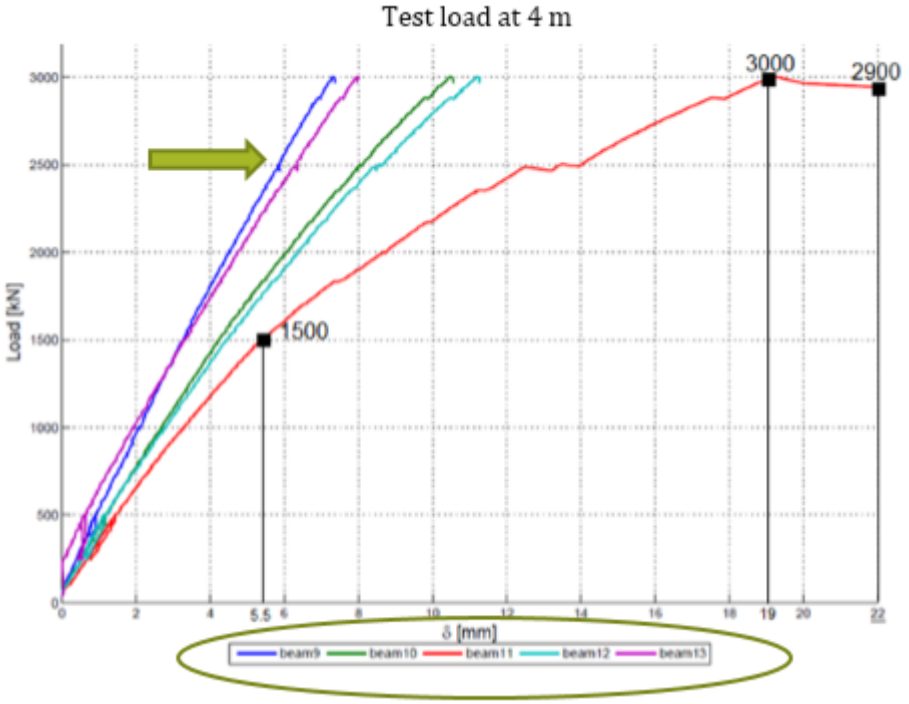


*Figure 126 five-girders take up a part of the load*

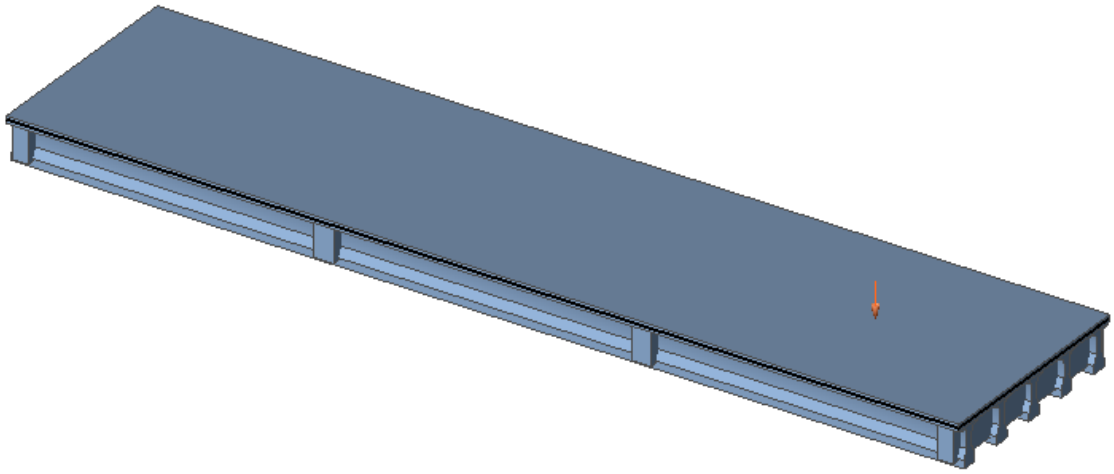

*Figure 127 five-girder numerical model with four crossbeams of 'De Vecht', with the load at 4 m from the end*

**Load distribution and deflections of the five-girder model**

Figure 128 displays that the outer beams take a significant part of external load (roughly $2 * 19 = 40\,\%$). So modelling with a three-girder model leads to a certain margin of error, compared to modelling with a five-girder model.

But even with a five-girder model the relative displacement is still too low (the difference between the neighbor and main beam is 1%). And a low relative girder displacement means that one is not certain whether the critical deflection is reached and membrane action is developed. That is why now a seven-girder model is considered as well, to determine the load distribution and corresponding deflection.

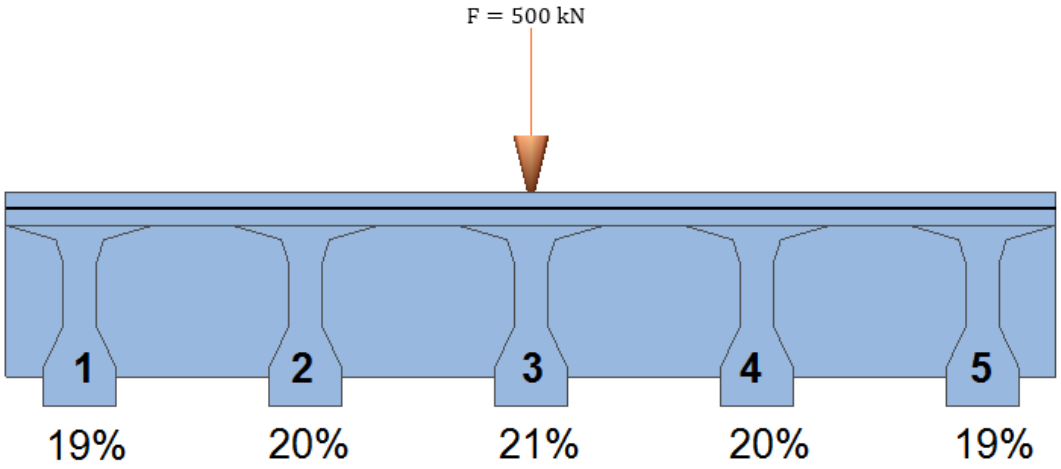


*Figure 128 load distribution of a five-girder model*

### Load distribution seven-girder model

The load distribution of the seven-girder numerical model was determined. Beams 1 and 7 carry 18.6% of the load, and beam 2 and 6, 27.8% (Figure 130). Which gives a summation of 46.4%. So it is shown that modelling with three-girders is not sufficient, since almost half of the load is distributed to the outer girders. The same calculation is done for the load at 2.25 m in Appendix H (Figure 243).

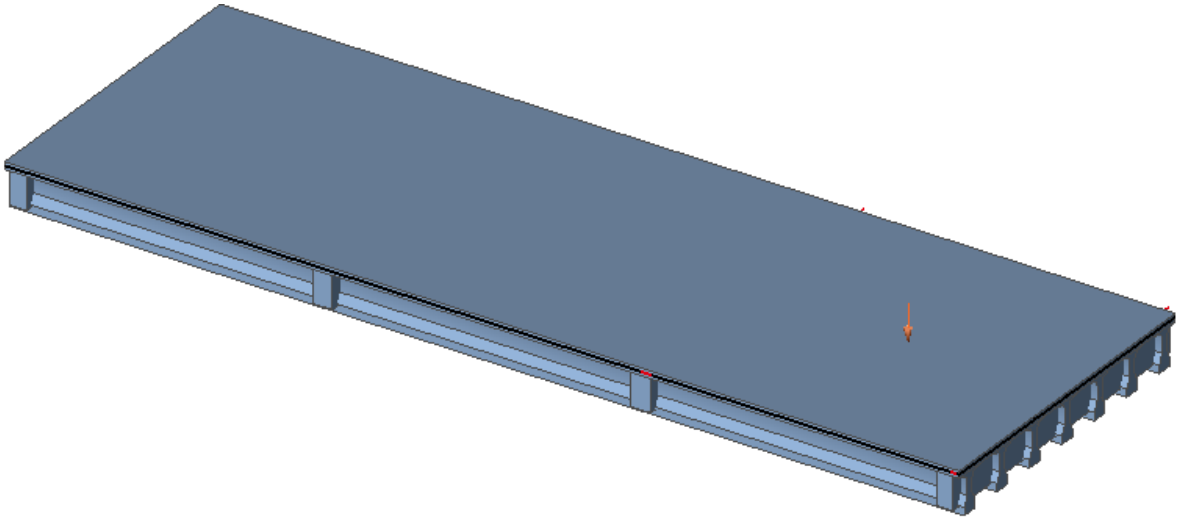

*Figure 129 seven-girder numerical model with four crossbeams of 'De Vecht', with the load at 4 m from the end*

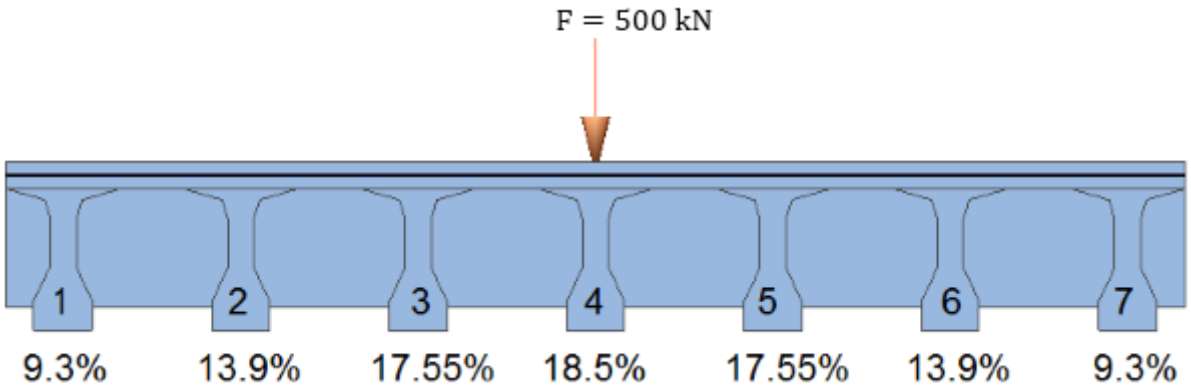


*Figure 130 load distribution over the seven girders determined numerically*

Furthermore, using the deflections (Figure 131), the margin of error of the three-girder model is determined, comparing it to the seven-girder one. For beam 1 and 7 this gives (using the deflections in Figure 131):

$$2 * \frac{2.3}{(2 * 2.3 + 2 * 2 * 2.5 + 2 * 2.9 + 3.4)} * 100\% = 24\%$$

The same calculation is done but for beam 2 and 6:

$$2 * \frac{2.5}{(2 * 2.3 + 2 * 2 * 2.5 + 2 * 2.9 + 3.4)} * 100\% = 27\%$$

This means that the three-girder numerical model displayed a total margin of error of 51% for the deflections.

The loaded main beam and its neighbor beams were assumed to take more of the external load than they actually did. While in fact the outer beams (beam 1,2,6,7 in Figure 131), shown with a seven-girder model, should take up a significant part of the load (46.4%), and their deflections are 51% of the summation of the deflections.

Information regarding the material properties of the numerical models can be found in Appendix H. Basically, the same numerical model was used as the one described in Chapter 9, only the amount of girders that were used as ribs under the plate increased.

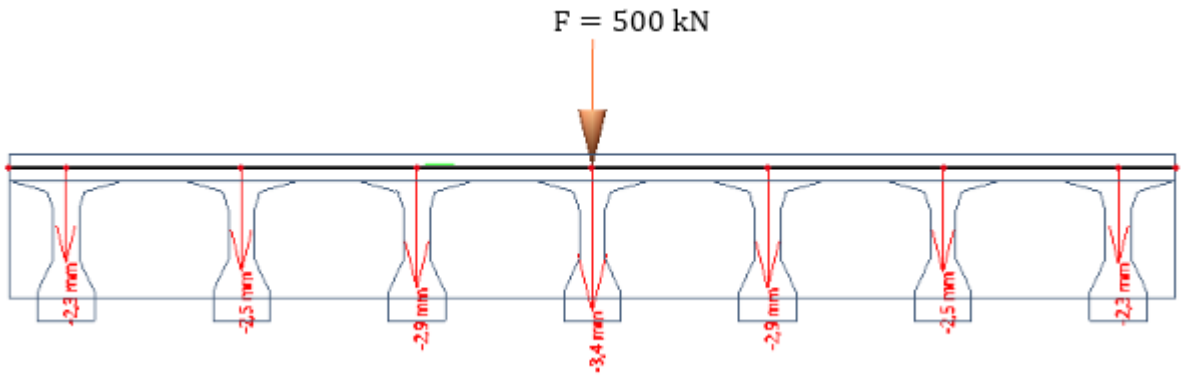


*Figure 131 deflections determined numerically of the seven girders with a load of 500 kN, placed at 4 m from the end*

## Nonlinear modelling of the main beam

The tests indicate that the bridge showed nonlinear behavior. In order to model the nonlinearity the same numerical plate model with seven girders and four crossbeams is used, only this time the main beam is modelled with a lower stiffness, lower than the neighbor beams. The main beam has an elasticity modulus E2, and the neighbors E1 (Figure 132). The stiffness is determined with the test results. The load-displacement relations are converted to stress-strain relations:

$$\sigma = E * \epsilon$$
$$\sigma = \frac{F}{A}\,[\text{MPa}]$$
$$\epsilon = \frac{\Delta l}{l_0} = \frac{\delta}{L_s}[-]$$
$$E = \frac{\sigma}{\epsilon}[\text{MPa}]$$

For the main beam, the secant modulus is determined. The peak load and its ultimate deflection are used. For the neighbor beam the tangent up to the linear load is determined (Figure 133).

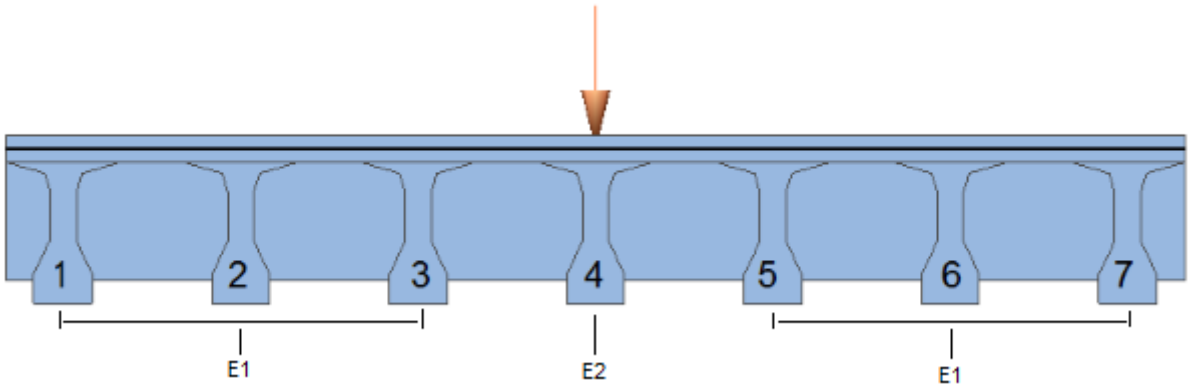


*Figure 132 different stiffness of main and neighbor beams*

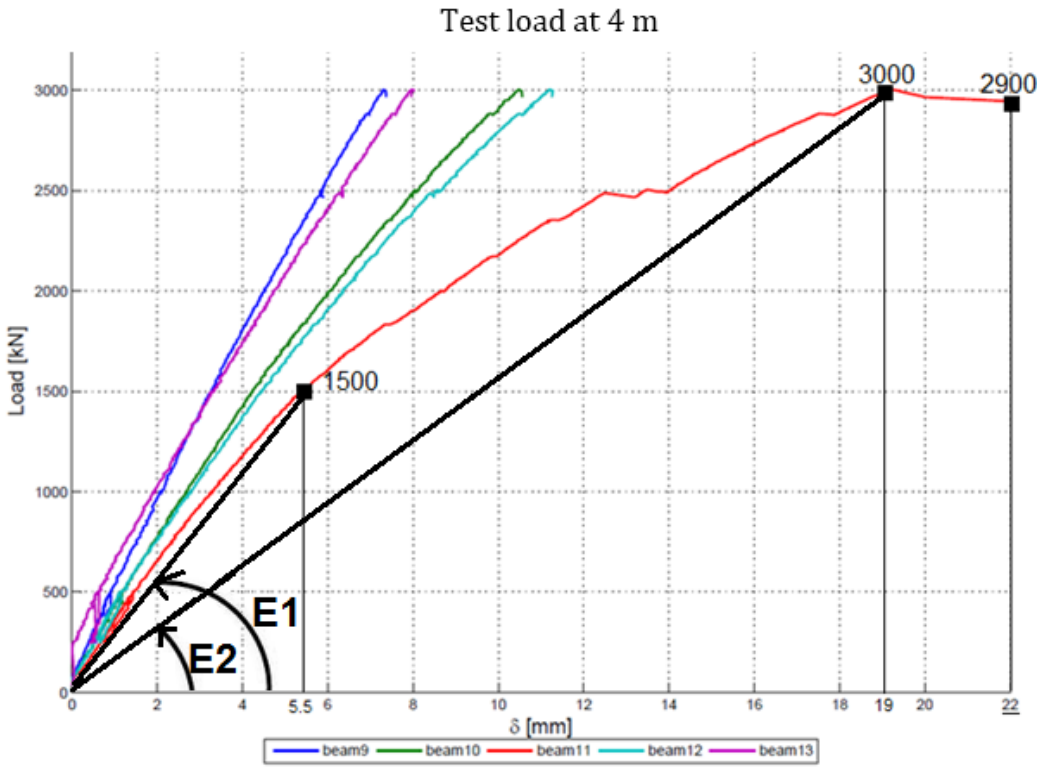


*Figure 133 determining the stiffness for the main and neighbor beams*

For the load at 4 m this gives:

$F_{peak} = 3000 * 10^3$ N
$\sigma = \frac{F}{A} = 18.75$ MPa
$A = 400 * 400$ mm (test load surface)
$\epsilon = \frac{\delta}{L_s} = 7.9 * 10^{-4}$
$\delta_{peak} = 19$ mm $= 19 * 10^{-3}$ m (from Figure 133)
$L_s = 24$ m (beam span)
$E_2 = \frac{\sigma}{\epsilon} = 23.7 * 10^3$ MPa

The same was done for the neighbor beam, giving: $E_1 = 40.9 * 10^3$ MPa
The difference between E1 and E2: $\frac{E_1}{E_2} = 1.7$

And then with the numerical model the load distribution was determined again. The new situation with the main beam with the lower stiffness shows a slightly higher load spread. The three center beams take 1.4% less of the load and distribute it to the outher four beams (Figure 134).

The method of decreasing the stiffness of the main beam has some effect but is not very large. The same is true for the test load at 2.25 m. E2 and E1 are also determined for the test load at 2.25 m: $E_2 = 48.6 * 10^3$ MPa; $E_1 = 81.4 * 10^3$ MPa; $\frac{E_2}{E_1} = 1.7$

And the load distribution is determined again with the lower stiffness for the main beam. And here it is shown that the effect is not large. The three center beams take 0.6% less of the load and spreads it to the outer four beams (Figure 135).

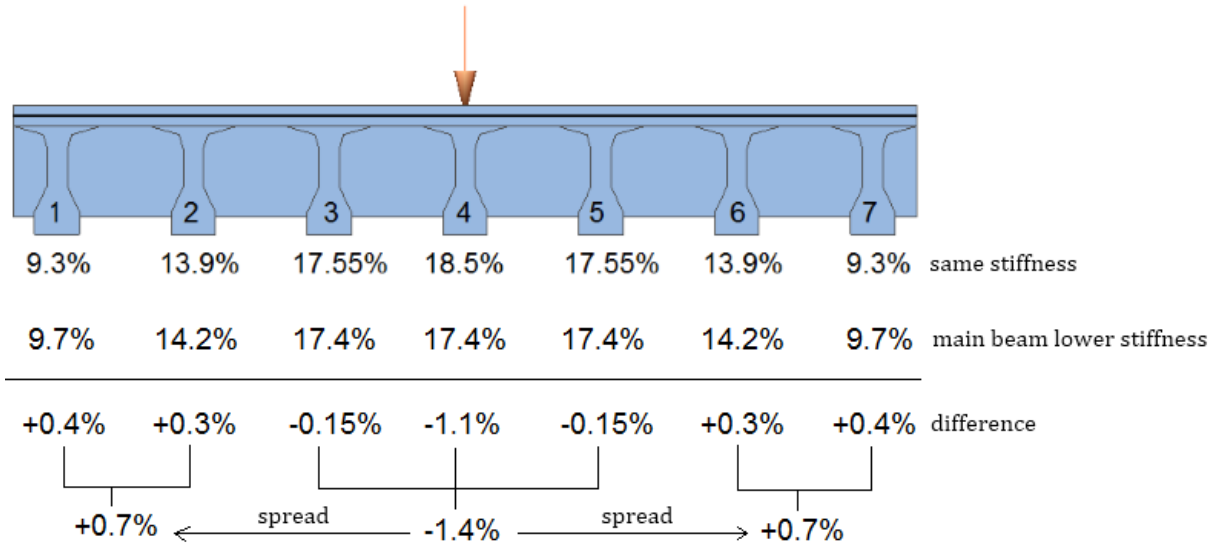


*Figure 134 effect of lower stiffness of main beam on load spread: load at 4 m*

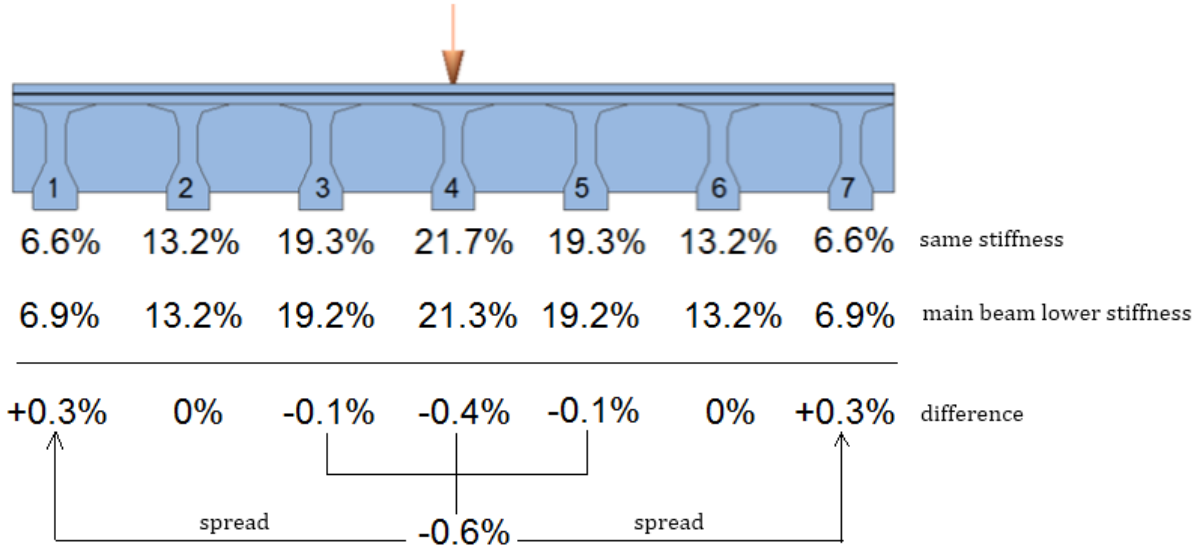


*Figure 135 effect of lower stiffness of main beam on load spread: load at 2.25 m*

**Conclusions nonlinear numerical modelling of the main beam**

Even when the loaded beam was modelled less stiff than the neighboring ones, the load is still almost spread equally over the three middle beams. This means that the relative displacement is still to low to determine whether the critical displacement is reached and whether compressive membrane action is developed in the slab.

## Conclusions on CMA in 'De Vecht' bridge

First, the bridge reached a high capacity in the order of 3000 kN (Figure 251). It is hard to comprehend how the bridge would reach such a maximum load without compressive membrane action. The girders themselves only have a maximum capacity of 1000 or 1700 kN (Appendix H). Calculating with normal flexural theories that do not include membrane action, lead to a slab capacity of around 200-300 kN (mentioned in part 1). This would have resulted in capacities between roughly 1200-2000 kN.

Furthermore, the load distribution determined with the test results gives a relative deflection of $19 - 10.5 = 8.5\,mm$ (Figure 136). It is possible that this deflection is high enough to reach the critical deflection, and to develop cracking and membrane action, but this is not certain.

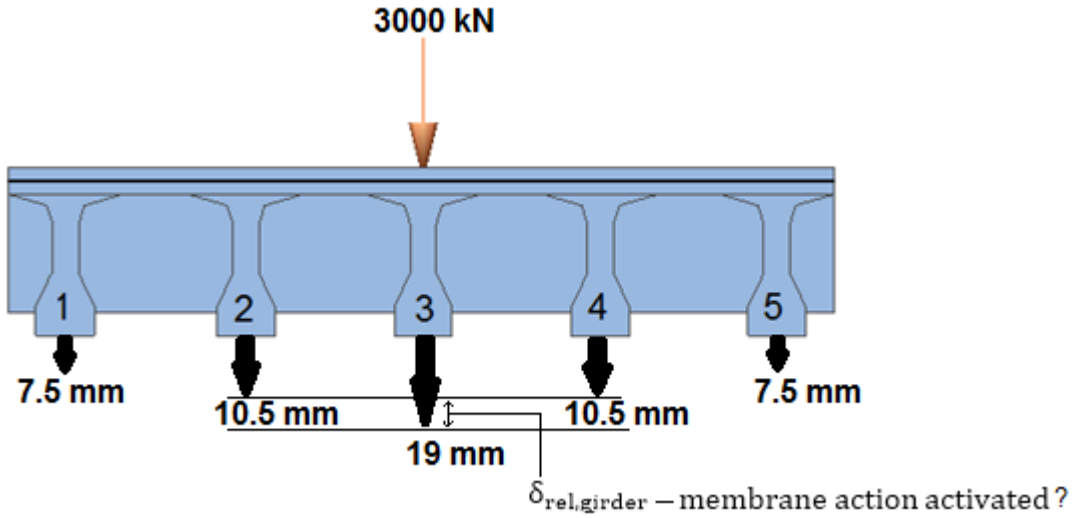


*Figure 136 possible activation of membrane action according to deflections derived from the test results (Appendix H)*

However, the numerically determined load distribution showed that the three center beams were loaded similarily (Figure 137). This means that the relative girder displacement of the main beam is too low. Therefore, it is uncertain whether cracking occurs and membrane action is activated (Figure 137). So when one uses the numerical method (discussed in Chapter 6 and 7), it is uncertain whether compressive membrane action develops in the slab.

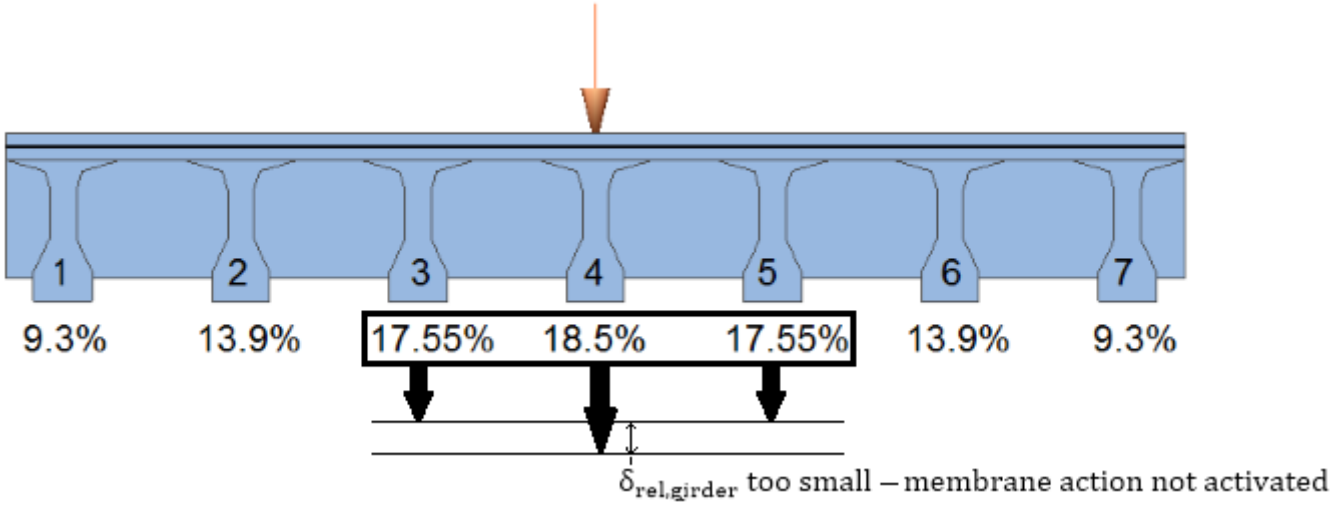


*Figure 137 using the method: CMA not activated due to to low relative displacements*

**Sufficient slab bending capacity**

Even with a seven-girder numerical model the relative girder displacement is too low. This low relative displacement means that numerically it is uncertain whether cracking occurs in the slab. Ultimately, it is uncertain if cracking occurs and consequently if compressive membrane action develops in the slab.

But the fact that compressive membrane action did not develop *during* loading, does not necessarily mean that the mechanism will not develop in the slab after the maximum loading point is reached.

The mechanism and its corresponding slab bending capacity can still play a part after the bridge system reaches a certain maximum capacity. It is assumed that this happens when the loaded beam reaches its maximum capacity. The maximum beam capacity was derived from the test done on an individual beam loaded at 4 m from the end (Figure): $F_{maxgirder} = 1000\ kN$.

After the loaded beam fails, it is the question whether the slab has sufficient bending capacity with use of compressive membrane action to carry the load that was on the beam. Therefore, the slab bending capacity $F_{slab}$ has to be determined to check if: $F_{slab} \geq F_{maxgirder}$ (Figure 138). This kind of check with use of the slab bending capacity was also mentioned in Chapter 1 and Chapter 5.

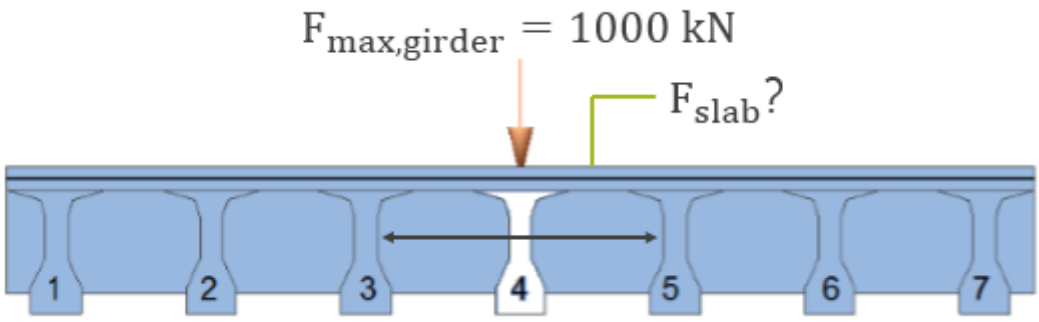


*Figure 138 loaded beam reaches its maximum capacity; slab needs to carry the load*

The slab bending capacities were determined (Appendix G) and mentioned earlier (Chapter 9). For the UK method 560 kN was determined and for the RK method 1200 kN.

This gives the following check:

$$F_{slab,uk} = 560 < F_{maxgirder} = 1000 \text{ kN (Not sufficient)}$$
$$F_{slab,rk} = 1200 > F_{maxgirder} = 1000 \text{ kN (Not sufficient)}$$

It is concluded that the UK method determines an insufficient slab bending capacity. However, the RK method gives a sufficient slab bending. So according to Rankin, the slab is able to carry the maximum load and redistribute it to the neighbor beams.

It is noted that the UK method is a safe but conservative method (mentioned already in Chapter 4). Moreover, prestressing of the concrete slabs is not taken into account in determining the slab's capacity. And the prestressing effect might influence the capacity in a positive manner, which is recommended to be studied more in depth in further research. However, for the test load at 2.25, $F_{maxgirder} = 1700$ kN (Appendix H). Both calculated slab capacities will not be able to carry this load.

**Neighbor beam failure**

Assuming that the slab is able to redistribute the load to the neighbor beams, leads to to the question whether the neighbor beams can carry the load.

First, the loaded beam is modelled with 10% of its original stiffness (Appendix H) to take into account its behavior after reaching maximum girder capacity. In Figure 139 it is found numerically that the neighbor beam is loaded more than the main beam. Since it is assumed that all beams have the same capacity, the neighbor beam cannot be loaded more than the main one, causing it to fail as well. The failure of one neighbor beams sets in motion a chain reaction of failures of the other beams. This mechanism is recommended for further research.

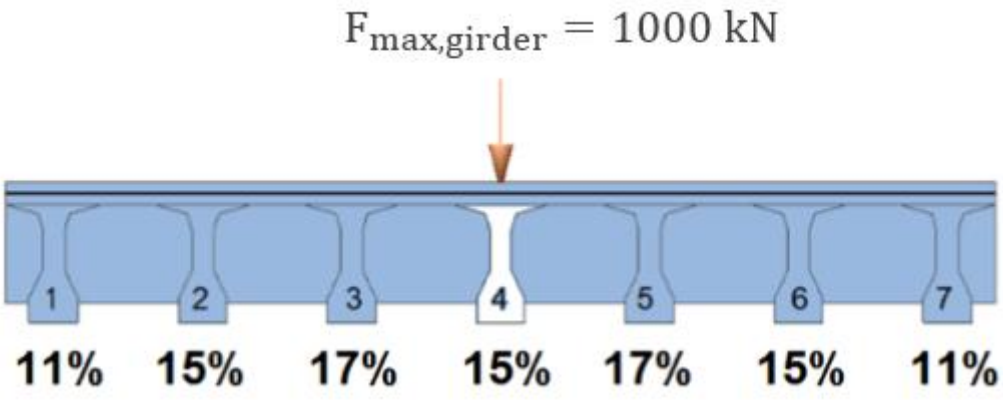


*Figure 139 linear load distribution after loaded beam reaches its maximum girder capacity*

### Distributed load

All the calculations and modelling were done with use of a point load. The point load assumes that all of the load is concentrated on a very small surface area. In reality, the traffic load is more spread out through axle loads.

Finally, after the main beam fails, the load is spread more to the neighbor beams (bottom picture in Figure 140). The point load then should be modelled more as a distributed load (Figure 140). The width over which the load is spread might be determined with the effective width method of Taylor mentioned in Chapter 3.

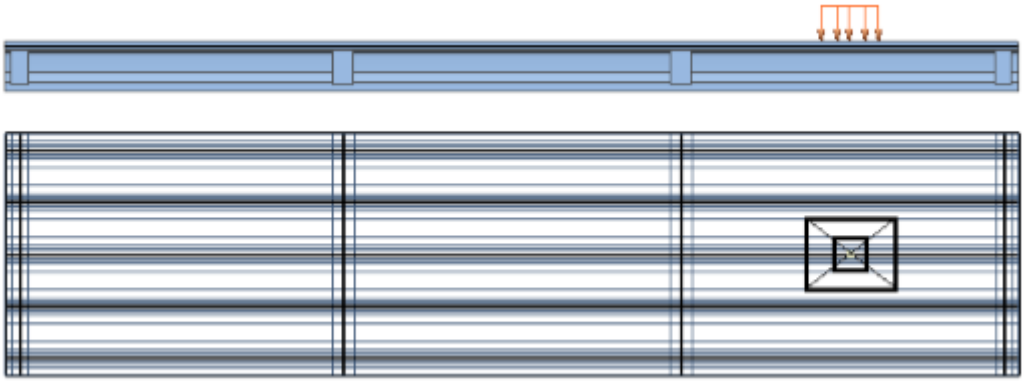

*Figure 140 load changes from point to distributred load after failure of the loaded beam*

## General recommendations from the other parts

### Recommendations from part 1

Explore other methods, beside the ones discussed, to calculate the slab bending capacity due to CMA, for example: method of Park.

### Recommendations from part 2

Use a FEM numerical model (e.g. Diana, Athena), with multiple girders and crossbeams to take into account the spreading, to understand the bridge system non-linear behavior. Use a FEM model for the individual girders to gain more insight in their behavior, capacity, deflection, at what deflection when does peak load occur, and failure. Use a FEM for slab behavior, peak arching action, deflection range, and failure.

### Recommendations from part 3

More research on laterally restraint slabs with different slenderness ratios and concrete strengths, to create more trend lines. And also the influence of the load location needs to be tested more, since the load at 2.25 m displayed a higher deflection at peak load and ultimate deflection.

Also more research and tests needs to be done on real size bridges. For example when another test is done on a bridge, cut off the main beam and test the slab to get the midspan slab displacement.

Redo all the calculations but with the actual concrete strength obtained from drilled concrete cores from the bridge for more accurate results.

# Appendix A

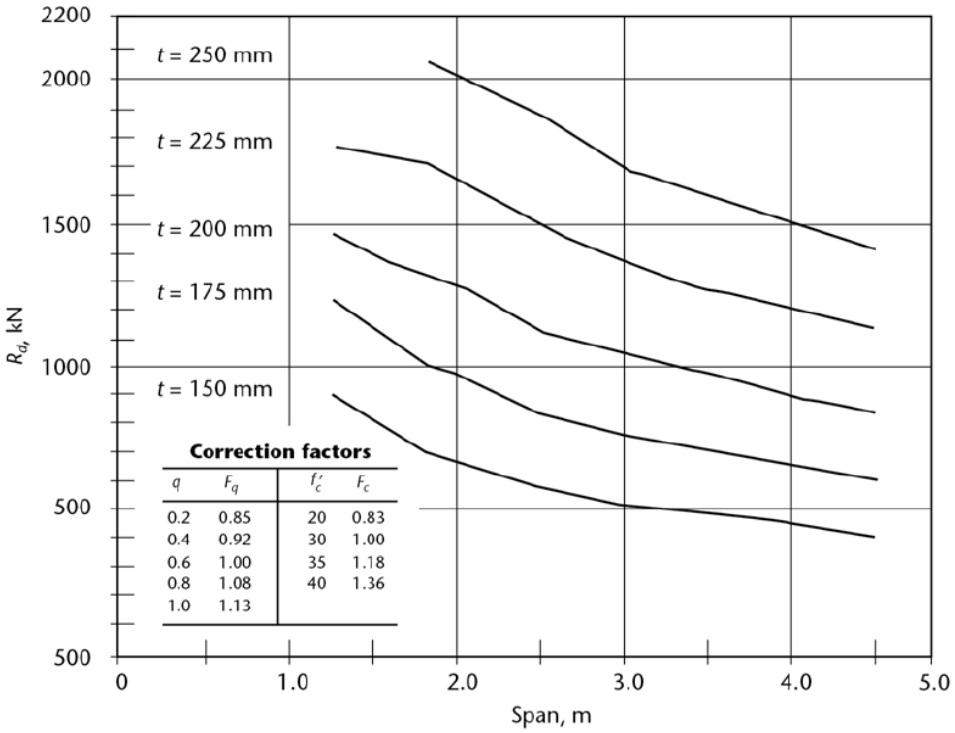


*Figure 141 Rd (kN) values for composite concrete deck slabs (new zealand transport agency, 2014)*

$$CRR = \frac{\text{total length visible cracks}}{\text{total length bottom reinforcement both directions}} * 100 \tag{41}$$

*Table 23 Strength reduction factors (new zealand transport agency, 2014)*

| Superstructure condition | Slab section properties based on: | |
|---|---|---|
| | construction drawings and assessed sound material | measured dimensions or verified as-built drawings, and measured sound material |
| Good or fair (CRR ≤40%) | $0.90\phi_D$ | $1.00\phi_D$ |
| Deteriorated (CRR = 70%) | $0.60\phi_D$ | $0.70\phi_D$ |
| Seriously deteriorated (CRR = 100%) | $0.30\phi_D$ | $0.40\phi_D$ |

**Calculation real size Brienenoord**

**Empirical method (NZ/CAN)**

Graphs from the Transit Bridge manual (new zealand transport agency, 2014) are used to determine $R_i$ since they are comparable with the ones in the CHBDC. Using interpolation, and reading the "composite" graph Figure 141, where reinforcement percentage is 0.23% (0.33% prestress streel in transverse direction, and 0.125 % reinforcement steel in longitudinal direction). This gives the following:

$R_i = 1140\ kN$

For:

$f_c' = 40\ MPa$
$h = 200\ mm,$
$L_s = 3.21\ m$

Calculated capacity:

$$P_{axle} = \frac{\frac{\phi * 0.6 * R_i}{\gamma_L * 40 * I} * 8200}{100} = \mathbf{369\ kN}$$

$\phi = 1.0 * \phi_d = 1.0 * 0.5 = 0.5$
$CRR \leq 40\%$, deck in good conditon, mostly the case in the Netherlands
$\gamma_L = 1.9$
$I = 1.0$

The code is for a load surface area of 250*250 mm and does not give a solution for other wheel prints, such as the one used on 'De Vecht' (400*400 mm).

So using linear extrapolation the capacity is estimated: $\frac{400}{250} * P_{axle} = 590\ kN$

A characteristic load of 300 kN is present in LM1 (NEN-EN 1991-2, 2005).

So the unity check gives:

$$\frac{300}{590} = 0.51\ [-]$$

The check is in order.

**Simplified method (UK)**

Input parameters:

$$f_c' = 0.8 * \frac{f_{cu}}{1.5} = 26.7 \frac{N}{mm^2}$$

$h = 200\ mm$
$d = 0.5 * h = 0.5 * 200 = 100\ mm$

It is noted that the effective depth d is defined as up till the halfway point of the main centrical reinforcement.

$$L_r = 0.5 * L_s = 0.5 * 3400 = 1700\ mm$$

Deformation:

$$\varepsilon_c = (-400 + 60 * 26.7 - 0.33 * 26.7) * 10^{-6} = 0.965 * 10^{-3}$$

$$R = \varepsilon_c * \frac{{L_r}^2}{d^2} = 0.965 * \frac{(1700)^2}{(200)^2} = 0.070 \leq 0.26$$

$$k = 0.0525 * \left(4.3 - 16.1 * \sqrt{3.3 * 10^{-4} + 0.1243 * 0.070}\right) = 0.145$$

Arch moment capacity:

$$M_{ar} = k * f_c' * h^2 = (0.145 * 26.7 * 200^2) = 155 \left[\frac{kNm}{m}\right]$$
$$P_b = \frac{M_{ar}}{0.23} = \mathbf{675\ kN}$$

Equivalent reinforcement ratio:

$$\rho_e = \frac{M_{ar}}{f_{ye} * d * z} = \frac{155 * 10^6}{320 * 0.75 * 100^2} = 0.0645\ \%$$
$z = 0.75 * d$
$d = 0.5 * h = 0.5 * 200 = 100\ mm$

Punching capacity:

$$P_p = 1.52 * (\phi + d) * d * \sqrt{f_c'} * (100 * \rho_e)^{0.25}$$
$\phi = 509\ mm$ (load surface $400 * 400$)

$$P_p = \left(1.52 * (340 + 100) * 100 * \sqrt{26.7} * (100 * 0.0645)^{0.25}\right) * 10^{-3} = 762\ kN$$

When two wheelloads are applied together:

$$P_{pd} = 0.65 * P_p = 495\ kN$$

Unity check:

$$\frac{\frac{300}{2}}{\frac{495}{1.5}} = 0.6$$

The check is in order. (NEN-EN 1991-2, 2005) prescribes a load of 150 kN (for a load surface of 400*400 mm), and the loadfactor 1.5 comes from BD (81/02, 2002).

**Conclusions and important notes**

The slenderness is an issue, and a very low reinforcement ratio is applied as well, whereas 0.3% is recommended. The slenderness issue will be addressed in the second part. It is possible that the present centrical prestress compensates for these issues. Finally, the "tussenstort" is cast later than the girders and is not part of the deck as whole and induces joints/interfaces. These joints might have been an issue, but they have been tested (Amir, 2014), and have been proven *not* to be decisive in failure.

### Rankin Method

The same clear span is considered (Figure 38). Which gives the following effective width:

$b_{eff} = c_y + 2 * L_e + 2 * h = \mathbf{3800\ mm}$
$c_y = 400\ mm$
$c_x = 400\ mm$
$L_e = \frac{L_s}{2} - \frac{c_x}{2} = 1500\ \text{mm}$
$h = 200\ mm$
$L_s = 3400\ mm$

#### Stiffness parameters

$E_c = 4.23 * f_{cu}^{0.5} = 21.8 \frac{kN}{mm^2}$
$f_{cu} = 26.7\ MPa$

$K_s = \frac{E_c * b_{eff} * h}{L_e} = 10375 \frac{kN}{mm}$

$K_d = \sum \frac{A_d * E_c}{L_e} = 86 * 10^3 \frac{kN}{mm}$
$A_d = 2 * (700 * 1620) = 2.3 * 10^6\ mm^2$

$K_b = \frac{A_b * E_c}{L_e} = 51.7 * 10^4 \frac{kN}{mm}$
$A_b = \frac{\zeta * I_b * L_e}{b_{eff}} = 37.9 * 10^6\ mm^2$
$\zeta = 985$ (FE)
$I_b = 1.32 * 10^{12}\ mm^4$

$K_r = \frac{1}{(\frac{1}{K_b} + \frac{1}{K_d})} = 73.8 * 10^3\ kN/mm$

#### Flexural Capacity

#### Flexural parameters

$\beta = 1 - 0.003 * f_{cd} = 0.92 > 0.9.$
$So\ \beta = 0.9$

$$x = \frac{f_y * A_s}{0.67 * f_{cd} * \beta * b_{eff}} = 13\ mm$$
$f_y = 320\ MPa$
$A_s = 660 \frac{mm^2}{m}$ (For transverse reinforcement percentage of 0.33%)

$z = d - 0.5 * \beta * x = 94\ mm$
$d = 100\ mm$

$M_b = f_y * A_s * z = 75\ kNm/m$

For fixed ended:

$$P_b = \frac{8 * L_s}{M_b} = 177\ kN$$

Arching section

$2 * d_1 = h - 2 * x * \beta$
$d_1 = 88\ mm$

$d_1$ from the previous iteration is used. The contact area due to arching is then given by:

$A = \alpha * b_{eff} * d_1 = 310619 mm^2$
$\alpha = 1$ for the first iteration, after 2 iterations $\alpha = 0.927$
$$L_R = L_e \sqrt[3]{\left(\frac{E * A}{K * L_e}\right) + 1} = 1528\ mm$$

Arching parameters

$\varepsilon_u = 0.0043 - [(f_{cd} - 60) * 2.5 * 10^{-5}] = 5.1 * 10^{-3} > 0.0043. So\ \varepsilon_u = 0.0043$
$\varepsilon_c = 2 * \varepsilon_u * (1 - \beta) = 8.6 * 10^{-4}$

Deformation

$$R = \frac{\varepsilon_c * {L_r}^2}{4 * d_1^2} = 0.073$$
$0 < R < 0.26;\ u = -0.15 + 0.36 * \sqrt{0.18 + 5.6 * R} = 0.127$

**Contact Depth**

$$\alpha = 1 - \frac{u}{2} = 0.936$$

$\alpha * d_1$ is used for refined arching section above until value remains constant (iterative process).

**Arching Capacity**

$$0 < R < 0.26;\ M_r = \ 4.3 - 16.1 * \sqrt{3.3 * 10^{-4} + 0.1243 * R}\ ) = 2.73$$
$$M_{ar} = 0.168 * b_{eff} * f_c' * d_1^2 * M_r * \frac{L_e}{L_r} = 367\ kNm/m$$

When both sides are restrained (Pucher, 1964) gives:

$$P_a = \frac{M_{ar}}{0.23} = 1597\ kN$$

**Flexural punching capacity**

The ultimate capacity is the sum of the flexural and arching capacity:

$$P_{pf} = P_b + P_a = \mathbf{1775\ kN}$$

However punching shear is governing, which is calculated with:

$$P_{pv} = \frac{0.43}{r_f} * \sqrt{f_{cd}} * (\phi + d)\pi * d * (\rho_e)^{0.25} = 501\ kN$$
$$r_f = 1.15 \text{ (rectangular wheel load)}$$

Ultimate capacity

$$P_{pf} > P_{pv}$$

Punching shear is governing, then: $P_u = P_{pv}$

**Prototype Brienenoord**

**Empirical method (NZ/CAN)**

The concrete deck was in good condition, as is common practice in the Netherlands. So $CRR \leq 40\%$, $\phi = 1.00 * \phi_D = 1.00 * 0.5 * 0.5$.

$$q = 50 * \left(\frac{A_{sl}}{b * d_l} + \frac{A_{st}}{b * d_t}\right) = 0.5\%$$

$A_{sl} = 141\ mm^2/m$ (reinforcement steel)
$A_{st} = 442\ mm^2/m$ (prestress steel)
$b = 1000\ mm$
$d_l = 91\ mm$
$d_t = 50\ mm$

Using extrapolation and the graph from Figure 141 the following parameters are determined:

$F_q = 0.96$, $F_c = 1.29$
$R_d = 500\ kN$, so $R_i = 0.96 * 1.29 * 500 = 619\ kN$

(Amir, 2014) suggested extrapolation of the correction factors might create unsafe impressions of strength. In the conclusion of this chapter, the calculated strength and test results will be compared.

Finally, the calculated strength is:

$$P_{axle} = \frac{\frac{0.5 * 0.6 * 619}{1.9 * 40 * 1} * 8200}{100} = \ 200\ kN$$

$\phi = \phi_{\mathrm{d}} * 1 = 0.5$ (low cracking)
$\gamma_L = 1.9$
$I = 1.0$

**Simplified method (UK)**

Input parameters:

$$f_c' = 0.8 * \frac{f_{cu}}{1.5} = 38 \frac{N}{mm^2}$$
$$h = 100\ mm$$
$$d = 0.5 * h = 50\ mm$$

Again the effective depth d is defined as up till the halfway point of the main reinforcement.

$$L_r = 0.5 * L_s = 0.5 * 1650 = 825\ mm$$

Deformation:

$$\varepsilon_c = (-400 + 60 * 26.7 - 0.33 * 26.7) * 10^{-6} = 1.4 * 10^{-3}$$

$$R = \varepsilon_c * \frac{{L_r}^2}{d^2} = 0.096 \leq 0.26$$

$$k = 0.0525 * \left(4.3 - 16.1 * \sqrt{3.3 * 10^{-4} + 0.1243 * 0.096}\right) = 0.198$$

Arch moment capacity:

$$M_{ar} = k * f_c' * h^2 = (0.198 * 38 * 100^2) = 75 \left[\frac{kNm}{m}\right]$$

Equivalent reinforcement ratio:

$$\rho_e = \frac{M_{ar}}{f_{ye} * d * z} = \frac{75 * 10^6}{525 * 0.75 * 50^2} = 0.076$$
$$z = 0.75 * d$$
$$d = 0.5 * h = 0.5 * 100 = 50\ mm$$

Punching capacity:

$$P_p = 1.52 * (\phi + d) * d * \sqrt{f_c'} * (100 * \rho_e)^{0.25}$$
$$P_p = \left(1.52 * (255 + 50) * 50 * \sqrt{38} * (100 * 0.076)^{0.25}\right) * 10^{-3} = 237\ kN$$
$$\phi = 255\ mm$$

**Rankin method**

The same clear span is considered (Figure 41). Which gives the following effective width:

$b_{eff} = c_y + 2 * L_e + 2 * h = 1850\ mm$
$c_y = 200\ mm$
$c_x = 200\ mm$
$L_e = \frac{L_s}{2} - \frac{c_x}{2} = 725\ \text{mm}$
$h = 100\ mm$
$L_s = 1650\ mm$

Stiffness parameters

$E_c = 4.23 * f_{cu}^{0.5} = 26 \frac{kN}{mm^2}$
$f_{cu} = 38\ MPa$

$K_s = \frac{E_c * b_{eff} * h}{L_e} = 6653 \frac{kN}{mm}$

$K_d = \sum \frac{A_d * E_c}{L_e} = 57 * 10^3 \frac{kN}{mm}$
$A_d = 2 * (700 * 1620) = 5.7 * 10^5\ mm^2$

$K_b = \frac{A_b * E_c}{L_e} = 28.4 * 10^4 \frac{kN}{mm}$
$A_b = \frac{\zeta * I_b * L_e}{b_{eff}} = 7.9 * 10^6\ mm^2$
$\zeta = 985$ (FE)
$I_b = 70.2 * 10^9\ mm^4$

$K_r = \frac{1}{(\frac{1}{K_b} + \frac{1}{K_d})} = 47.4 * 10^3\ kN/mm$

### Flexural Capacity

#### Flexural parameters

$\beta = 1 - 0.003 * f_{cd} = 0.886 < 0.9.$

$$x = \frac{f_y * A_s}{0.67 * f_{cd} * \beta * b_{eff}} = 10\ mm$$

$f_y = 525\ MPa$
$A_s = 442.5\ mm^2/m$
$z = d - 0.5 * \beta * x = 45\ mm$
$d = 50\ mm$
$M_b = f_y * A_s * z = 20\ kNm/m$

For fixed ended:

$$P_b = \frac{8 * L_s}{M_b} = 95\ kN$$

#### Arching section

$2 * d_1 = h - 2 * x * \beta$
$d_1 = 41\ mm$

$d_1$ from the previous iteration is used. The contact area due to arching is then given by:

$A = \alpha * b_{eff} * d_1 = 70.4 * 10^3\ mm^2$
$\alpha = 1$ for the first iteration, after 2 iterations $\alpha = 0.932$

$$L_R = L_e \sqrt[3]{\left(\frac{E * A}{K * L_e}\right) + 1} = 737\ mm$$

### Arching parameters

$\varepsilon_u = 0.0043 - [(f_{cd} - 60) * 2.5 * 10^{-5}] = 0.00485 > 0.0043$
$So\ \varepsilon_u = 0.0043$
$\varepsilon_c = 2 * \varepsilon_u * (1 - \beta) = 9 * 10^{-4}$

### Deformation

$R = \frac{\varepsilon_c * {L_r}^2}{4 * d_1^2} = 8 * 10^{-2}$
$0 < R < 0.26;\ u = -0.15 + 0.36 * \sqrt{0.18 + 5.6 * R} = 0.13$

### Contact Depth

$\alpha = 1 - \frac{u}{2} = 0.932$

$\alpha * d_1$ is used for refined arching section above until value remains constant (iterative process).

### Arching Capacity

$0 < R < 0.26;\ M_r = 4.3 - 16.1 * \sqrt{3.3 * 10^{-4} + 0.1243 * R}) = 2.7$
$M_{ar} = 0.168 * b_{eff} * f_{cd} * d_1^2 * M_r * \frac{L_e}{L_r} = 52\ kNm/m$

When both sides are restrained (Pucher, 1964) gives:

$P_a = \frac{M_{ar}}{0.23} = 225\ kN$

### Flexural punching capacity

The ultimate capacity is the sum of the flexural and arching capacity:
$P_{pf} = P_b + P_a = \mathbf{320\ kN}$

However punching shear is governing, which is calculated with:
$P_{pv} = \frac{0.43}{r_f} * \sqrt{f_{cd}} * (\phi + d)\pi * d * (\rho_e)^{0.25} = 140\ kN$
$r_f = 1.15$ (rectangular wheel load)

$P_{pf} > P_{pv}$, then: $P_u = P_{pv}$

### Girder Shear Capacity

First the critical T-girder is considered, which is loaded close the supports. Depending on the location of the point load, the girder can fail in different ways, with different shear capacities. At least two fail mechanisms are possible: tensile splitting and flexural shear. Tensile splitting failure is more common when the girder is not reinforced heavily with shear braces. Here the principle tensile stress exceeds the concrete tensile strength, failure occurs in the web of the girder without warning, failing brittle.

(Vugts, 2012) determines the zone where tensile splitting shear failure could occur, using the design flexural cracking moment $M_{cr}$ and $M_{Ed}$ (Figure 142 and Figure 143). In the uncracked zones, for ULS, the design value for the shear resistance of the concrete is calculated. The mean tensile concrete strength $f_{ctm}$ is used for the lab experiment instead of the lower $f_{ctd}$, giving the linear tensile splitting shear capacity:

$$V_{Rd,c} = \frac{I * b_w}{S} * \sqrt{f_{ctd}^2 + \alpha_l * \sigma_{cp} * f_{ctd}}$$

$$V_{Rd,c} = \frac{70.2295 * 10^9 * 150}{70.9 * 10^6} * \sqrt{4.16^2 + 1.0 * \frac{0.85 * 4951 * 10^3}{342900} * 4.16} \quad (42)$$

$$V_{Rd,c} = 1229\ kN$$

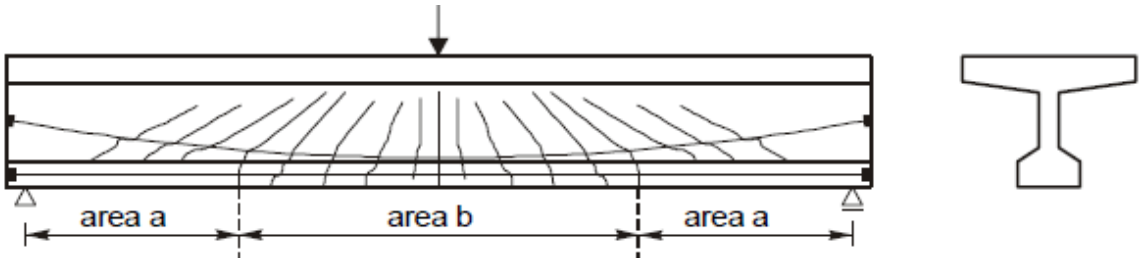


*Figure 142 cracking prestressed beam*

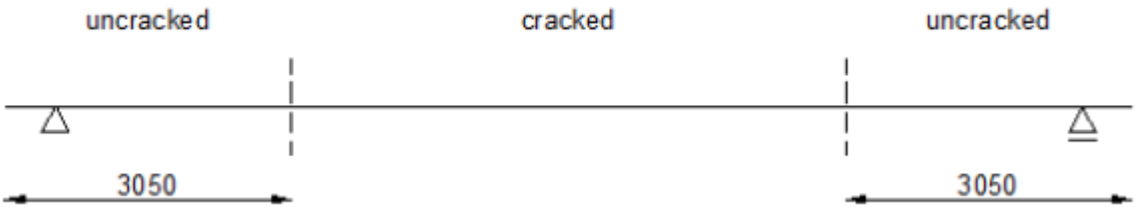


*Figure 143 crack zones*

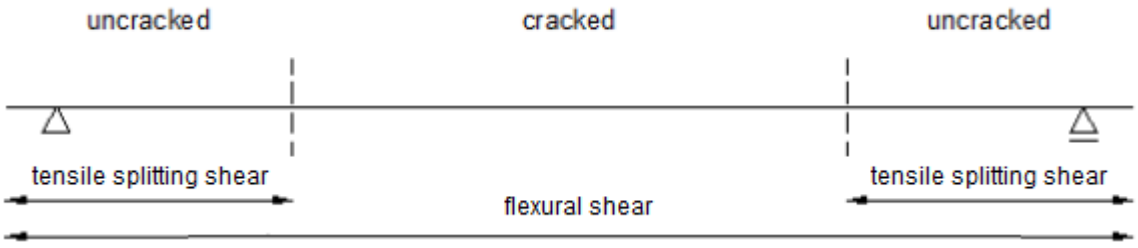


*Figure 144 locations where failure modes occur*

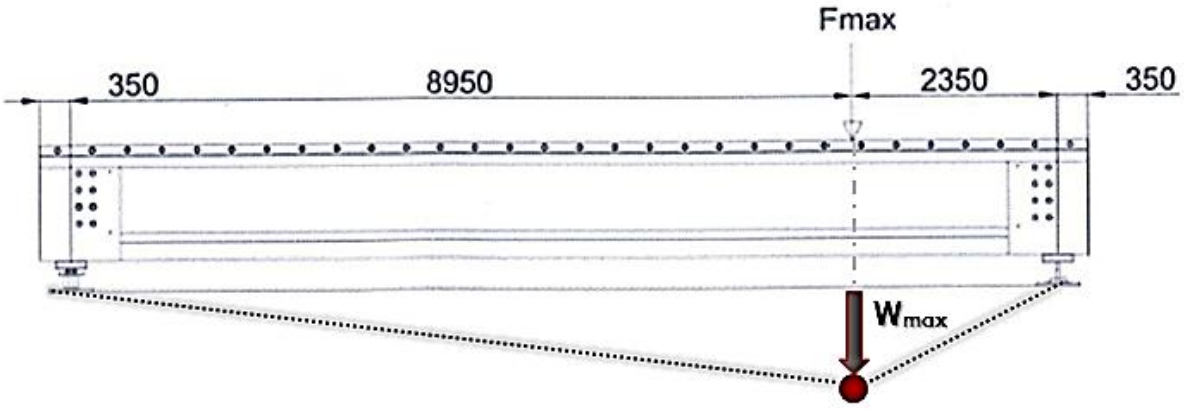


*Figure 145 load location and relative deflection of the girder over its span*

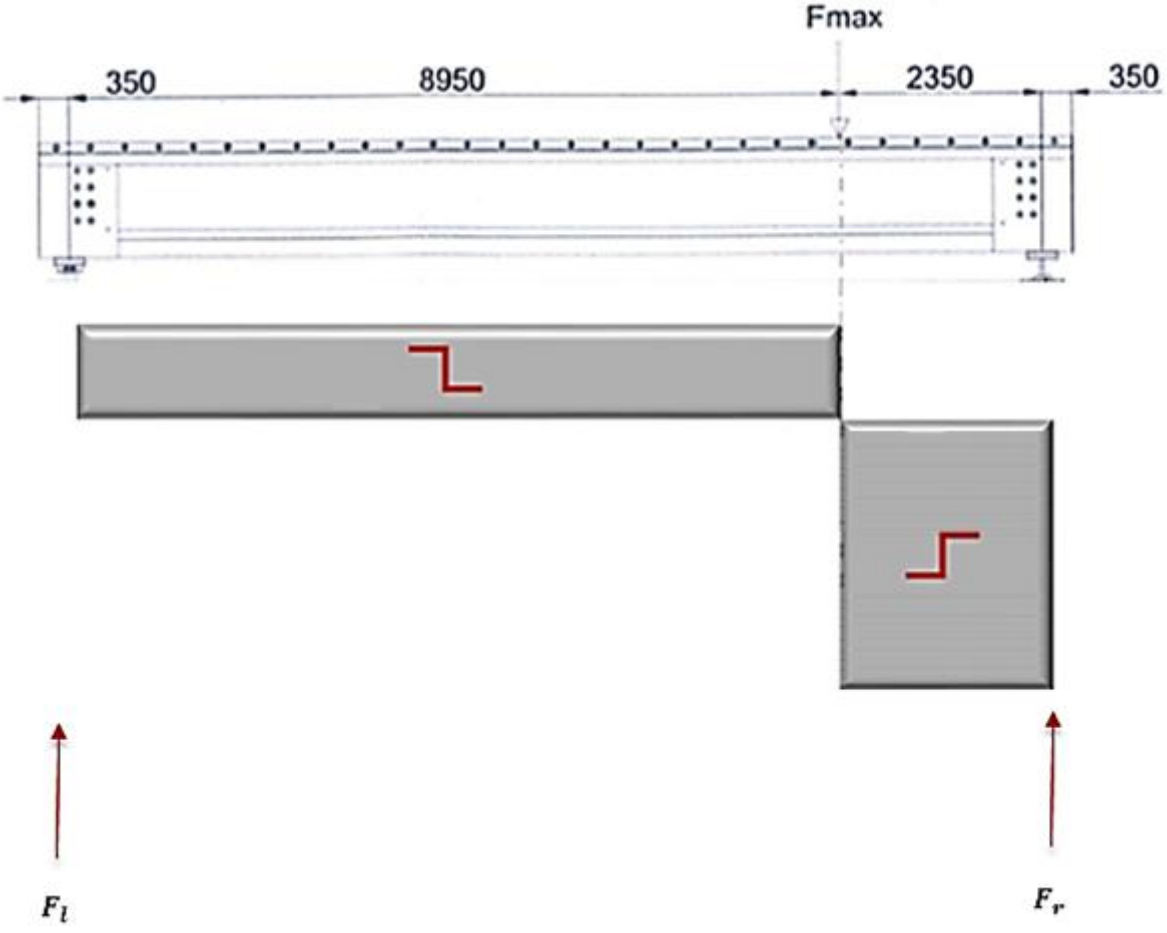


*Figure 146 Shear force distribution*

If the girder is loaded at a point near the supports within the uncracked zone, it is possible failure due to tensile splitting shear occurs. Comparing Figure 143 with Figure 145, one sees that the point of loading is 2350 mm from the end, this falls in the marked uncracked zone of 3050 mm. Here, it is possible the girder fails in tensile shear splitting. However, because of the presence of high shear reinforcement in the girder, the other fail mode flexural shear is more likely. The flexural shear capacity with shear reinforcement for this loading situation is assumed to be $V_{rd,max} = 1189\ kN$ (Vugts, 2012). And usually this capacity is higher than the tensile splitting capacity, which is usually calculated with $f_{ctd}$ instead of $f_{ctm}$. The highest capacity between tensile splitting and flexural shear, though, can be taken when loading in the uncracked zone (Figure 144).

Therefore with equilibrium of forces and the load position, the support reactions are known. Using that the maximum design shear force equals the tensile splitting strength, this gives:

$$F_{max} = \frac{11.3}{8.95} * F_r = 1.26 * V_{Ed} = 1.26 * 1229 \approx 1550\ kN$$
$$F_{max} = 1.26 * 1189$$

$$V_{Ed} = V_{Rd,c} \text{ (tensile splitting shear)}$$

Or

$$V_{Ed} = V_{Rd,max} \text{ (flexural shear)} \qquad (43)$$

**Example calculation slab bending capacity for prototype Brienenoord**

**Determine effective width**

The considered clear span is 3450 mm. This gives an effective width of 3650 mm.

$$b_{eff} = c_y + 2 * L_e + 2 * h = 200 + 2 * 1625 + 2 * 100 = \mathbf{3650\ mm} \quad (44)$$

$c_y$ = length of load area in y − direction
$L_e$ = effective span of the slab subjected to arching force
$L_e = \frac{L_s}{2} - \frac{c_x}{2} = \frac{3450}{2} - \frac{200}{2} = 1625\ mm$
$c_x$ = length of load area in x − direction
$L_s$ = clear span of considered slab
$L_s = 2 * L_{c.t.c} - 2 * d_{web} = 2 * 1800 - 2 * 75 = 3450\ mm$

**Lower bound slab bending capacity**

The linear girder load, 1500 kN, is reached around 7 mm, derived from the single beam prototype test result. For now, at this instant, membrane action is assumed to activate for a determined effective width with a bending capacity that can be calculated (Figure 58). This is the lower bound slab bending capacity of a laterally restraint concrete strip. For a simply supported slab Rankin gives a bending capacity of 133 kN, and the effective width is 3650 mm.

**Upper bound slab bending capacity**

The assumed maximum deflection $\delta_{ultm}$, which is 37 mm, is derived from the single beam test results. And at the maximum deflection, the activated beam span is about 9.2 m (Figure 62).

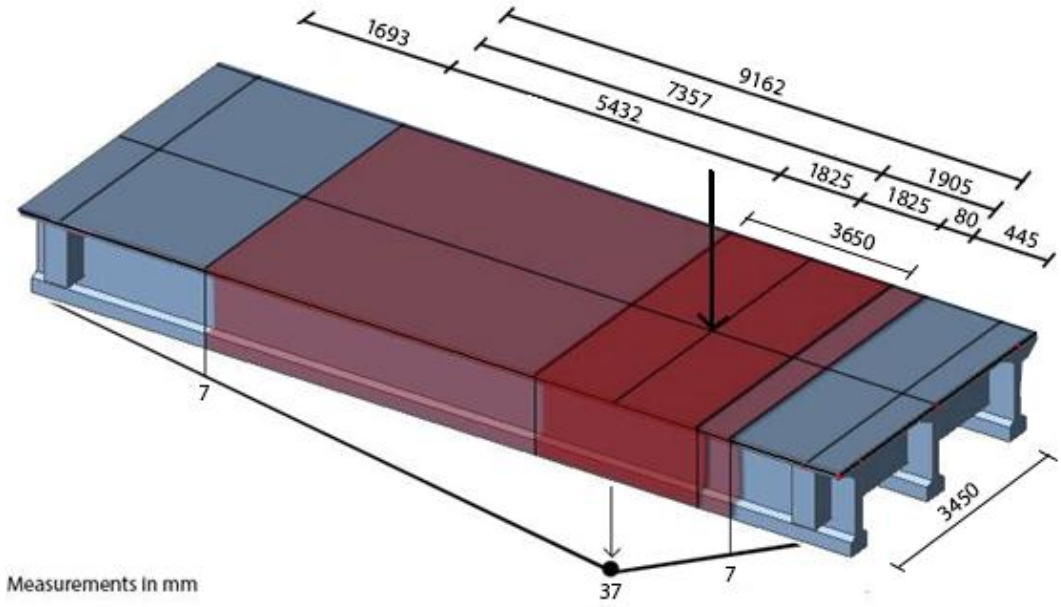


*Figure 147 Activated slab area, top view with measurements (not on scale)*

**Total slab capacity**

The calculation is done for the activated span length of 9.2 m. An effective width of 3.65 m and an assumed slab bending capacity of 133 kN per activated slab strip, gives the following total slab capacity:

$$n\,[-] = \frac{\text{activated slab span [m]}}{\text{effective width slab strip [m]}}$$

$$\text{total slab capacity [kN]} = n * \textbf{bending capacity slab strip}$$

$$F_{slab,upper} = n * F_{slab,lower}$$

$$n = \frac{9.2}{3.65} = 2.5$$

$$F_{slab,upper} = 2.5 * 133 = 333\ kN$$

The linear girder load of 1550 kN can be added to give the total load, since it is assumed that slab and beam work together

$$F_{total} = F_{girder} + F_{slab,upper} = 1550 + 333 = 1883\ kN$$

The same calculations are done again, for Rankin (SS/FE), (FE) and the UK method. For the last method the same effective width is assumed to be present. The CAN method does not calculate a bending capacity. Results are summarized (Table 24).

*Table 24 results total slab capacity and total bridge capacity*

| Method | Slab Bending capacity $\mathbf{F_{slab,lower}}$ [kN] | Activated beam span [m] | Total slab capacity $\mathbf{F_{slab,upper}}$ [kN] | Total bridge load [kN] |
|---|---|---|---|---|
| **Rankin (SS)** | 133 | 9.2 | **333** | **1883** |
| **Rankin(SS/FE)** | 172 | 9.2 | 430 | 1980 |
| **Rankin (FE)** | 178 | 9.2 | 445 | 1995 |
| **Simplified(UK)** | 75 | 9.2 | 188 | 1738 |

# Appendix B

### Numerical model 1 Elastic plate

### General information plate

Concrete class: C45/55.
Concrete density: 2500 kg/m$^3$.
E-modulus: 36300 MPa.
G-modulus: 15125 MPa.
Poisson ratio: 0.2 [-]
FEM-model: orthotropic plate.
Linear numerical model.
Thickness: 100 mm.
Spring supports.
Spring stiffness: 17.7 MN/m.
Crossbeams: 0
Amount of girders: 0.
Size 2D-plate element: 0.25 m.
Plate theory: Mindlin-reissner.
Type solver: direct.

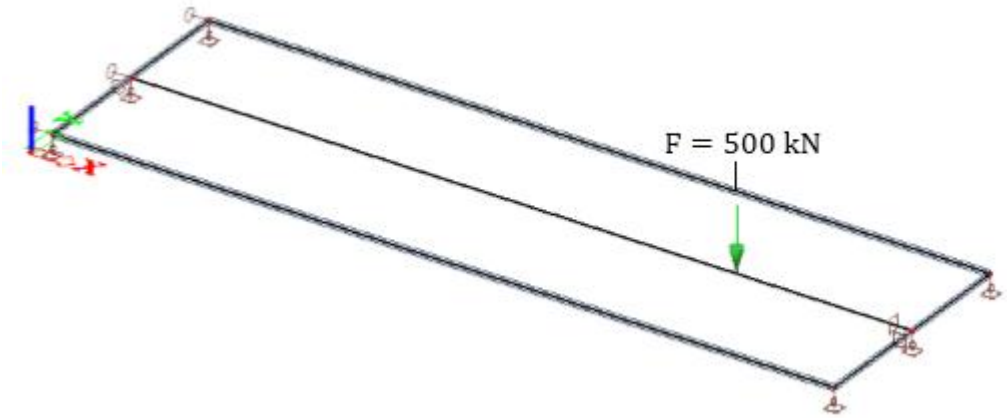


*Figure 148 linear elastic plate model*

**Load distribution**

The key element involved in the distribution of the load is the deck, modeled as a plate. So first, a linear elastic plate was modeled with three supports at each end.

A load distribution of 20.5% **59%** 20.5% over the supports was found, for a load of 500 kN. A rough estimation beforehand expects the load to divide over the three supports with a ratio of 25:50:25, the model corresponds with that notion.

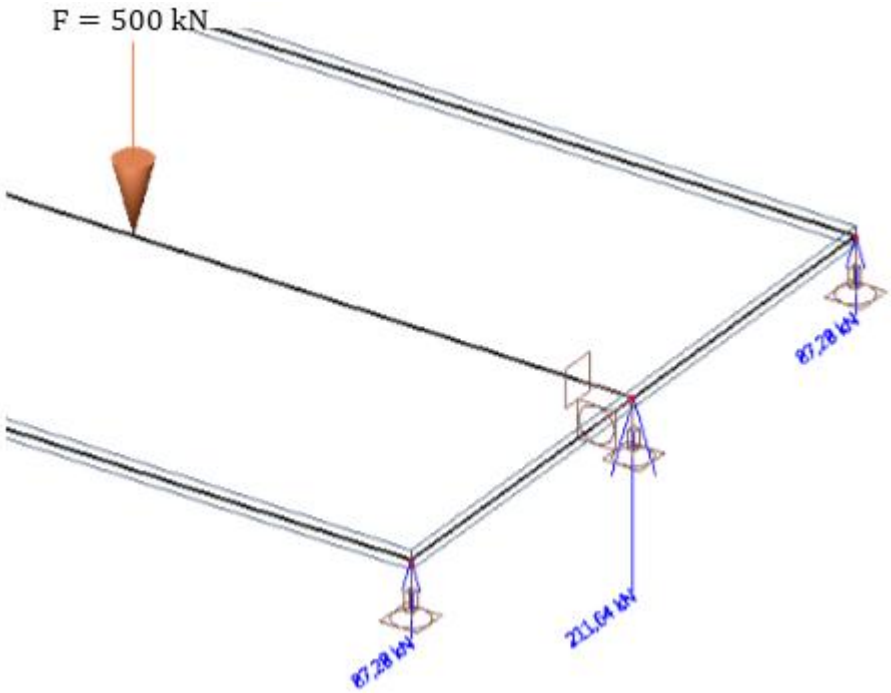


*Figure 149 load distribution over the three supports*

.

**Numerical model 2 Elastic plate with three girders**

**General information plate**

Concrete class: C45/55.
Concrete density: 2500 kg/$m^3$.
E-modulus: 36300 MPa.
G-modulus: 15125 MPa.
Poisson ratio: 0.2 [-]
FEM-model: orthotropic plate.
Linear numerical model.
Thickness: 100 mm.
Spring supports.
Spring stiffness: 59.5 MN/m.
Crossbeams: 0.
Amount of girders: 3.
Size 2D-plate element: 0.25 m.
Plate theory: Mindlin-reissner.
Type solver: direct.

**General information girder**

Concrete class: C55/67
Concrete density: 2500 kg/$m^3$.
E-modulus: 38400 MPa.
G-modulus: 15917 MPa.
Poisson ratio: 0.2 [-]
A: 0.2634 $m^2$.
$I_y$: 4.42*$10^{-2}$ $m^4$.
$W_{ely}$: 7.33*$10^{-2}$ $m^3$.

### Load distribution

After the basic model, T-girders were implemented as ribs to consider their effect on the spreading of the load. The load distribution became 11.5 % **77%** 11.5%, for a load of 500 kN. The critical girder takes up more of the load. This change is explained by the increased bending stiffness of the plate due to implementing the T-girders as a ribs under the loaded area. This stiffer part takes up more of the load and directly transfers it via the heavily loaded T-girder to its supports, and thus distributes it less laterally via the slab and to the other girders.

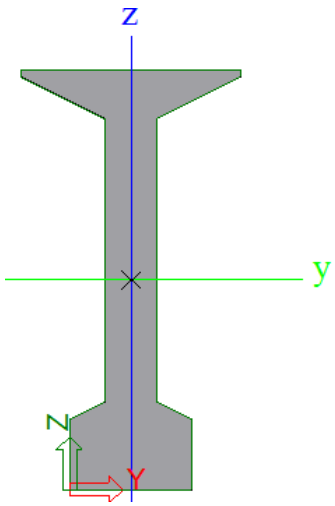


*Figure 150 cross section beam*

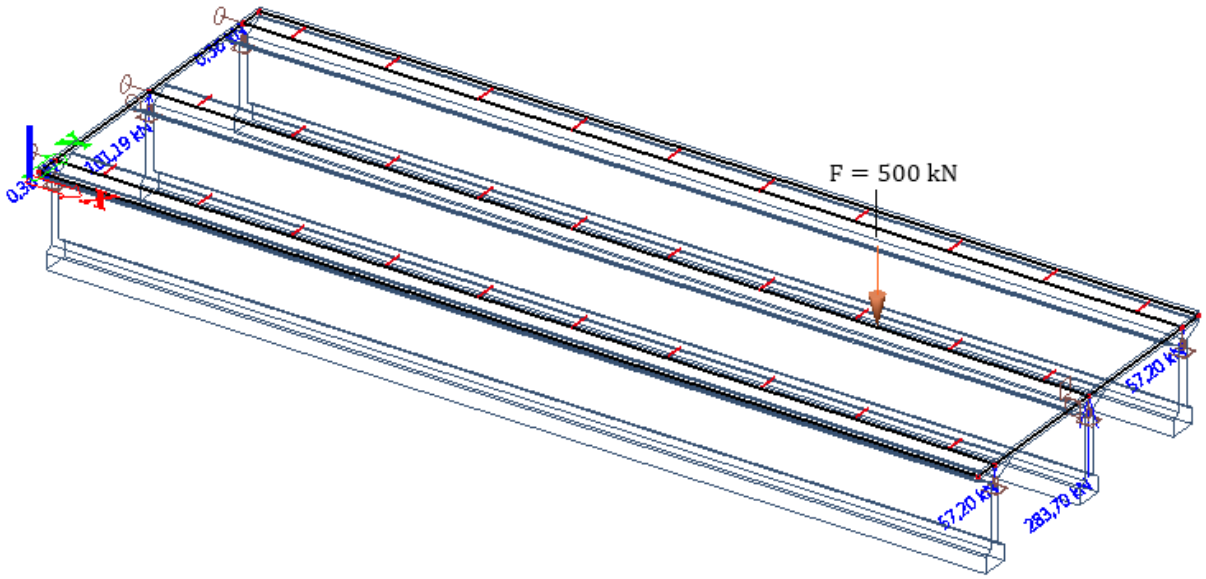


*Figure 151 plate with three girders*

**Numerical Model 3 Elastic plate with three girders and two crossbeams**

**General information plate**

Concrete class: C45/55.
Concrete density: 2500 kg/m$^3$.
E-modulus: 36300 MPa.
G-modulus: 15125 MPa.
Poisson ratio: 0.2 [-]
FEM-model: orthotropic plate.
Linear numerical model.
Thickness: 100 mm.
Spring supports.
Spring stiffness:  69.3 MN/m.
Crossbeams: 2.
Amount of girders: 3.
Size 2D-plate element: 0.25 m.
Plate theory: Mindlin-reissner.
Type solver: direct.

**General information girder**

Concrete class: C55/67
Concrete density: 2500 kg/m$^3$.
E-modulus: 38400 MPa.
G-modulus: 15917 MPa.
Poisson ratio: 0.2 [-]
A: 0.2634 m$^2$.
$I_y$: 4.42*10$^{-2}$ m$^4$.
$W_{ely}$: 7.33*10$^{-2}$ m$^3$.

**General information crossbeam**

Concrete class: C45/55
Concrete density: 2500 kg/m$^3$.
E-modulus: 38400 MPa.
G-modulus: 15917 MPa.
Poisson ratio: 0.2 [-]
Cross section: 810*350 mm.
A: 2.84*10$^{-1}$ m$^2$.

$I_y$: 1.55*10$^{-2}$ m$^4$.
$W_{ely}$: 3.83*10$^{-2}$ m$^3$.

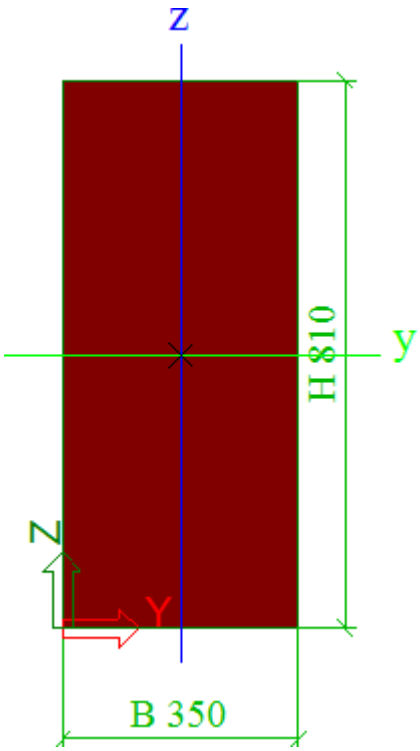

*Figure 152 cross section cross beam*

### Load distribution

The next step was to build on the previous model by adding crossbeams which are present in the lab prototype (Figure 153). The load distribution now becomes 32.5 % **35 %** 32.5 %, for a load of 500 kN. The spreading of the load has increased, causing the critical girder to be loaded with almost a third of the total load (of one side of the deck). This significant increase in spreading is caused by the inserted concrete crossbeam.

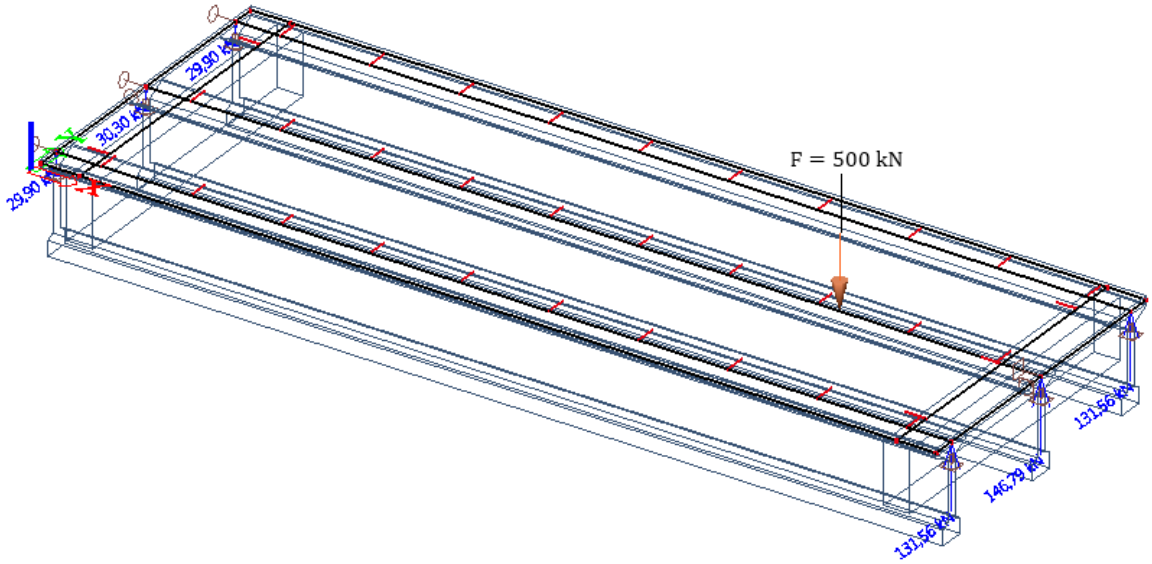


*Figure 153 plate with three girders and two crossbeams*

**Numerical model 4 Elastic Plate with four girders**

**General information plate**

Concrete class: C45/55.
Concrete density: 2500 kg/$m^3$.
E-modulus: 36300 MPa.
G-modulus: 15125 MPa.
Poisson ratio: 0.2 [-]
FEM-model: orthotropic plate.
Linear numerical model.
Thickness: 100 mm.
Spring supports.
Spring stiffness: 60.9 MN/m.
Crossbeams: 0.
Amount of girders: 4.
Size 2D-plate element: 0.25 m.
Plate theory: Mindlin-reissner.
Type solver: direct.

**General information girder**

Concrete class: C55/67
Concrete density: 2500 kg/$m^3$.
E-modulus: 38400 MPa.
G-modulus: 15917 MPa.
Poisson ratio: 0.2 [-]
A: 0.2634 $m^2$.
$I_y$: 4.42*$10^{-2}$ $m^4$.
$W_{ely}$: 7.33*$10^{-2}$ $m^3$.

### Load distribution

In the lab prototype four girders are present in the bridge. Model 4 takes a look at a plate with four girders. The load distribution is 11 % **73%** 9% 7%, for a load of 500 kN. The extra girder and deck surface area causes an increase in spreading relative to model 2. The effect on load spreading of this added girder is not as strong as by addition of the crossbeam as shown in Model 3.

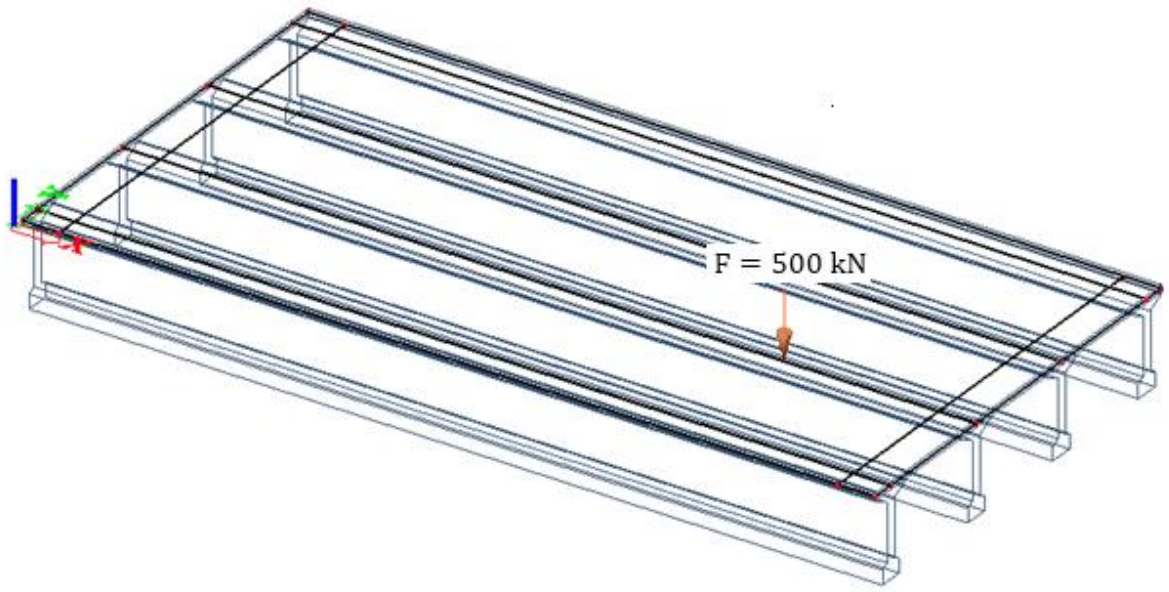


*Figure 154 plate with four girders*

**Numerical model 5 Elastic plate with four girders and two crossbeams**

**General information plate**

Concrete class: C45/55.
Concrete density: 2500 kg/$m^3$.
E-modulus: 36300 MPa.
G-modulus: 15125 MPa.
Poisson ratio: 0.2 [-]
FEM-model: orthotropic plate.
Linear numerical model.
Thickness: 100 mm.
Spring supports.
Spring stiffness:  71.37 MN/m.
Crossbeams: 2.
Amount of girders: 4.
Size 2D-plate element: 0.25 m.
Plate theory: Mindlin-reissner.
Type solver: direct.

**General information girder**

Concrete class: C55/67
Concrete density: 2500 kg/$m^3$.
E-modulus: 38400 MPa.
G-modulus: 15917 MPa.
Poisson ratio: 0.2 [-]
A: 0.2634 $m^2$.
$I_y$: 4.42*$10^{-2}$ $m^4$.
$W_{ely}$: 7.33*$10^{-2}$ $m^3$.

**General information crossbeam**

Concrete class: C45/55
Concrete density: 2500 kg/$m^3$.
E-modulus: 38400 MPa.
G-modulus: 15917 MPa.
Poisson ratio: 0.2 [-]
Cross section: 810*350 mm.
A: 2.84*$10^{-1}$ $m^2$.
$I_y$: 1.55*$10^{-2}$ $m^4$.
$W_{ely}$: 3.83*$10^{-2}$ $m^3$.

**Load distribution**

The final model takes into account the whole the lab prototype: four girders and two crossbeams. The load distribution is 31% **32%** 25% 12%, for a load of 500 kN. It is clear that adding crossbeams has a significant effect on the load distribution. Causing the support of the critical girder to be loaded with roughly a third of the load. The added fourth girder, compared to Model 3, causes the small difference in loading of 3%.

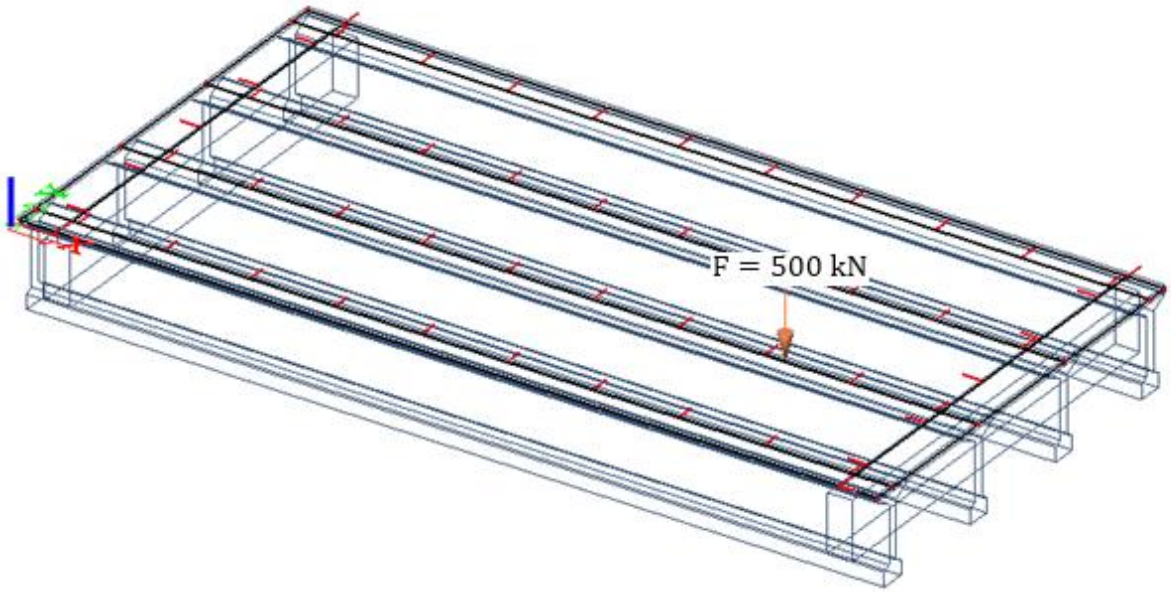


*Figure 155 plate with four girders and two crossbeams*

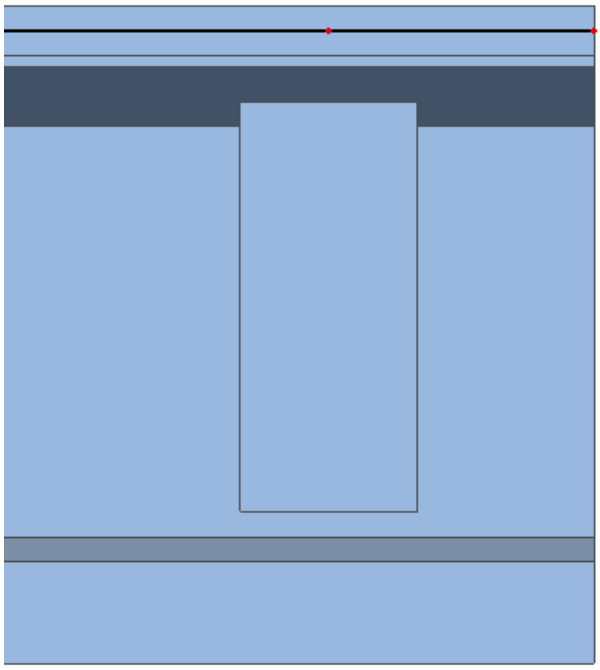

*Figure 156 eccentricity of crossbeam in numerical model*

The effect of the eccentricity of the crossbeam is also relevant. The eccentricity relative to the top of the deck is 190 mm as stated by (Amir, 2014). If one were to increase this eccentricity the spreading of the load increases.

The differences in spring stiffness is caused by the difference in self-weight of each model.

### Conclusions Linear distribution

Every single one of the models display a significant load distribution under linear conditions. Meaning that the critical loaded girder, the girder expected to fail in shear, can take up more load than it would have, if loaded solely. In reality the critical girder is never loaded with a full hundred percentage of the load since it spreads and distributes the load to the neighbor girders via the plate

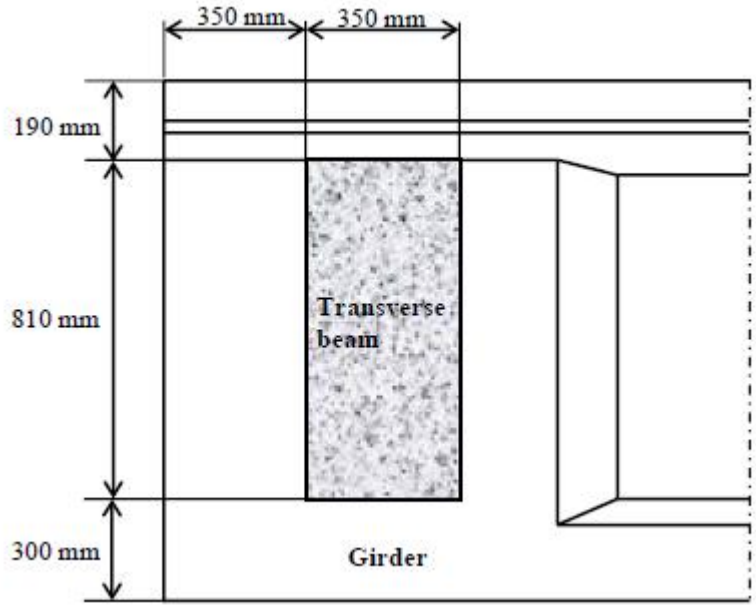


*Figure 157 eccentricity crossbeam in prototype*

*Table 25 overview input and output of the five models*

| Model | T-beams | Supports per side | Crossbeams | Spring stiffness [MN/m] | Load percentage main beam [%] |
|---|---|---|---|---|---|
| **1** | 0 | 3 | | 17.7 | 59 |
| **2** | 3 | 3 | | 59.5 | 77 |
| **3** | 3 | 3 | X | 69.3 | 36 |
| **4** | 4 | 4 | | 60.9 | 73 |
| **5** | 4 | 4 | X | 71.4 | **32** |

# Appendix C

## Neighbor beam experiment

### Introduction

It was questioned what the influence of the load location is in chapter 7. So an experiment on the prototype 'Brienenoord is discussed where the loading point changes location. The same numerical plate model is used again. The comparison is made to verify the model and see how the results obtained from the model hold up to reality.

**Background experiment**

The tests were done on the lab prototype of the 'Brienenoord'. The goal of the experiment was to see how the loads distribute over the neighbor beams before and after cracking of the loaded main beam (Ensink, 2014). The experiment was executed on the middle of the second bottom beam, between prestressing point FP15 and FP16 (Figure 158).

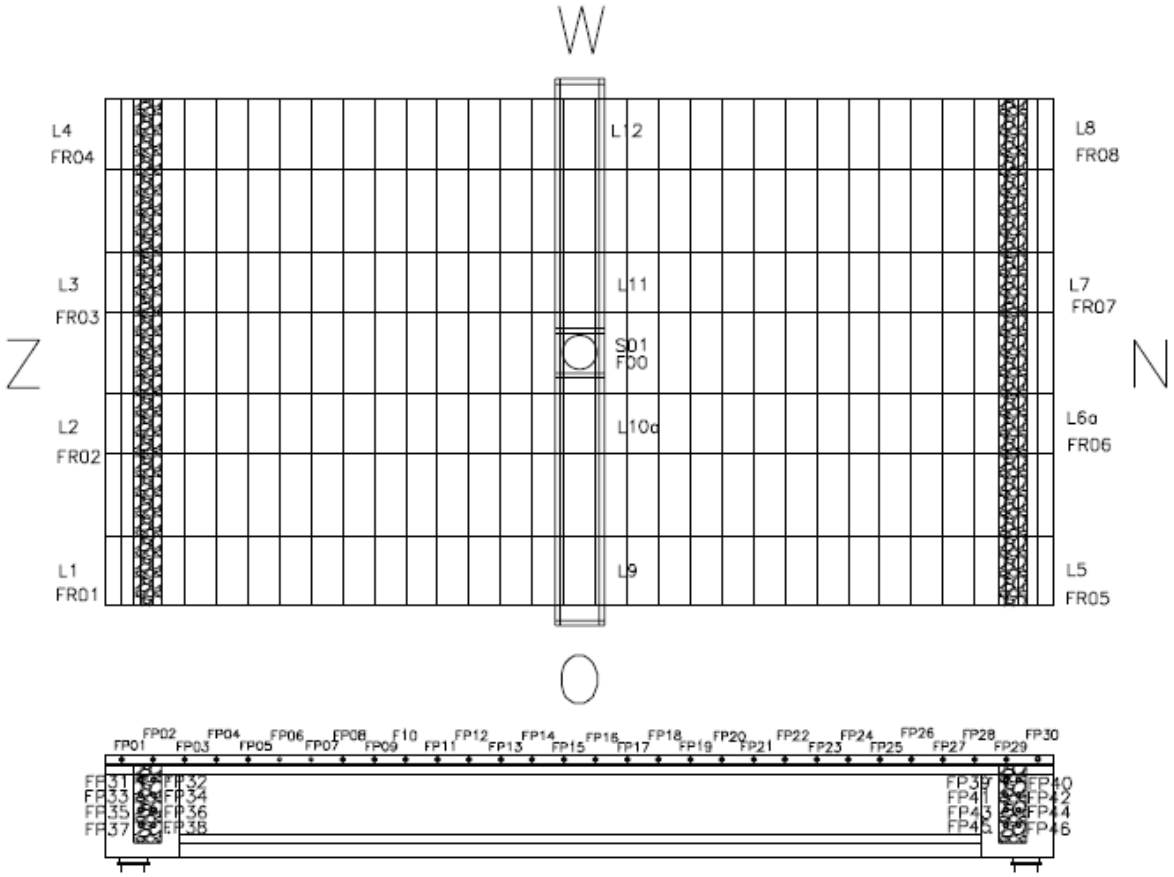


*Figure 158 loading point of experiment (Ensink, 2014)*

The first test loaded the beam up to 1700 kN, but then the test was stopped, because diagonal cracks appeared in the web of the girder and insufficient shear capacity was possible. With analysis of the test results and use of hand calculations, it was assumed that the load could be increased up to 2200 kN, while maintaining a certain safety margin However, the machine, that was used, could only go to a load of 1950 kN. Figure 159 shows the load displacement curve from the test.

.

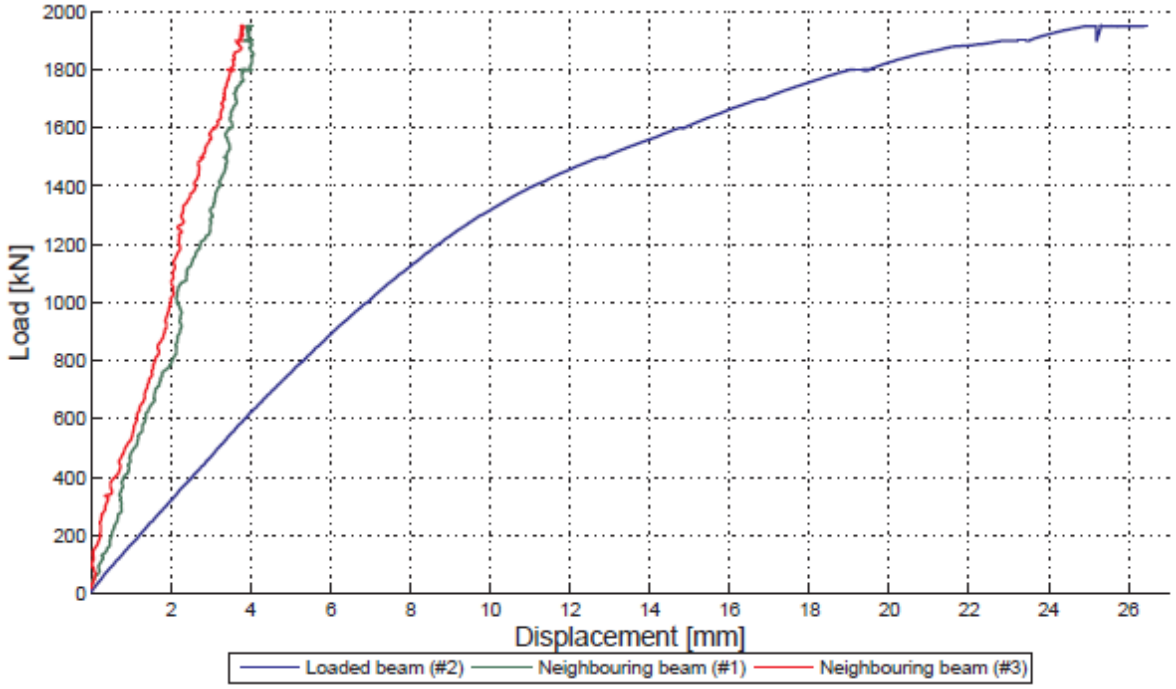


*Figure 159 load-displacement graph bottom three girders during the test (Ensink, 2014)*

**Activation of membrane action**

In Chapter 5 and 7 it was discussed that membrane action could activate earlier in the linear loading phase of the main beam, before it reaches its linear capacity. Chapter 7 suggest numerically that this assumption is plausible. However, the test results in this chapter do not show a significant increase of capacity and seem to reach a plateau in the loading graph (Figure 159).

And redistribution of the loads does not seem to be taken place. A reasonable conclusion is that membrane action is possibly not activated, or not to its full extent. This means that the slab strength contribution is also not present, or not very large (Figure 159). There are a few possible reasons why membrane action is not activated:

- Too high slenderness ratio $\lambda$
  - Long clear span
  - Thin deck
- Critical deflection criteria $\delta_{rel,girder} > \delta_{midspan}$ not met

For the first reason, concerning the slenderness, the criteria from Part 1 are reconsidered. These criteria need to be met for membrane action to activate, and the slenderness condition in particular is important. Again, the considered clear span is 3450 mm (Figure 158).

- $\lambda = \frac{3450}{100} = 34.5 > 20$
- $h = 100\,mm < 150\,mm$

Since the slenderness criteria is not met, the system does not have a restraint factor of $\eta = 0.5$ or higher. This means that the deck is not laterally restraint enough according to the criteria. This is a possible reason why membrane action does not activate. And it is added, that when one of the criteria is not met, membrane action cannot be assumed to be present in the system, and is not allowed to be calculate with, according to the research from part 1.

The other reason is the critical deflection condition: the relative girder deflection needs to exceed the slab midspan deflection. It is possible that this condition was not met. This is required to be met to activate membrane action. This was checked numerically.

The considered clear span was 3450 mm. For a slab bending capacity $F_{slab} = 172\ kN$, a slab midspan deflection $\delta_{slab} = \delta_{crit} = 10\ mm$ was determined (Figure 159). This bending capacity has not changed and was already determined (Table 9).

In the test results, at a load of 1500 kN, a displacement of 12.5 mm is reached with a relative girder displacement of, after rounding, 10 mm (after subtracting the average deflection from the neighbor girders of 2.5 mm). And it is shown that the critical deflection condition is met (Figure 161). $\delta_{rel,girder} = \delta_{crit} = 10\ mm$

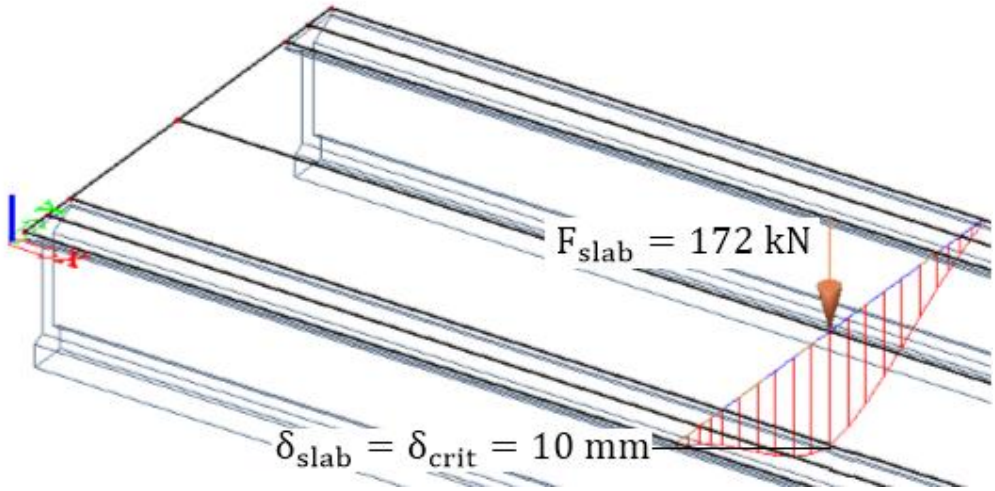


*Figure 160 section at middle of girder to determine the slab's midspan displacement for Rankin (SS/FE)*

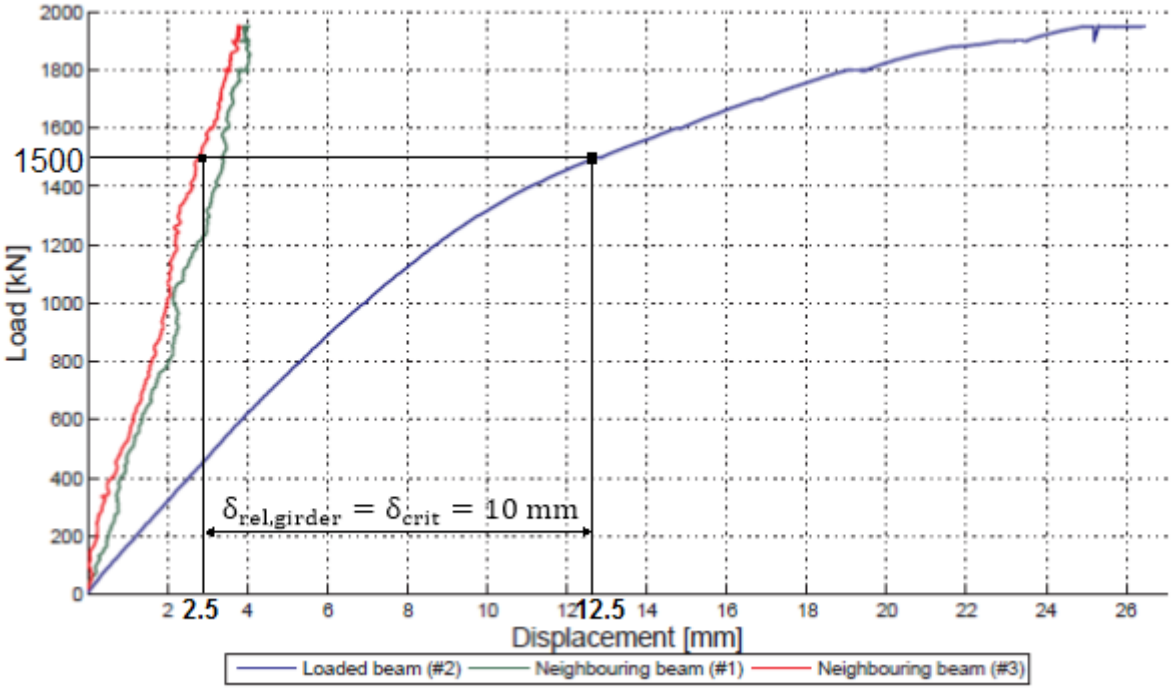


*Figure 161 critical displacement and critical girder load in load displacement graph*

**Conclusions**

Ultimately, the numerical model and Figure 161 show that the relative girder displacement does exceed the midspan displacement. This means that membrane action would activate. So the more likely reason why it does not activate, is because the deck is too slender.

The lateral restraint also depends on the position of the load relative to the end cross-beams. And the restraint stiffness increases if the load area moves toward the ends of the bridge, closer to the diaphragms. Therefore, by loading the deck exactly in the middle (Figure 158), the loading point is placed the furthest away from the end cross-beams and is at its least stiff point.

### Neighbor experiment numerical model

A comparison between load displacement graphs is made to determine a range wherein a linear numerical model is applicable to this experiment, and where it is safe to work with a linear model. The same three-girder numerical model from the previous chapters is used, only now the loading point is relocated to the middle of the main beam (Ensink, 2014).First, the experiment behaves stiffer than the three-girder numerical model in the linear phase (Figure 162). And generally the numerical model shows a safe underestimate of the the test (Figure 164). This is apparent up till the maximum load of the test around 1950 kN, here the numerical model starts to deviate around 24 mm (Table 26).

Furthermore, end beams were added (Figure 163) and the deflections were determined again, and plotted in the same graph (Figure 164). Now it is shown that the numerical model seems more similar to the test. With end beams the numerical model starts to deviate at 1600 kN. So the presence of the end beams influences the load-displacement behavior significantly, this is mentioned and taken into account in later chapters.

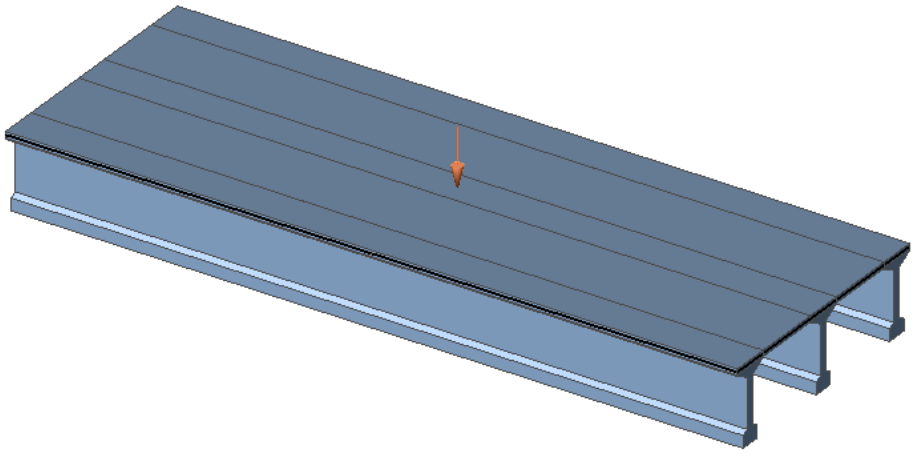

*Figure 162 three-girder numerical model: neighbor test with point load in the middle of the main beam*

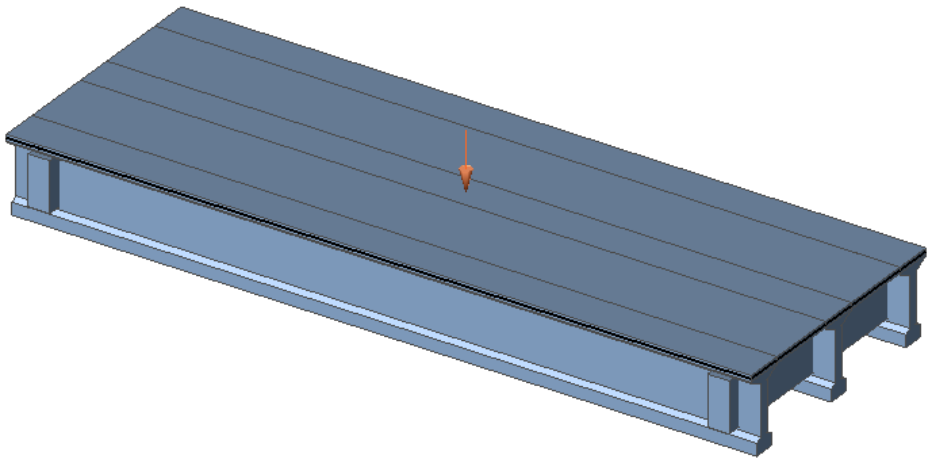

*Figure 163 three-girder numerical model with endbeams: neighbor test with point load in the middle of the main beam*

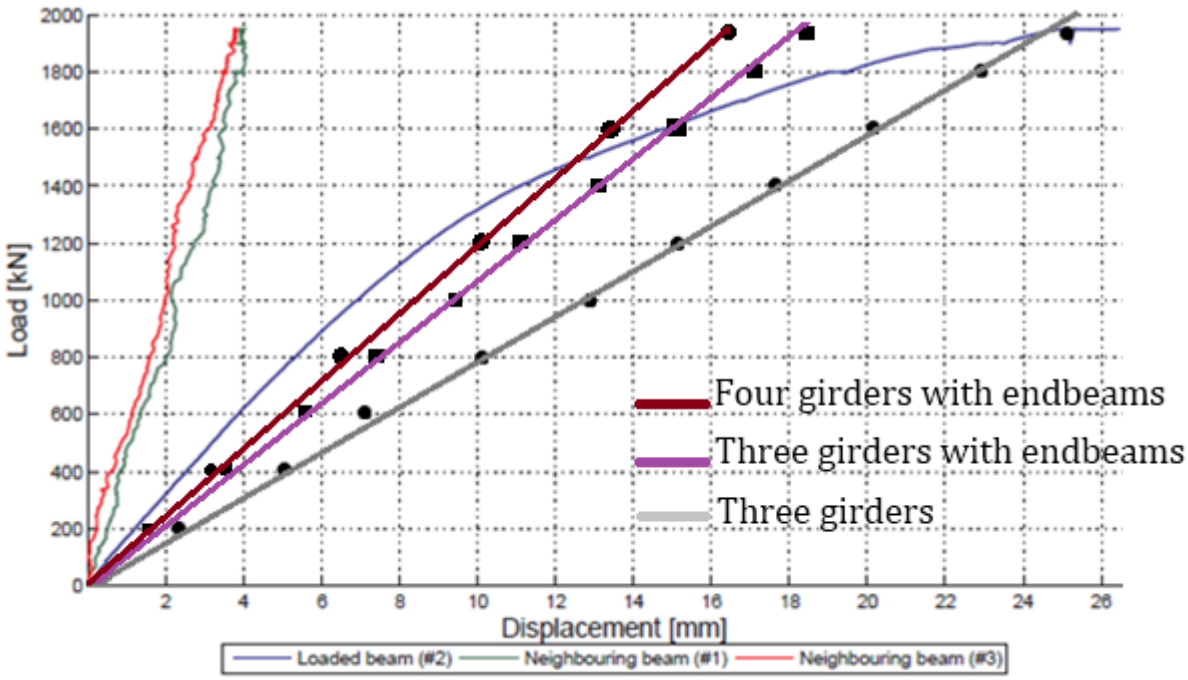


*Figure 164 comparison main loaded girder load displacement graph experiment vs linear plate model*

*Table 26 comparison main girder displacements experiment vs model*

| Load [kN] | Displacement [mm] | |
|---|---|---|
| | Experiment | Model |
| 200 | 1.5 | 2.5 |
| 400 | 2.5 | 5.1 |
| 600 | 4 | 7.6 |
| 800 | 5.5 | 10.2 |
| 1000 | 7 | 12.7 |
| 1200 | 8.5 | 15.3 |
| 1400 | 11 | 17.8 |
| 1600 | 15 | 20.4 |
| 1800 | 19.5 | 22.9 |
| 1950 | 26 | 24.8 |

*Table 27 comparison neighbor girder displacements experiment vs model*

| Load [kN] | Displacement [mm] | |
|---|---|---|
| | Experiment | Model |
| 200 | 0,5 | 0,7 |
| 400 | 0,7 | 1,4 |
| 600 | 1,2 | 2,2 |
| 800 | 1,8 | 2,9 |
| 1000 | 2 | 3,6 |
| 1200 | 2,2 | 4,3 |
| 1400 | 3 | 5 |
| 1600 | 3,2 | 5,8 |
| 1800 | 3,8 | 6,5 |
| 1950 | 4 | 7 |

Finally, the neighbor beams of the numerical model behave less stiff than the ones of the experiment (Figure 165). The comparison between the neighbor girder displacements is given in Table 27, where the experimental displacements are estimated with use of the load displacement graphs in Figure 164.

**Conclusions**

Overall, all numerical models show a safe underestimate up to a certain point. The three-girder model with end beams deviates at 1600 kN from the experiment, and the four-girder model with endbeams at 1500 kN.

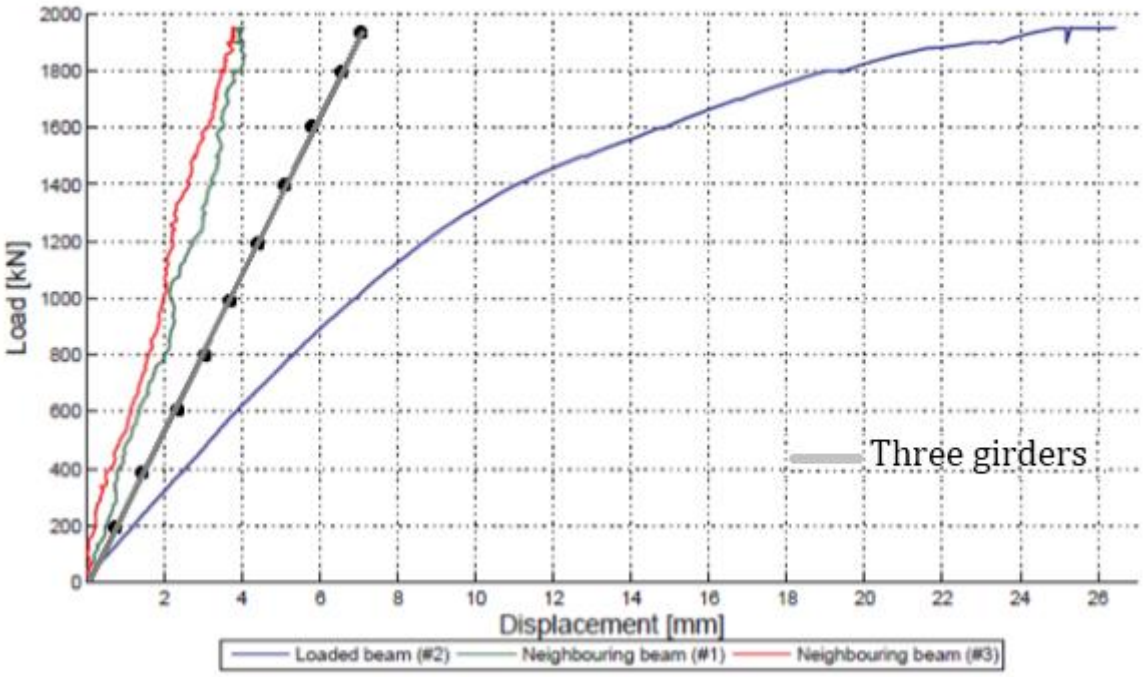


*Figure 165 comparison neighbor girder load displacement graph experiment vs linear plate model*

**Calculation neighbor experiment**

A calculation is given where it is assumed that membrane action is activated. This is done to see what the potential capacity of the slab is (using the same method from Chapter 7). A numerical three-girder model is considered, for its symmetry, to determine the relative girder deflections.

- Build a numerical linear plate model

Only three beams are modeled to simplify the calculation and easily determine the load distribution, relative girder and slab midspan displacements.

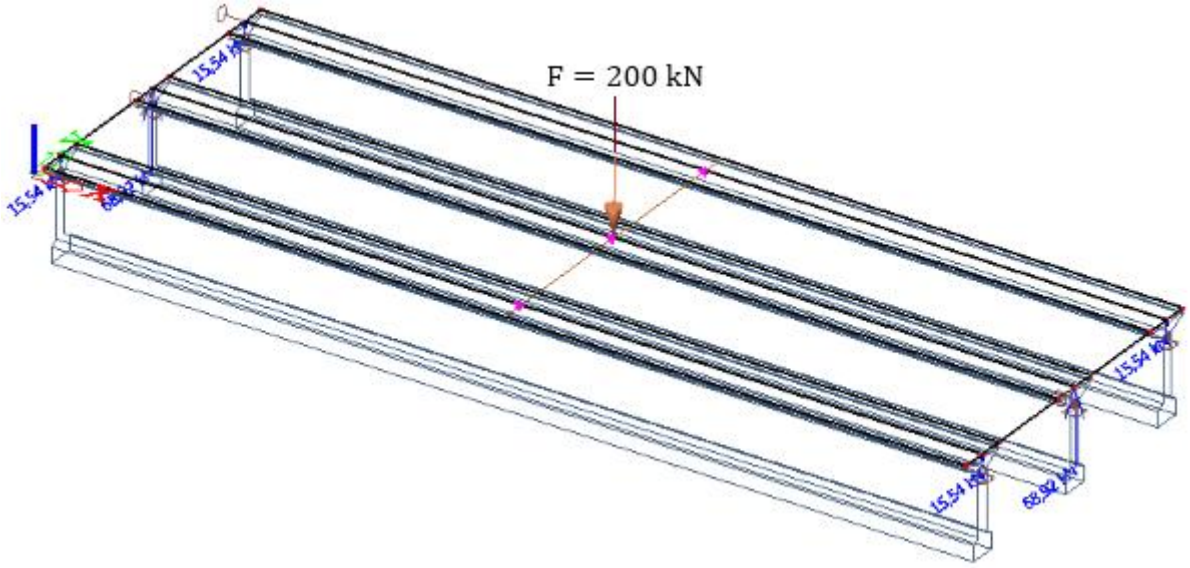


*Figure 166 load distribution of the model*

- Determine the linear load distribution of the model

At a load of 200 kN, the linear elastic distribution of the plate was determined (Figure 166): 15.5% 69% 15.5%. Meaning that, after replacing the loading point in the middle of the critical girder, the load distribution changed slightly. The main beam takes 69 percent of the load, previously this was 72 percent. So, the loading point does indeed have an influence on the linear load distribution as stated in Chapter 6.

Using the reaction forces from the experiment (Ensink, 2014), the linear load distribution can be determined roughly as well. Here it is shown that for the three bottom girders, the middle one is loaded with about 54% of the load. This differs from the model and might explain differences regarding the critical girder load determined with the model and the one found in Figure 159. Ultimately this difference in load distribution causes differences in the calculated total slab capacity (Equation (45)).

- Establish $\delta_{girder,max}$

In the experiment the girder reached a maximum load of 1950 kN with a maximum displacement $\delta_{girder,max} = 26\,mm$ (Figure 159).

- Determine capacity of single slab strip

The Rankin method is used with simply supported conditions (SS), fixed ended (FE), and (SS/FE) (Table 28).

- Determine the slab midspan displacement

A section is made to determine the slab midspan displacement (Figure 167). First, the slab bending capacity for Rankin (SS), where the slab is assumed to be simply supported, was determined: $F_{slab} = 133$.

The midspan displacement for which the slab bending capacity was reached, was determined with the model (Figure 167).

The same was done for Rankin (SS/FE) and (FE), and the midspan displacements are given in Table 28. The considered clear span for this method is 3450 mm.

The slab midspan displacements are considered as the critical deflections: $\delta_{slab} = \delta_{crit}$. The relative girder deflection need to exceed the critical deflections for membrane action to activate.

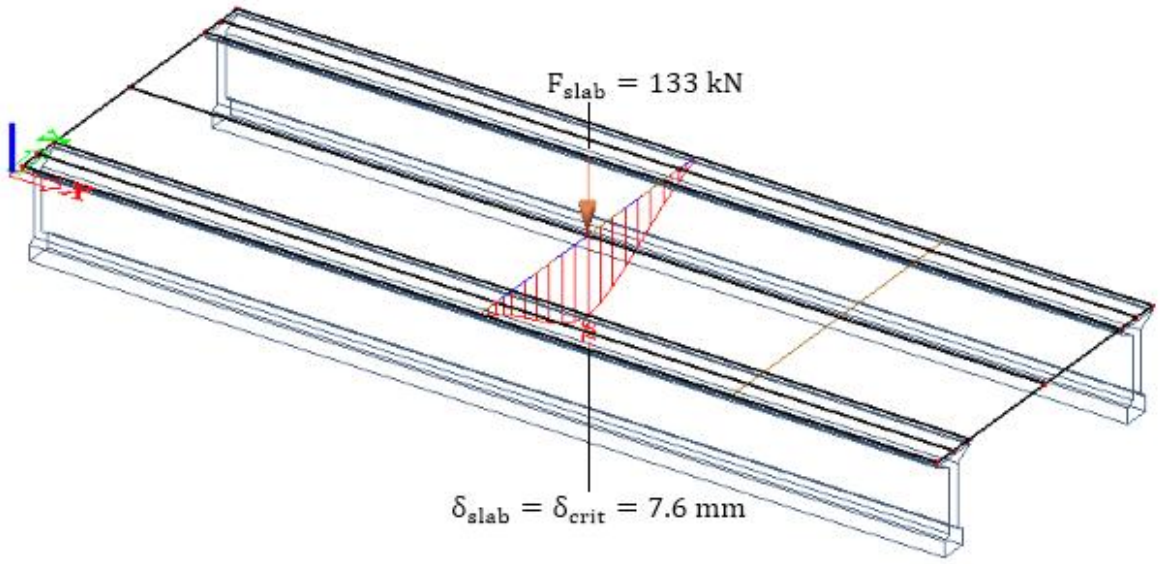


*Figure 167 midspan displacement for Rankin (SS) for loading point at middle of the girder*

*Table 28 overview of midspan displacements and critical girder loads*

| Method | Slab Bending capacity $\mathbf{F_{slab,lower}}$ [kN] | Slab Midspan/Critical displacements $\boldsymbol{\delta_{slab} = \delta_{crit}}$[mm] |
|---|---|---|
| **Rankin (SS)** | **133** | **7.6** |
| **Rankin(SS/FE)** | 172 | 9.8 |
| **Rankin (FE)** | 178 | 10.1 |

- Determine the critical girder load

The loading point has changed location, meaning that the midspan displacements are different, and this means that the relative girder displacements are different. Moreover the loads at which these girder displacements are reached, the critical girder loads, are also different.

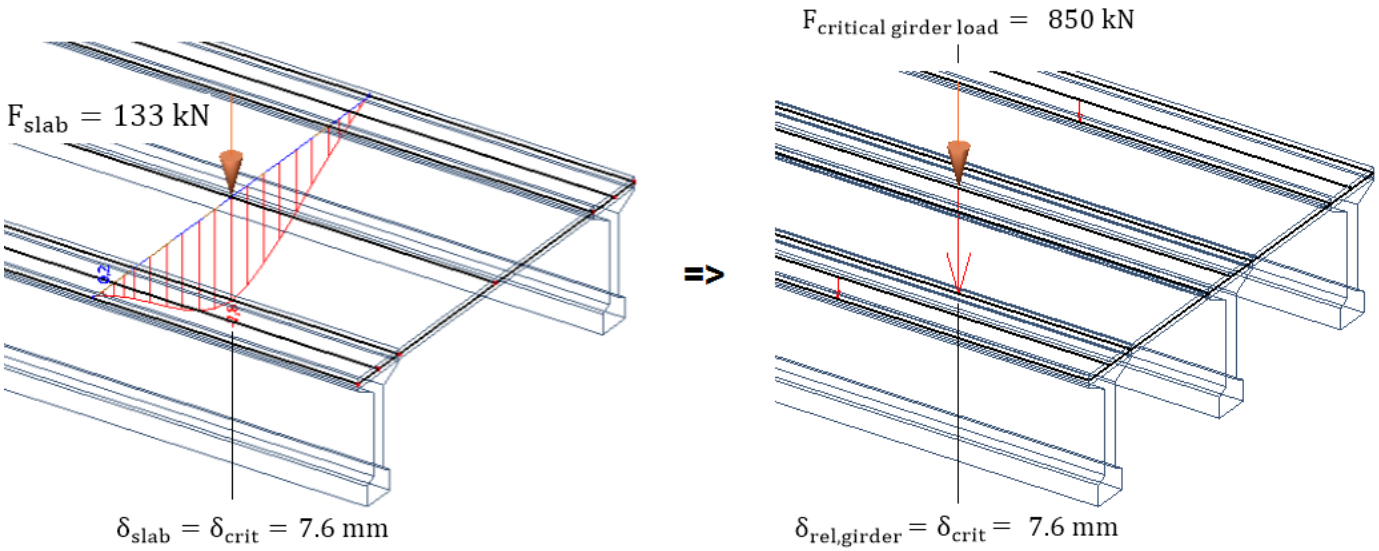


*Figure 168 determining critical girder load*

*Table 29 slab displacement, critical displacement, and critical girder load*

| Method | Slab Bending capacity [kN] | Midspan/Critical displacements [mm] | Critical Girder load [kN] |
|---|---|---|---|
| **Rankin (SS)** | **133** | **7.6** | **850** |
| **Rankin(SS/FE)** | 172 | 9.8 | 1075 |
| **Rankin (FE)** | 178 | 10.1 | 1113 |

- Determine the activated beam span

The activated beam span and slab area is determined with $\delta_{max,girder} = 26\,mm$ and the critical displacement of 7.6 mm. A length of 8 m is activated (Figure 169).

- Determine the effective width of a single slab strip

The effective width $b_{eff} = 3650\,mm$ (Figure 170), the same as calculated in Chapter 7, since bridge parameters such as the considered span have not changed. Only the load point changed locations.

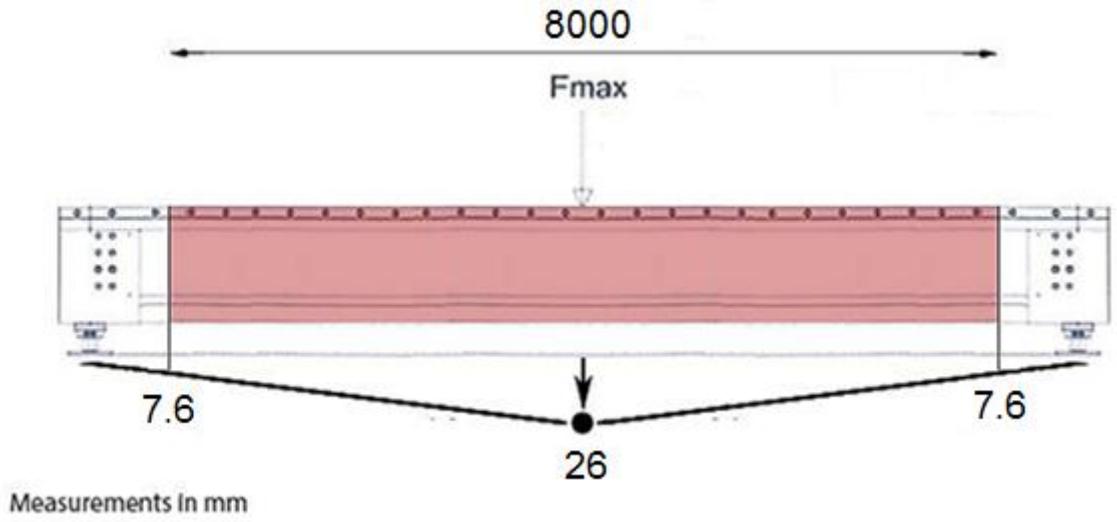


*Figure 169 activated beam span (not on scale)*

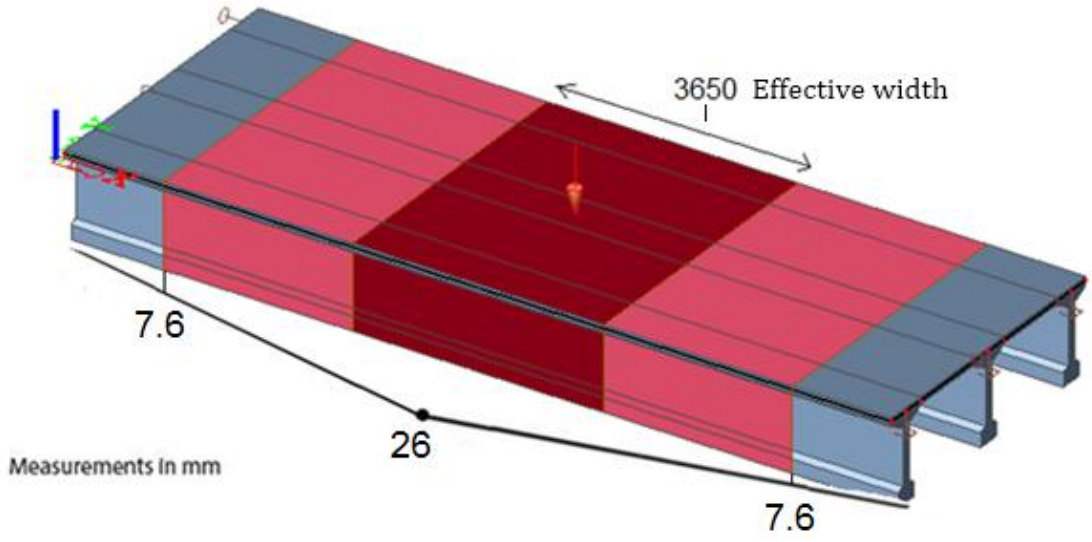


*Figure 170 effective width (not on scale)*

- Determine the total slab capacity

A length of 8 m is activated. And with an effective width of 3.65 m and an assumed bending capacity of 133 kN per activated slab strip, this gives the following total slab capacity:

$$n[-] = \frac{\text{activated slab span[m]}}{\text{effective width slab strip[m]}}$$

$$\text{total slab capacity } F_{slab,upper}[kN] = n * \textbf{bending} \text{ capacity slab strip} \tag{45}$$

$$F_{slab,upper} = n * F_{slab,lower}$$

$$n = \frac{8}{3.65} = 2.2$$

$$F_{slab,upper} = 2.2 * 133 = 292\ kN$$

- Determine the girder load and total bridge load

Since the girder is loaded in the middle, the flexural shear capacity $V_{rd,max} = 1189\ kN$ (Vugts, 2012). First, converting this load with equilibrium of forces gives: $F_{max} = 2 * V_{rd,max} = 2378\ kN$.

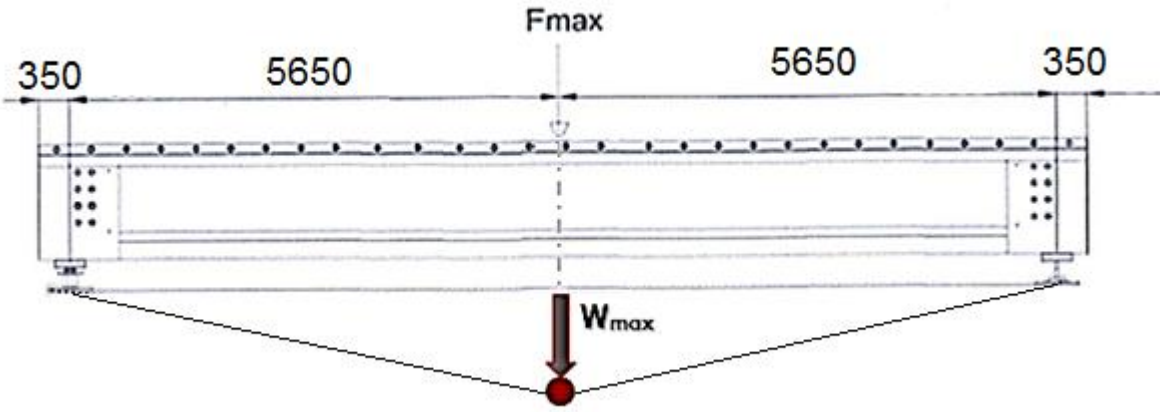


*Figure 171 displacement neighbor test*

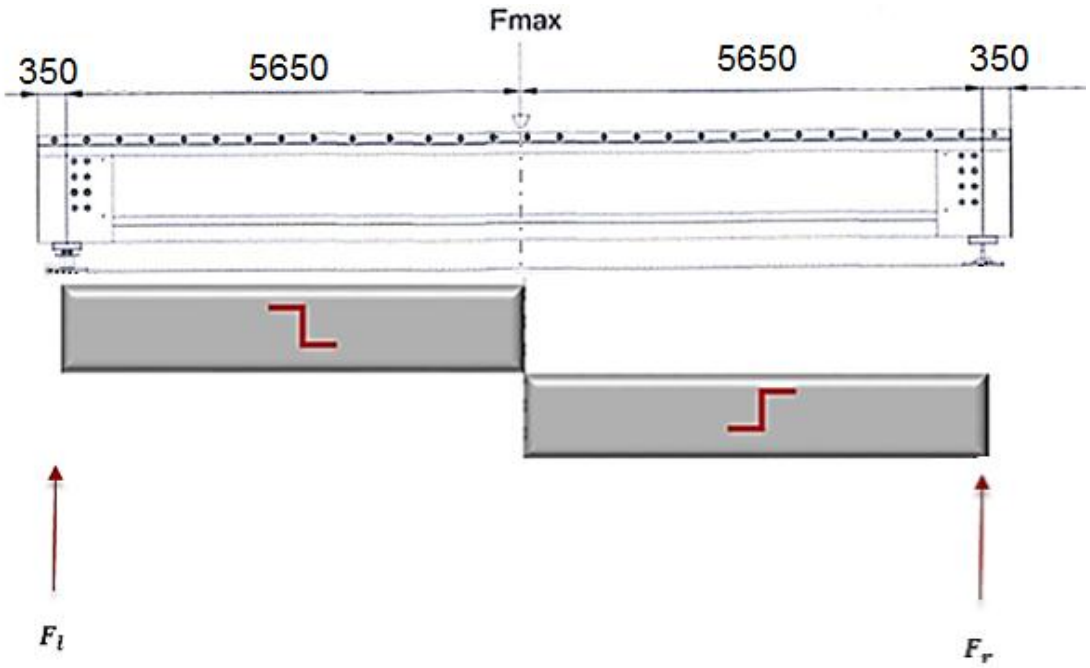


*Figure 172 shear distribution neighbor test*

And then the girder load is converted to an equivalent bridge load using the load distribution:

$$F_{bridge} = \frac{F_{single}}{0.69} = 3446\ kN$$

The linear girder load, 3446 kN, after calculating the equivalent bridge load, is added to the slab capacity, since it is assumed that slab and girder work together, as soon as the relative girder displacement exceeds the midspan displacement, already shown before. The results are given in Table 30. A visual representation of the lower and upper bound limit is given (Figure 174).

As a quick check the lower and upper bound failure load is converted for a single girder, using the load distribution:

$$0.69 * 3446 = 2378\ kN \text{ and } 0.69 * 3783 = 2610\ kN$$

This means the girder failure load is calculated to be between 2378 and 2610 kN (Figure 175), which is plausible since the single beam test indicated a possible strength of about 3000 kN.

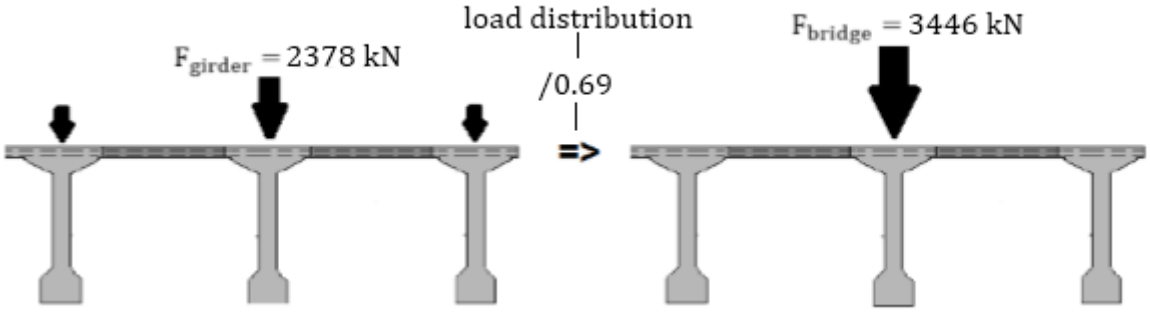


*Figure 173 converting girder load to bridge load*

*Table 30 results total deck capacity*

| Method | Slab bending capacity [kN] | Activated girder span [m] | Total slab capacity [kN] | Total bridge load [kN] |
|---|---|---|---|---|
| **Rankin (SS)** | 133 | 8 | 292 | 3738 |
| **Rankin(SS/FE)** | 172 | 7 | 330 | 3776 |
| **Rankin (FE)** | 178 | 6.9 | 337 | **3783** |

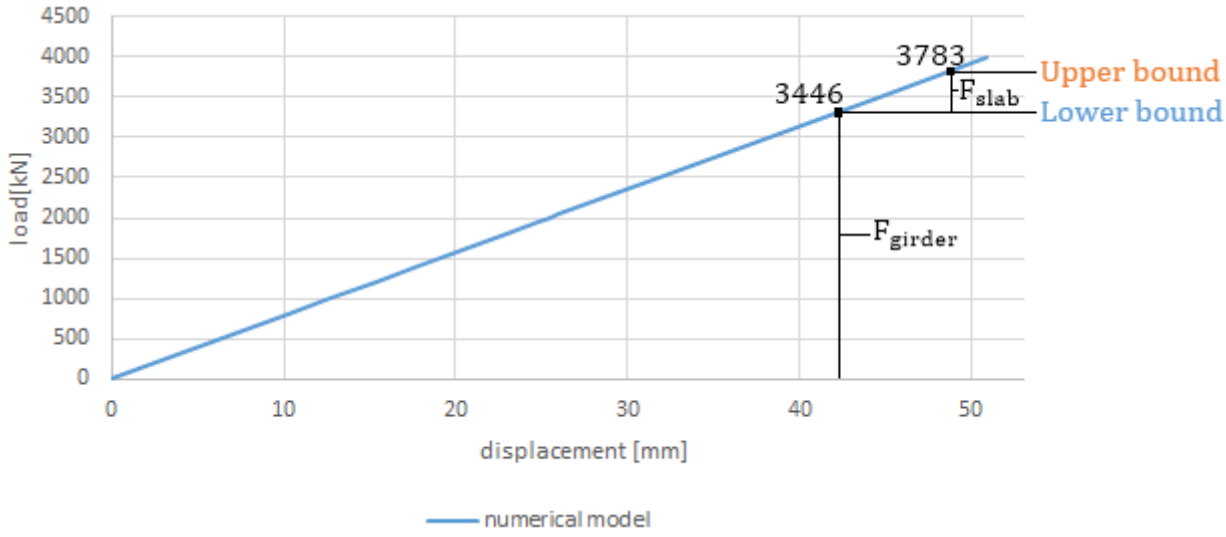


*Figure 174 range of the bridge's total load: lower, and upper bound limit using the numerical model*

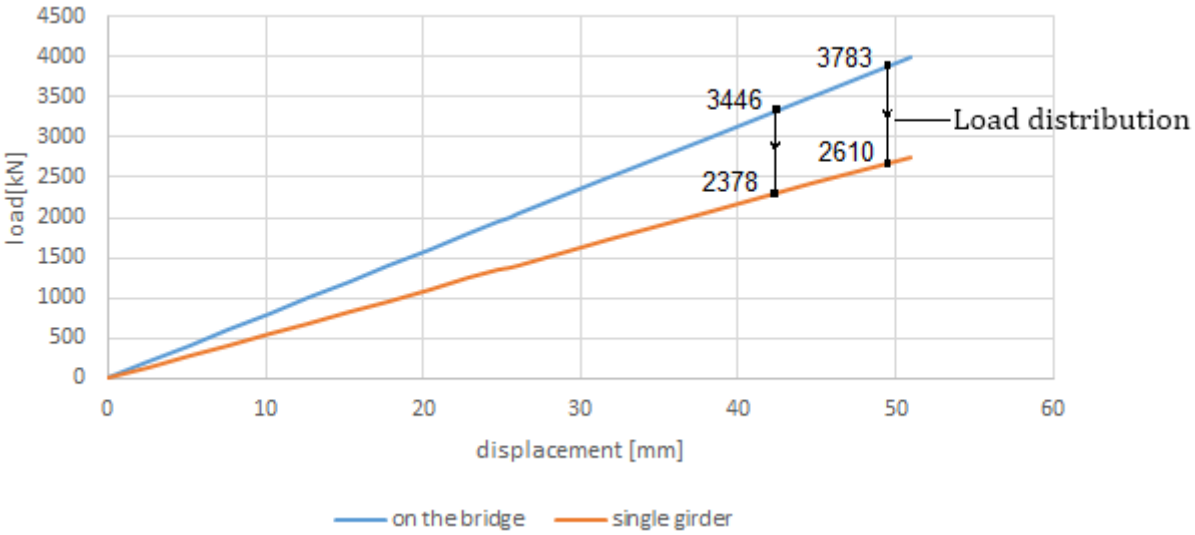


*Figure 175 load on the single girder after load distribution for the lower and upper bound limit values*

### Conclusions

Up to 24 mm, the linear plate model with three girders is a safe underestimate of reality. After the maximum test load of 1950 kN, the test was stopped, so the deflections after that are not know. But the rest of the nonlinear behavior is estimated and compared with the numerical model.

It is shown that the numerical model overestimates the total load after 24 mm. For the part between 24 and 48 mm, a nonlinear numerical model is needed or one can calculate with a lower stiffness for the main beam in the numerical model.

Comparing the results from Chapter 8 with Chapter 7 shows a few differences. First, for the load point in the middle of the deck, the activated span is shorter (Table 30).

Second, the difference in activated span in turn gives a difference in total deck capacity, the difference in strength is about 40 to 50 kN. So the contribution of the slab for the failure load is less when loaded in the middle. The contribution of the beam, though, is higher in this case.

But ultimately, the strength contributed by slab membrane action, considering both situations, never exceeds an average strength of 450 kN. The reason why is because the effective width is long, 3.65 m, shown in Equation (45). And the effective width is dependent on the considered clear span, which is 3.45 m, long as well. Both resulting in a low total slab capacity that can be calculated.

So, further research is done by placing the beams closer to each other, reducing the considered span and making the slab less slender. And the total slab capacity will be determined again and compared.

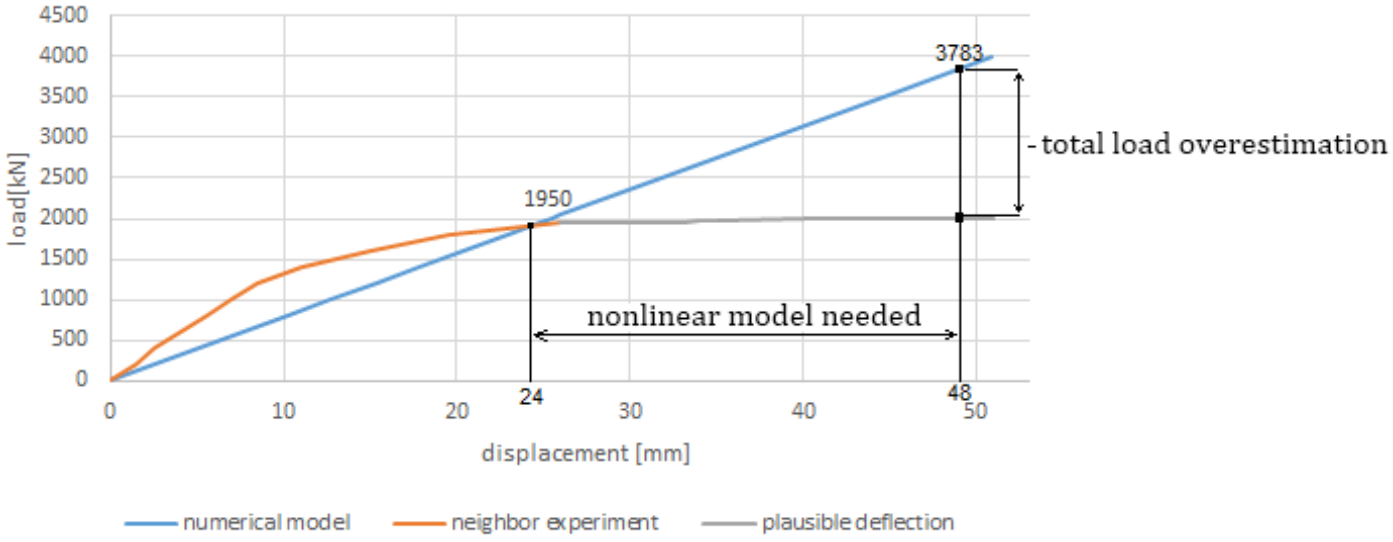


*Figure 176 overestimation of the total bridge load*

# Parameter study of deflection field and slenderness

## Introduction

In this chapter the deflection field of the neighbor beams is researched with use of the numerical model. Furthermore the slenderness issue is addressed: the neighbor beams are placed closer together to study the effect of the slab's considered span and the span/depth ratio. And then the comparison is made between two situations, for a long span and a shorter span. Finally a calculation is done to compare the slab's contributed strength in both situations.

**Deflection field neighbor beams**

A few points are taken as starting points: the loads and deflections of the neighbor girders are determined there (Figure 177). Then these deflections and loads are compared with the ones from the numerical model, for two spans, 1650 and 3450 mm (Table 31).

Table 31 shows similarities between the displacements of the experiment and the model: the difference in displacement never exceeds 0.5 mm and increases as the load increases (Table 31).

When the shorter span, 1650 mm, is considered, differences in displacements are noticed. The displacements of the neighbor girders increased, almost twice as much (Table 31). This is because the girders are now placed closer to the load, meaning that the load path is shortened, and the load gets distributed faster to the neighbor girders, causing them to be loaded more and displace more. Finally this means that the main girder displaces less for the shorter situation, since it distributes more of the load to the neighbor girders (Table 32).

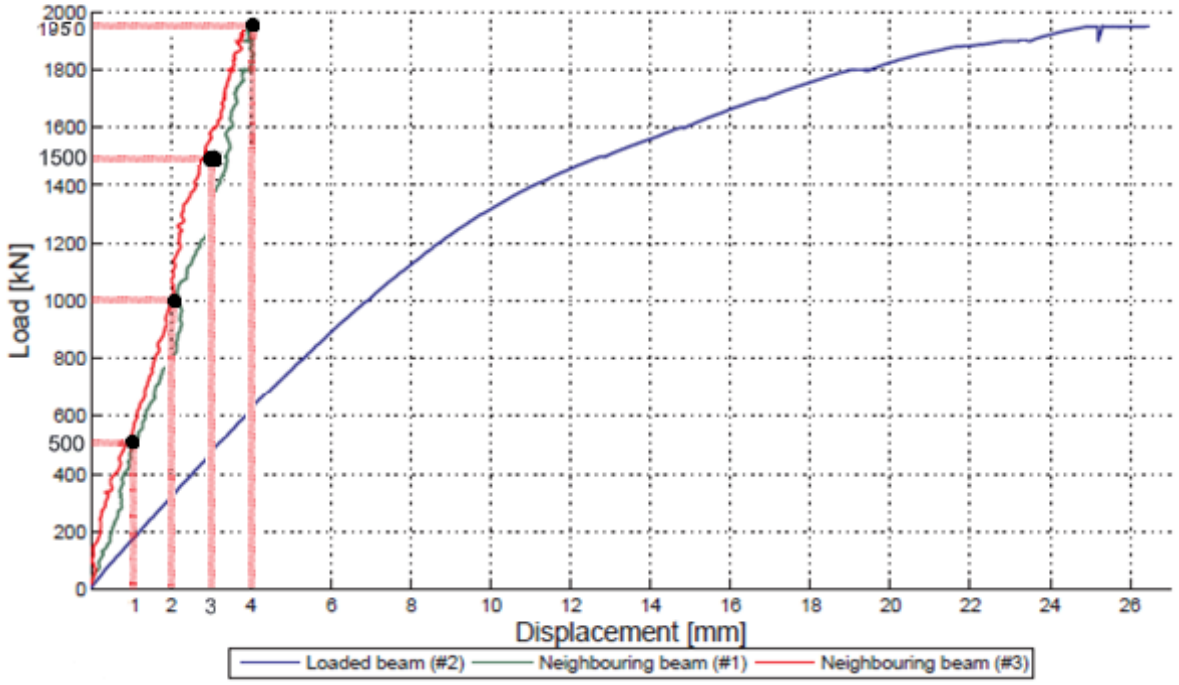


*Figure 177 displacements and loads from the experiment to compare with the numerical model (for c.t.c 1650 and 3450 mm)*

*Table 31 comparison relative displacement neighbor girders considering two clear spans*

| Load [kN] | $\delta_{rel,experiment}$ [mm] L=3450 mm | $\delta_{rel,model}$ [mm] L=3450 mm | $\delta_{rel,model}$ [mm] L=1650 mm |
|---|---|---|---|
| **500** | 1 | 1.1 | 2 |
| **1000** | 2 | 2.3 | 3.9 |
| **1500** | 3 | 3.4 | 5.9 |
| **1950** | 4 | 4.5 | 7.6 |

*Table 32 comparison relative displacement critical girders considering two clear spans*

| Load [kN] | $\delta_{rel,experiment}$ [mm] L=3450 mm | $\delta_{rel,model}$ [mm] L=3450 mm | $\delta_{rel,model}$ [mm] L=1650 mm |
|---|---|---|---|
| **500** | 2 | 3.5 | 2.8 |
| **1000** | 5 | 7 | 5.6 |
| **1500** | 9 | 10.4 | 8.4 |
| **1950** | 22 | 13.6 | 11 |

The displacements of the experiment in Table 32 are determined by using the load displacement graph in Figure 177. In Table 32 for the load 500 till 1500 kN, the numerical model shows a higher displacement than the experiment, this has to do with differences between the load distribution. In the numerical model the loaded beam takes more of the load than in the experiment. The difference in displacement is not that large, in the order of 1 to 2 mm. But for the maximum load of 1950 kN a significant difference is noted. Probably due to the fact that the beam in the experiment behaved nonlinear, displacing more as the load increased, whereas the model is linear. This was already mentioned in Chapter 8, and any calculations done above 1950 kN should be considered with caution, since the numerical model deviates there.

For simplification of the calculation in Chapter 5 till 8 the deflection was assumed to be linear with a plastic hinge located at maximum deflection, and the rest of the girder acted as rigid bodies. In reality the deflections of the girders display a more parabolic nature (Figure 178).

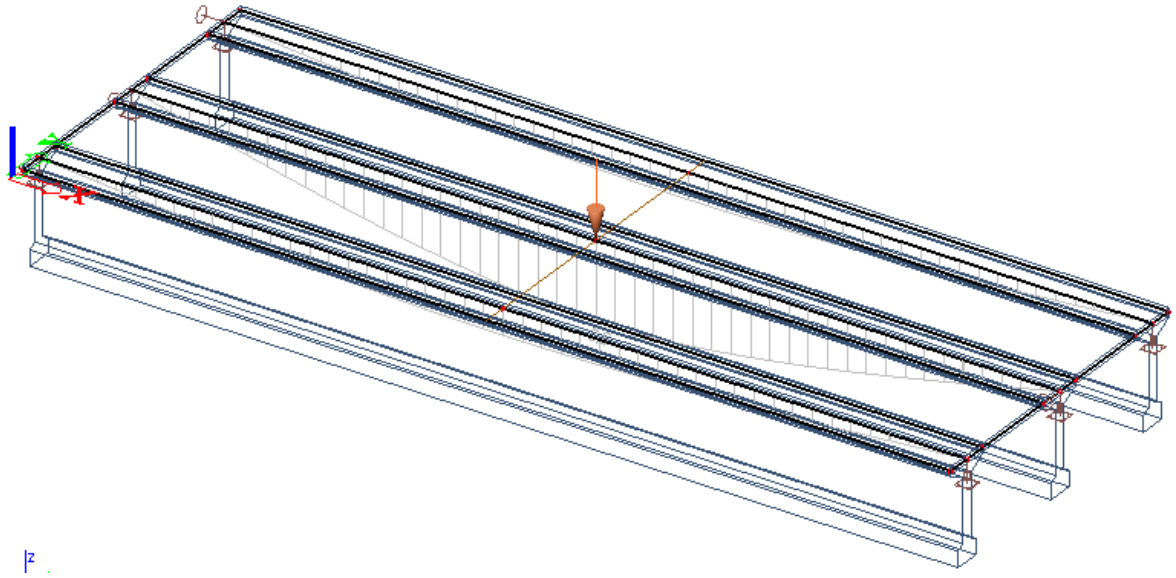

*Figure 178 relative deflection fields girders*

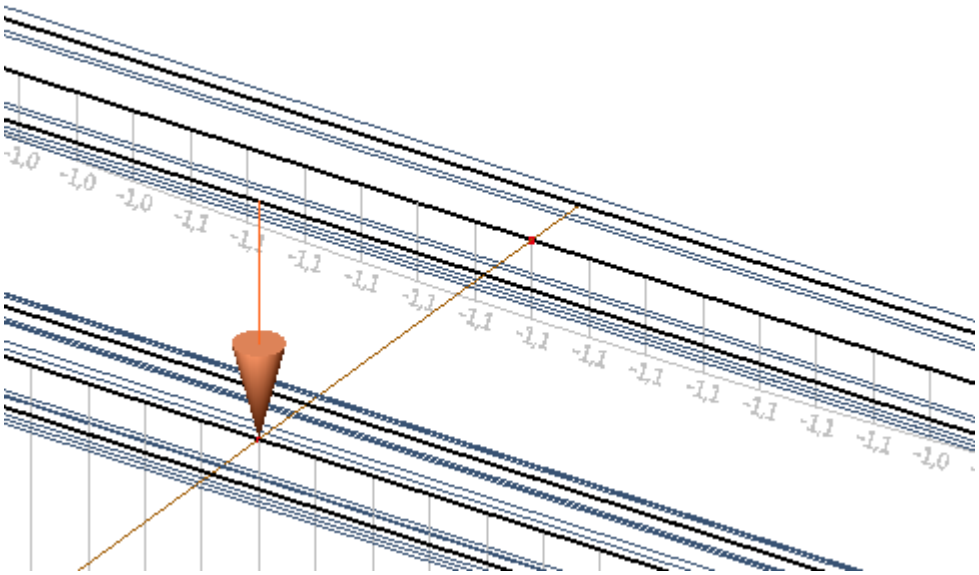


*Figure 179 displacement of neighbor girder at the middle of the girder*

### Calculation for shortened situation (1)

To study the parameter of the span/depth ratio, the calculative process is done again, but this time the considered clear span is 1650 mm, creating a less slender situation. A new model uses the shorter clear span, placing the girders closer together, with the point load still in the middle. Other geometrical and material properties stayed the same.

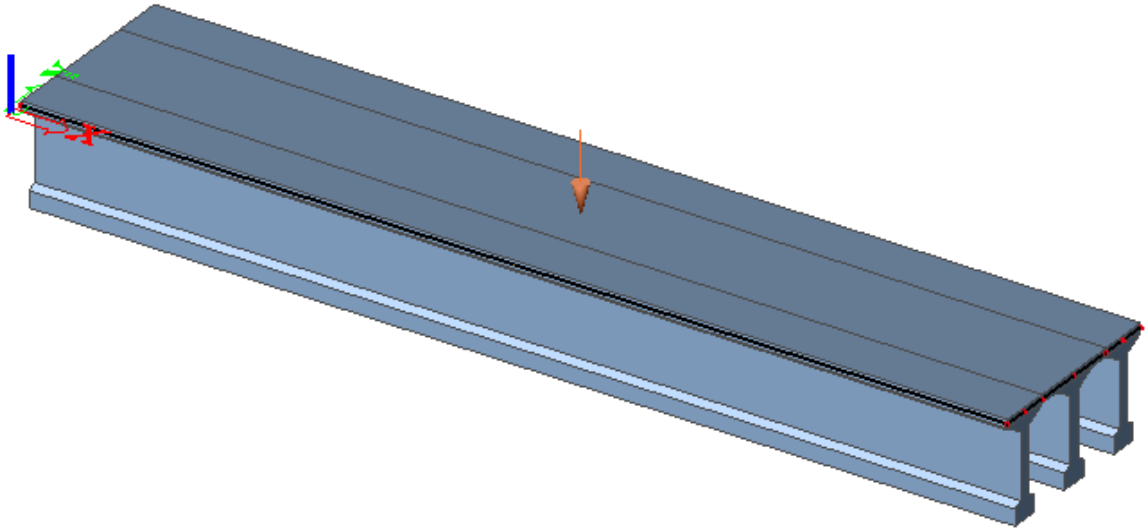

*Figure 180 loading point in the middle of the critical girder for a shortened situation*

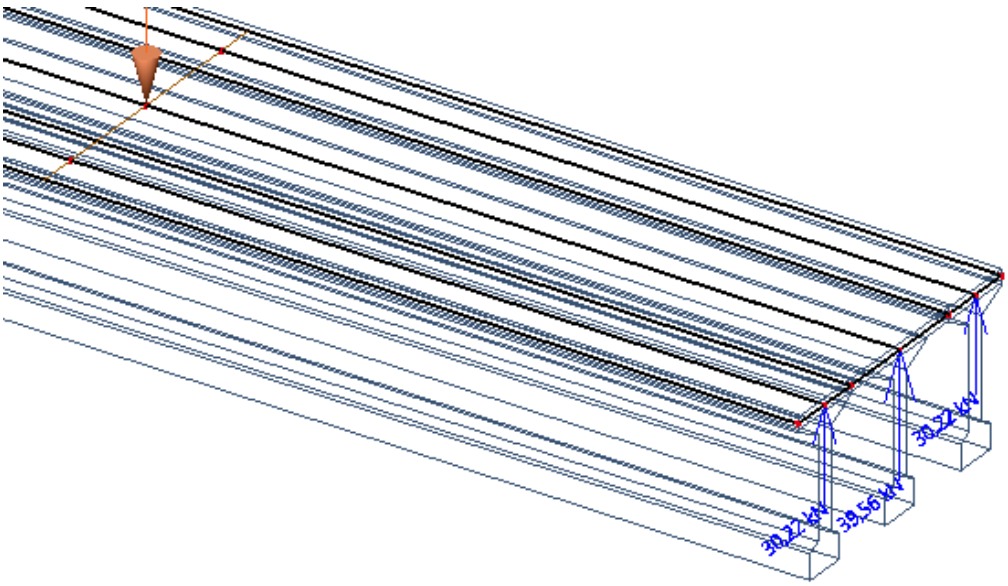


*Figure 181 load distribution of the model*

The linear load distribution was determined (Figure 181). This gave the following load distribution: 30% 40% 30%. Meaning that after placing the neighbor girders closer, the load distribution changed, the critical girder now takes 40 percent of the load. This result is expected since the load gets distributed faster over the shorter span to the neighbor girders, increasing the spreading. Again this is an indication that for a situation with more than three girders, such as 'De Vecht', it is wise to consider a numerical model with at least five girders, because of the high load spreading and possible participation of multiple girders, outside of the main three.

Placing the girders closer together results in a higher spreading, but also means that less of the load can be redistributed if the main girder fails, and assuming the girder properties stay the same. For the short span, 1650 mm, redistribution is possible up to 80%. If this occurs, the two neighbor beams are assumed to fail. This means the neighbor beams and their respective capacities are governing for the bridge.Simply put, the bridge capacity is two times the neighbor beam capacity.

For the long span, 3450 mm, 100% redistribution was possible. This is important when modelling and calculating with the deck of 'De Vecht'.

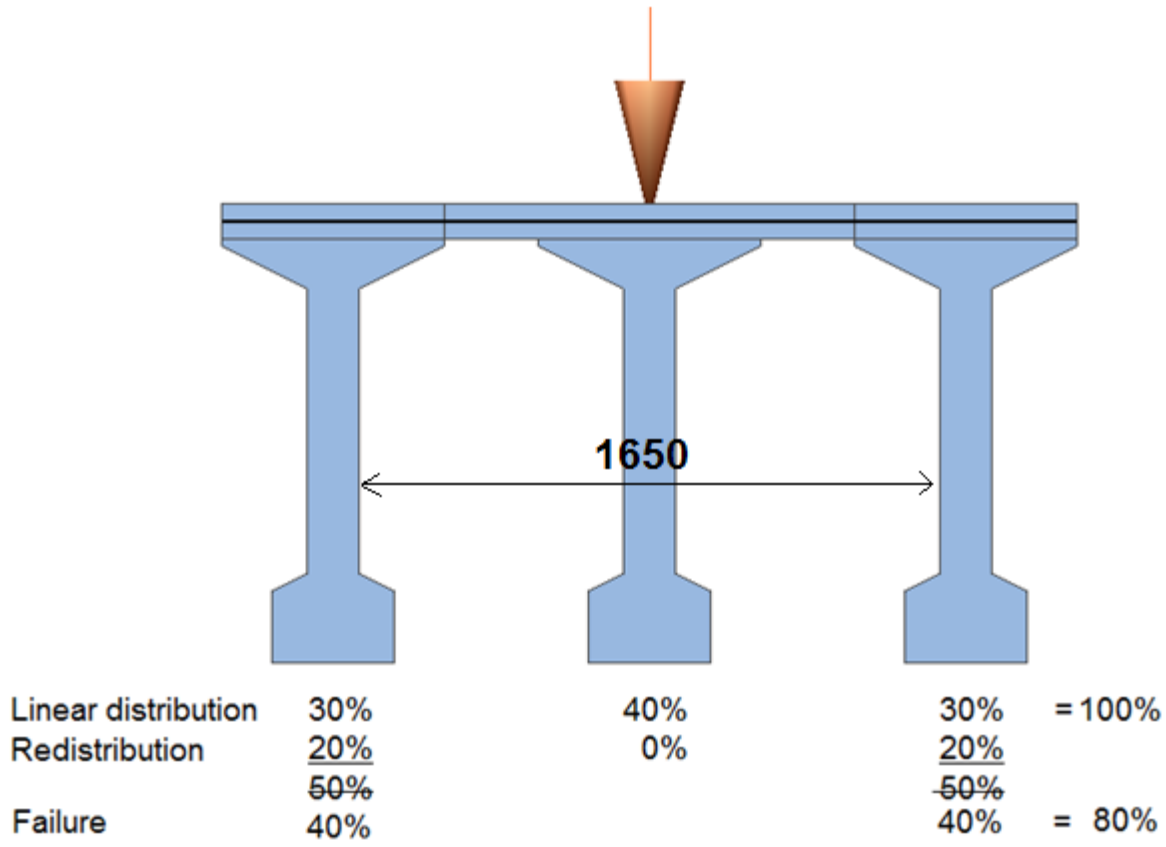


*Figure 182 linear load distribution for numerical model for shorter span*

The Rankin method is used, where simply supported (SS), fixed ended (FE), and the situation between these two (SS/FE) were considered (Table 33). The slab strip bending capacity increased, because the span was shortened.

First the midspan displacements are determined: a section in the numerical model is made to determine the midspan displacement (Figure 183). Then the midspan displacement, for which the slab strip bending capacity was reached, was determined with the numerical model (Figure 181). The shorter span is also the reason why the midspan displacements are smaller (Table 28), the slab acts stiffer, displacing less. An overview of the midspan displacements is given in Table 33.

The midspan displacements are the criteria that the relative girder displacements need to exceed in order for membrane action to activate in the slab. Now the numerical model (Figure 181) is used to determine at which loads these midspan displacements are exceeded, the critical girder loads (Table 33). Here it is found that the critical girder loads are larger than for the longer situation ($L = 3450\ mm$). The reason why is because the shortened slab acts stiffer, meaning that the critical girder load is reached later.

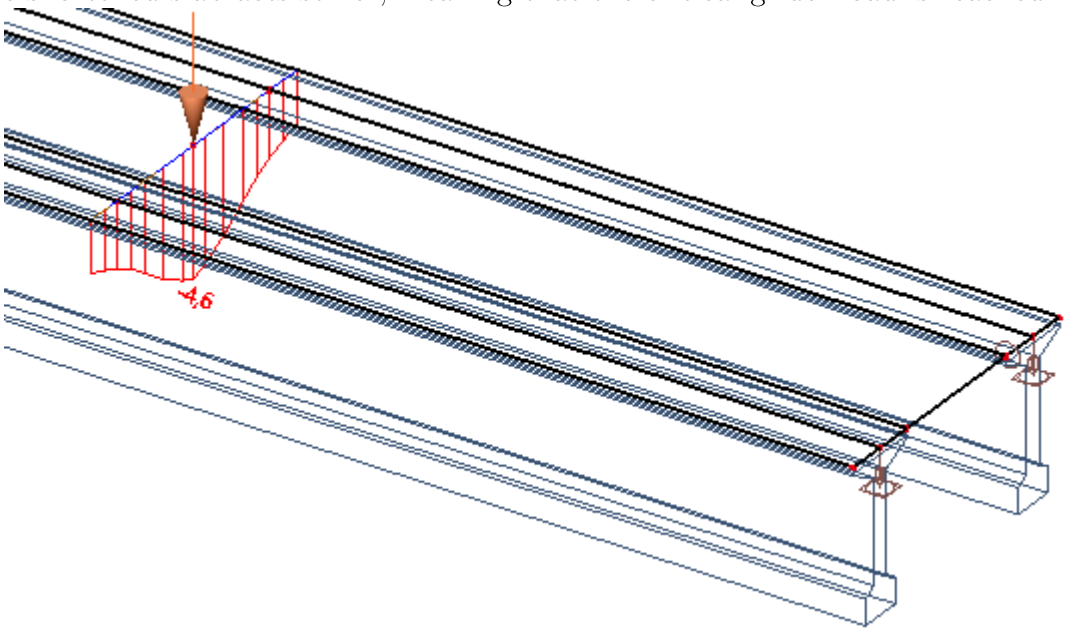


*Figure 183 midspan displacement for Rankin (SS) for loading point at middle of the girder*

*Table 33 overview of midspan displacements and critical girder loads*

| Method | Slab strip bending capacity [kN] | Midspan displacements [mm] | Critical Girder load [kN] |
|---|---|---|---|
| **Rankin (SS)** | 226 | 4.6 | 1763 |
| **Rankin(SS/FE)** | 232 | 4.7 | 1800 |
| **Rankin (FE)** | 233 | 4.7 | 1800 |

The new effective width $b_{eff} = 1850\ mm$ (Figure 184). Previously the effective width was 3650 mm, for clear span $L = 3450\ mm$. The effective width has changed and reduced significantly, since the considered clear span is reduced as well. The change in effective width eventually effects the total deck capacity.

$b_{eff} = c_y + 2 * L_e + 2 * h = 200 + 2 * 725 + 2 * 100 = 1850\ mm$
$c_y =$ length of load area in y − direction
$L_e =$ effective span of the slab subjected to arching force
$L_e = \frac{L_s}{2} - \frac{c_x}{2} = \frac{1650}{2} - \frac{200}{2} = 725\ mm$
$c_x =$ length of load area in x − direction
$L_s =$ clear span of considered slab $= 1650\ mm$
$L_s = 1650$ mm (assumed shorter span)

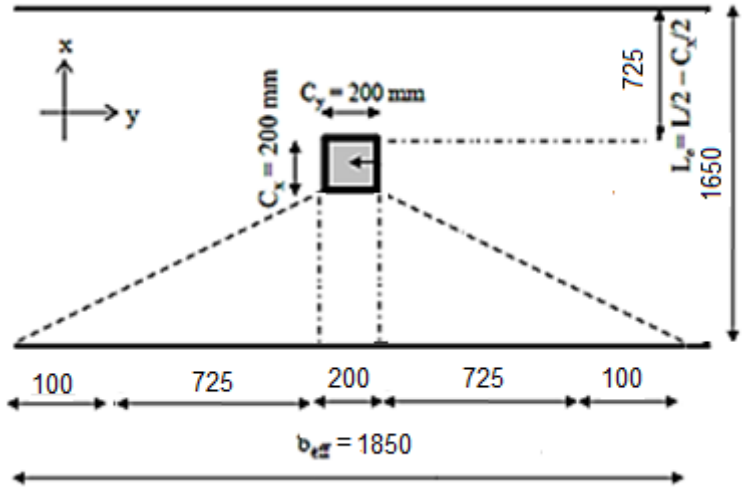


*Figure 184 effective width*

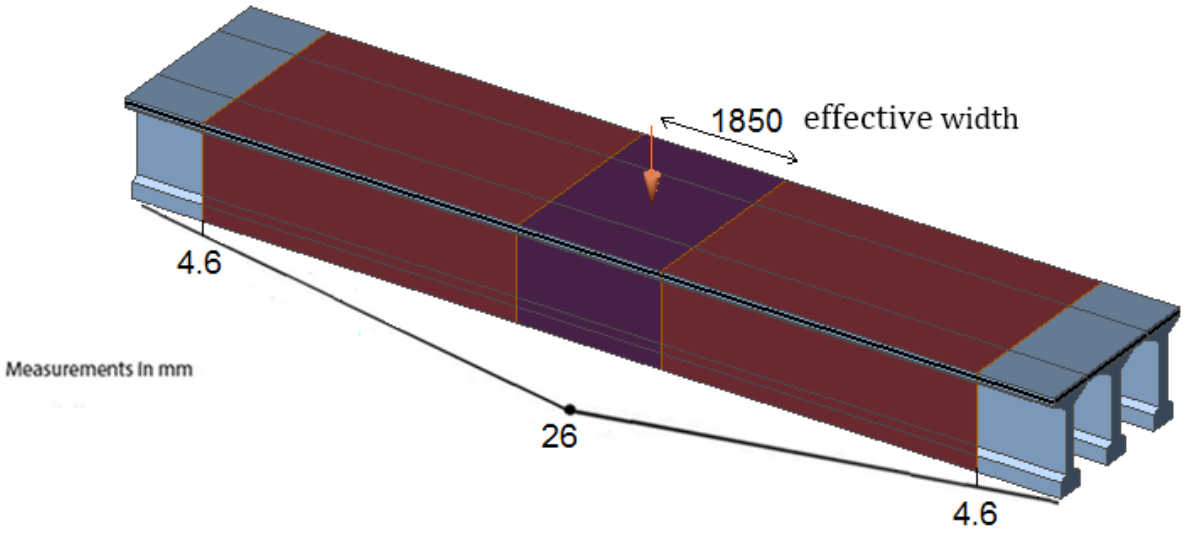


*Figure 185 effective width and activated span for L=1650 mm*

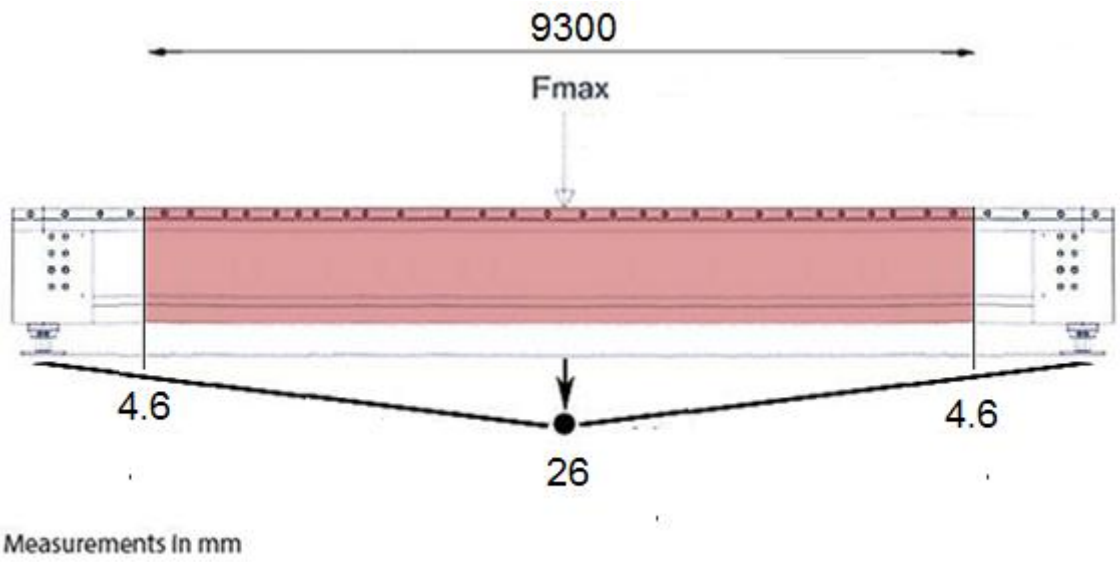


*Figure 186 activated girder length (not on scale)*

Now the activated girder span and slab area can be determined with the maximum of 26 mm and the critical displacement of 13.8 mm. A length of 5.3 m is activated (Figure 169), and an effective width of 1.85 m and an assumed capacity of 226 kN per activated slab strip, gives the following total provided deck capacity:

$$n = \frac{\text{activated slab span}}{\text{effective width slab strip}}$$

$$\text{total capacity activated slab area} = n * \text{capacity slab strip} \tag{46}$$

$$\frac{9.3}{1.85} \approx 5$$

$$5 * 226 = 1136\ kN$$

*Table 34 results total deck capacity L=1650 mm for neighbor test model*

| Method | Slab strip bending capacity [kN] | Activated girder span [m] | Total deck capacity [kN] |
|---|---|---|---|
| **Rankin (SS)** | 226 | 9.3 | 1136 |
| **Rankin(SS/FE)** | 232 | 9.2 | 1154 |
| **Rankin (FE)** | 233 | 9.2 | 1158 |

*Table 35 results total deck capacity L=3450 mm for neighbor test model*

| Method | Slab strip bending capacity [kN] | Activated girder span [m] | Total deck capacity [kN] |
|---|---|---|---|
| **Rankin (SS)** | 133 | 8 | 292 |
| **Rankin(SS/FE)** | 172 | 7 | 330 |
| **Rankin (FE)** | 178 | 6.9 | 337 |

**Conclusions shortened span neighbor test**

There is a difference in total deck capacity. Partly, this has to do with the fact that in Equation (45) the effective width is very large, 3650 mm, this is for the long span, 3450 mm. When the span is reduced to 1650, the effective width also is reduced, to 1850 mm, meaning the total activated span will be divided by slab strips with a smaller effective width. Leading to a total deck capacity that is more than three times than that was found previously (comparing Table 34 and Table 35). The larger total deck capacity seems plausible, since the deck was shortened, making it act stiffer and more restraint, which would lead to more membrane action and a higher capacity.

**Calculation for shortened situation (2)**

A shorter clear span is also considered for the earlier test situation, with the point load located near the supports. The same clear span is used, 1650 mm, and the same calculative process is followed. Results are shown in Table 36 and Table 37. Table 36 shows the results of the shortened situation, $L = 1650\,mm$. And Table 37 shows the results from Chapter 7 for $L = 3450\,mm$.

Comparing Table 36 and Table 37 shows that the shortened situation gives a higher deck capacity compared to the longer situation. This is caused by a smaller effective width, causing the deck to be divided in smaller strips of concrete with a higher capacity of their own, resulting in a total deck capacity almost three times larger than found previously.

*Table 36 results total capacity for L=1650 mm*

| Method | Slab strip bending capacity [kN] | Activated girder span [m] | Total deck capacity [kN] |
|---|---|---|---|
| **Rankin (SS)** | 226 | 10.59 | 1294 |
| **Rankin(SS/FE)** | 232 | 10.37 | 1302 |
| **Rankin (FE)** | 233 | 10.37 | 1307 |

*Table 37 results total capacity for L=3450 mm*

| Method | Slab strip bending capacity [kN] | Activated girder span [m] | Total deck capacity [kN] |
|---|---|---|---|
| **Rankin (SS)** | 133 | 8.9 | 325 |
| **Rankin(SS/FE)** | 172 | 8.2 | 386 |
| **Rankin (FE)** | 178 | 8 | 390 |

# Summary

## Conclusions

Comparing the results from the neighbor and shear test models from Table 34 to Table 37 gives a few conclusions, and a clear overview of the tables are given in Appendix C.

First, the location of the load is significant, it influences the whole calculative process and causes differences when comparing different loading situations, for example loading in the middle of the girder (Chapter 8), or near the supports (Chapter 7). In general when the point load is in the middle of the girder, the total deck capacity, theoretically activated with membrane action, is lower than when loading the girder near the supports. But, when loading the middle of the girder, the girder shear capacity is higher. Ultimately resulting in a higher total theoretical capacity when the load is in the middle of the girder.

Second, the less slender the bridge deck is, shorter or thicker, the more capacity it has. The shorter situations result in slab strips with each a smaller effective width and higher capacities. Which leads to a higher total deck capacity, and a higher total bearing capacity.

Ultimately the capacity of the deck due to membrane action can be calculated with certain methods. But slenderness issues need to be taken into account, and one must be aware of the consequences following the change of the loading location.

## List of important parameters

- Slenderness, the ratio between clear span and deck thickness
- Effective width of a single slab strip (dependent on clear span)
- Location of the point load
- Capacity of the girder (changes for different loading locations)
- Capacity of a single slab strip (effected by the slenderness)
- Total deck capacity (dependent on strip capacity)
- Total capacity (influenced by capacity of girder and deck)

## Short overview results parameter study

### Neighbor experiment

*Table 38 results total deck capacity L=1650 mm for neighbor test model*

| Method | Slab strip bending capacity [kN] | Activated girder span [m] | Total deck capacity [kN] |
|---|---|---|---|
| **Rankin (SS)** | 226 | 9.3 | 1136 |
| **Rankin(SS/FE)** | 232 | 9.2 | 1154 |
| **Rankin (FE)** | 233 | 9.2 | 1158 |

*Table 39 results total deck capacity L=3450 mm for neighbor test model*

| Method | Slab strip bending capacity [kN] | Activated girder span [m] | Total deck capacity [kN] |
|---|---|---|---|
| **Rankin (SS)** | 133 | 8 | 292 |
| **Rankin(SS/FE)** | 172 | 7 | 330 |
| **Rankin (FE)** | 178 | 6.9 | 337 |

### Shear experiment

*Table 40 results total capacity for L=1650 mm for shear test*

| Method | Slab strip bending capacity [kN] | Activated girder span [m] | Total deck capacity [kN] |
|---|---|---|---|
| **Rankin (SS)** | 226 | 10.59 | 1294 |
| **Rankin(SS/FE)** | 232 | 10.37 | 1302 |
| **Rankin (FE)** | 233 | 10.37 | 1307 |

*Table 41 results total capacity for L=3450 mm for shear test*

| Method | Slab strip bending capacity [kN] | Activated girder span [m] | Total deck capacity [kN] |
|---|---|---|---|
| **Rankin (SS)** | 133 | 8.9 | 325 |
| **Rankin(SS/FE)** | 172 | 8.2 | 386 |
| **Rankin (FE)** | 178 | 8 | 390 |

# Appendix D

### Overview research deck slabs

Table 42 and Table 43 show an overview of the research on the load displacement behavior of concrete slabs. Because of the many differences between the researches, the following is roughly divided in the first three that discusses restrained slab strips, and the last two that discusses prototype models on scale.

Table 44 shows test results from different researches for restrained reinforced concrete slabs. Here a value $\frac{\delta_u}{h}$ of 0.5 with span to depth ratios in the range 20 to 40, seems to be conservative estimate. Where $\delta_u$ is the central deflection for the ultimate load. For smaller span to depth ratios, the ultimate load is reached for significantly smaller $\frac{\delta_u}{h}$ than 0.5.

These tests are commonly done on thinner deck slabs of about 40 to 50 mm, which is used to create Figure 188, where the deflection is given in mm. Here it is estimated that in the slenderness range 10 to 20, a deflection from 15 to 20 mm occurs, and for slenderness 20 to 40, a deflection from 20 to 25, if the linear trend is followed. It is noted that the graph is comprised of the data from Table 44, where most of the slabs are square, meaning they are supported on four sides, and behave more like two-way supported slabs than one-way. This is an important note when using the information from Figure 187 and Figure 188.

*Table 42 overview research load displacement for laterally restrained reinforced concrete slab strips*

| Research | Failure mode | Fail Load [kN] | Ultimate deflection [mm] | Concrete Strength [MPa] | Reinforcement | Thickness [mm] | Slenderness [-] |
|---|---|---|---|---|---|---|---|
| **(Muthu, 2006)** | Snapping reinforcement | 14.2-64 | 8.3-16.9 | 34-54 | Reinforced steel | 50 and 65 | 8.5 and 11 |
| **(Taylor, Rankin, & D.J., 2001)** | Crushing | 46-500 | 30-50 | 30-100 | Reinforced steel | 150 | 9.5 |
| **(Taylor & Mulin, 2005)** | Crushing/bending | 33-210 | 20-30 | 40-80 | GFRP (glass fibre reinforced polymer) reinforcement | 150 | 9.5 |
| **(Taylor & Tharmarajah, 2010)** | Crushing | 295.1-343.5 | 11.4-19.4 | 66.3-72.6 | GFRP reinforcement | 150 | 9.5 |
| **(Taylor & Tharmarajah, 2014)** | Crushing | 295.1--343.5 | 14.6-19.4 | 65.7-69.3 | BFRP (basalt) and GFRP reinforcement | 150 | 9.5 |

*Table 43 overview research load displacement for scale prototypes*

| Research | Failure mode | Fail Load [kN] | Ultimate deflection [mm] | Scale | Concrete Strength [MPa] | Reinforcement | Thickness [mm] | Slenderness [-] |
|---|---|---|---|---|---|---|---|---|
| **(Poston, 1988)** | Punching Shear (expected) | 224 | 5.6 | half scale | - | Prestressed steel tendons | 210 | 5.7 |
| **(Marshe, 1997)** | Punching Shear | 72-95 | 7.3-10.1 | 1/4.04 | 40 | Prestressed CFRP tendons | 43 | 13.2 |
| **(Amir, 2014)** | Punching shear | 257-359 | 4.15-13.96 | half scale | 65 | Prestressed steel tendons | 100 | 16.5 |
| **(Batchelor, 1987)** | Punching shear | 12-24 | 3-8 | 1/8 | - | Reinforced steel | 178 | 17.2 |

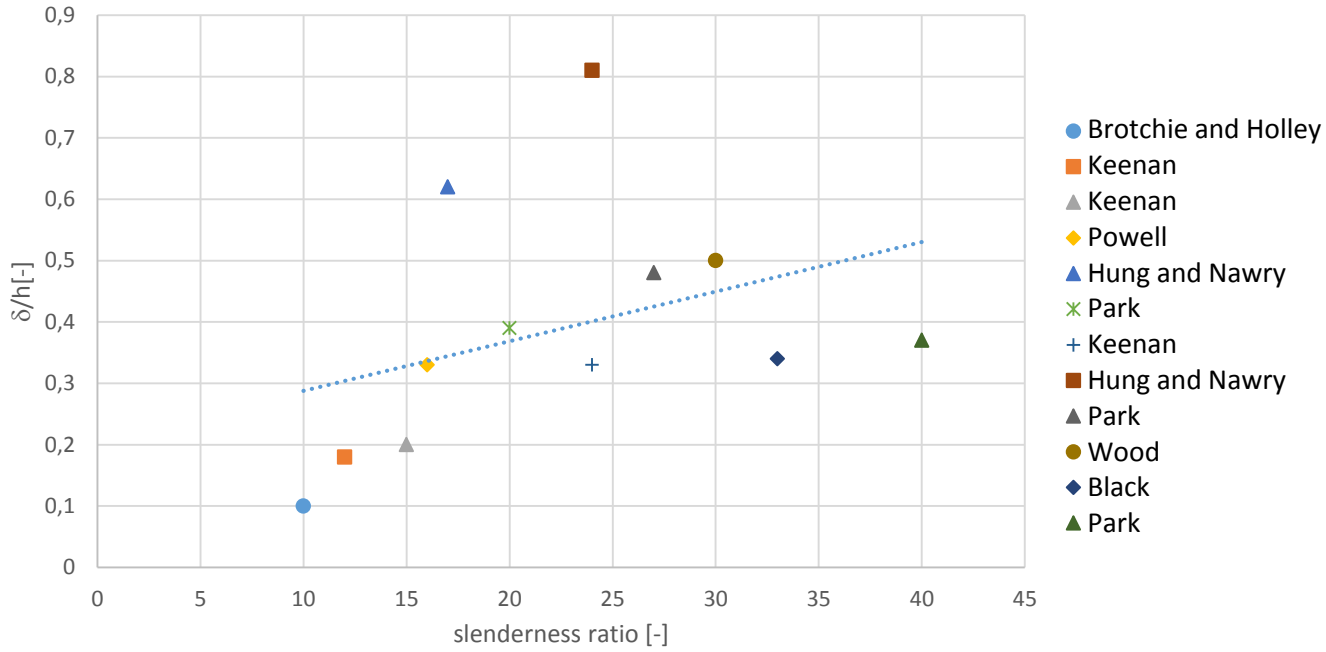


*Figure 187 slenderness vs deflection/thickness derived from Table 44*

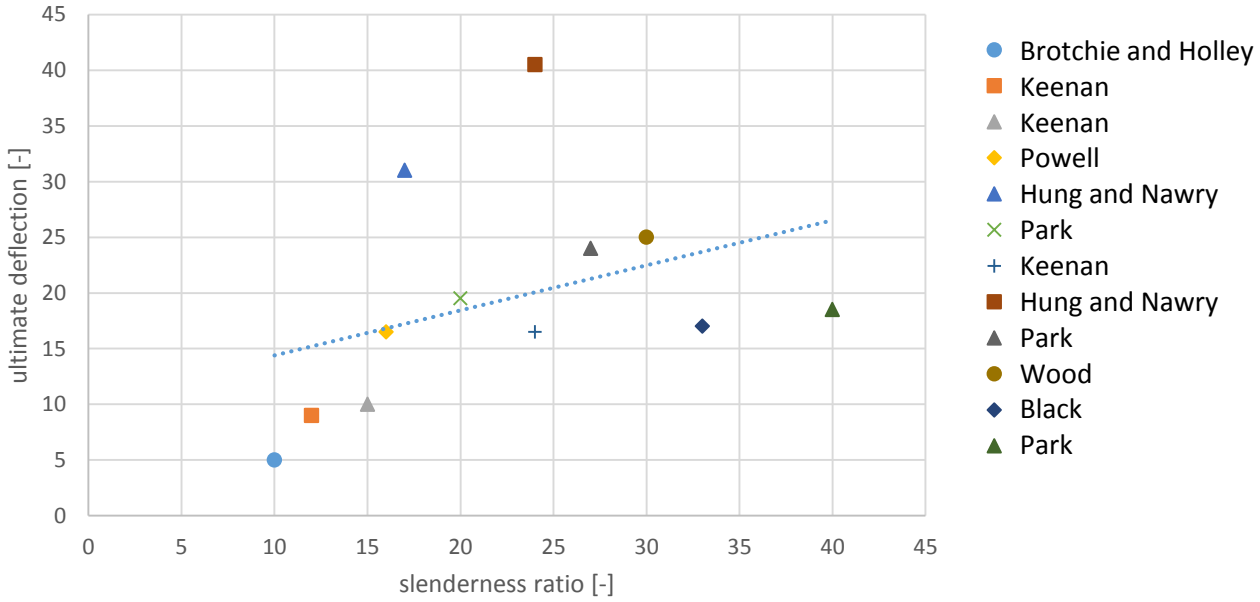


*Figure 188 slenderness vs ultimate deflection derived from Table 44*

*Table 44 measured central deflection/slab thickness at ultimate load of uniformly loaded laterelly restrained slabs*

| Investigator | Number of Slabs | $\frac{l_x}{l_y}$ | $\frac{l_y}{h}$ | $\frac{\delta_u}{h}$ | $\frac{\delta_u}{l_y}$ |
|---|---|---|---|---|---|
| Powell[12.4] | 15 | 1.75 | 16 | 0.33–0.44 | 0.021–0.028 |
| Wood[12.5] | 3 | 1.0 | 30 | 0.5 | 0.017 |
| Park[12.8] | 5 | 1.5 | 20 | 0.39–0.50 | 0.020–0.025 |
| | 1 | 1.5 | 27 | 0.48 | 0.018 |
| | 3 | 1.5 | 40 | 0.37–0.50 | 0.009–0.013 |
| Brotchie and Holley[12.14] | 4 | 1.0 | 20 | 0.36–0.57 | 0.018–0.029 |
| | 3 | 1.0 | 10 | 0.10–0.11 | 0.010–0.011 |
| Keenan[12.16] | 4 | 1.0 | 24 | 0.33–0.51 | 0.014–0.021 |
| | 1 | 1.0 | 15 | 0.20 | 0.013 |
| | 1 | 1.0 | 12 | 0.18 | 0.018 |
| Hung and Nawy[12.19] | 7 | 1.0 | 24 | 0.81–0.89 | 0.034–0.038 |
| | 5 | 1.43 | 17 | 0.62–0.74 | 0.037–0.044 |
| Black[12.21] | 4 | 1.0 | 33 | 0.34–0.71 | 0.010–0.022 |

(Muthu, 2006)

*Table 45 details restrained slab stripa and summary test data (Muthu, 2006)*

| Slab no | Edge beam dimension (mm) | Thickness of slab (mm) | Spacing of reinforcement (mm) | | Cube strength $f_{ck}$ (MPa) | Experimental ultimate load ($Q_{ue}$) (kN) | Deflection at ultimate load ($\delta_{ue}$) (mm) | Ratio ($\delta_{ue}/D$) | Edge rigidity factor ($\lambda$) |
|---|---|---|---|---|---|---|---|---|---|
| | | | Shorter direction ($S_Y$) | Longer direction ($S_X$) | | | | | |
| M1 | 150 × 300 | 50 | 150 | 150 | 43.5 | 19.6 | 12.81 | 0.26 | 0.03 |
| M2 | 150 × 275 | 50 | 125 | 150 | 43.4 | 28.8 | 11.10 | 0.22 | 0.04 |
| M3 | 150 × 250 | 50 | 95 | 150 | 50.57 | 35.2 | 16.81 | 0.34 | 0.04 |
| M4 | 150 × 225 | 50 | 75 | 150 | 51.30 | 39.2 | 16.92 | 0.34 | 0.05 |
| M5 | 150 × 200 | 50 | 65 | 150 | 54.40 | 14.2 | 16.08 | 0.32 | 0.06 |
| M6 | 150 × 300 | 65 | 167 | 200 | 34.73 | 21.0 | 8.25 | 0.13 | 0.07 |
| M7 | 150 × 275 | 65 | 125 | 200 | 40.50 | 34.4 | 10.24 | 0.16 | 0.08 |
| M8 | 150 × 250 | 65 | 95 | 200 | 45.30 | 42.6 | 10.82 | 0.17 | 0.11 |
| M9 | 150 × 225 | 65 | 75 | 200 | 53.60 | 54.8 | 12.71 | 0.20 | 0.11 |
| M10 | 150 × 200 | 65 | 65 | 200 | 54.36 | 64.0 | 13.89 | 0.21 | 0.13 |

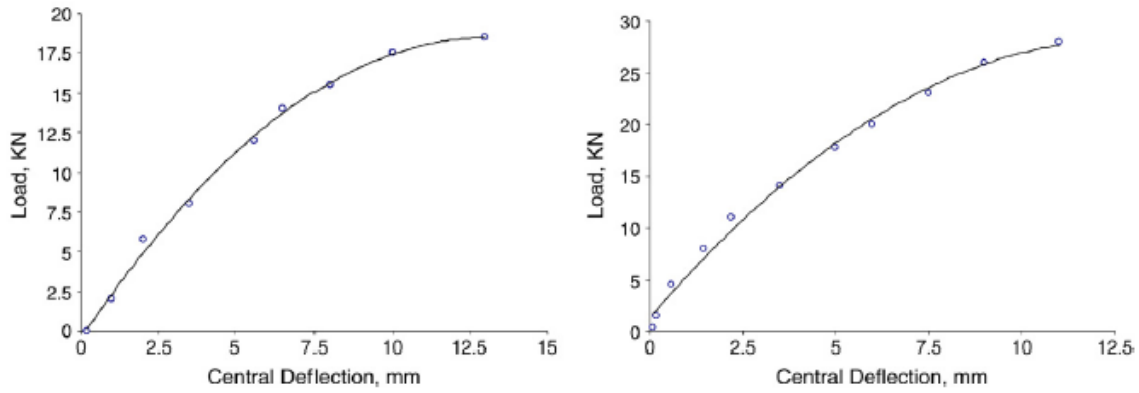


*Figure 189 load deflection plot of partially restrained slabs M1 and M2 (Muthu, 2006)*

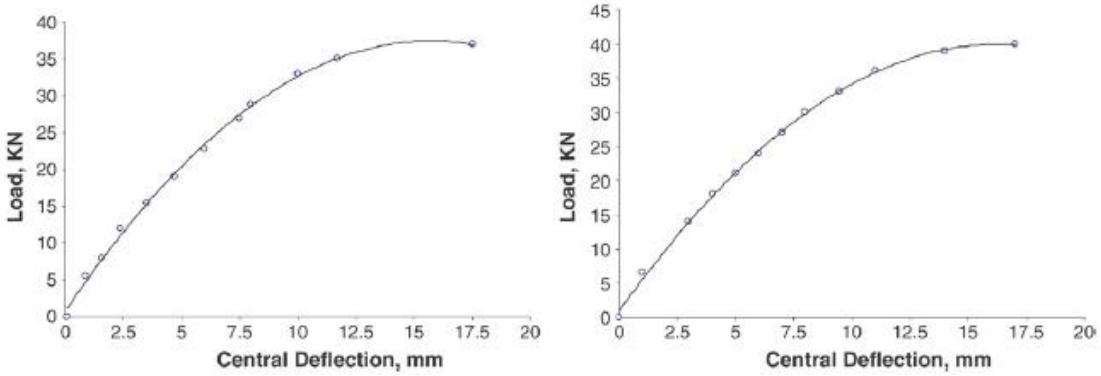


*Figure 190 load deflection plot of partially restrained slabs M3 and M4 (Muthu, 2006)*

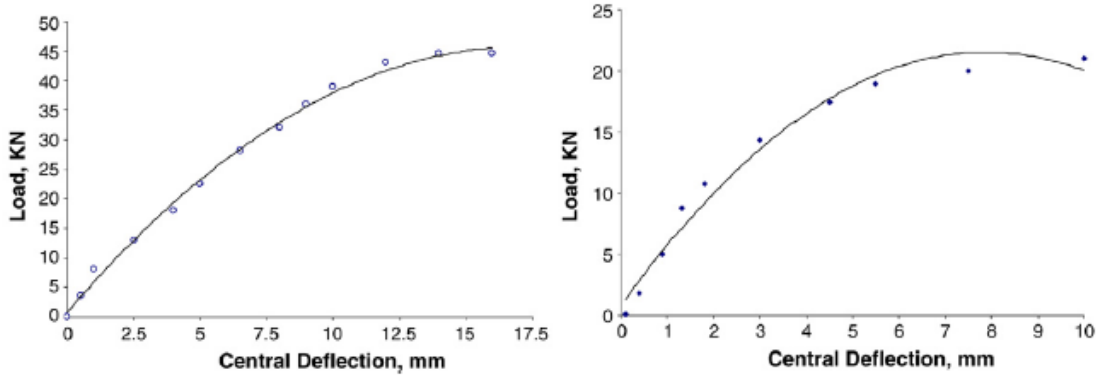


*Figure 191 load deflection plot of partially restrained slabs M5 and M6 (Muthu, 2006)*

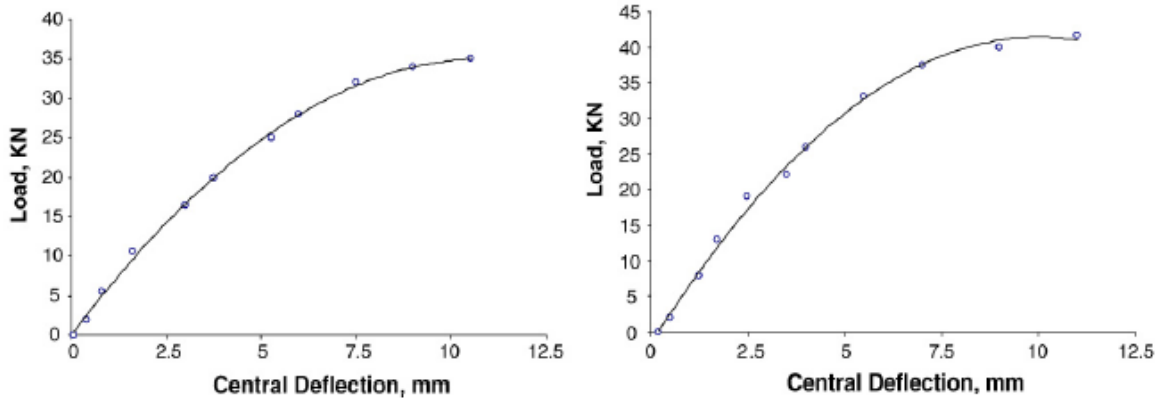


*Figure 192 load deflection plot of partially restrained slabs M7 and M8 (Muthu, 2006)*

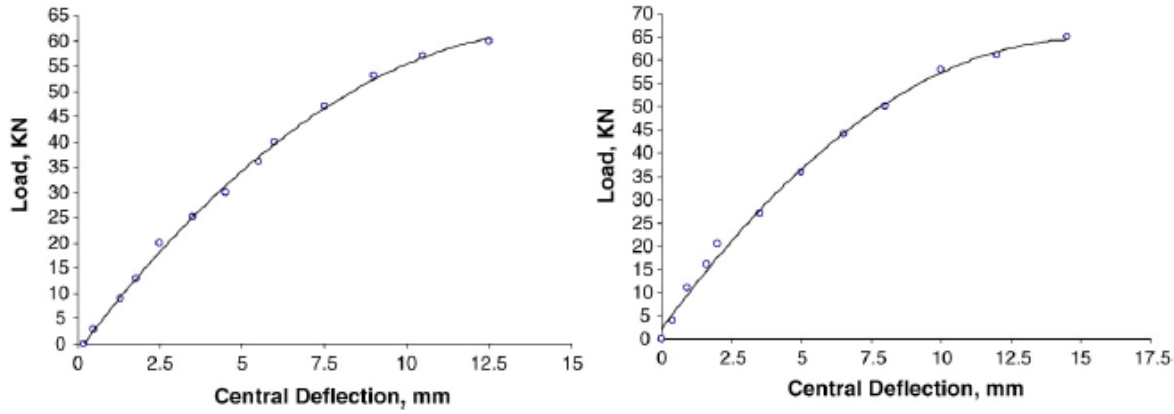


*Figure 193 load deflection plot of partially restrained slabs M9 and M10 (Muthu, 2006)*

(Taylor, Rankin, & D.J., 2001)

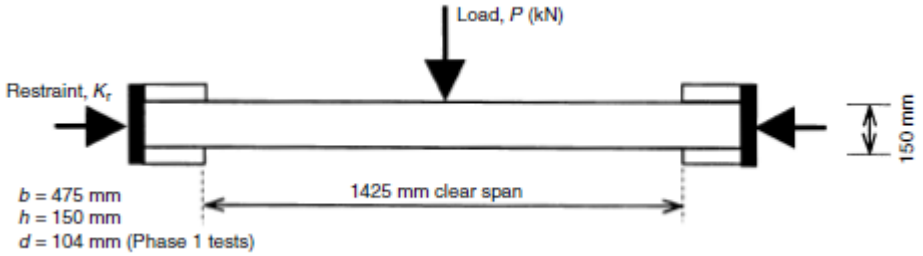


*Figure 194 model test load arrangement for F/E and L/R boundary conditions (Taylor, Rankin, & D.J., 2001)*

*Table 46 test variables (Taylor, Rankin, & D.J., 2001)*

| Phase No. | Slab No. | Slab No. | Reinforcement | Boundary condition | $f_{cu}$: N/mm$^2$ | $f_t$: N/mm$^2$ | Ratio $f_t/f_{cu}^{1/2}$ | Ratio $K_r/K_s$ |
|---|---|---|---|---|---|---|---|---|
| 1 | S1 | 1 | 0·68% T & B | F/E + L/R | 31·2 | 3·0 | 0·54 | 0·12 |
| | S2 | 2 | 0·68% T & B | F/E + L/R | 40·8 | 3·3 | 0·52 | 0·11 |
| | S3 | 3 | 0·68% T & B | F/E + L/R | 64·5 | 4·3 | 0·54 | 0·09 |
| | S4 | 4 | 0·68% T & B | F/E + L/R | 82·2 | 6·7 | 0·74 | 0·08 |
| | S5 | 5 | 0·68% T & B | F/E + L/R | 101·1 | 4·9 | 0·49 | 0·08 |
| | S6 | 6 | 0·68% B | S/S | 34·8 | 2·3 | 0·39 | n/a |
| | S7 | 7 | 0·68% B | S/S | 91·0 | 6·1 | 0·64 | n/a |
| | S8 | 8 | 0·68% B | S/S + L/R | 100·1 | 6·6 | 0·66 | 0·08 |
| 2 | S9 | 9 | 0·68% T & B | F/E + L/R | 89·3 | 5·6 | 0·59 | 0·18 |
| | S10 | 10 | none | F/E + L/R | 90·5 | 5·3 | 0·56 | 0·18 |
| | S11 | 11 | 0·68% centre | F/E + L/R | 96·8 | 6·1 | 0·62 | 0·17 |
| | S12* | 12 | 0·68% T & B | F/E + L/R | 101·0 | 6·4 | 0·64 | 0·17 |
| | S13 | 13 | fibres only | F/E + L/R | 104·9 | 6·8 | 0·66 | 0·17 |
| | S14 | 14 | 0·68% T & B | F/E + L/R | 39·5 | 3·0 | 0·48 | 0·29 |
| | S15 | 15 | 0·68% T & B | F/E + L/R | 60·9 | 3·7 | 0·47 | 0·22 |

F/E = fixed end
L/R = lateral restraint
S/S = simple support
* quarter span load points

*Table 47 comparison failure loads to predicted strengths (Taylor, Rankin, & D.J., 2001)*

| Phase No. | Slab No. | Failure Load: kN | BS 5400 F. Load: kN | Ratio Actual/ BS 5400 | QUB F. Load: kN | Ratio Actual/ QUB | Park F. Load: kN | Ratio Actual/ Park |
|---|---|---|---|---|---|---|---|---|
| 1 | S1 | 135 | 91·5 | 1·48 | 125 | 1·08 | 146·0 | 0·92 |
| | S2 | 145 | 93·4 | 1·55 | 138 | 1·05 | 162·3 | 0·89 |
| | S3 | 175 | 94·7 | 1·85 | 157 | 1·11 | 190·0 | 0·92 |
| | S4 | 187 | 94·7 | 1·97 | 168 | 1·11 | 210·2 | 0·89 |
| | S5 | 192 | 94·7 | 2·03 | 178 | 1·08 | 231·9 | 0·83 |
| | S6 | 46 | 46·2 | 1·00 | 46·2 | 1·00 | 46·2 | 1·00 |
| | S7 | 50 | 48·4 | 1·03 | 48·4 | 1·03 | 48·4 | 1·03 |
| | S8 | 183 | 64·6 | 2·83 | 153 | 1·20 | 229·0 | 0·80 |
| 2 | S9 | 252 | 94·7 | 2·66 | 214 | 1·18 | 263·9 | 0·95 |
| | S10 | 200 | 0·0 | — | 144 | 1·39 | 212·4 | 0·94 |
| | S11 | 223 | 68·3 | 3·27 | 194 | 1·15 | 222·5 | 1·00 |
| | S12 | 500 | 194·2 | 2·57 | 453 | 1·10 | 569·6 | 0·88 |
| | S13 | 225 | 0·0 | — | 158 | 1·42 | 235·2 | 0·96 |
| | S14 | 195 | 93·3 | 2·09 | 153 | 1·27 | 182·6 | 1·07 |
| | S15 | 211 | 94·7 | 2·23 | 182 | 1·16 | 220·2 | 0·96 |
| | | Average | | 2·04 | | 1·16 | | 0·94 |
| | | Standard Deviation | | 0·65 | | 0·12 | | 0·07 |
| | | Coeff. variation | | 31·9% | | 10·3% | | 7·8% |

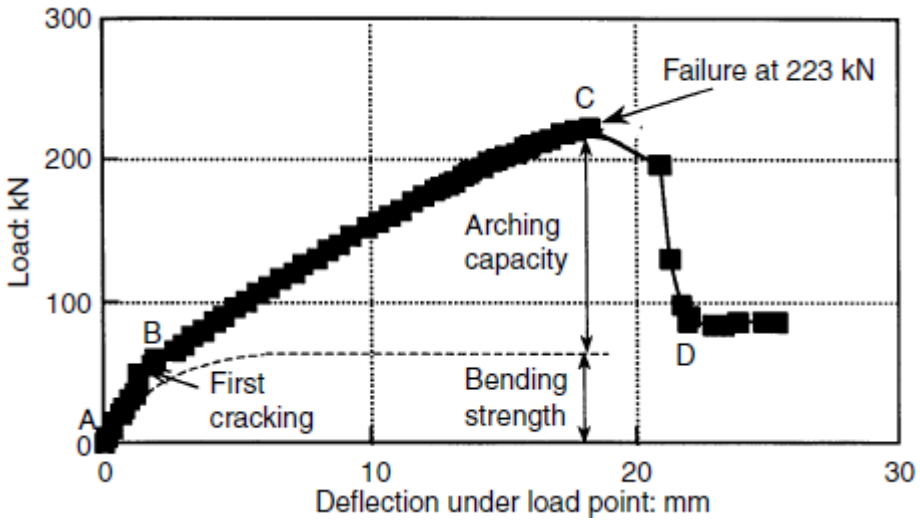


*Figure 195 load plotted against displaement slab S11 (Taylor, Rankin, & D.J., 2001)*

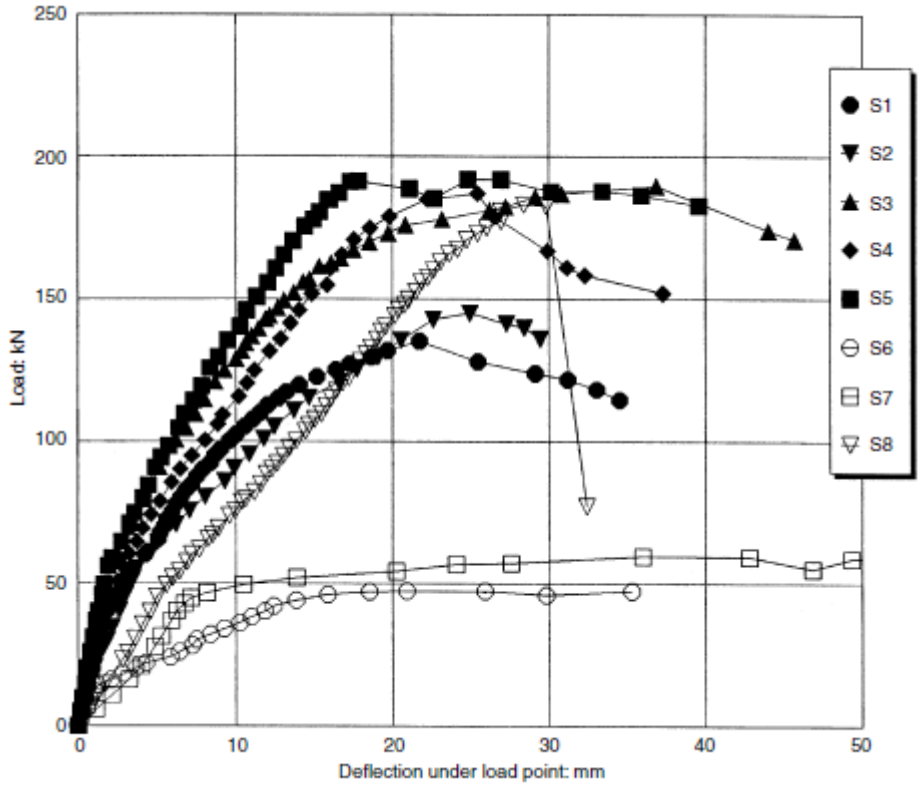


*Figure 196 comparison of test phase 1 results--load plotted against deflection under load point (Taylor, Rankin, & D.J., 2001)*

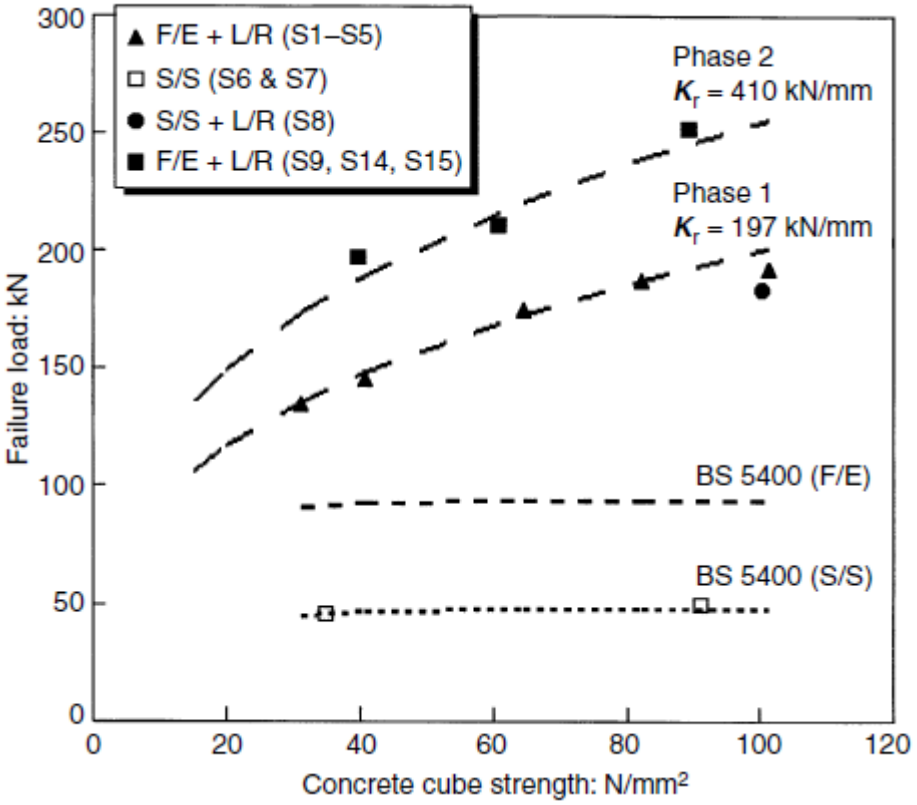


*Figure 197 summary of failure load vs concrete compressive strength (Taylor, Rankin, & D.J., 2001)*

(Taylor & Mulin, 2005)

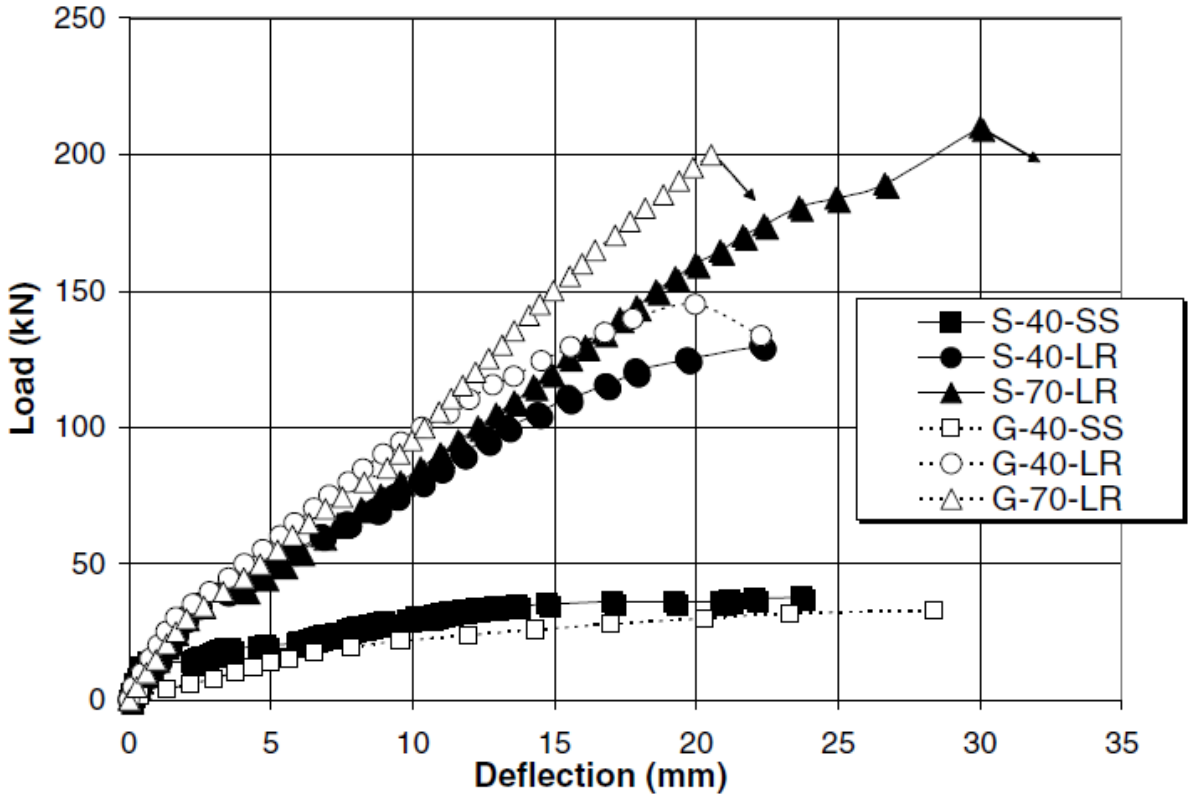


*Figure 198 load vs vertical deflection at midspan (Taylor & Mulin, 2005)*

*Table 48 test results (Taylor & Mulin, 2005)*

| Slab no. | $f_{cu}$ (N/mm$^2$) | $f_t$ (N/mm$^2$) | Failure load (kN) | Deflection @ failure (mm) | Failure mode |
|---|---|---|---|---|---|
| S-40-SS | 39.7 | 2.9 | 37.4 | 22 | Steel yielding |
| S-40-LR | 41.0 | 3.1 | 129.8 | 22 | Crushing/bending |
| S-70-LR | 85.0 | 2.9 | 210 | 30 | Crushing/bending |
| G-40-SS | 39.9 | 3.7 | 33 | 28 | Crushing |
| G-40-LR | 38.6 | 3.3 | 145 | 20 | Crushing/bending |
| G-70-LR | 67.9 | 3.3 | 200 | 21 | Crushing/bending |

(Taylor & Tharmarajah, 2010)

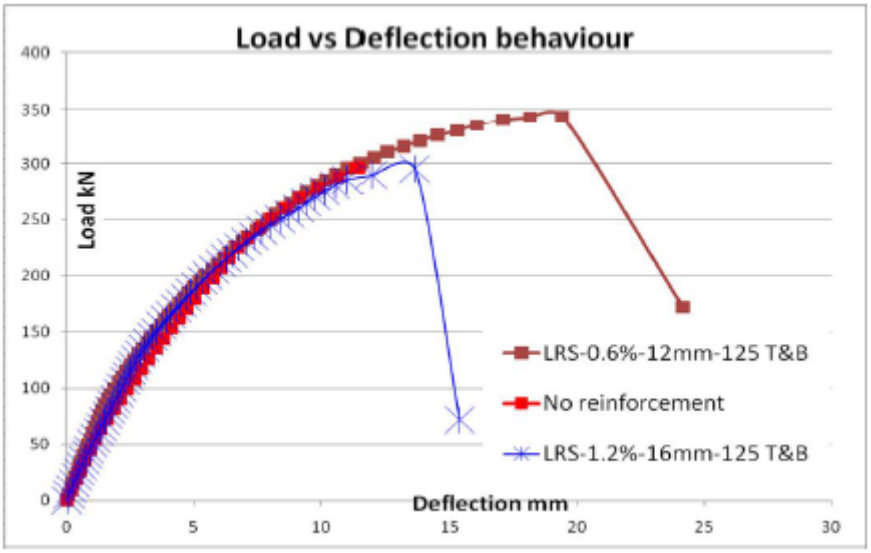


*Figure 199 load deflection behavior of three GFRP reinforced laterally restraint slabs (Taylor & Tharmarajah, 2010)*

*Table 49 test results of slabs (Taylor & Tharmarajah, 2010)*

| Test slab | Concrete strength ($N/mm^2$) | Effective depth (mm) | Failure load (kN) | Deflection at failure (mm) |
|---|---|---|---|---|
| SLAB 1 | 68.1 | 119 | 343.5 | 19.4 |
| SLAB 2 | 72.6 | N/A | 296.7 | 11.4 |
| SLAB 3 | 66.3 | 117 | 295.1 | 13.6 |

(Taylor & Tharmarajah, 2014)

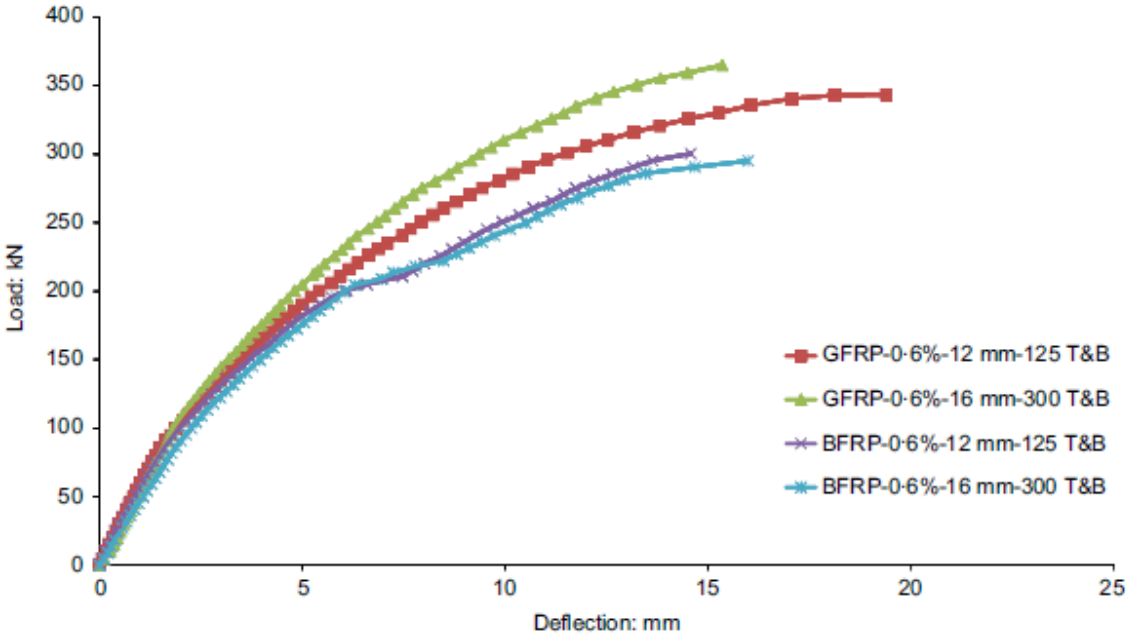


*Figure 200 load against deflection of the test slabs*

*Table 50 summary of the tests*

| Test slab | Concrete strength: MPa | Deflection at 150 kN | Maximum strain at 150 kN: % of ultimate strain | Crack width at 150 kN: mm | Deflection at failure: mm | Failure load: kN |
|---|---|---|---|---|---|---|
| GFRP-0·6%-12-125 T&B | 68·1 | L/407 | 20% | 0·33 | 19·4 | 343·5 |
| GFRP-0·6%-16-300 T&B | 65·7 | L/445 | 17% | 0·31 | 15·4 | 364·9 |
| BFRP-0·6%-12-125 T&B | 69·3 | L/385 | 10% | 0·33 | 14·6 | 300·4 |
| BFRP-0·6%-16-300 T&B | 66·1 | L/356 | 16% | 0·28 | 16·0 | 295·1 |

(Poston, 1988)

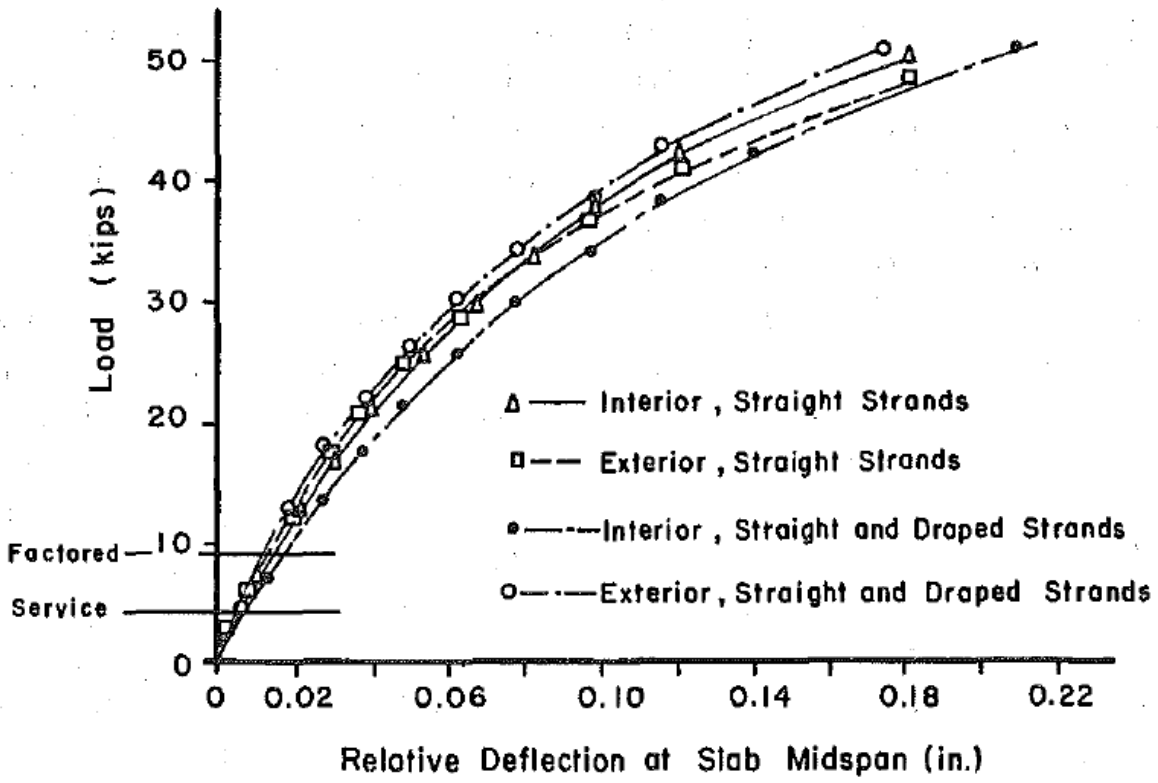


*Figure 201 load deflection curve for tested slabs (Poston, 1988)*

Scale deflection: from 0.5 to 5.6 mm, with steps of about 1 mm. Scale load: 0 to 224 kN, steps of 45kN.

(Marshe, 1997)

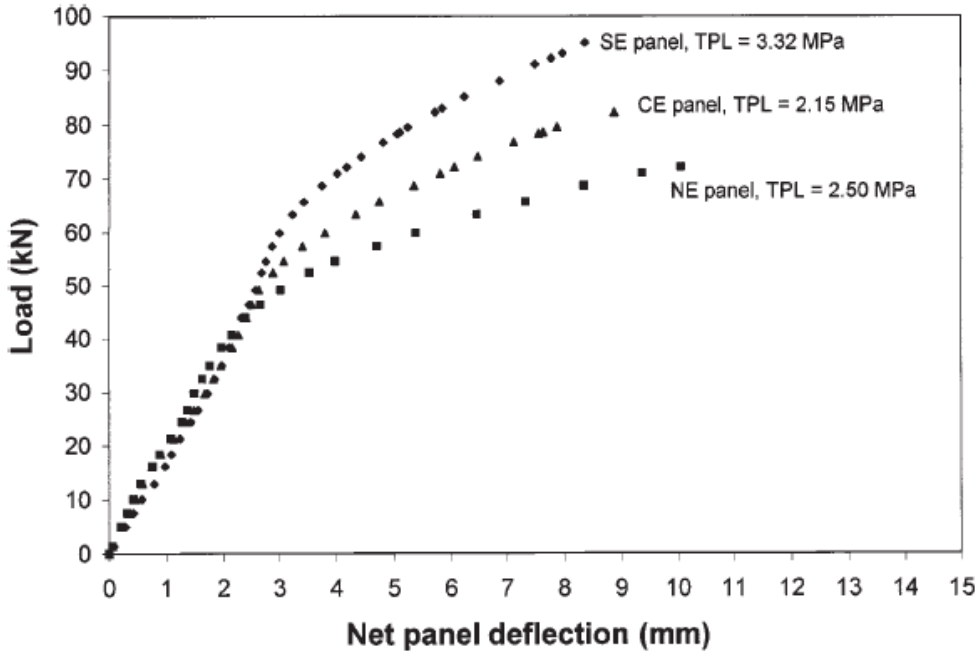


*Figure 202 net panel deflections with different TPL, loaded between tendons (Marshe, 1997)*

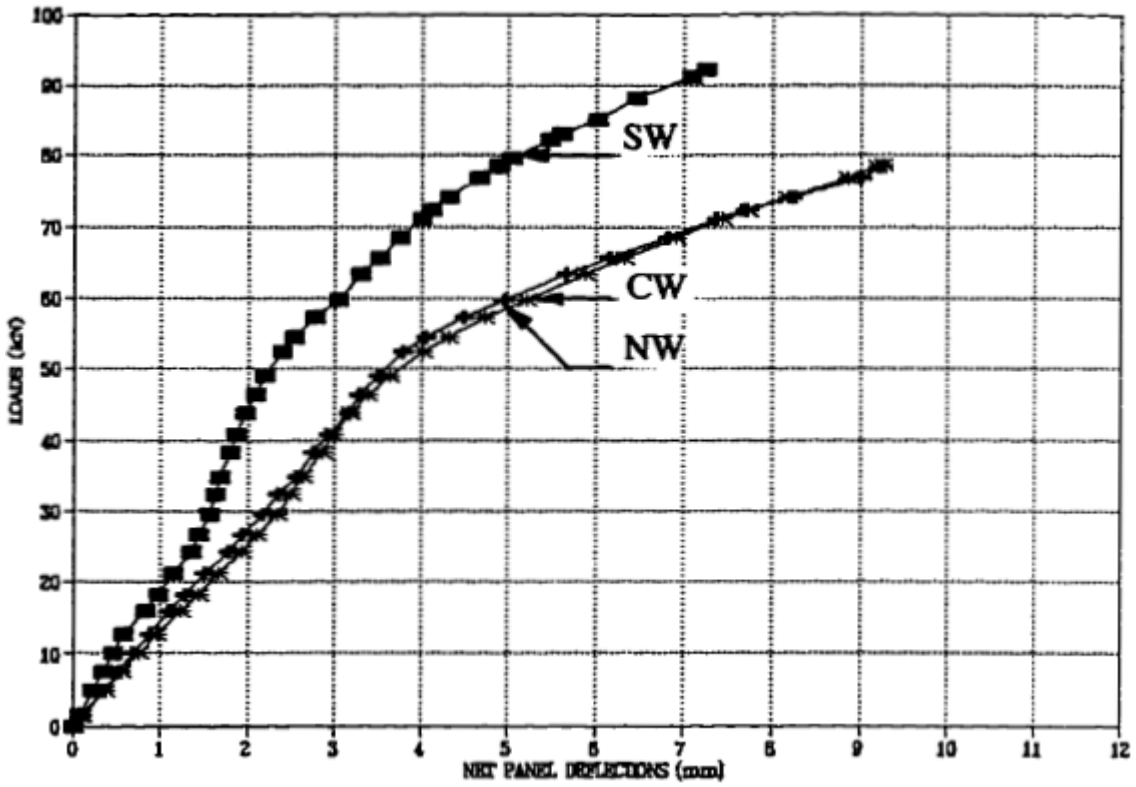


*Figure 203 net panel deflections with different TPL, loaded above tendons (Marshe, 1997)*

*Table 51 summary of test results (Marshe, 1997)*

| | | CFRP deck | | | | |
|---|---|---|---|---|---|---|
| Panel (1) | TPL (MPa) (2) | Ultimate panel deflection $\delta_u$ (mm) (3) | Cracking load $P_{cr}$ (kN) (4) | Model punching load $P_u$ (kN) (5) | Prototype punching load (5) × $4.04^2$ (kN) (6) | Safety factor (6)/140 (7) |
| CW | 2.15 | 9.3 | 38 | 79 | 1283 | 9.2 |
| CE | 2.15 | 8.9 | 44 | 82 | 1343 | 9.6 |
| NW | 2.50 | 9.4 | 38 | 78 | 1276 | 9.1 |
| NE | 2.50 | 10.1 | 35 | 72 | 1178 | 8.4 |
| SW | 3.32 | 7.3 | 60 | 92 | 1503 | 10.7 |
| SE | 3.32 | 8.4 | 60 | 95 | 1551 | 11.1 |

(Batchelor, 1987)

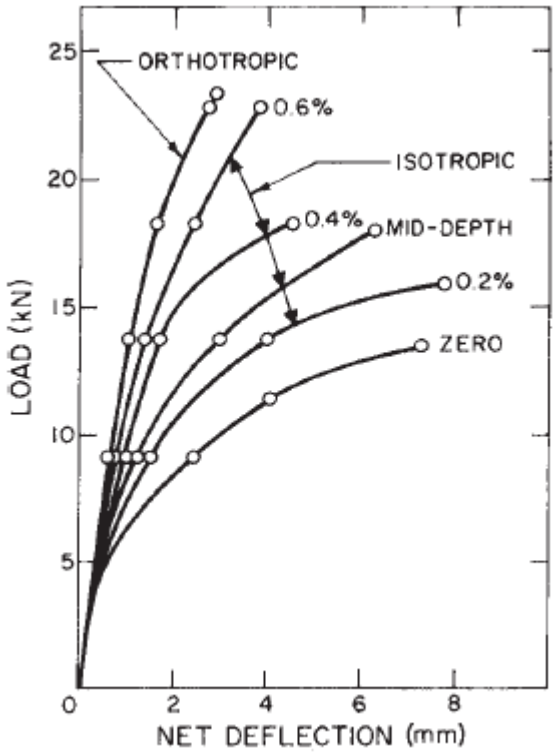


*Figure 204 typical load-deflection curves for slabs of four beam bridge model (Batchelor, 1987)*

# Appendix E

**Breedte: 800 mm**

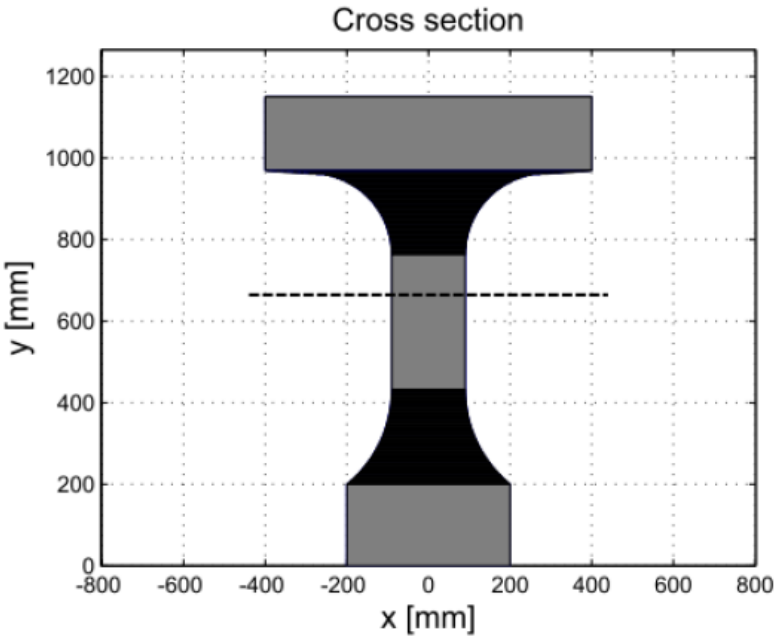


$A_c$ = 398878.9536 mm$^2$
$z_o$ = 664.20 mm
$z_b$ = 485.80 mm
$I_{yy}$ = 6.0478e+10 mm$^4$
$W_o$ = 9.1054e+07 mm$^3$
$W_b$ = 1.2449e+08 mm$^3$

*Figure 205 cross section properties girder "de Vecht"*

**Breedte: 800 + 425 = 1225 mm**

(incl. meewerkende breedte tussenstort)

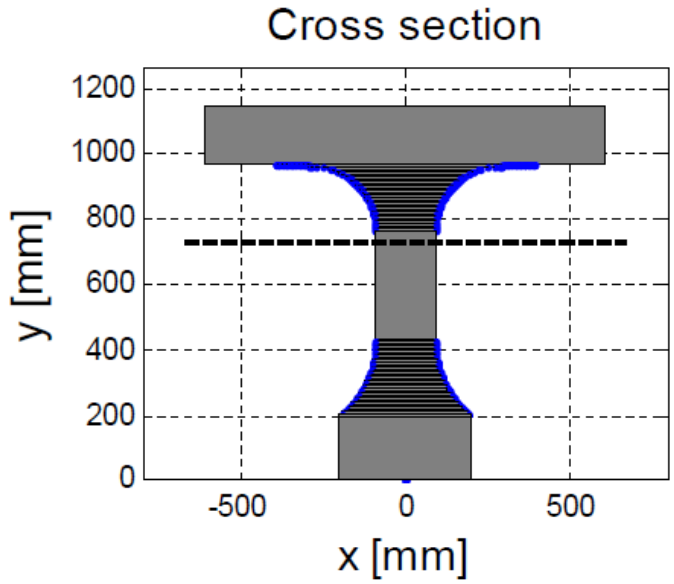


$A_c$ = 475378.9536 mm$^2$
$z_o$ = 727.89 mm
$z_b$ = 422.11 mm
$I_{yy}$ = 7.0741e+10 mm$^4$
$W_o$ = 9.7186e+07 mm$^3$
$W_b$ = 1.6759e+08 mm$^3$

*Figure 206 cross section properties girder "de Vecht"*

*Table 52 load distributions for the three-girder model, for the point loads at 4 and 2.25 m, with and without crossbeams*

| Load location [m] | Crossbeams | Load percentage on main beam [%] | Percentage of load after redistribution [%] |
|---|---|---|---|
| 4 | | 40 | 80 |
| 4 | X | 33.3 | 67 |
| 2.25 | | 47 | 94 |
| 2.25 | X | 34 | 68 |

# Appendix F

**Slab bending capacity calculations 'De Vecht'**

**Empirical method (NZ/CAN)**

Graphs from the Transit Bridge manual (new zealand transport agency, 2014) are used to determine $R_i$. Using interpolation, and reading the "composite" graph Figure 141, where reinforcement percentage is 0.45% (0.44% prestress streel in transverse direction, and 0.027 % reinforcement steel in longitudinal direction). This gives the following:

$R_i = 903\ kN$

For:

$f_c' = 23.3\ MPa$
$h = 180\ mm,$
$L_s = 2.239\ m$

Calculated capacity:

$$P_{axle} = \frac{\frac{\phi * 0.6 * R_i}{\gamma_L * 40 * I} * 8200}{100} = \mathbf{292\ kN}$$

$\phi = 1.0 * \phi_d = 1.0 * 0.5 = 0.5$
$CRR \leq 40\%$, deck in good conditon, mostly the case in the Netherlands
$\gamma_L = 1.9$
$I = 1.0$

The code is for a load surface area of 250*250 mm and does not give a solution for other wheel prints, such as the one used on 'De Vecht' (400*400 mm).

So using linear extrapolation the capacity is estimated: $\frac{400}{250} * P_{axle} = 467\ kN$

A characteristic load of 300 kN is present in LM1 (NEN-EN 1991-2, 2005).

So the unity check gives:

$$\frac{300}{467} = 0.64\ [-]$$

The unity check is OK.

**Simplified method (UK)**

Input:

$$f_c' = 0.8 * \frac{f_{cu}}{1.5} = 23.3 \frac{N}{mm^2}$$

$h = 180\ mm$
$d = 0.5 * h = 90\ mm$

$L_r = 0.5 * L_s = 0.5 * 2270 = 1135\ mm$

Deformation:

$$\varepsilon_c = (-400 + 60 * 26.7 - 0.33 * f_c') * 10^{-6} = 8 * 10^{-4}$$

$$R = \varepsilon_c * \frac{{L_r}^2}{d^2} = 0.03 \leq 0.26$$

$$k = 0.0525 * \left(4.3 - 16.1 * \sqrt{3.3 * 10^{-4} + 0.1243 * R}\right) = 0.17$$

Arch moment capacity:

$$M_{ar} = k * f_c' * h^2 = 128 \left[\frac{kNm}{m}\right]$$

Bending Capacity:

$$\boldsymbol{P_b = \frac{M_{ar}}{0.23} = 558\ kN}$$

Equivalent reinforcement ratio:

$$\rho_e = \frac{M_{ar}}{f_{ye} * d * z} = 0.07\ \%$$

$f_{ye} = 525\ MPa$
$z = 0.75 * d$
$d = 0.5 * h = 0.5 * 180 = 90\ mm$

Punching capacity:

$$P_p = 1.52 * (\phi + d) * d * \sqrt{f_c'} * (100 * \rho_e)^{0.25}$$

$\phi = 509\ mm$
$\boldsymbol{P_p = 635\ kN}$

When two wheelloads are applied together:

$$P_{pd} = 0.65 * P_p = 237\ kN$$

Unity check:

$$\frac{\frac{300}{2}}{\frac{237}{1.5}} = 0.9$$

The check is in order. (NEN-EN 1991-2, 2005) prescribes a load of 150 kN, and the loadfactor 1.5 comes from BD (81/02, 2002).

For the UK method the bending capacity is governing for slab failure: $P_p = 635\ kN > P_b = 558\ kN$

**Rankin Method**

The considered clear span is 2270 mm (Figure 109). Which gives the following effective width:

$$b_{eff} = c_y + 2 * L_e + 2 * h = 2630\ mm$$
$$c_y = 200\ mm$$
$$c_x = 200\ mm$$
$$L_e = \frac{L_s}{2} - \frac{c_x}{2} = 1035\ \text{mm}$$
$$h = 180\ mm$$
$$L_s = 2270\ mm$$

**Stiffness parameters**

$$E_c = 4.23 * f_{cu}^{0.5} = 20.4 \frac{kN}{mm^2}$$
$$f_{cu} = 23.3\ MPa$$

$$K_s = \frac{E_c * b_{eff} * h}{L_e} = 9345\ \frac{kN}{mm}\ (Fixed\ ended, \eta = 1)$$

$$K_d = \sum \frac{A_d * E_c}{L_e} = 10.5 * 10^3 \frac{kN}{mm}$$
$$A_d = 2 * (500 * 820) + 2 * (400 * 820) = 1.5 * 10^6\ mm^2$$

$$K_b = \frac{A_b * E_c}{L_e} = 66 * 10^4 \frac{kN}{mm}$$
$$A_b = \frac{\zeta * I_b * L_e}{b_{eff}} = 3 * 10^6\ mm^2$$
$$\zeta = 985 \text{ (FE)}$$
$$I_b = 6.0478 * 10^{10}\ mm^4$$

$$K_r = \frac{1}{(\frac{1}{K_b} + \frac{1}{K_d})} = 41 * 10^3\ kN/mm$$

**Flexural Capacity**

**Flexural parameters**

$$\beta = 1 - 0.003 * f_{cd} = 0.93 > 0.9.\ So, \beta = 0.9$$

$$x = \frac{F_s}{0.67 * f_{cd} * \beta * b_{eff}} = 0.07\ mm$$
$$F_s = F_{cable} * \left(\frac{A_p * b_{eff} * 10^{-3}}{A_{p,cable}}\right)$$
$$F_{cable} = 400\ kN$$
$$A_p = 1155 \frac{mm^2}{m}\ (1\ cable\ per\ 400\ mm)$$
$$A_{p,cable} = 462\ mm^2\ (Prestress\ Freyssinet\ 12\phi 7)$$
$$z = d - 0.5 * \beta * x = 90\ mm$$
$$d = 91\ \ mm$$

$$M_b = f_y * A_s * z = 237\ kNm/m$$

For fixed ended:

$$P_b = \frac{8 * L_s}{M_b} = 833\ kN$$

**Arching section**

$$2 * d_1 = h - 2 * x * \beta$$
$$d_1 = 90\ \ mm$$

$d_1$ from the previous iteration is used. The contact area due to arching is then given by:

$A = \alpha * b_{eff} * d_1 = 228 * 10^3\ mm^2$
$\alpha = 1$ for the first iteration, after 2 iterations $\alpha = 0.967$

$$L_R = L_e \sqrt[3]{\left(\frac{E * A}{K * L_e}\right) + 1} = 970\ mm$$

### Arching parameters

$\varepsilon_u = 0.0043 - [(f_{cd} - 60) * 2.5 * 10^{-5}] = 5.2 * 10^{-3} > 0.0043. So, \varepsilon_u = 0.0043$
$\varepsilon_c = 2 * \varepsilon_u * (1 - \beta) = 8.6 * 10^{-4}$

### Deformation

$$R = \frac{\varepsilon_c * {L_r}^2}{4 * d_1^2} = 0.03$$
$0 < R < 0.26;\ u = -0.15 + 0.36 * \sqrt{0.18 + 5.6 * R} = 0.063$

### Contact Depth

$$\alpha = 1 - \frac{u}{2} = 0.976$$

$\alpha * d_1$ is used for refined arching section above until value remains constant (iterative process).

### Arching Capacity

$0 < R < 0.26;\ M_r = 4.3 - 16.1 * \sqrt{3.3 * 10^{-4} + 0.1243 * R}\ ) = 3.3$
$$M_{ar} = 0.168 * b_{eff} * f_c' * d_1^2 * M_r * \frac{L_e}{L_r} = 269\ kNm/m$$

When both sides are restrained (Pucher, 1964) gives:

$$P_a = \frac{M_{ar}}{0.23} = 1172\ kN$$

### Flexural punching capacity

The ultimate capacity is the sum of the flexural and arching capacity:

$$P_{pf} = P_b + P_a = 2006\ kN$$

**Brittle Punching Capacity**

$$P_{pv} = \frac{0.43}{r_f} * \sqrt{f_{cd}} * (\phi + d)\pi * d * (\rho_e)^{0.25} = \mathbf{503\ kN}$$

$\phi = 509\ mm$ (load surface $400 * 400$)

$r_f = 1.15$ (rectangular wheel load)

The bending capacity is higher than the punching capacity. However, the bridge system is expected not to fail in punching and the higher slab bending capacity is used for the calculations in the main report.

**Girder shear capacity 'De Vecht'**

$$V_{Rd,c} = \frac{I * b_w}{S} * \sqrt{f_{ctd}^2 + \alpha_l * \sigma_{cp} * f_{ctd}} = 997\ kN$$
$$I = 60.478 * 10^9\ mm^4$$
$$b_w = 180\ mm$$
$$S = 70.9 * 10^6\ mm^3 \quad (47)$$
$$f_{ctd} = 4.21\ MPa$$
$$\alpha_l = 1.0$$
$$\sigma_{cp} = 6.6\ MPa$$

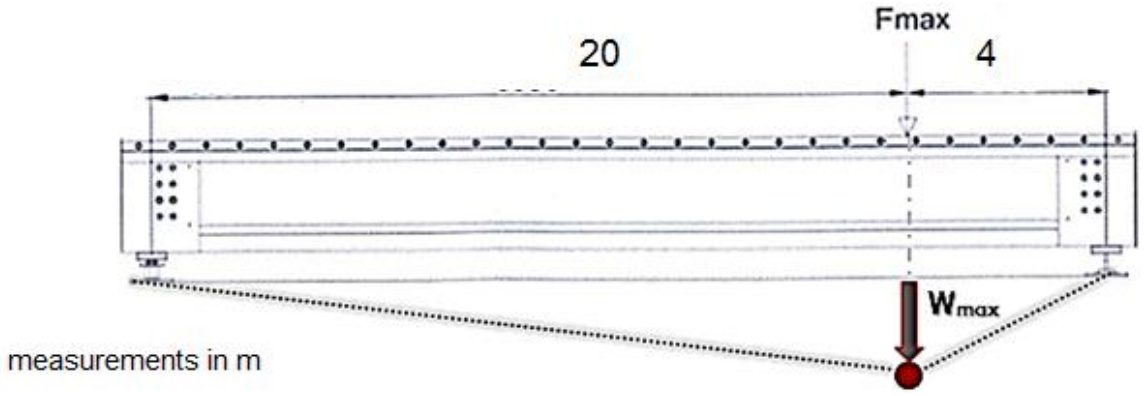


*Figure 207 load location and relative deflection of the girder over its span*

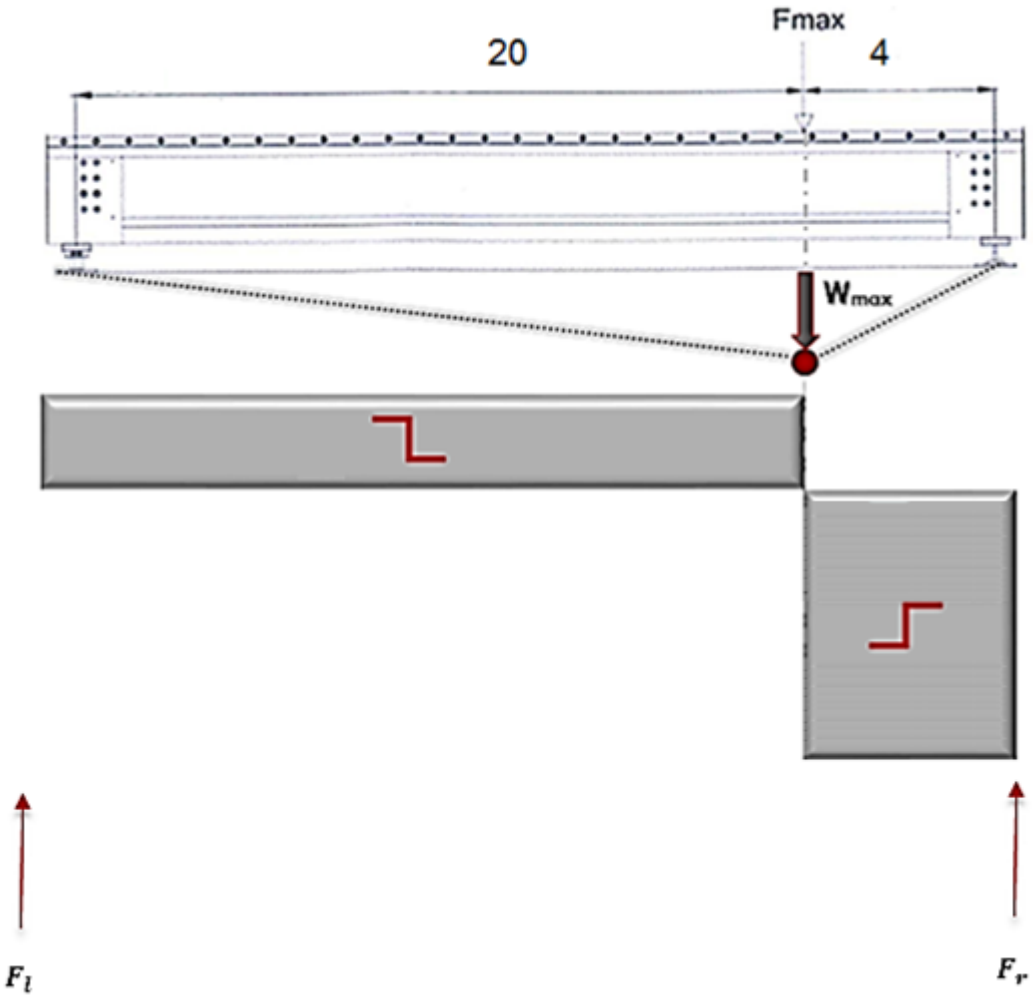


*Figure 208 Shear force distribution*

Two failure modes are possible: tensile splitting and flexural shear. Tensile splitting failure is more likely to occur since the girder is not reinforced heavily with shear stirrups. The mean tensile concrete strength $f_{ctm}$ is used, giving the tensile splitting shear capacity (calculation is given in Appendix F). With equilibrium of forces and the load position, the support reactions are known. Using that the maximum design shear force equals the tensile splitting strength, gives:

$$F_{max} = \frac{24}{20} * F_r = 1.2 * V_{Ed} = 1197\ kN$$

$$V_{Ed} = V_{Rd,c} \text{ (tensile splitting shear)} \tag{48}$$

For the test load at 2.25 m from the end, the following holds:

$$F_{max} = \frac{24}{21.75} * F_r = 1.1 * V_{Ed} = 1097\ kN$$
$$V_{Ed} = V_{Rd,c} \quad (49)$$

$F_{max}$ is for when loading only a single beam. This means that when the beam is integrated in a bridge system a higher bridge load is possible because of the load distribution. The load distribution is used to determine an equivalent load for the bridge $F_{bridge}$ (Figure 209):

$$F_{bridge} = \frac{F_{single}}{0.4} = \frac{1197}{0.4} = 3420\ kN \text{ (load at 4m)}$$
$$F_{bridge} = \frac{F_{single}}{0.47} = \frac{1097}{0.47} = 2812\ kN \text{ ( load at 2.25 m)}$$

However only redistribution was only possible up 80% of the total load (Figure 115): $0.8 * 3420 = 2736\ kN$
For the test load at 2.25 m, the percentage was 94%: $0.94 * 2812 = 2286\ kN$

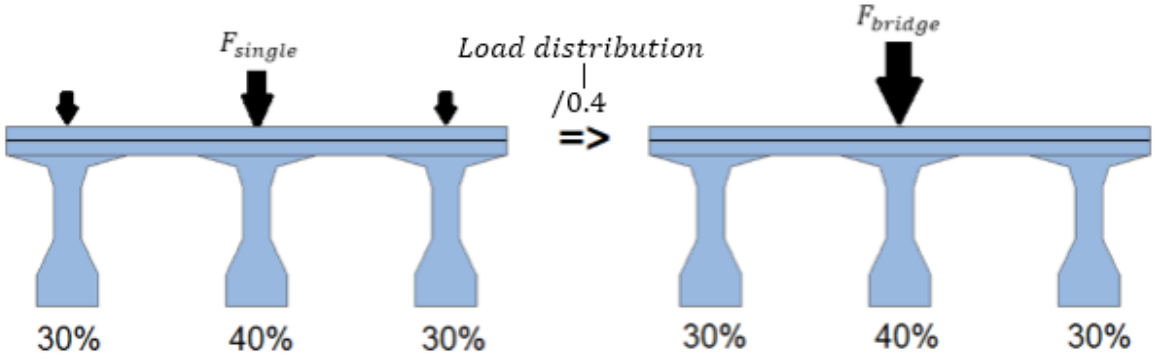


*Figure 209 converting single girder load, top, to full load on the bridge, bottom, using the linear load distribution for test load at 4 m*

*Table 53 girder and equivalent load, and redistributed capacity for three-girder model without crossbeams*

| Load location [m] | $F_{single}$[kN] | $F_{bridge}$[kN] | $F_{redistr}$[kN] |
|---|---|---|---|
| 4 | 1197 | 3420 | 2736 |
| 2.25 | 1097 | 2812 | 2286 |

*Table 54 girder and equivalent load, and redistributed capacity for three-girder model with crossbeams*

| Load location [m] | $F_{single}$[kN] | $F_{bridge}$[kN] | $F_{redistr}$[kN] |
|---|---|---|---|
| 4 | 1197 | 3627 | 2430 |
| 2.25 | 1097 | 3226 | 2194 |

# Appendix G

## Deflections estimated with use of Taylor tests

### Deflections

Using the research from Chapter 8, an ultimate deflection of 35 mm and a deflection of 25 mm at peak load (Figure 211 and Figure 212) is estimated. This means that it is possible a deflection plateau, showing plastic behavior, of 10 mm is available for the bridge during which the slab has the opportunity to redistribute loads. These deflections are considered upper bound deflections, since they occur when the slab fails in bending, which gives an upper bound slab capacity. When the slab's failure mode punching is governing, a deflection of 10 mm is assumed as a lower bound (Figure 210). The slab is assumed to be fixed ended (FE) and laterally restraint, since the stiffness factor $K_r$ is much larger than 1221 kN/mm (Figure 30).

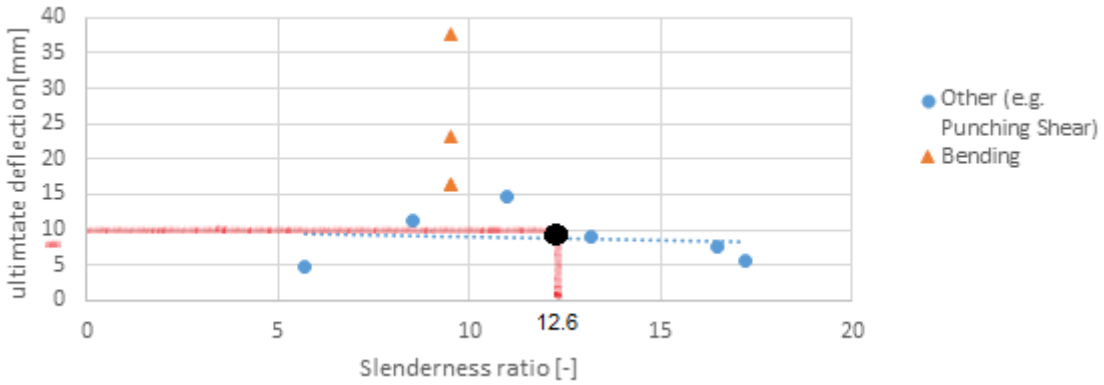


*Figure 210 lower bound ultimate deflection estimated, using Vecht slenderness 12.6*

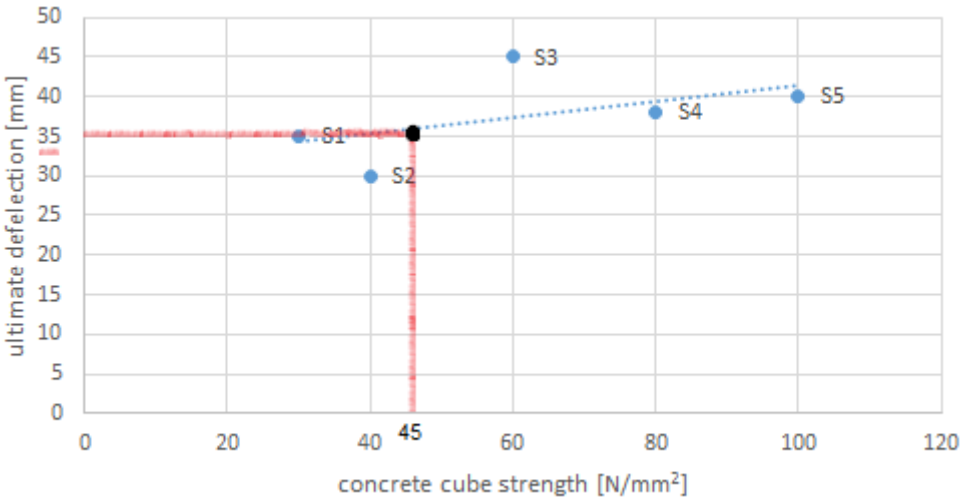


*Figure 211 upper bound ultimate deflection using Taylor's test results of concrete strength vs ultimate deflection*

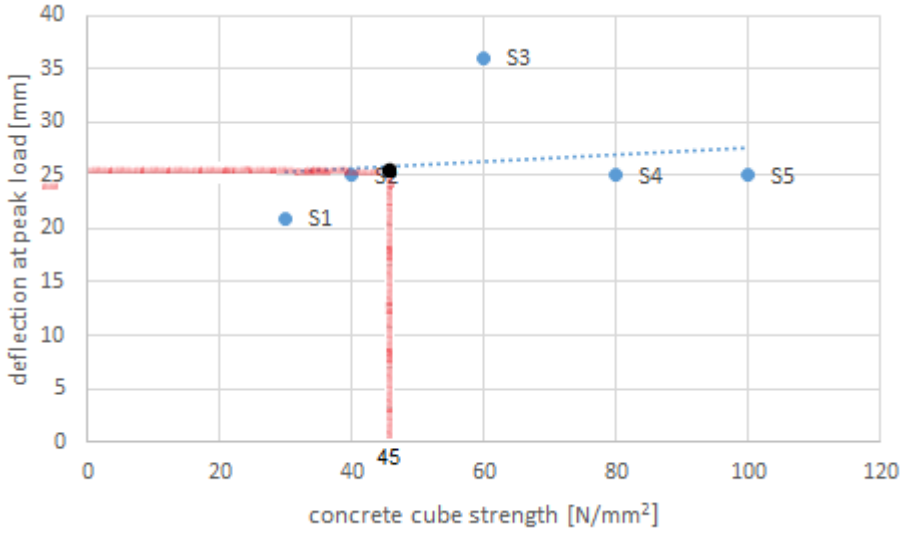


*Figure 212 upper bound delection at peak load using Taylor results*

*Table 55 estimated values using test results*

| Estimated values | |
|---|---|
| Deflection at peak load (upper) | 25 mm |
| Ultimate deflection (upper) | 35 mm |
| Plastic deflection plateau | 10 mm |
| Ultimate deflection (lower) | 10 mm |

The values determined from Figure 210 till Figure 212 are given in Table 55. Basically there are two possibilities for the slab, an upper and lower bound deflection pattern. For the first, bending is the governing failure mode, and for the second, punching shear.

The slab is assumed to reach its full bending capacity and arching action at peak load. After that, the deflection plateau starts and eventually ends at the ultimate deflection. During this period of deflection, redistribution of loads is assumed to be possible.

### Total bridge load

Using the numerical model (Figure 114), the linear bridge load of the system is determined, using the ultimate slab deflection of 35 mm as a limit for the numerical model (Figure 211).

The two most important elements are the slab and main beam. On one hand, the slab is governing, since after it fails, redistribution cannot take place anymore, and the main beam, not able to take the load anymore, fails as well. So the slab bending capacity and slab deflections are important.

But on the other hand the beam is important too. Especially the beam capacity and deflection. An ultimate deflection of 37 mm for a single girder was observed earlier (Figure 47). The beams of 'De Vecht' could displace more or less. They are less reinforced, possibly causing it to behave less ductile and deflect less. The actual deflections obtained from test results of 'De Vecht' beams are discussed later.

For an ultimate deflection of 35 mm, a total bridge load of 2469 kN, without crossbeams, is found (Figure 213). Which is an upper bound value, because the ultimate deflection of 35 mm was assumed to be an upper bound limit, which only occurs when bending of the slab is the governing failure mode.

The slab is governing in this case, and the maximal load, for the maximal assumed deflection, is considered an upper bound limit of the bridge (Table 56).

Furthermore, the numerical model behaved stiff, and the neighbor beams as well, due to the short considered span. This resulted in very low relative girder deflections of the main beam, which is of importance in the calculation of activated parts of the deck.

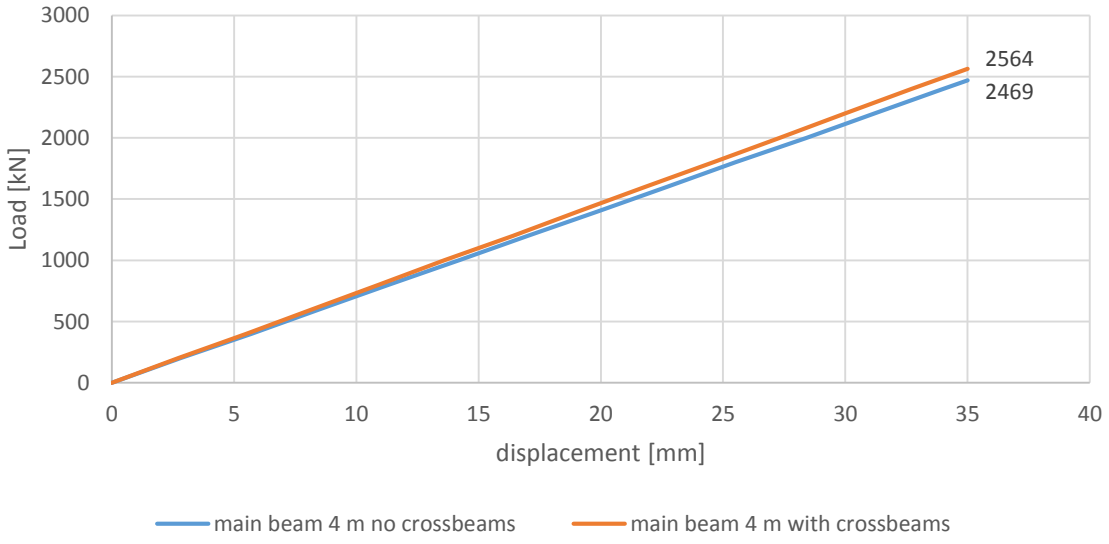


*Figure 213 load displacement graph bearing capacity with and without crossbeams*

The same test load was placed on the numerical model with cross beams--at the ends, one-third, and two-third of the length--to see the difference in capacity. A bearing capacity of 2564 kN was found (Figure 213), and a small difference in capacity is found 95 kN, with a factor 1.04 larger, compared to the model without cross beams.

But for the remainder of the calculations in this chapter the numerical model with crossbeams is used since one wants the most realistic representation of the actual bridge system, and the most accurate calculations and predictions. And the crossbeams are especially important for the load distribution and the determined deflections. Concluding, 'De Vecht' has four crossbeams, two at the end and two intermediate ones, and leaving them out is a significant deviation of the reality.

**Redistribution of load**

For the three methods, SCIA, UK, and RK Bending, redistribution of the load is assumed to be possible after the slab reaches its peak load and starts to behave plastically, indicated with the deflection plateau. For the possibilities where punching occured, redistribution is assumed not to occur, since the slab would have failed brittlely, failing without warning and without a chance to redistribute the loads.

**Deflection condition**

The relative girder displacements are very low, since the clear span was very short, and the neighbor girders displaced almost as much as the main girder. This results in relative girder deflections not exceeding the slabs deflections at midspan, the critical condition in order for membrane action to activate. At the maximal deflection of the bridge, the calculation shows the relative girder deflection to be about 2 mm, since the neighbor beams displaced almost as much as the main beam (Figure 214). Again, the fact that the three girders displace almost the same makes it logical to use a numerical model with more girders, five or seven.

So, instead of the relative deflection, just the deflection of the bridge system is used (e.g. Figure 216), in order to make the calculation for the total slab capacity provided by membrane action. This capacity is necesary for redistribution. The critical deflections are considered to be the deflections occuring at the peak load of the slab (Figure 216 and Figure 221).

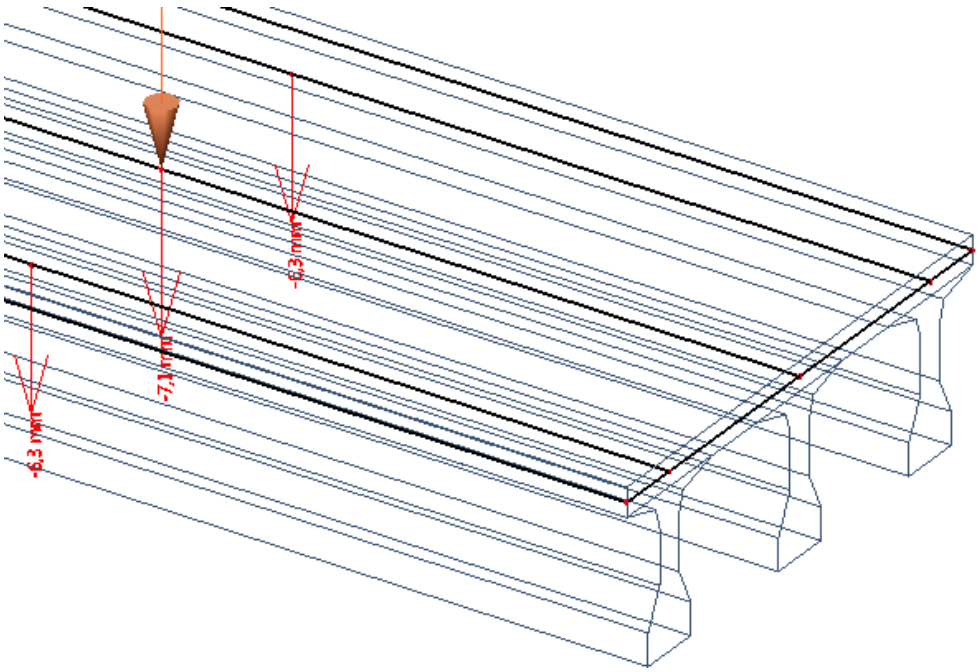


*Figure 214 deflections of main and neighbor beams, which are similar, resulting in low relative deflections*

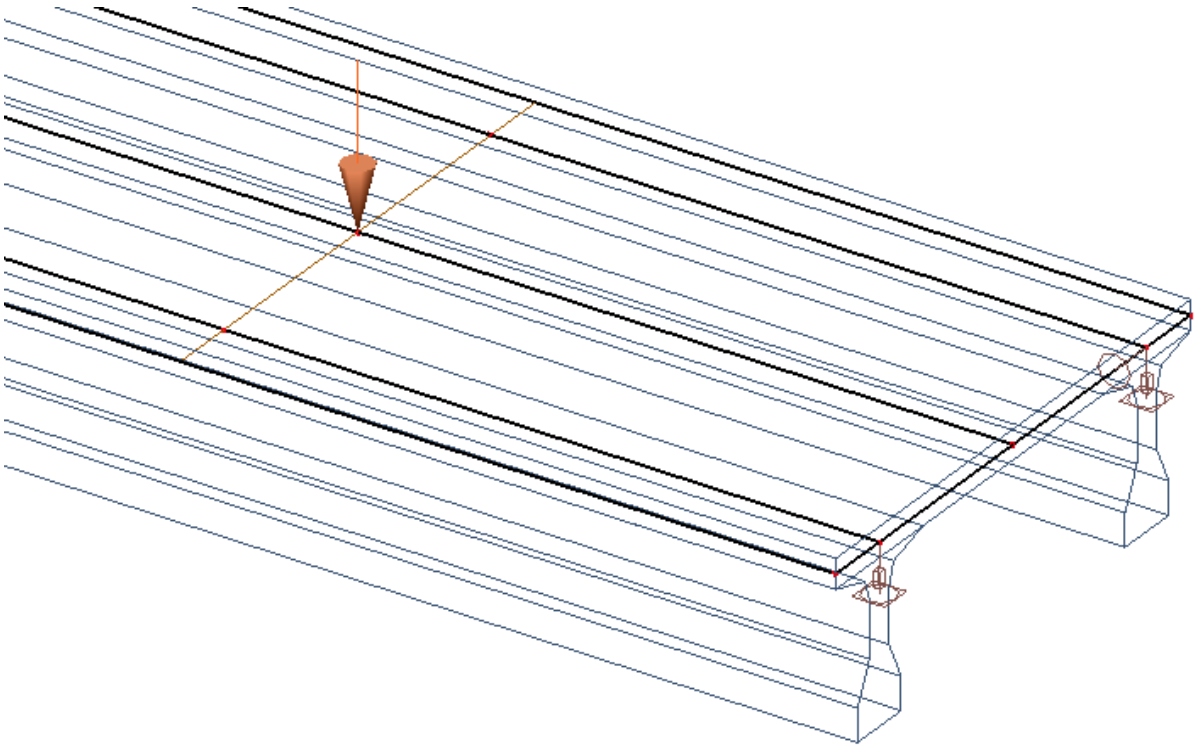

*Figure 215 numerical slab model to determine deflections at midspan*

### SCIA punching capacity (lower bound limit)

A slab punching capacity of 455 kN was found (Table 16 and Figure 216). No redistribution is assumed to occur after punching slab failure. However, it is assumed that it is not likely that punching occurs at all, since the main beam (Figure 109) is loaded directly. But, however, if punching occurs, the bridge is assumed not to have any capacity left, since the slab fails brittle and instantly without warning.

### SCIA bending capacity (upper bound limit)

A slab bending capacity of 1136 kN was found (Table 16 and Figure 216). Redistribution is assumed to be only possible after the slab reaches full arching action at its peak load, 1136 kN. The remaining load that the activated slab needs to carry and redistribute, using the model with crossbeams: $2546 - 1830 = 716\,kN$ (Figure 216). Simply said, the slab, after reaching the full arching action, needs to activate a surface area which can contribute a capacity of 716 kN.

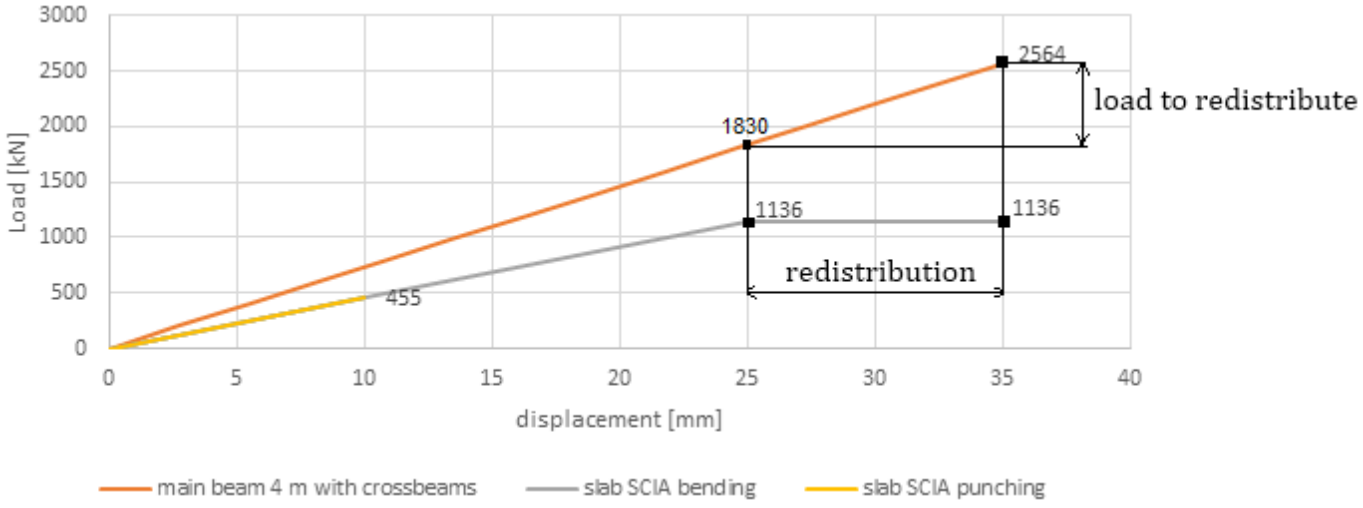


*Figure 216 total bridge load capacity and slab bending capacity determine with SCIA and Taylor test results*

### CAN punching capacity (lower bound limit)

Using the empirical method (CAN) the punching capacity was determined: 467 kN (Figure 219). And using a numerical slab model of 'De Vecht' (Figure 215) the displacement, at which this load occurs, was determined at 11 mm, which is in the same order as 10 mm, derived from the Taylor slab test results (Chapter 8) for failure in punching. So, the numerical model and the calculation seem to correspond with that.

### UK method punching capacity (lower bound limit)

Using the UK method the slab punching capacity was determined: 635 kN (Figure 218). And using a numerical slab model of 'De Vecht' (Figure 215) the displacement, at which this load occurs, was determined: 14 mm.

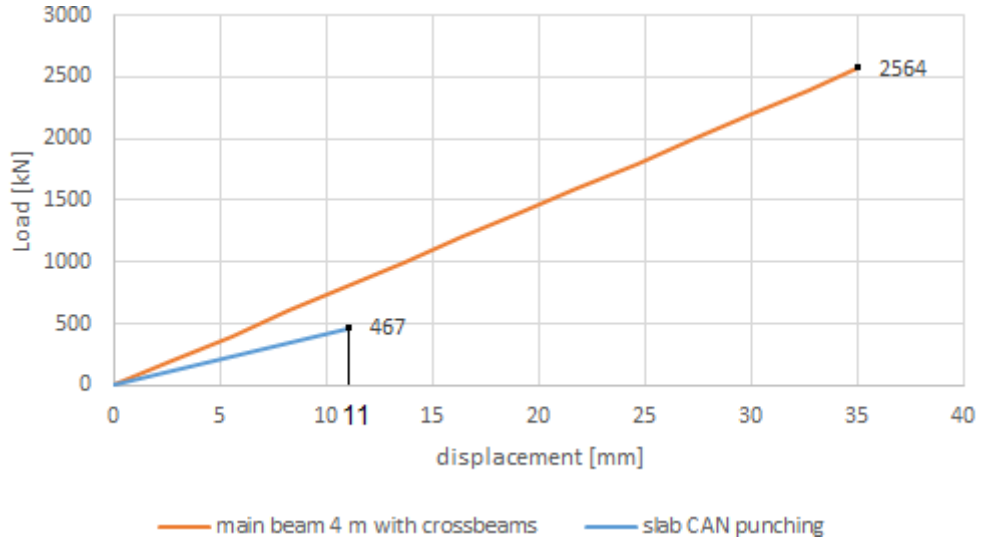


*Figure 217 total bridge load and slab punching capacity according to empirical method*

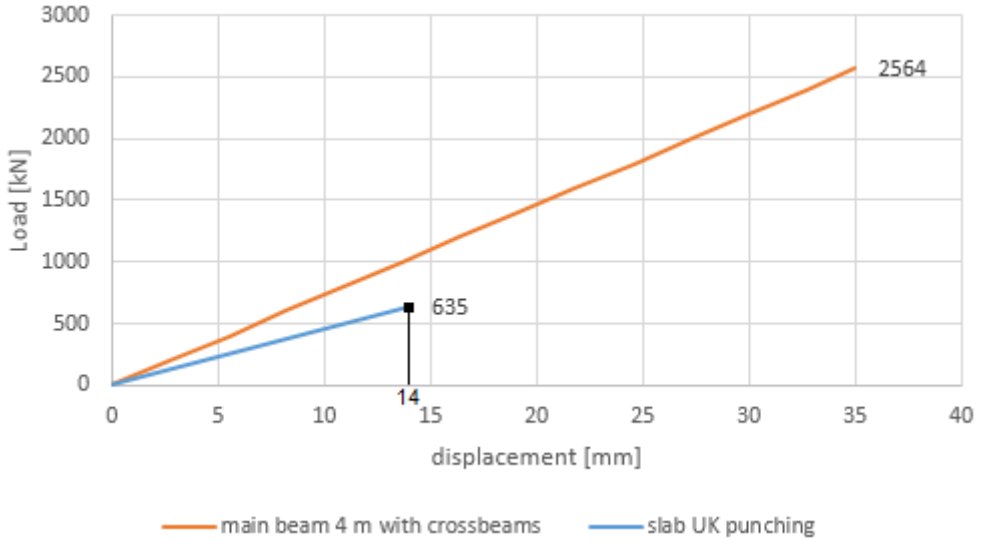


*Figure 218 total bridge load and slab punching capacity UK method*

**UK method bending capacity (upper bound limit)**

The slab bending capacity with the simplified method (UK) was 558 kN (Figure 219). Then using a numerical slab model of 'De Vecht' (Figure 215), the displacement, at which this load occurs, was determined: 12.3 mm. This is the deflection at peak load, and it was estimated that the slab behaves plastically for 10 mm, giving the slab an ultimate deflection of about 22.3 mm. Which is reached around 1635 kN.

Redistribution is only possible after the slab's peak load, 558 kN, is reached, and so the load that the slab needs to carry and redistribute is: $1635 - 900 = 735\ kN$ (Figure 219). Bending is assumed to be the governing failure mechanism and not punching.

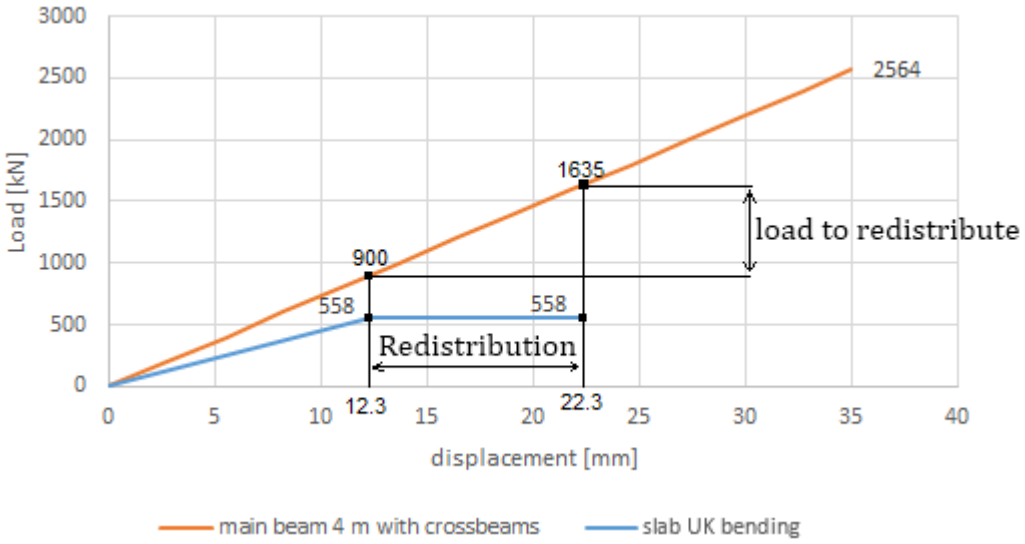


*Figure 219 bearing capacity, slab bending determined with UK method*

### Rankin method punching capacity (lower bound limit)

Using the RK method the punching capacity was determined: 509 kN (Figure 220). And using a numerical slab model of "De Vecht" (Figure 215) the displacement, at which this load occurs, was determined: 12 mm.

### Rankin method bending capacity (upper bound limit)

The bending capacity, determined by the Rankin method was 2006 kN (Figure 116). And using a numerical slab model of 'De Vecht' (Figure 215) the displacement, at which this load occurs, was determined: 43.5 mm. The slab could behave plastically for 10 mm, which gives an ultimate deflection of 53.5 mm. However, the main girder reaches its maximal failure load, 2564 kN, before the slab reaches its full capacity and is able to redistribute the loads (Figure 220). Redistribution seems not possible in this situation, using this specific method.

Also, the numerically determined deflections are larger than the estimated ultimate slab deflection of 35 mm. In (Taylor, Rankin, & D.J., 2001), slab deflections above 40 mm were not measured, possibly meaning that the calculated slab capacity is too high, or the numerical model behaves too stiff. Also, the heavily reinforced single girder test in Chapter 5 showed a maximum deflection of 45 mm. And the girder of "De Vecht" is not as heavily reinforced, so deflections this high might not occur. This is discussed later.

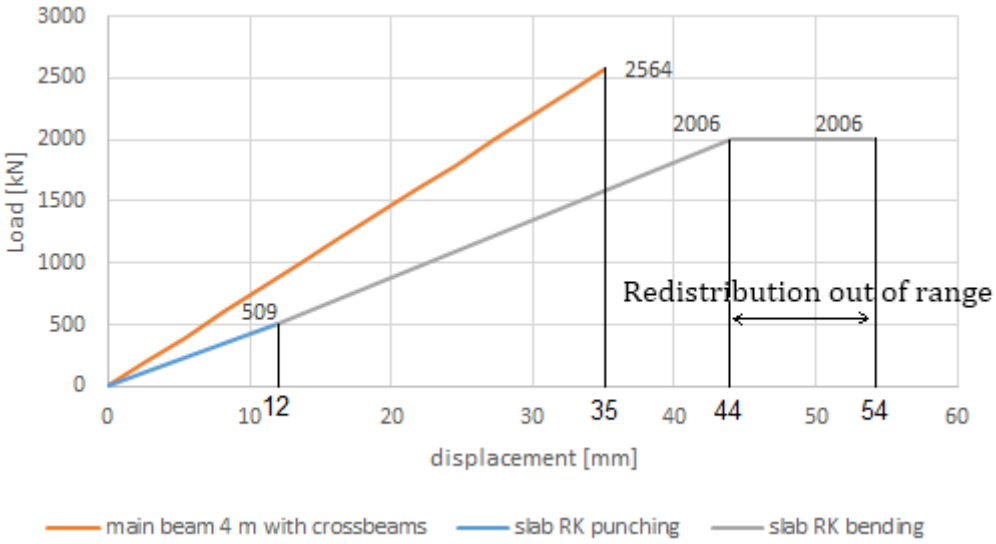


*Figure 220 bearing capacity and slab bending and punching capacity according to RK method*

**Prediction for the bridge load**

The results of all the methods are given in Table 56. It is assumed that only for the methods which calculate bending capacities redistribution is possible. In this case, for a linear situation (Figure 115), where the redistribution possibility limits the bearing capacity, the slab capacity, and ductility, governs the upper bound capacity of the bridge (Table 56).

*Table 56 predictions bearing capacity bridge test load at 4m*

| Method | Lower Bound Capacity [kN] | Upper Bound Capacity [kN] | Load to redistribute [kN] |
|---|---|---|---|
| **SCIA Punching** | 455 | - | N/A |
| **SCIA Bending** | 1830 | 2546 | 716 |
| **CAN Punching** | 467 | - | N/A |
| **UK Punching** | 635 | - | N/A |
| **UK Bending** | 900 | 1635 | 735 |
| **RK Punching** | 509 | - | N/A |
| **RK Bending** | - | 2546 | N/A |

### Activated span

Now the slab capacity is determined that is available for redistribution of the loads (Table 56). First, the activated span is determined. For SCIA bending, the activated span is 8600 mm (Figure 221). A maximal deflection of 35 mm is used (for the maximal load of 2564 kN after redistribution), and the critical deflection is 25 mm, at which maximum arching action of the slab is assumed (Figure 216).

For UK bending, the activated span is 10800 mm (Figure 222), which is more than the effective width, meaning extra capacity is available. But only the span activated outside of the range of the effective width can provide extra capacity for redistribution, since the effective width itself is responsible for the initial slab bending capacity and maximum arching action. A maximum deflection of 22.3 mm is used, and the critical deflection is 12.3 mm, at which maximum arching action of the slab, 558 kN, is assumed (derived from Figure 219).

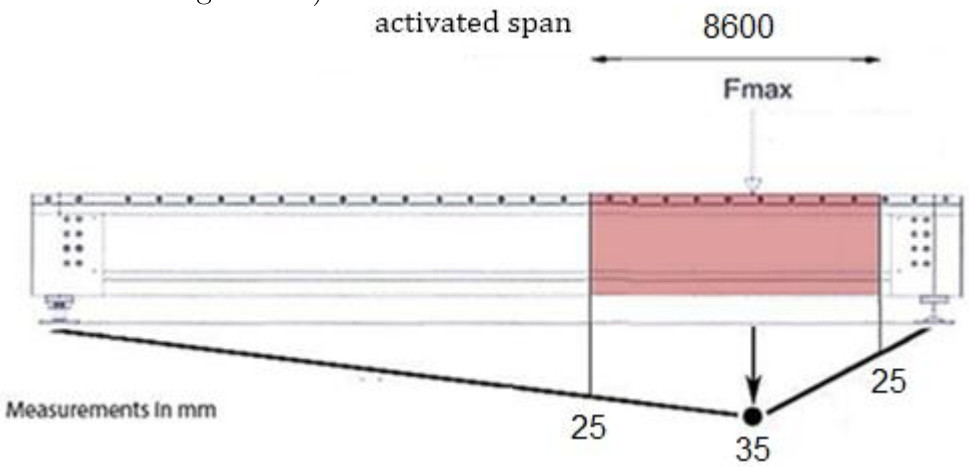


*Figure 221 activated span SCIA bending (not on scale) for the test load at 4 m from the end*

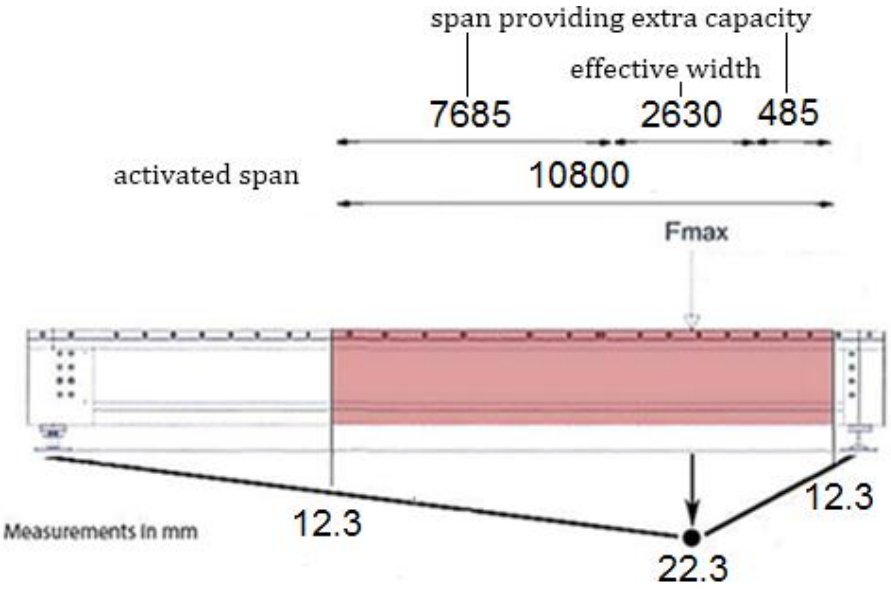


*Figure 222 activated span UK bending (not on scale) for the test load 4 m from the end*

**Total slab capacity**

Now the total slab capacity is determined. For UK bending:

The effective width (Figure 222) is smaller than the total activated span. So both parts on the right and left side of effective width can provide extra capacity:

$$\text{activated span for extra capacity: } L_{extra} = \text{activated span} - \text{effective width}$$
$$n = \frac{L_{extra}}{b_{eff}}$$
$$\text{total extra capacity} = n * \text{slab } \mathbf{bending} \text{ capacity}$$

$$10{,}8 - 2.63 = 8.17\ m$$
$$\frac{8.17}{2.63} = 3\ [-]$$
$$3 * 558 = \ 1675\ kN > 735 \text{ (Redistribution possible)}$$

The same effective width calculated in the RK method is used for the UK method (Figure 108). The same calculation is done for SCIA bending method as well (Table 57).

*Table 57 redistribution methods*

| Method | Activated span [m] | Total slab capacity [kN] | Extra Capacity for redistribution [kN] | Redistribution |
|---|---|---|---|---|
| **SCIA bending** | 8.6 | 1894 | 1894>716 | Possible |
| **UK bending** | 10.8 | 1675 | 1675>735 | Possible |
| **RK bending** | - | - | - | - |

### Nonlinear distribution

Earlier, a linear elastic distribution was assumed, which limited the maximal failure load that the bridge could take, after redistribution (Figure 115). Assuming a nonlinear situation, where the girder properties could change, the neighbor girders could take up more of the distributed load (Figure 223). And here, the slab could deflect more until its full plastic deflection plateau is developed, resulting in an overall higher bearing capacity and failure load of the bridge (Figure 224). For RK bending the slab is assumed to be able to deflect up till 53.5 mm, redistributing during that, and finally reaches the highest possible capacity, which is calculated. Figure 225 shows the newly activated span.

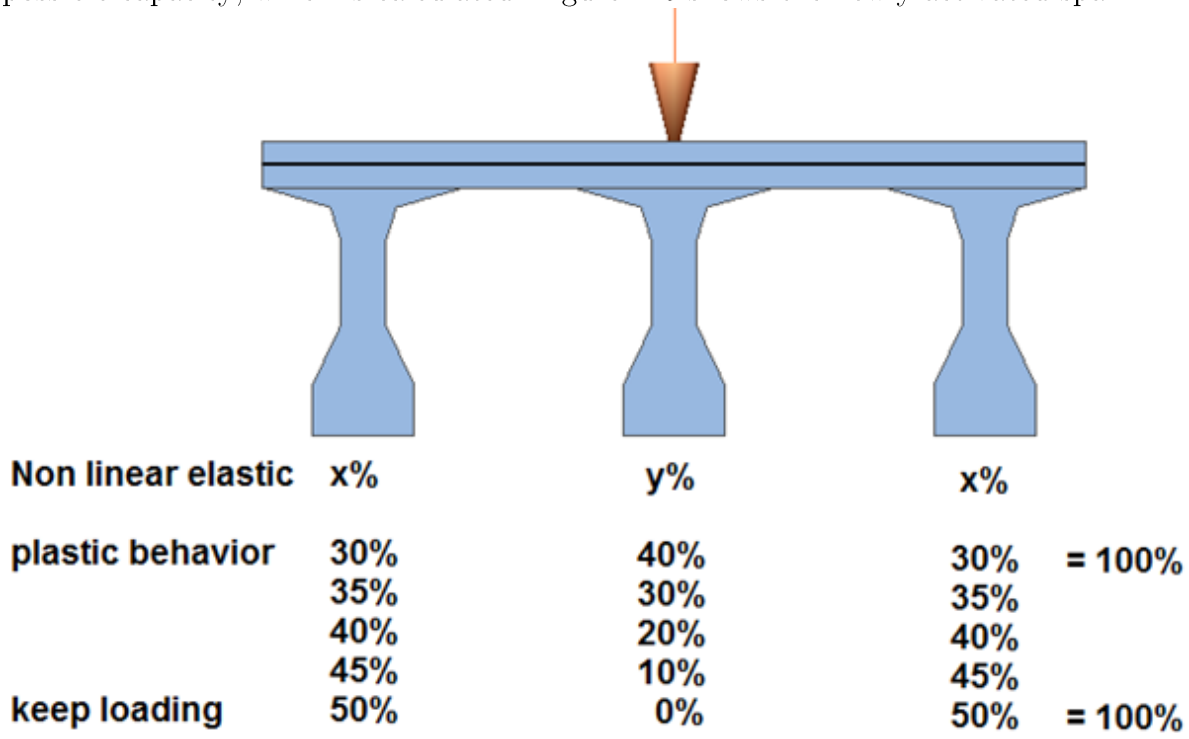


*Figure 223 nonlinear behavior*

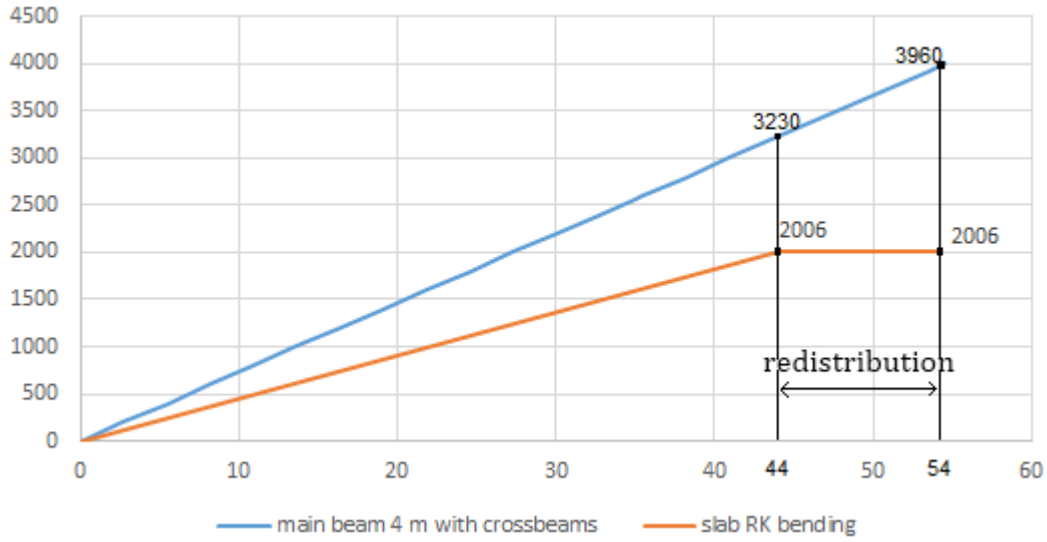


*Figure 224 nonlinear situation where slab is governing providing extra redistribution for RK bending*

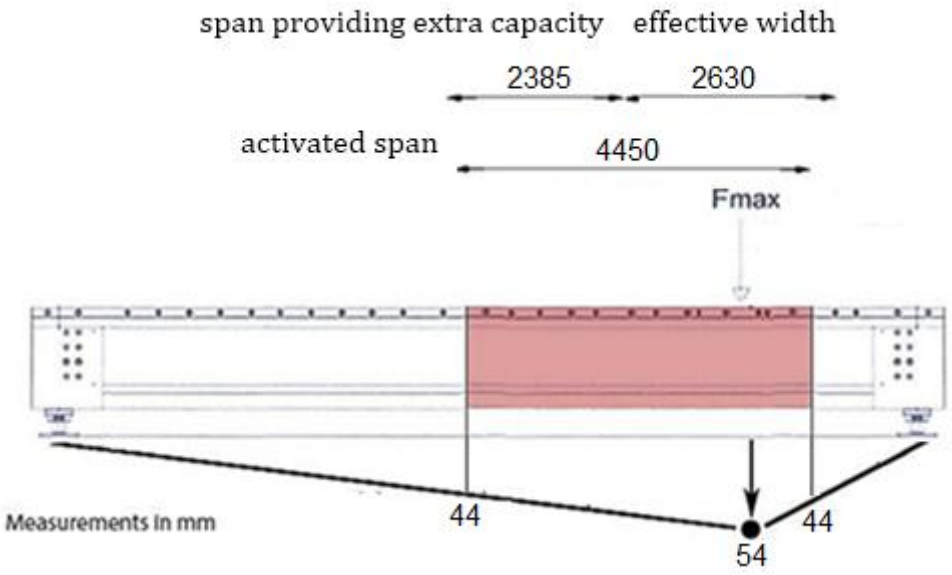


*Figure 225 activated span RK bending nonlinear (not on scale)*

**Total slab capacity**

For RK bending the calculation is as followed:

The effective width overlaps the right side of the activated span, so only the left side of the activated span can provide extra capacity (Figure 225)

$$3.7 - \frac{2.63}{2} = 2.385\ m$$

$$\frac{2.385}{2.96} = 0.9\ [-]$$

$$0.9 * 2006 = 1800\ kN > 730\ \text{(Redistribution possible)}$$

**Summary**

From the calculation for RK bending, in the nonlinear situation, it shows that for the assumed deflection plateau of 10 mm the load which needs to be redistributed is around 730 kN. Which means about 73 kN/mm needs be redistributed, this is useful to know when assuming other plateau sizes for other slabs.

It was shown that redistribution is possible. And Table 58 gives the new lower and upper bound capacity of the bridge, where RK bending gives the highest possible capacity of all the three considered methods.

A quick check with a linear load distribution to determine what the maximal load is for the single main girder gives, $3230 * 0.4 = 1290\ kN$ and $3960 * 0.4 = 1500$ kN. It is plausible that the main girder could be loaded up to this range of loads.

*Table 58 prediction bearing capacity with upper and lower bound limit nonlinear situation*

| Method | Lower bound capacity [kN] | Upper bound capacity [kN] |
|---|---|---|
| **RK bending** | 3230 | 3960 |

**Second test load: 2.25 m from the end**

The same calculations are done, but now the point load changes location (Figure 106). The same slab capacities are used, as they do not change with the change of point load location.

When the point load changes location, at 2.25 m from the end, closer to the supports, the numerical model behaves stiffer. Therefore it reaches a higher maximal bearing capacity of 5422 kN for the estimated ultimate deflection of 35 mm, compared to the test load at 4 m with. So, shifting the load from 4 to 2.25 m from the end, leads to almost double the capacity according to the numerical model. The reason why is probably because the load is placed closer to the end beams.

However, redistribution was only possible up till 2194 kN, which is governing as an upper limit value of the bridge load in this case.

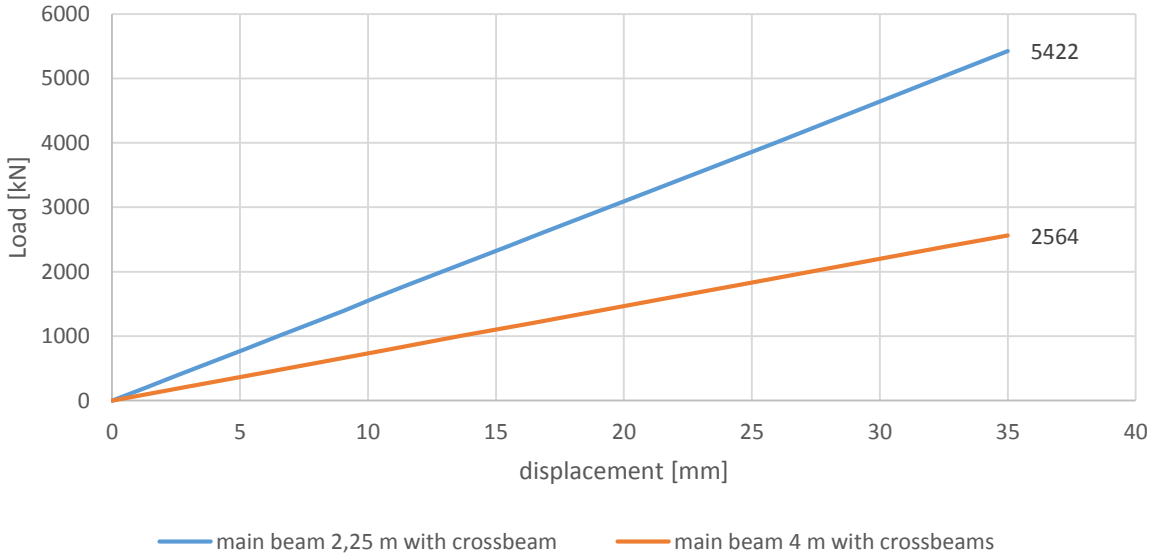


*Figure 226 comparing bearing capacity with the load at 2.25 and 4 m with crossbeams*

*Table 59 overview deflections test at 2.25 m from the end*

| Method | Deflection [mm] | |
|---|---|---|
| | **For Punching** | **For Bending** |
| **SCIA** | 10 | 25-35 |
| **Empirical (CAN)** | 6 | N/A |
| **Simplified (UK)** | 8.4 | 7.4-17.4 |
| **Rankin (FE)** | 6.7 | 26.4-36.4 |

**Deflections**

In Table 59 an overview of the deflections are shown. A plastic plateau of 10 mm is assumed again, since the slab properties have not changed, during which redistribution is possible (Figure 227). For punching, deflections below 10 mm were found, since the numerical model behaved stiffer, and this is still in the order of the estimated range for slabs failing in punching, according to the Taylor tests in Chapter 8.

**Redistribution**

The three methods, SCIA, UK, and RK Bending, for which redistribution is possible, are given with their respective slab capacities (Figure 227 and Figure 228). Here, it is shown that only for UK bending the maximal assumed load, 2194 kN (Table 54), falls within the range of the deflection plateau, the decisive period when redistribution can take place. Then the load which needs to be redistributed after the slab reaches its peak load: $2194 - 1170 = 1024\ kN$

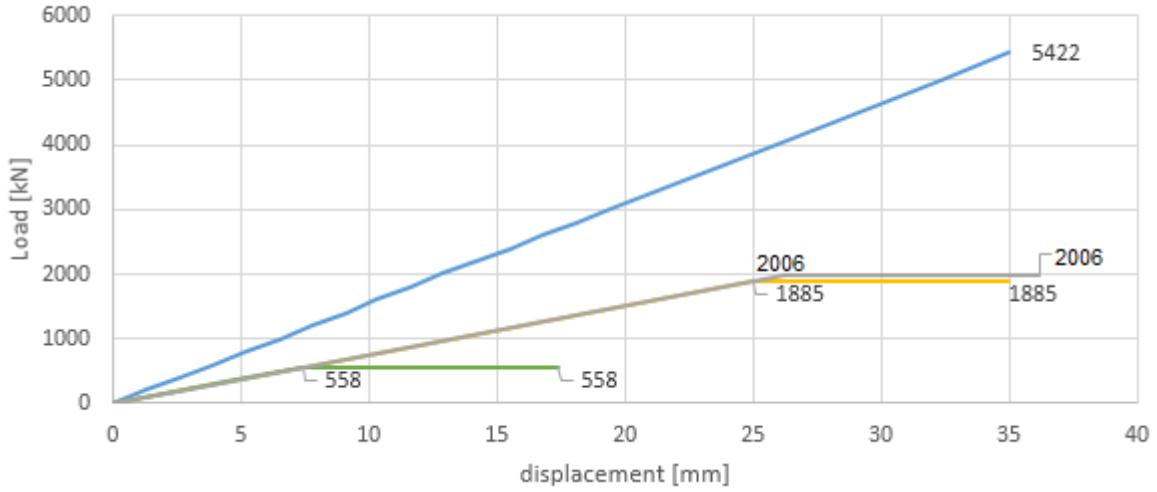


*Figure 227 bearing capacities and slab bending capacites with possible redistribution*

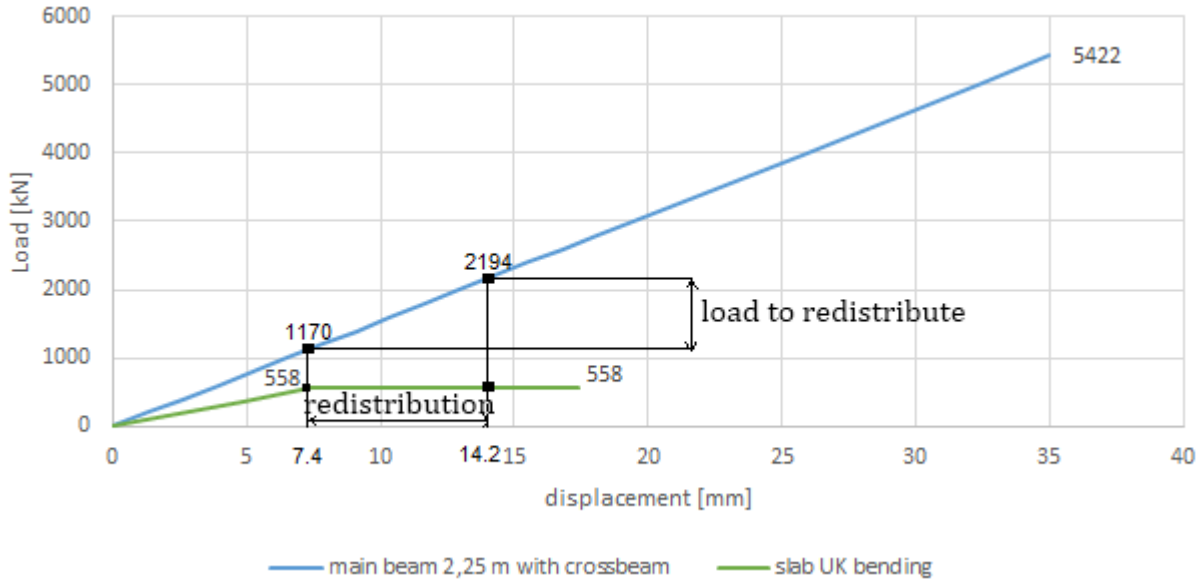


*Figure 228 slab bending capacity according to UK method with possible redistribution*

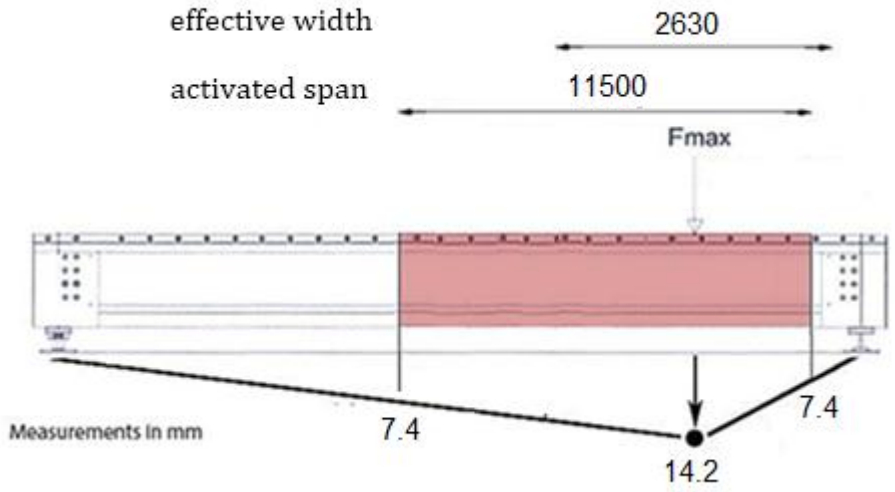


*Figure 229 activated span UK Bending*

### Activated span

The maximum deflection for the maximal assumed load, 2194 kN, is 14.2 mm (Figure 227 and Figure 229). The critical deflection is 7.4 mm (Table 59), since this is the instant at which the plastic plateau initiates and redistribution is possible.

### Total deck capacity

For UK bending the calculation is as followed:

The effective width overlaps the right side of the activated span, so extra capacity is provided only by the left side for redistribution of the loads (Figure 229).

$$11.5 - \frac{2.63}{2} = 10.185\ m$$

$$\frac{10.185}{2.63} = 3.8\ [-]$$

$$3.8 * 558 = 2160\ kN > 1024 \text{ (Redistribution possible)}$$

### Prediction capacity of the bridge

*Table 60 predictions bearing capacity bridge test load at 2.25 m*

| Method | Lower Bound Capacity [kN] | Upper Bound Capacity [kN] | Load to redistribute [kN] |
|---|---|---|---|
| **SCIA Bending** | - | 2194 | - |
| **SCIA Punching** | 754 | - | N/A |
| **CAN Punching** | 467 | - | N/A |
| **UK Bending** | 1170 | 2194 | 1024 |
| **UK Punching** | 635 | - | N/A |
| **RK Bending** | - | 2194 | - |
| **RK Punching** | 509 | - | N/A |

### Nonlinear situation

A nonlinear situation is possible again (like Figure 223). Figure 230 shows the load redistribution and Figure 231 shows the activated span for RK bending. The rest of the load redistribution in the load-displacement graphs and activated spans are given in Appendix G (Figure 232 and Figure 235).

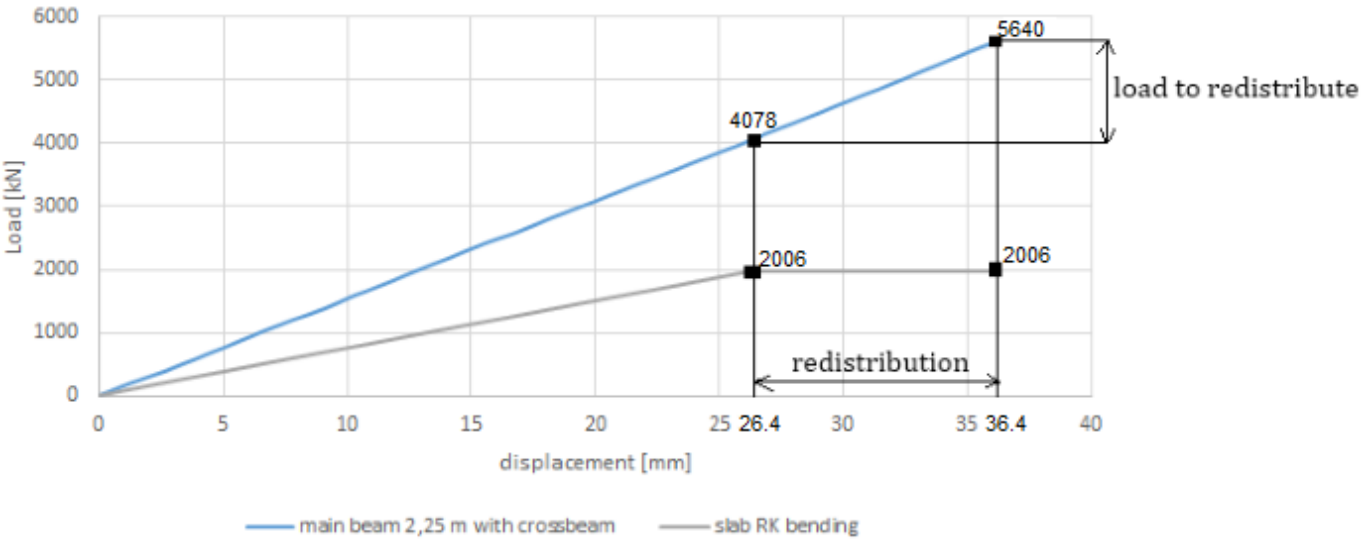


*Figure 230 full slab capacity nonlinear behavior for RK bending*

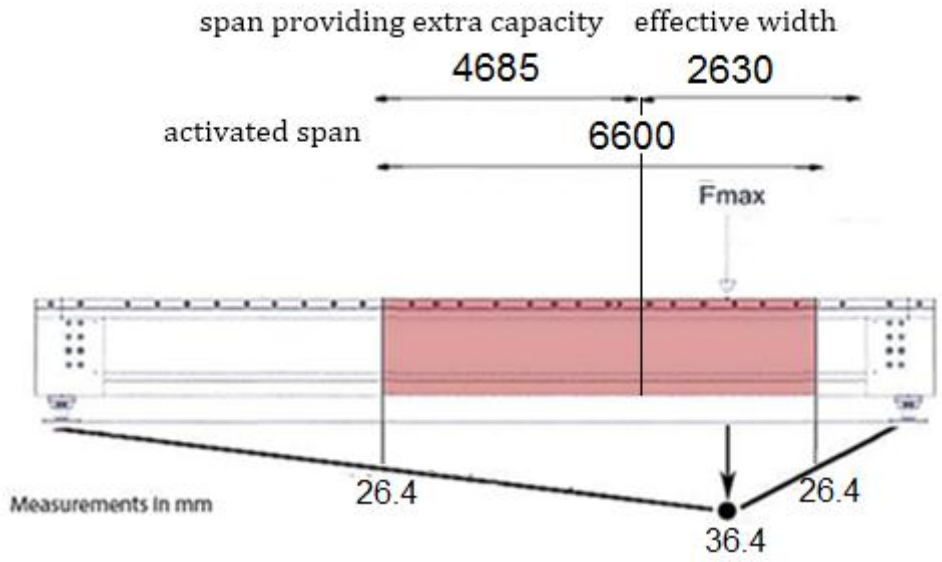


*Figure 231 activated span RK bending nonlinear (not on scale)*

**Total deck capacity**

For RK bending the calculation is as followed:

The effective width overlaps the right side of the activated span, so only the left side of the activated span can provide extra capacity (Figure 231):

$$6 - \frac{2.63}{2} = 4.685\ m$$
$$\frac{4.685}{2.63} = 1.8\ [-]$$
$$1.8 * 2006 = 3611\ kN > 1562\ \text{(Redistribution possible)}$$

The rest of the methods follow the same calculation process, and the results are given in (Table 61).

*Table 61 overview redistribution nonlinear situation*

| Method | Load to redistribute [kN] | Activated span [m] | Extra capacity for redistribution [kN] | Redistribution |
|---|---|---|---|---|
| **SCIA bending** | 1560 | 7.82 | 3720 > 1560 | Possible |
| **UK bending** | 1522 | 12.5 | 2373 > 1522 | Possible |
| **RK bending** | 1562 | 6.6 | 3611 > 1562 | Possible |

### Summary

Table 61 shows, for the assumed deflection plateau of 10 mm, the load which is redistributed, to be around 1550 kN, averaging the load for the three methods. Which means about 155 kN/mm needs to be redistributed, this is useful to know when assuming other plateau sizes for other slabs. Table 61 shows redistribution is possible for all three methods.

Table 62 gives the new range of lower and upper bound capacity of the bridge for the three methods. UK bending gives the most conservative capacity, and RK bending the maximum. Figure 236 of Appendix G summarizes the method used in this chapter.

*Table 62 prediction bearing capacity with upper and lower bound limit nonlinear situation*

| Method | Lower bound capacity [kN] | Upper bound capacity [kN] |
|---|---|---|
| **SCIA bending** | 3862 | 5422 |
| **UK bending** | 1170 | 2692 |
| **RK bending** | 4078 | 5640 |

### Nonlinear load distributions graphs for test load at 2.25 m on 'De Vecht'

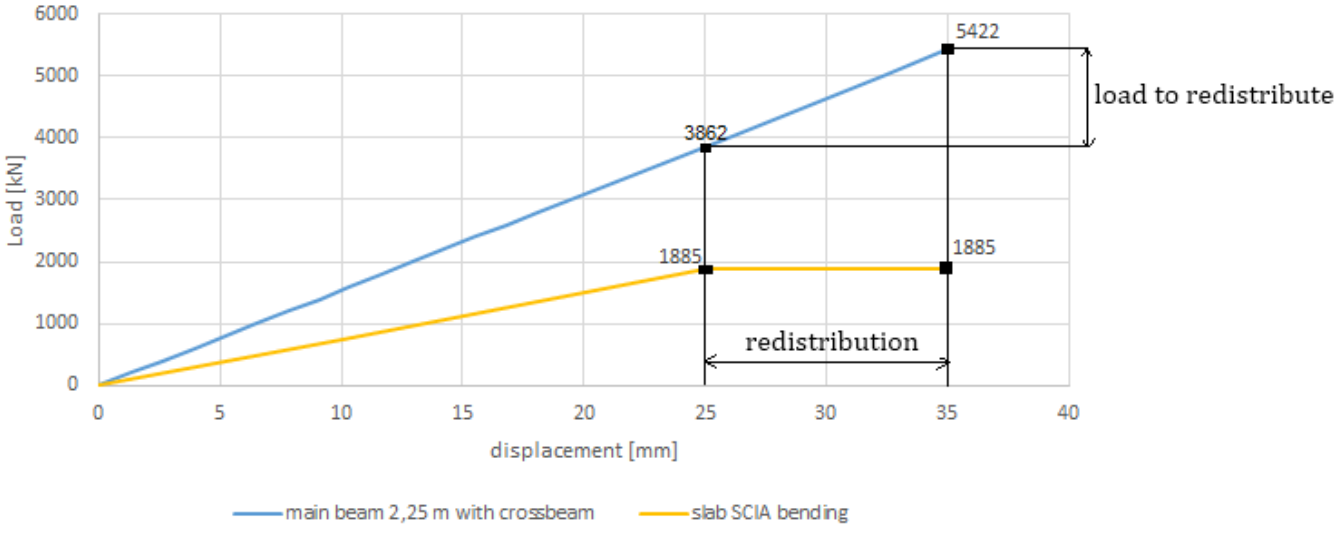


*Figure 232 full slab capacity nonlinear behavior for SCIA bending*

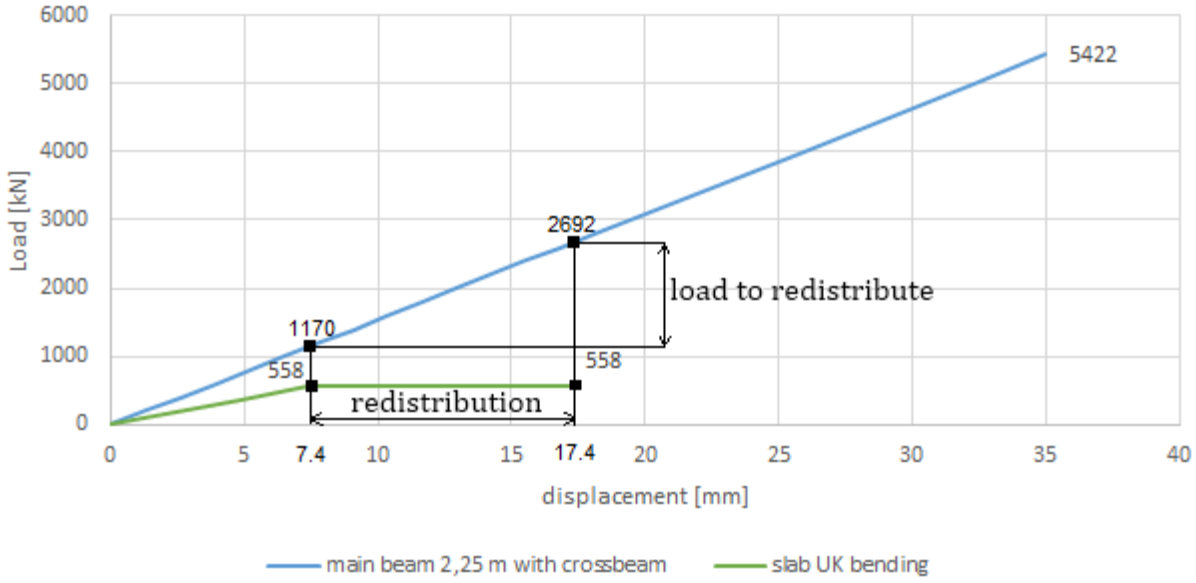


*Figure 233 full slab capacity nonlinear behavior for UK bending*

## Activated spans

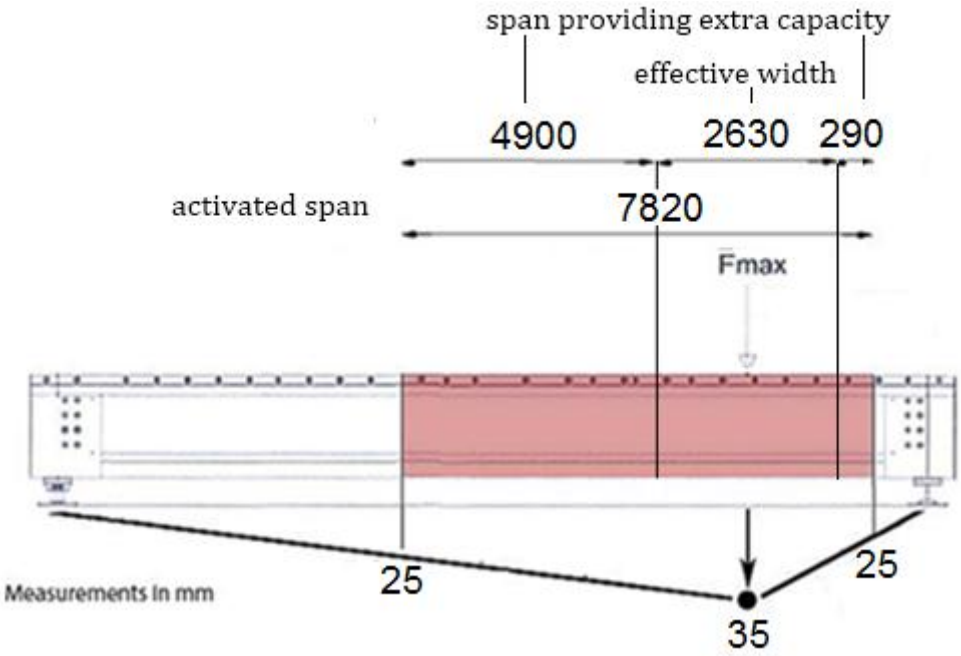


*Figure 234 activated span SCIA bending nonlinear (not on scale)*

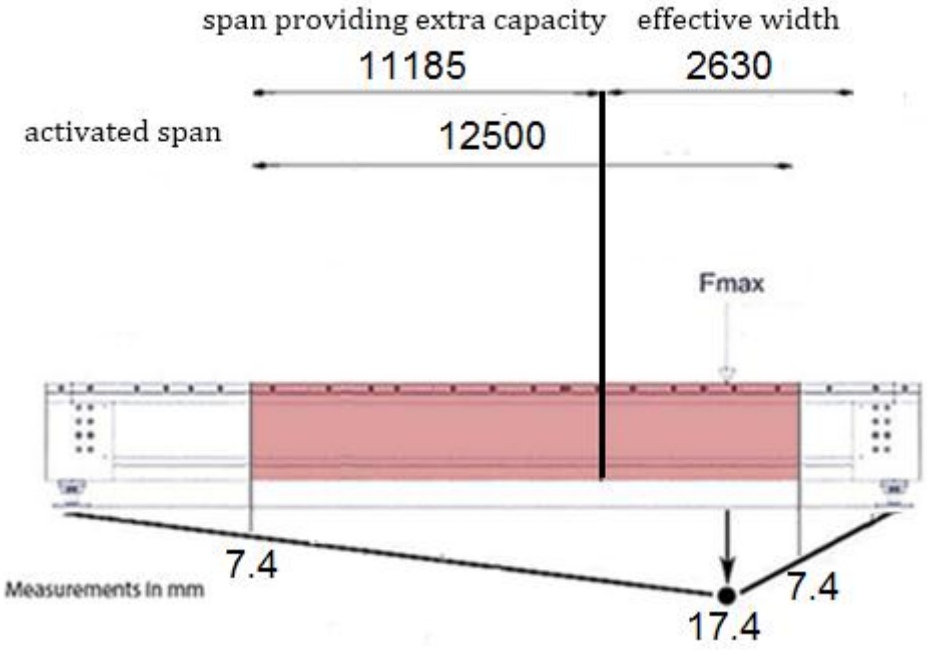


*Figure 235 activated span UK bending nonlinear (not on scale)*

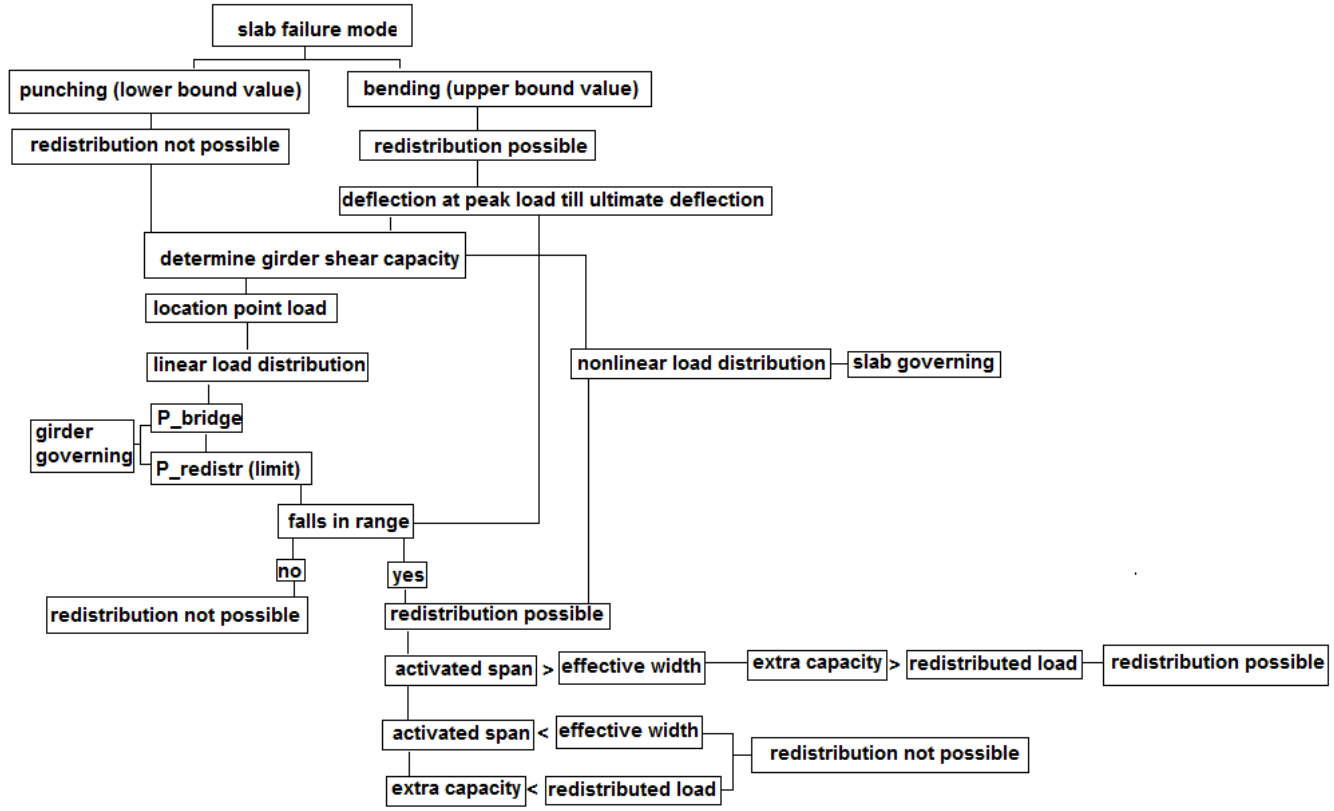


*Figure 236 flowchart calculative method Chapter 9*

# Appendix H

## Bridge system test results

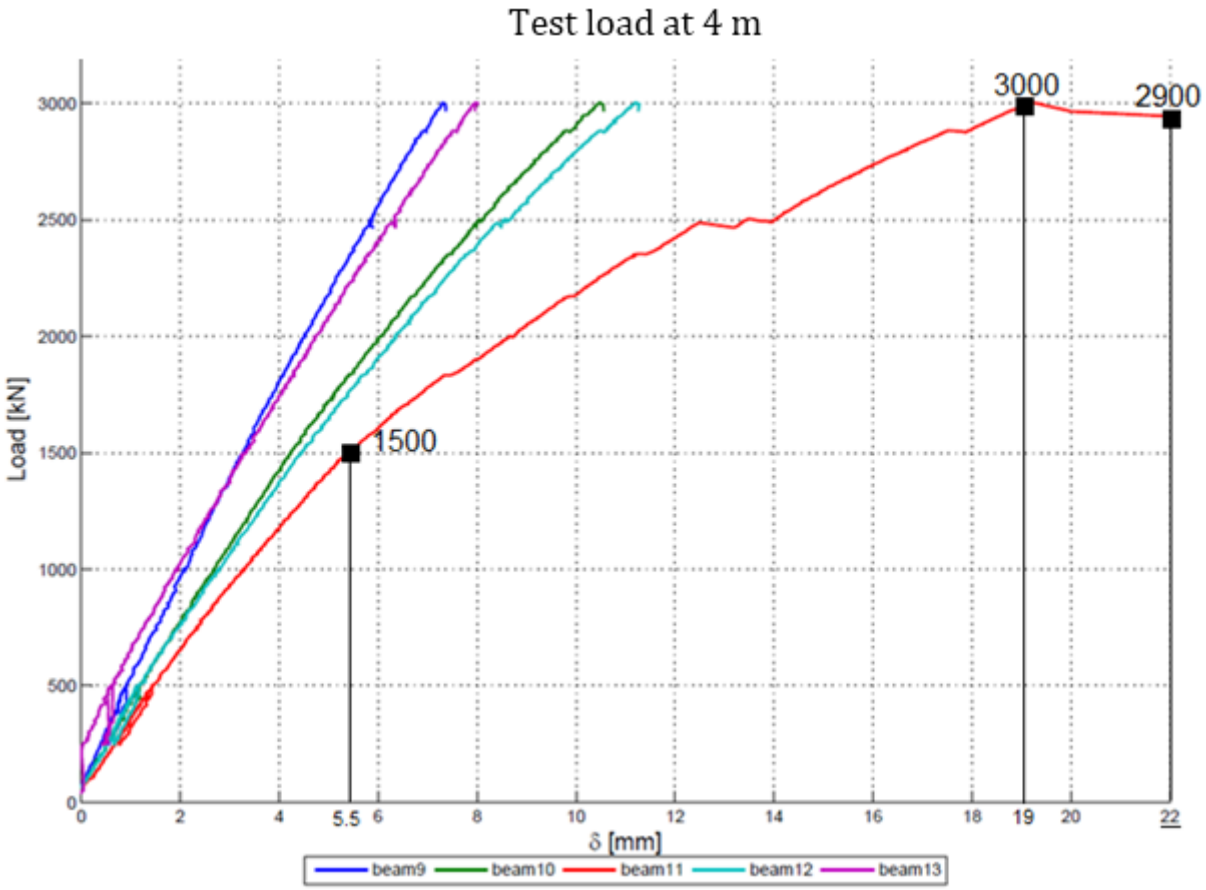


*Figure 237 load displacement graph for the load at 4 m*

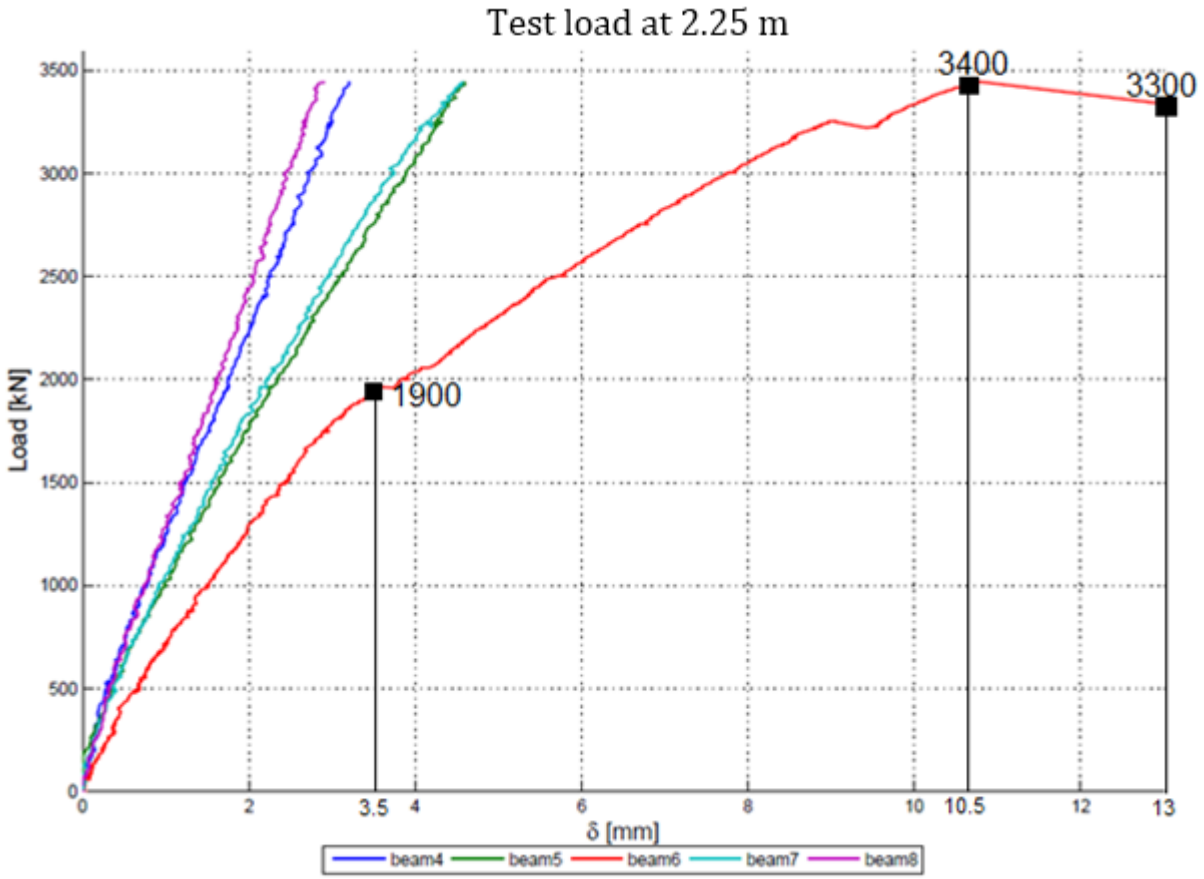


*Figure 238 load displacement graph for the load at 2.25 m*

## Single girder test results

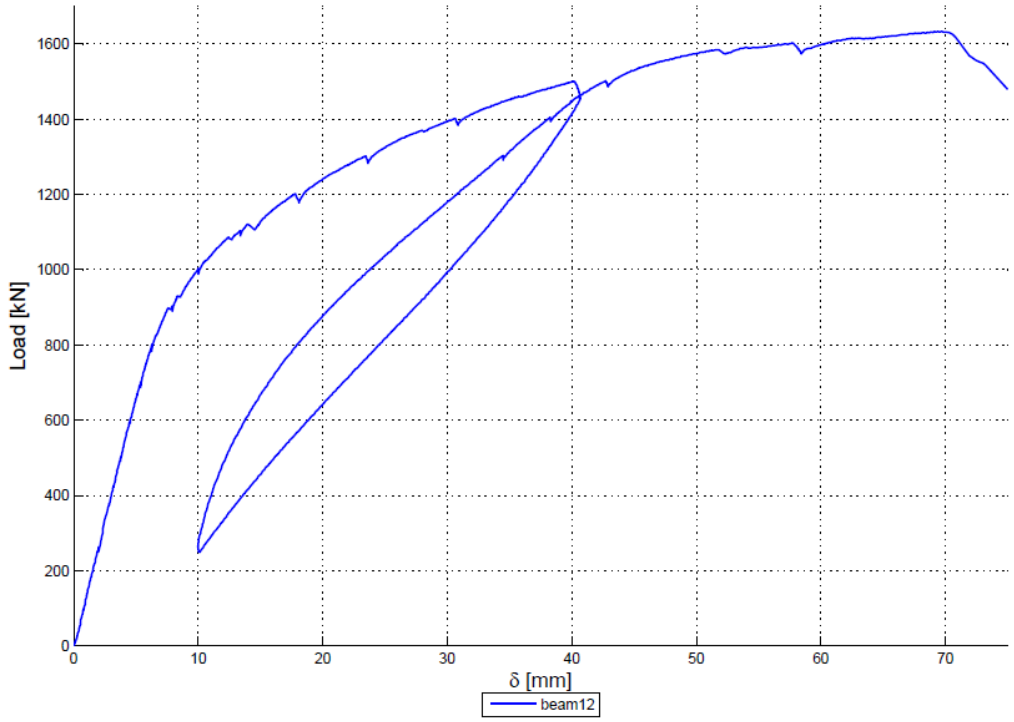


*Figure 239 load displacement test single girder with the load at 2.25 m (1)*

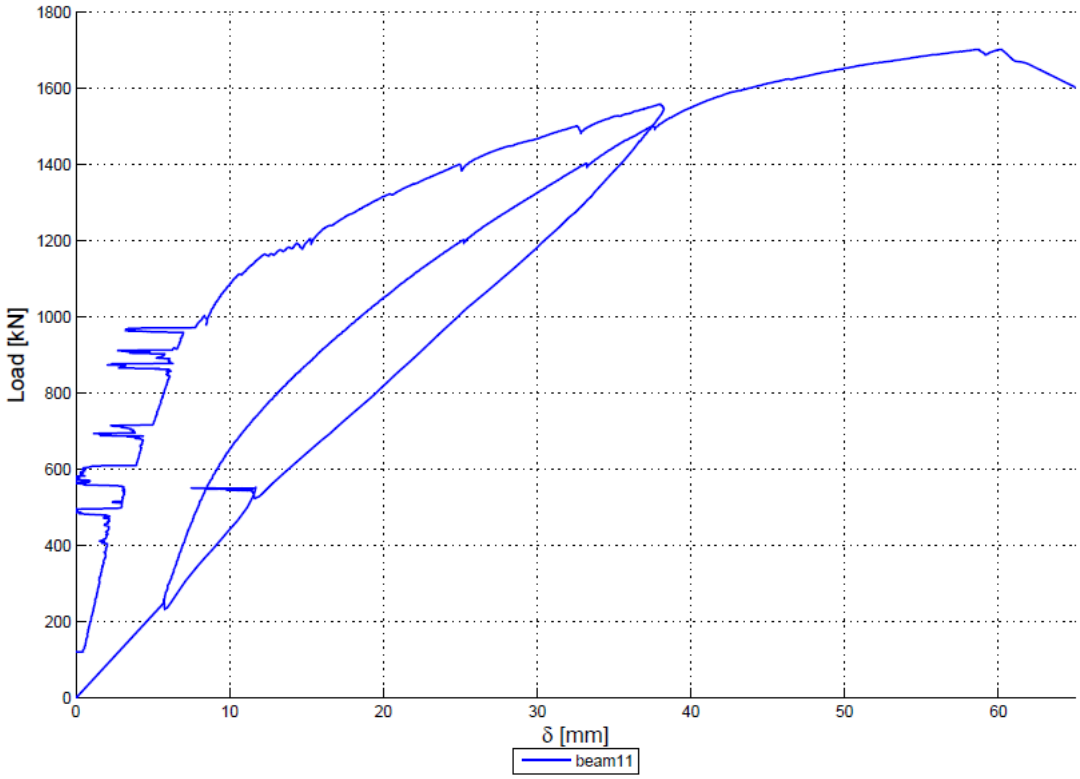


*Figure 240 load displacement test single girder with the load at 2.25 m (2)*

## Comparison test results with numerical models with multiple girders

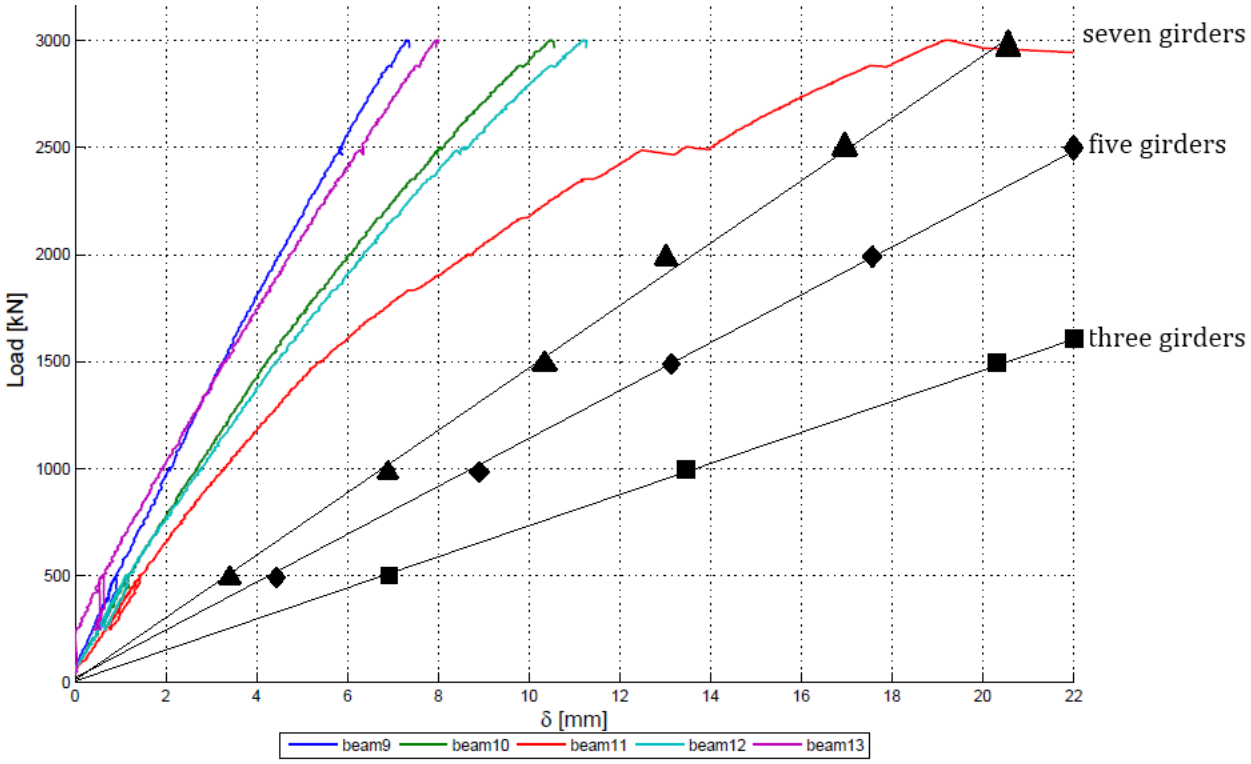


*Figure 241 comparison load-displacement behavior of 'De Vecht' with numerical model for three, five, and seven girders. The load is 4 m from the end.*

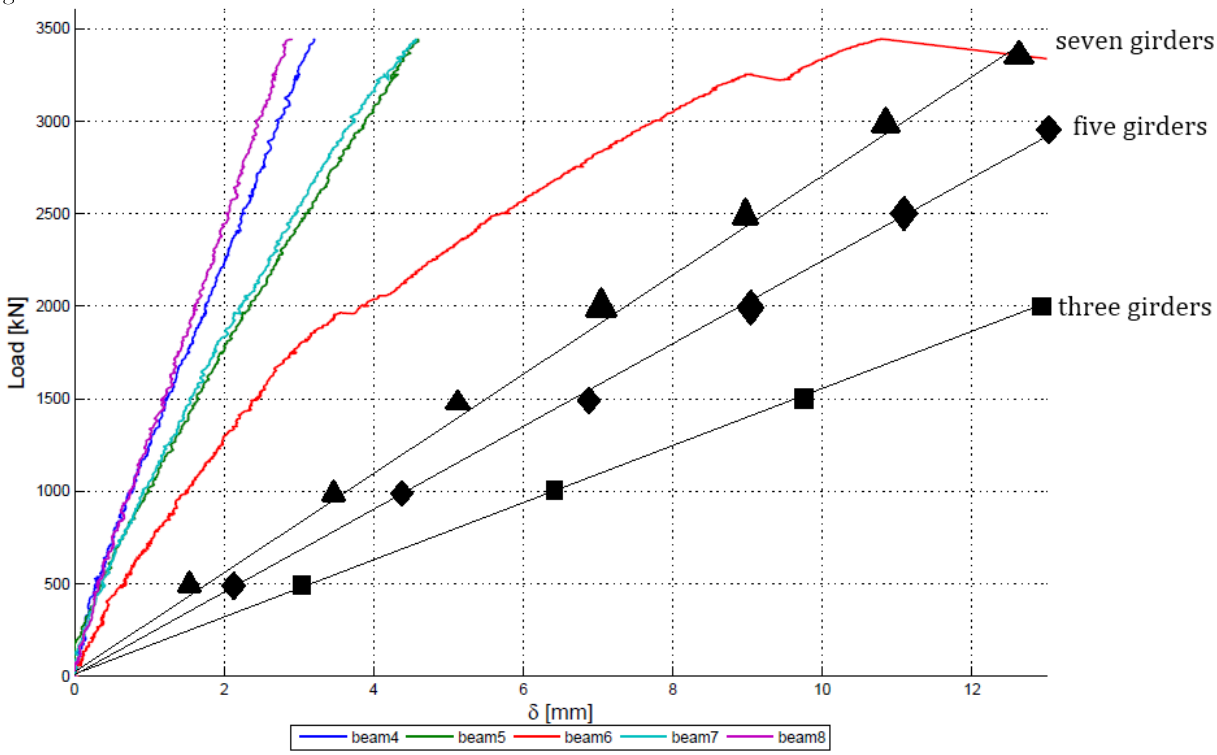


*Figure 242 comparison load-displacement behavior of 'De Vecht' with numerical model for three, five, and seven girders. The load is 2.25 m from the end.*

**Information of Numerical Model De Vecht**

**General information plate**

Concrete class: C35/45.
Concrete density: 2500 kg/$m^3$.
E-modulus: 34100 MPa.
G-modulus: 14000 MPa.
Poisson ratio: 0.2 [-]
FEM-model: orthotropic plate.
Linear numerical model.
Thickness: 180 mm.
Spring supports.
Size 2D-plate element: 0.25 m.
Plate theory: Mindlin-reissner.
Type solver: direct.

**General information girder**

Concrete class: C55/67
Concrete density: 2500 kg/$m^3$.
E-modulus: 38400 MPa.
G-modulus: 15917 MPa.
Poisson ratio: 0.2 [-]
A: 0.27 $m^2$.
$I_y$: 2.8*$10^{-2}$ $m^4$.
$W_{ely}$: 5.5*$10^{-2}$ $m^3$.

**General information crossbeam**

Concrete class: C35/45
Concrete density: 2500 kg/$m^3$.
E-modulus: 34100 MPa.
G-modulus: 14000 MPa.
Poisson ratio: 0.2 [-]
Cross section: 820*400 mm.
A: 0.328 $m^2$.
$I_y$: 1.8*$10^{-2}$ $m^4$.
$W_{ely}$: 4.4*$10^{-2}$ $m^3$.

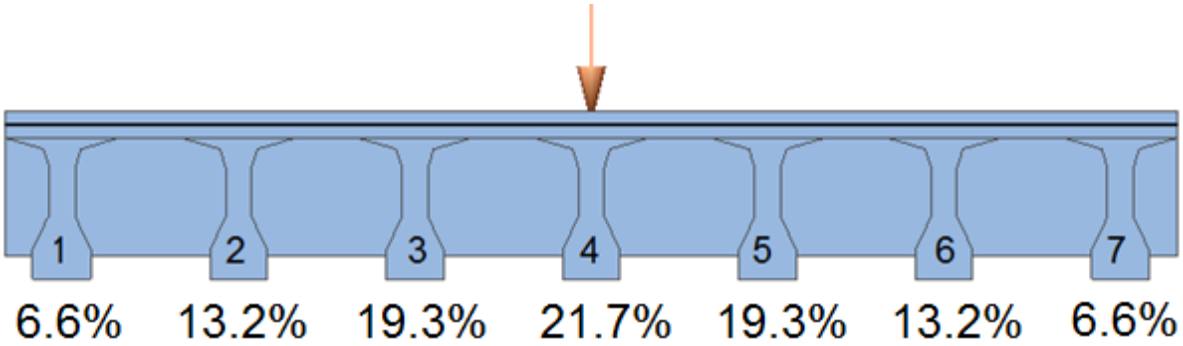


*Figure 243 load distribution determined with the seven-girder model of 'De Vecht' with the load at 2.25 m*

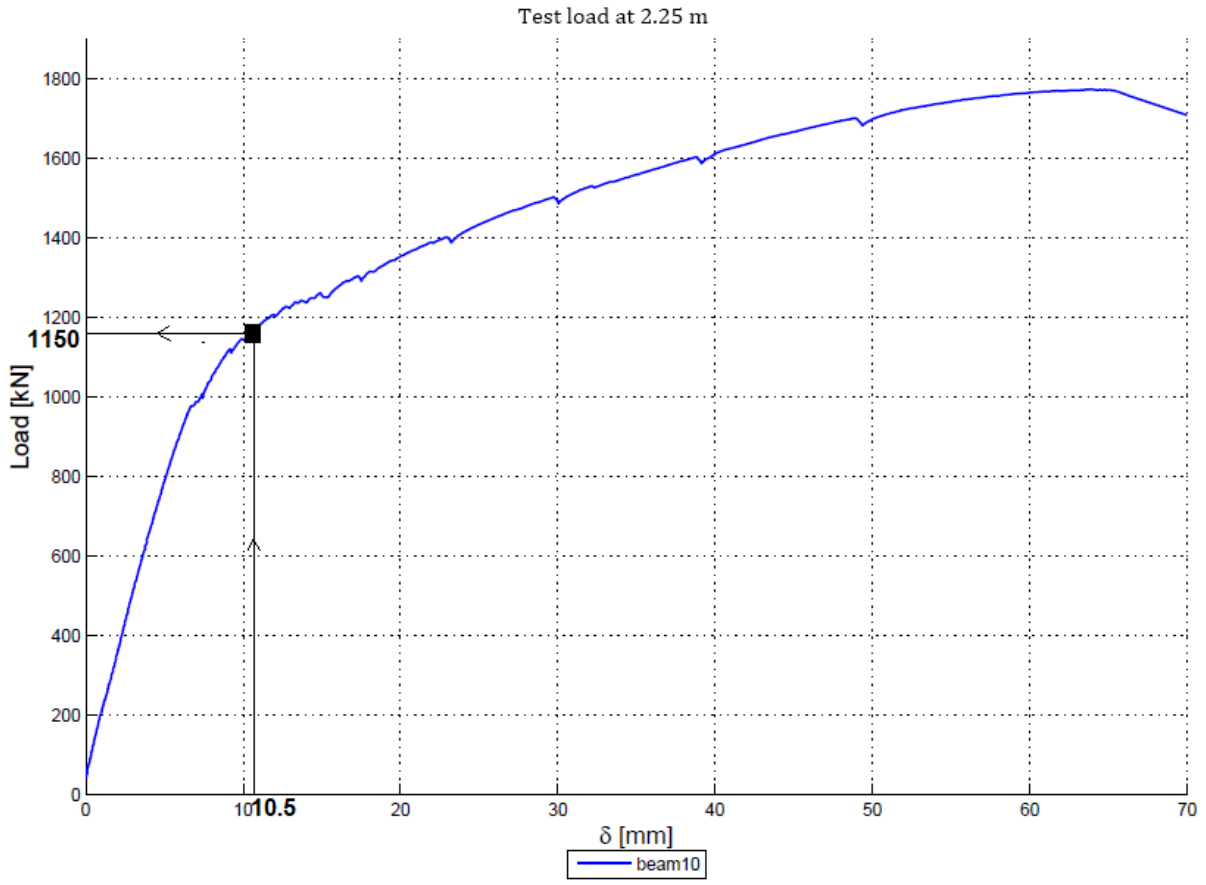


*Figure 244 determining at what load the ultimate deflection of the bridge system of the main beam is reached, for the load at 2.25m*

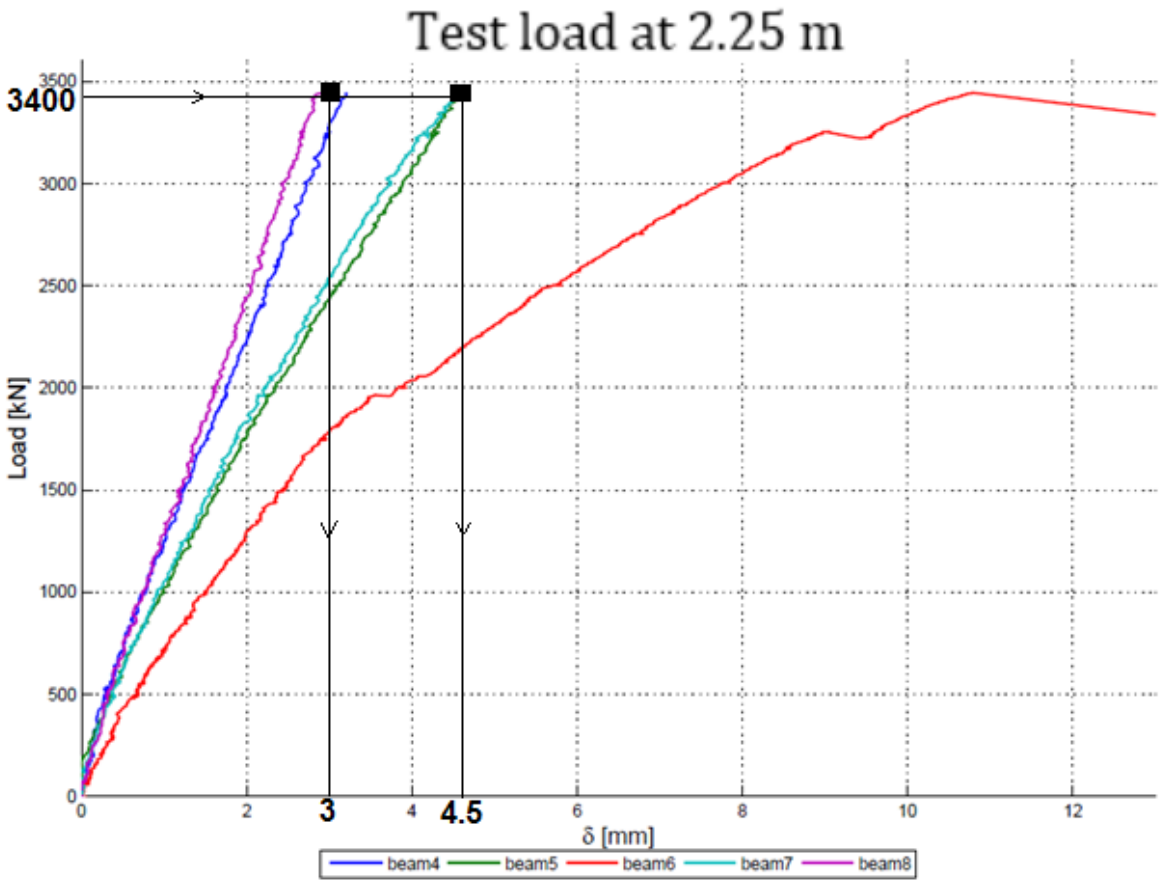


*Figure 245 determining ultimate deflections of the neighbor beams, witht the load at 2.25 m*

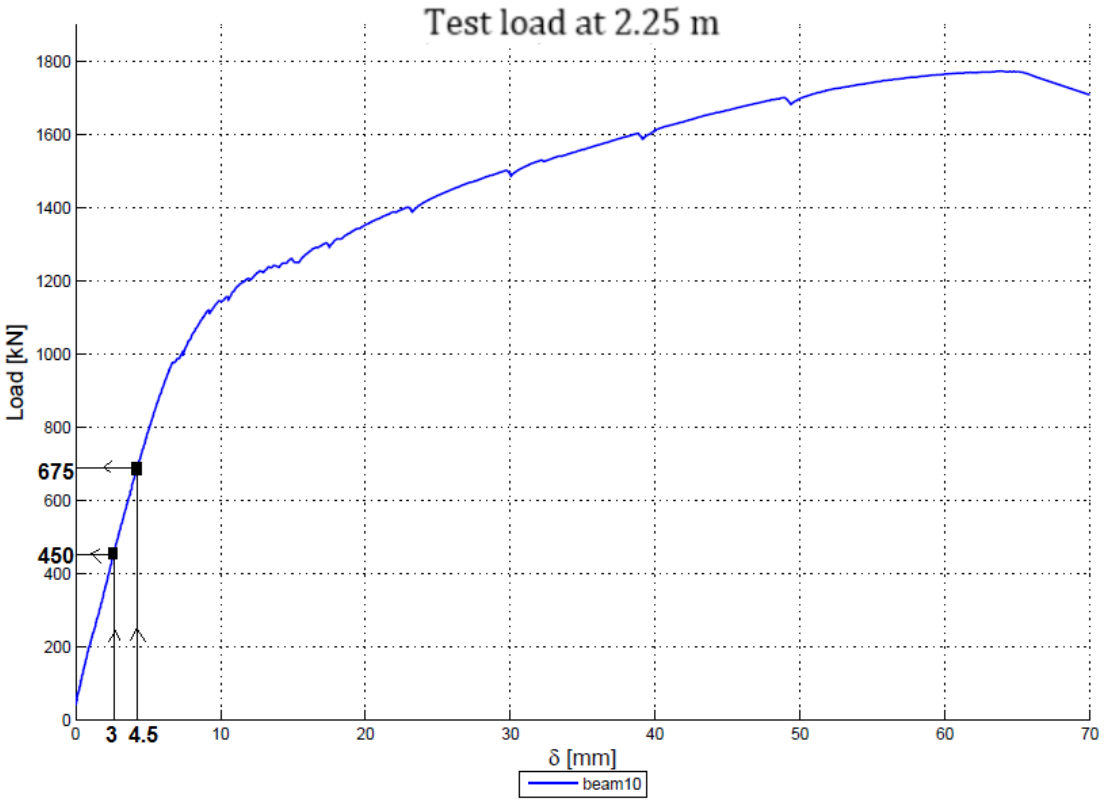


*Figure 246 determining at what load the ultimate deflection of neighbor beam is reached, for the load at 2.25m*

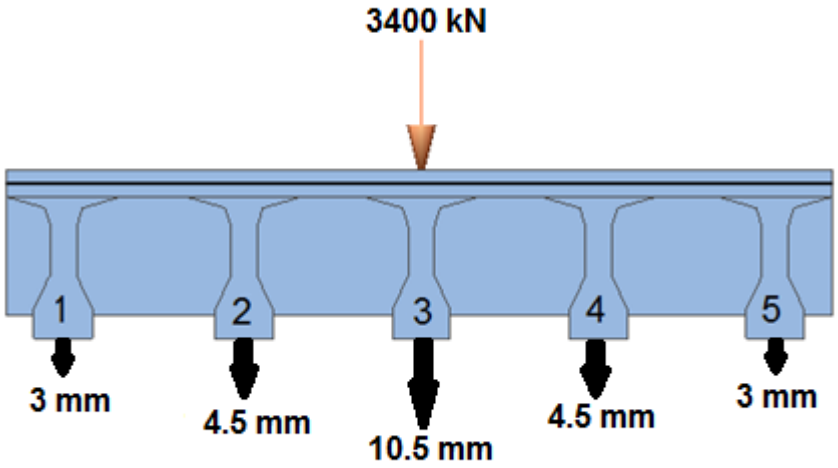


*Figure 247 displacements of the main beam and neighbor beams at the peak load 3400 kN, for the load placed at 2.25m*

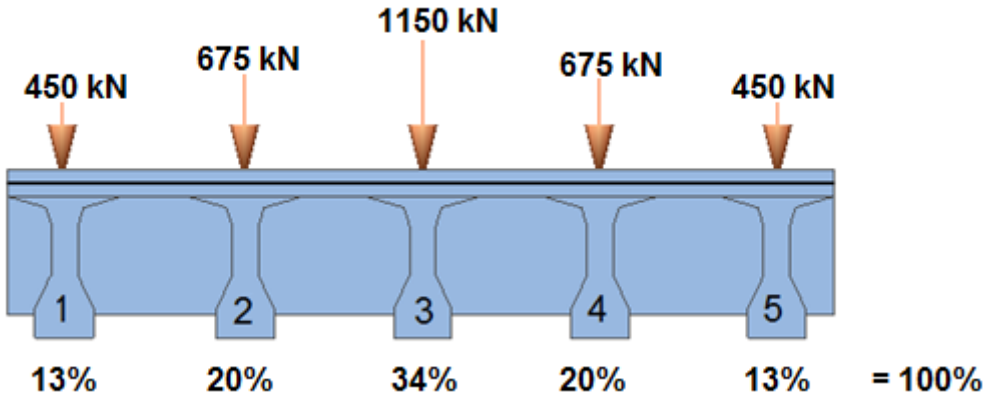


*Figure 248 load distribution determined with the tests results, over five girders with the girder load on each beam, for the load at 2.25 m*

### Required slab capacity

### Comparison actual and predicted slab capacity

Now the deck capacity, with compressive membrane action, that should have been activated, is estimated. In line with hypothesis one from Chapter 5, this is done by subtracting the girder capacity, obtained from the single girder test results (Table 20), from the total bearing capacities, obtained from the test results on the bridge system (Table 17). An initial estimation, option 1, of the required deck capacities is given in (Table 63).

For the load at 4 m, 2000 kN is needed, while for the load at 2.25 m, 1700 kN is needed. From all the slab capacities determined in Chapter 11, the RK bending method with a slab bending capacity of 2006 kN meets the requirement (Table 63 and Table 64). Moreover, the method of Rankin was shown in the Taylor tests to be an underestimate of the actual strength, with a margin of error of about 16%, leading to a strength of $1.16 * 2006 = 2327\ kN$. And the effect of prestressing is not taken into account into the calculation of the slab capacity. Also the design concrete strength was used instead of the actual one, taking into account hydration.

*Table 63 results bridge bearing capacity, girder capacity, and required deck capacity*

| load location [m] | total load [kN] | total girder load [kN] | required total slab capacity [kN] | calculated slab bending capacity RK [kN] |
|---|---|---|---|---|
| 2.25 | 3400 | 1700 | 1700 | 2006 |
| 4 | 3000 | 1000 | 2000 | 2006 |

*Table 64 comparison actual and predicted deck capacity*

| load location [m] | required total slab capacity [kN] | calculated slab bending capacity [kN] | | Margin of error [%] |
|---|---|---|---|---|
| 2.25 | 1700 | RK | 2006 | 18% |
| | | UK | 558 | 67% |
| | | SCIA | 1136 | 33% |
| 4 | 2000 | RK | 2006 | 0.3% |
| | | UK | 558 | 72% |
| | | SCIA | 1136 | 43% |

The calculated slab bending capacities generally are a safe but conservative underestimate of the reality, and with the RK bending having the smallest margin of error. The capacity determined with the SCIA numerical model and the estimated deflections, derived from the trendlines from the Taylor tests, also shows promise. If more data was available for more trendlines with the proper slenderness ratio, and the actual concrete strength was known, then the slab capacity could be determined again with the numerical model, probably with a lower margin of error.

**Option 2**

Aside from option 1, a nuanced calculation shows that the deck requires a capacity of $3400 - 1150 = 2250\ kN$ or $3000 - 625 = 2375\ kN$, for the load at 2.25 or 4 m (Table 65). The percentual difference between option 1 (Figure 249) and 2 (Figure 250) is given too. The calculation needs to be redone with the actual concrete strength to see if the required slab capacities are reached.

So there are two options to calculate the required slab capacity. Option 1 subtracts the girder load from the total load, leaving the required slab capacity. And option 2 uses the ultimate deflections determined from the load-displacement of the bridge system, and then finds the girder capacity at which these deflections are reached, using the load displacement graph of the single girder (Figure 121), and this girder capacity is then subtracted from the total load. Or options 1 and 2 could be combined, use option 1, but compensate for the percentual difference. For example: $\frac{1700}{(100-24.4)} * 100 = 2250\ kN$.

*Table 65 required deck capacities options 1 and 2*

| Load location [m] | Total load [kN] | Girder load [kN] | Required deck capacity | | |
|---|---|---|---|---|---|
| | | | Option 2 [kN] | Option 1 [kN] | Difference [%] |
| 2.25 | 3400 | 1150 | 2250 | 1700 | 24.4 |
| 4 | 3000 | 625 | 2375 | 2000 | 15 |

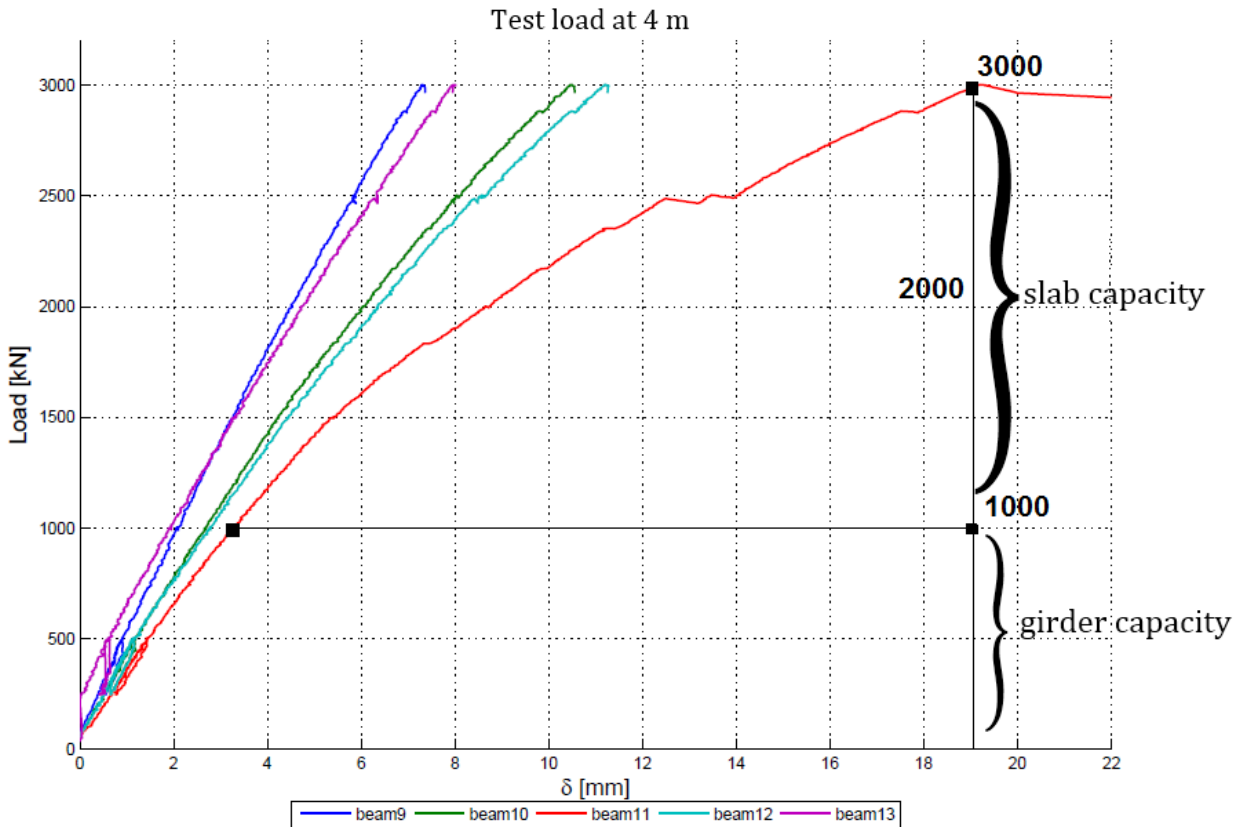


*Figure 249 determining slab capacity with total capacity and girder capacity, option 1, based on the first hypothesis*

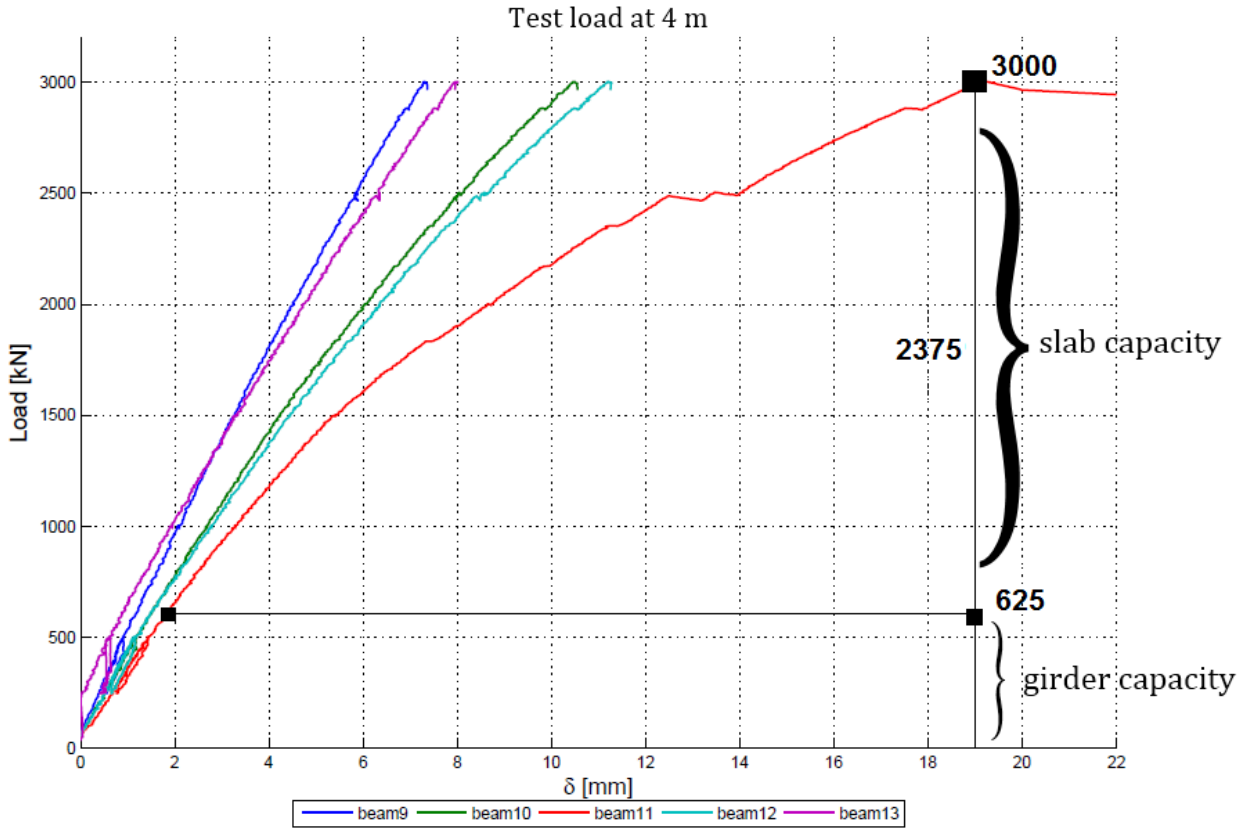


*Figure 250 determining slab capacity with total capacity and girder capacity, option 2, based on the test results of the bridge system and single girder*

**Critical deflection and deflection range**

Option 2 implies two other conclusions. First, the critical condition, to use membrane action, would have been met in the linear loading phase of the bridge system, before 1500 kN (Figure 237 and Table 17). Since only after this instant, membrane action is allowed to be summated with the girder capacity. The load, 625 kN, is reached around 2 mm (Figure 250). It is hard to say if the girder deflection at this point exceeds the deflection at midspan of the slab, which is the critical deflection condition in order for membrane action to be taken account, since there is no actual data for the slab's deflection, and modelling gives the same inaccuracies as discussed before.

Second, the slab is assumed to redistribute the loads, meaning it does not fail and keeps deflecting, starting at 2 mm, and the slab keeps contributing its capacity combined with the individual main beam capacity to form the total load. This happens up till 22 mm, when failure is reached.

Since the load distribution is known (Figure 125), this gives the load-displacement graph of the single girder (Figure 251). And if the girder load is known during the whole loading process, then by subtracting the total load with the girder load, the slab's load-displacement graph is also known (Table 66 and Figure 251).

The same is also done in Appendix H, for the neighbor beams for the load at 4 m (Figure 252, Table 67 and Table 68), and for the load at 2.25 m (Figure 253 and Figure 254, and Table 69 till Table 71).

Overall, the load-displacement behavior of the single girder, and the slab is shown to be non-linear. Since these two key elements, slab and girder, behave non-linear, it is wise to model these with a FEM model capable of non-linearity for future bridge situations.

*Table 66 determining the girder load, with use of the total load on the bridge system and the load distribution, and then subtracting the girder load from the total load, giving the slab load*

| Deflection of bridge system [mm] | Total load [kN] | Girder load (20.8% of total) [kN] | Slab load [kN] |
|---|---|---|---|
| **2** | 625 | 130 | 495 |
| **4** | 1200 | 250 | 950 |
| **6** | 1700 | 354 | 1346 |
| **8** | 1900 | 395 | 1505 |
| **10** | 2200 | 458 | 1742 |
| **12** | 2400 | 500 | 1900 |
| **14** | 2500 | 520 | 1980 |
| **16** | 2700 | 562 | 2138 |
| **18** | 2800 | 582 | 2218 |
| **19** | **3000** | **625** | **2375** |
| **22** | 2900 | 603 | 2297 |

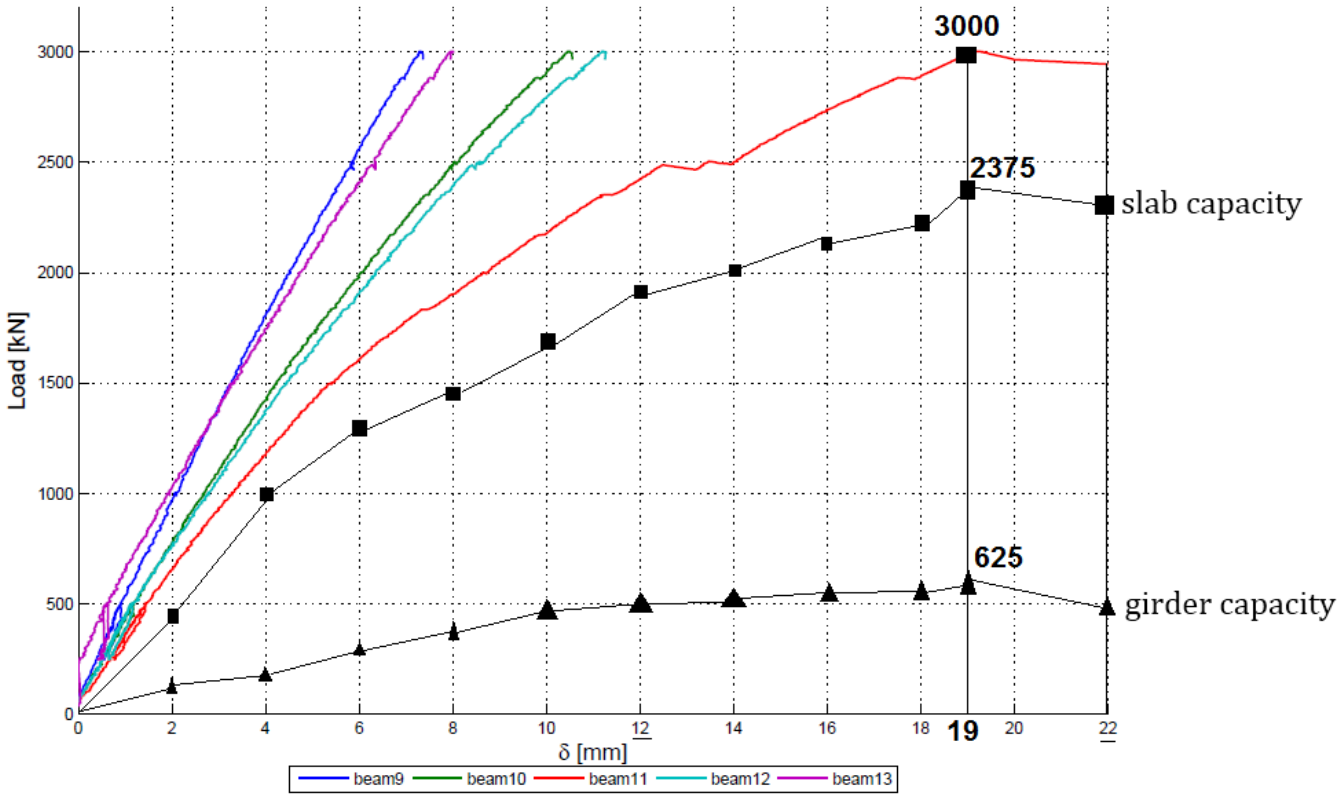


*Figure 251 girder and slab capacity determined with use of the load distribution*

**Important notes on option 2**

The slab is determined to carry 2375 kN. And RK slab bending capacity was between 2006-2327 kN. This two capacities are in the same order, so it is possible that the slab might carry this load.

However, the slab redistributest the load to the neighbor beams. And these beams do not have the capacity to carry this high load. In a linear approach, the neighbor beams are assumed to have same capacity as the main beam, and they will not carry more than the main beam.

*Table 67 determining the girder load for the neighbor beam 10,12, with use of the total load on the bridge system and the load distribution, and then subtracting the girder load from the total load, giving the slab load*

| Deflection of bridge system [mm] | Total load [kN] | Girder load (15.8% of total) [kN] | Slab load [kN] |
|---|---|---|---|
| 2 | 750 | 119 | 631 |
| 4 | 1400 | 221 | 1179 |
| 6 | 1900 | 300 | 1600 |
| 8 | 2400 | 380 | 2020 |
| 10.5 | 3000 | 475 | 2525 |

*Table 68 determining the girder load for the neighbor beam 11,13, with use of the total load on the bridge system and the load distribution, and then subtracting the girder load from the total load, giving the slab load*

| Deflection of bridge system [mm] | Total load [kN] | Girder load (11.7% of total) [kN] | Slab load [kN] |
|---|---|---|---|
| 2 | 1000 | 117 | 883 |
| 4 | 1750 | 205 | 1545 |
| 6 | 2500 | 293 | 2207 |
| 7.5 | 3000 | 350 | 2650 |

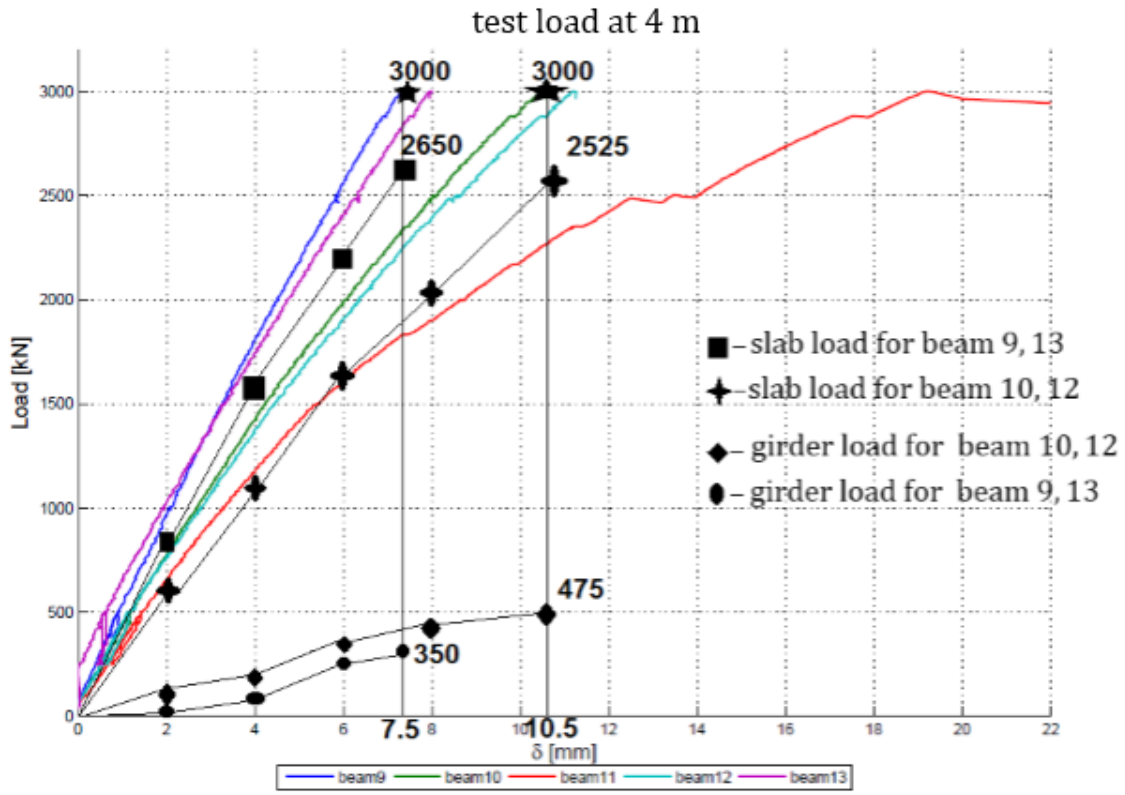


*Figure 252 girder and slab capacity determined for the neighbor beams with use of the load distribution*

*Table 69 determining the girder load for the main beam with the load at 2.25 m, with use of the total load on the bridge system and the load distribution, and then subtracting the girder load from the total load, giving the slab load*

| Deflection of bridge system [mm] | Total load [kN] | Girder load (34 % of total) [kN] | Slab load [kN] |
|---|---|---|---|
| **2** | 1250 | 425 | 825 |
| **4** | 2000 | 680 | 1320 |
| **6** | 2600 | 884 | 1716 |
| **8** | 3000 | 1020 | 1980 |
| **10.5** | 3400 | 1150 | 2250 |
| **13** | 3300 | 1122 | 2178 |

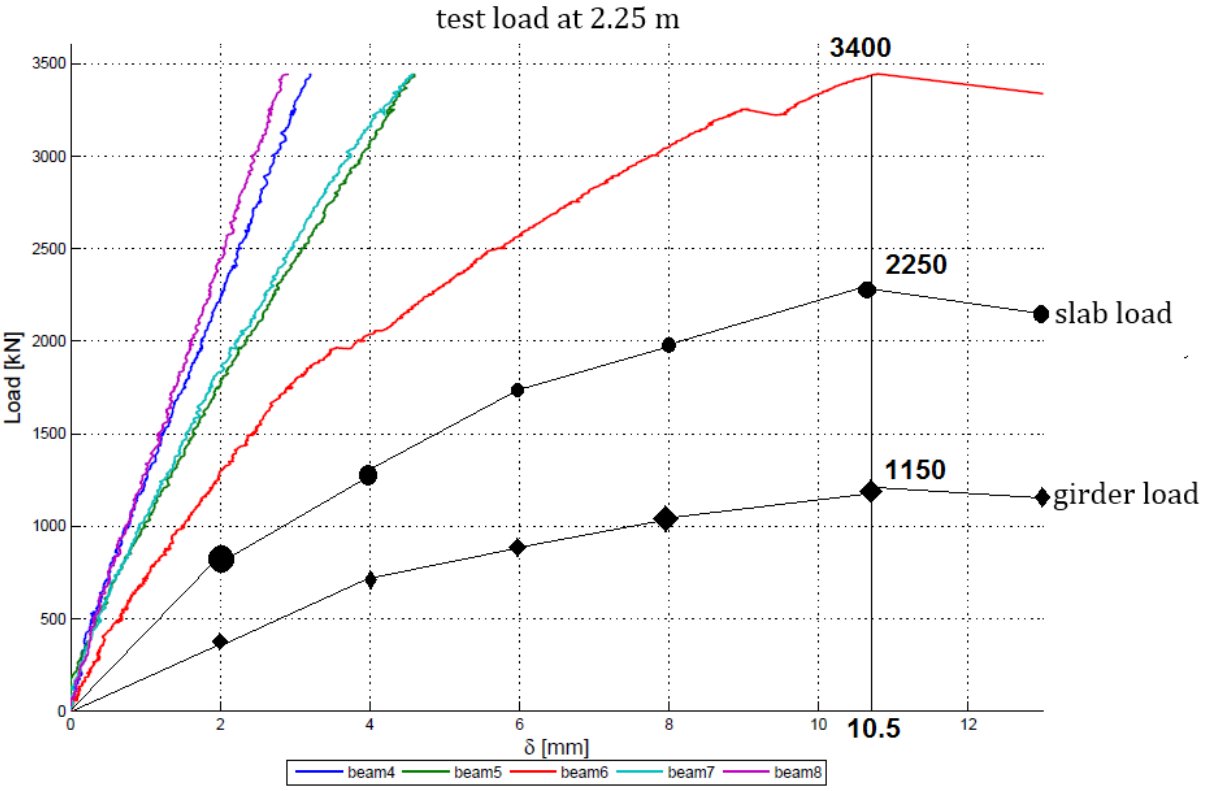


*Figure 253 girder and slab capacity determined for the main beam with use of the load distribution, for the load at 2,25 m*

*Table 70 determining the girder load for the neighbor beam 5,7, with use of the total load on the bridge system and the load distribution, and then subtracting the girder load from the total load, giving the slab load, for the load at 2,25 m*

| Deflection of bridge system [mm] | Total load [kN] | Girder load (20% of total) [kN] | Slab load [kN] |
|---|---|---|---|
| 2 | 1750 | 350 | 1400 |
| 4.5 | 3400 | 680 | 2720 |

*Table 71 determining the girder load for the neighbor beam 4, 8, with use of the total load on the bridge system and the load distribution, and then subtracting the girder load from the total load, giving the slab load, for the load at 2,25 m*

| Deflection of bridge system [mm] | Total load [kN] | Girder load (13 % of total) [kN] | Slab load [kN] |
|---|---|---|---|
| 2 | 2250 | 293 | 1957 |
| 3.5 | 3400 | 442 | 2958 |

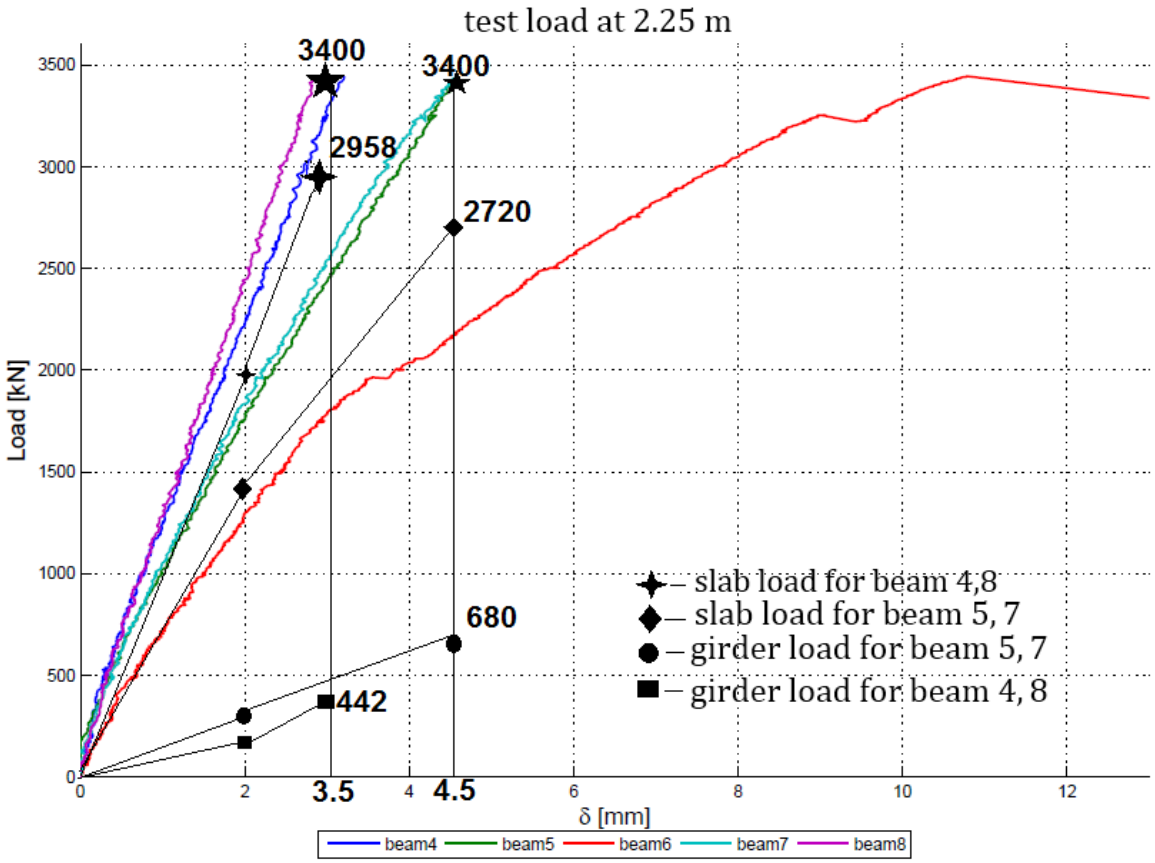


*Figure 254 girder and slab capacity determined for the neighbor beams with use of the load distribution, for the load at 2,25 m.*

# Bibliography


81/02, U. H. (2002). *Use of Compressive Membrane Action in bridge decks, Design Manual for roads and bridges* .

Amir, S. (2014). *Compressive Membrane Action in Prestressed Concrete deck slabs.* Delft.

Batchelor, B. (1987). *Membrane enhance in top slabs of concrete bridges.* Ontario: Queen's University.

CAN/CSA-S6-06. (2006). *Canadian Highway Bridge Design Code (CHBDC).* Ontario: Canadian Standard Association.

Christiansen, K. (1963). The effect of membrane stresses on the ultimate strength of an interior panel in a reinforced concrete slab. *Structural Engineer*, 261-265.

Dorton, R., & Csagoly, P. (1977). *The development of the Ontario Bridge Code.* Ministry of Transportations and Communications.

Ensink, S. (2014). *Proeven Buurliggers meetrapport.* Delft: Delft University of Technology.

Hewitt, B. E., & Batchelor, B. d. (1975). Punching shear strength of restrained slabs. *Journal of the Structural Division*, 1837-1853.

Hognestad, E., Hanson, N., & McHenry, D. (1955). Concrete stress distribution in ultimate strength design. *Journal of the American Concrete Institute*, 455-479.

Hon, A., Taplin, G., & Al-Mahaidi, R. (2005). Strength of reinforced concrete bridge decks. *ACI structural journal*, 393-401.

Hwang, H. (2010). punching and fatigue behavior of longspan prestressed concrete deck slabs. *Engineering structures*, 2861-2872.

Kirkpatrick, J., Long, A. E., & Thompson, A. (1982). Load distribution characteristics of MBeam bridge decks. *Structural Engineer* , 34-43.

Liebenberg, A. C. (1966). *Arch action in concrete slabs.* National Building Research.

Long, A. (1975). A two phase approach to the prediction of the punching strength of slabs. *Journal of the American Concrete Institute*, 37-45.

Marshe, S. (1997). *Punching behavior of composite bridge decks transversely prestressed with carbon fibre reinforced plastic tendons.* Ontario.

McDowell, E., McKee, K., & Sevin, E. (1956). Arching action theory of masonry walls. *Journal of Structural Division*, 915-918.

Muthu, K. (2006). *Load deflection behaviour of partially restrained slab strips.* Selengor: Elsevier.

(2007). *NEN 6706:2005; TGB 1990 Verkeersbelastingen op bruggen.*

(2005). *NEN-EN 1991-2.* Brussels.

(2005). *NEN-EN 1992-1-1.* Brussels.

new zealand transport agency. (2014). *New Zealand Bridge Manual, 3rd Edition.* Wellington: New Zealand Government.

Ockleston, A. J. (1955). Load tests on a three-storey reinforced concrete building in Johannesburg. *the structural engineer*, 304-322.

Park, R. (1964). Ultimate strength of rectangular concrete slabs under short-term uniform loading with edges restrained against lateral movement. *Proceedings of the Institution of Civil Engineers, Structures and Buildings*, 125-150.

Poston, R. (1988). effects of transverse prestressing in bridge decks. *Journal of structural engineering*.

Pucher, A. (1964). *Influence surfaces of elastic plates.* New York: Springer Verlag.

Rankin, G. (1982). *Punching failure and compressive membrane action in reinforced concrete slabs.* Belfast.

Rankin, G., & Long, A. (1997). Arching action strength enhancement in laterally restrained slabs. *ICE proceedings-Structures and Buildings*, 461-467.

Rijkswaterstaat. (2013). *Richtlijnen beoordelen kunstwerken (RBK) 1.1.* Rijkswaterstaat.

(2013). *Stevin Report No. 25.5.13-06.* Delft.

Taylor, S., & Mulin, B. (2005). *Arching action in FRP reinforced concrete slabs.* Belfast: Elsevier.

Taylor, S., & Mullin, B. (2006). Arching action in FRP reinforced concrete slabs. *Construction and building materials*, 71-80.

Taylor, S., & Tharmarajah, G. (2010). *Arching action in laterally resraint GFRP slabs.* Beijing: Queen's university.

Taylor, S., & Tharmarajah, G. (2014). *corosion resistant FRP reinforcement for concrete deck slabs.* ICE.

Taylor, S., Rankin, G., & Cleland, D. (2002, February). Guide to compressive membrane action in concrete bridge decks.

Taylor, S., Rankin, G., & D.J., C. (2001). Arching action in high strength concrete slabs. *Proc Inst Civil Engineers Struct. Buildings*, 353-362.

Van der Veen, C., & Gijsbers, F. (2014). *Stevinrapport nr. 25.5-10-04 Verkennende studie dunnen dekken en tussenstorts.* DElft.

Van der Veen, C., Gijsbers, J., & de Boer, A. (2012). Drukmembraanwerking. *Cement* , 68-74.

Vugts, M. W. (2012). *Experimental determination of bearing capacity of transversely prestressed concrete deck slabs.* Delft.

Wood, R. (1961). *Plastic and elastic design of slabs and plates.* London: Thames and Hudson.